Nonequilibrium Superconductivity : Part II

Yury Holubeu *

September 29, 2025

This draft is not aimed for distribution.

Contents

*https://yuriholubeu.github.io/, yuri.holubev@gmail.com

Preface

Amazing facts

(I'll reveal it later)

Puzzles for motivation

(I'll reveal it later)

Part VII
Other My Theories

Part VIII
Main Experiments

Part IX
Other Special Theories, Models

7 Nonequilibrium Cooper pairing in the nonadiabatic Regime by Yuzbashyan et al.

Abstract

We obtain a complete solution for the mean-field dynamics of the BCS paired state with a large, but finite number of Cooper pairs in the nonadiabatic regime. We show that the problem reduces to a classical integrable Hamiltonian system and derive a complete set of its integrals of motion. The condensate exhibits irregular multi-frequency oscillations ergodically exploring the part of the phase-space allowed by the conservation laws. In the thermodynamic limit however the system can asymptotically reach a steady state.

The study of the dynamics of the BCS superconductors has a long history[1]. Early attempts to describe nonstationary superconductivity were based on the time-dependent Ginzburg-Landau (TDGL) equation [2, 3, 4], which reduces the problem to the time evolution of a single collective order parameter $\Delta(t)$. The TDGL approach is valid only provided the system quickly reaches an equilibrium with the instantaneous value of $\Delta(t)$, i.e. a local equilibrium is established faster than the time scale of the order parameter variation, $\tau_\Delta \simeq 1/\Delta$. This requirement limits the applicability of the TDGL to special situations where pair breaking dominates, e.g. due to a large concentration of magnetic impurities. An alternative to TDGL is the Boltzmann kinetic equation[5, 6] for the quasiparticle distribution function coupled to a self-consistent equation for $\Delta(t)$. This approach is justified only when external parameters change slowly on the τ_Δ time scale, so that the system can be characterized by a quasiparticle distribution.

Is it possible to describe theoretically the dynamics of a BCS paired state in the nonadiabatic regime when external parameters change substantially on the τ_Δ time scale? In particular, an important question is whether, following a sudden perturbation, the condensate reaches a steady state on a τ_Δ time scale or on a much longer quasiparticle energy relaxation time scale τ_ϵ. In the nonadiabatic regime both TDGL and the Boltzmann kinetic equations fail and one has to deal with the coupled coherent dynamics of individual Cooper pairs. Recent studies[15, 16, 17, 18] of this outstanding problem were motivated by experiments on fermionic pairing in cold atomic alkali gases[8, 7]. The strength of pairing interactions in these systems can be fine tuned rapidly by a magnetic field, making it easier than in metals to access the nonadiabatic regime experimentally.

The main result of the present paper is an explicit general solution for the *dynamics* of the BCS model, which describes a spatially homogenous condensate at times $t \ll \tau_\epsilon$. We employ the usual BCS mean-field approximation, which is accurate when the number of Cooper pairs is large[10, 11]. It turns out that the mean-field BCS dynamics can be formulated as a nonlinear *classical Hamiltonian* problem. We obtain the exact solution for all initial conditions and a complete set of integrals of motion for the mean-field BCS dynamics.

In this paper we assume that the number of Cooper pairs in the system is arbitrary large, but *finite*. In this case the typical evolution at times $t \ll \tau_\epsilon$ is *quasi*-periodic with a large number of incommensurate frequencies. The condensate exhibits irregular multi-frequency oscillations ergodically exploring the part of the phase-space allowed by the conservation laws. The system returns arbitrarily close to its initial state at irregular time intervals. However, the return time diverges in the thermodynamic limit for most physical initial conditions, while the solution

asymptotically reaches a *steady* state on the τ_Δ time scale. The system thermalizes on a much larger energy relaxation time scale τ_ϵ[9].

The dynamics of the BCS condensate following a sudden change of external parameters has been previously discussed by a number of authors[11, 12, 13, 14, 15, 16, 17, 18, 19]. Most notably, a linear analysis around the BCS ground state has been performed[11, 12] and some simple particular solutions for the nonlinear mean-field dynamics in the context of superconductivity have been reported[14, 15]. We discuss below how these results fit into the general picture.

We begin our description of the nonequilibrium Cooper pairing in the non-dissipative regime, $t \ll \tau_\epsilon$, with the BCS model[20, 21, 22].

$$\hat{H}_{BCS} = \sum_{j,\sigma} \epsilon_j \hat{c}^\dagger_{j\sigma}\hat{c}_{j\sigma} - g\sum_{j,q} \hat{c}^\dagger_{j\uparrow}\hat{c}^\dagger_{j\downarrow}\hat{c}_{q\downarrow}\hat{c}_{q\uparrow} \tag{7.1}$$

where ϵ_j are single-particle energies. The pairing is between time reversed states $|j\uparrow\rangle$ and $|j\downarrow\rangle$[23]. Our goal is to determine the evolution of a state that was driven out of equilibrium at, say, $t = 0$.

There are several equivalent ways to derive mean-field equations of motion. One can start with the BCS product state, $\prod_j \left(U_j(t) + V_j(t)c^\dagger_{j\uparrow}\hat{c}^\dagger_{j\downarrow}\right)|0\rangle$, and use Bogoliubov-de Gennes equations for the time-dependent amplitudes $U_j(t)$ and $V_j(t)$. Alternatively, one can study the evolution of the normal, $G_j(t) = -i\langle[\hat{c}_{j\uparrow}(t), \hat{c}^\dagger_{j\uparrow}(t)]\rangle$, and anomalous, $F_j(t) = -i\langle[\hat{c}_{j\uparrow}(t), \hat{c}_{j\downarrow}(t)]\rangle$, Green's functions at coinciding times[12].

The most convenient for us approach to the BCS mean-field dynamics is based on the Anderson pseudospin representation[11]. Within this approach the mean-field equations are Hamiltonian equations of motion for a classical spin chain. Pseudospin-1/2 operators are related to fermion creation and annihilation operators via $\hat{K}^z_j = (\hat{n}_{j\uparrow} + \hat{n}_{j\downarrow} - 1)/2$ and $\hat{K}^-_j = \hat{c}_{j\downarrow}\hat{c}_{j\uparrow} = (\hat{K}^+_j)^\dagger$. Pseudospins are defined on empty and doubly occupied (unblocked) single-particle orbitals ϵ_j. Singly occupied orbitals are decoupled from the dynamics. For n unblocked orbitals the Hamiltonian has the form

$$\hat{H}_{BCS} = \sum_{j=0}^{n-1} 2\epsilon_j \hat{K}^z_j - g\sum_{j,q} \hat{K}^+_j\hat{K}^-_q \tag{7.2}$$

The mean field approximation is accurate[11, 10] in the thermodynamic limit due to the infinite range of interactions between spins in the Hamiltonian (7.2). Therefore, the effective field seen by each pseudospin in (7.2) can be replaced with its quantum mechanical average, $\mathbf{b}_j(t) = (-2\Delta_x(t), -2\Delta_y(t), 2\epsilon_j)$, where $\Delta(t) \equiv \Delta_x(t) - i\Delta_y(t) \equiv g\sum_j\langle\hat{K}^-_j(t)\rangle$ is the BCS gap function. In this approximation, each spin evolves in the self-consistent field: $\dot{\hat{\mathbf{K}}}_\mathbf{j} = \mathbf{i}[\hat{\mathbf{H}}_\mathbf{BCS}, \hat{\mathbf{K}}_\mathbf{j}] \approx \mathbf{b_j}\times\hat{\mathbf{K}}_\mathbf{j}$. Taking the quantum mechanical average of these equations with respect to the time-dependent state of the system, we obtain for $\mathbf{s}_j(t) = \langle\hat{\mathbf{K}}_j(t)\rangle$

$$\dot{\mathbf{s}}_j = \mathbf{b}_j\times\mathbf{s}_j \quad \mathbf{b}_j = (-2gJ_x, -2gJ_y, 2\epsilon_j) \quad \mathbf{J} = \sum_{q=0}^{n-1}\mathbf{s}_q \tag{7.3}$$

The components of the classical spins $s^z_j(t)$ and $s^\pm_j = s^x_j \pm is^y_j$ are related to Bogoliubov amplitudes and equal times Green's functions as $2s^z_j = |V_j|^2 - |U_j|^2$, $s^-_j = \bar{U}_jV_j$ and $G_j(t) = is^z_j(t)$, $F_j(t) = is^-_j(t)$, respectively. Evolution equations (7.3) conserve the square of the average for each spin: $d\mathbf{s}^2_j/dt = 0$. If the spins initially were in a product state, $\mathbf{s}^2_j = 1/4$. Note also that $\Delta(t) = gJ_-(t)$.

One can check that Eqs. (7.3) are equations of motion for a *classical* spin Hamiltonian

$$H_{BCS} = \sum_{j=0}^{n-1} 2\epsilon_j s^z_j - g\sum_{j,q} s^+_j s^-_k \tag{7.4}$$

It means that Eqs. (7.3) are Hamilton equations $\dot{\mathbf{s}}_j = \{H_{BCS}, \mathbf{s}_j\}$ derived from Hamiltonian (7.4) using the usual angular momentum Poisson brackets

$$\left\{s_j^a, s_k^b\right\} = -\varepsilon_{abc}\delta_{jk}s_j^c \tag{7.5}$$

where a, b, and c stand for spatial indexes x, y, and z. The classical model (7.4) can be obtained from its quantum counterpart (7.2) by replacing operators with classical dynamical variables and commutators with Poisson brackets.

Both the classical (7.4) and quantum models (7.1) and (7.2) are integrable[24, 25, 26]. To show this, one can introduce a vector function (Lax-vector) of an auxiliary parameter u

$$\mathbf{L}(u) = -\frac{\hat{\mathbf{z}}}{g} + \sum_j \frac{\mathbf{s}_j}{u - \epsilon_j}, \tag{7.6}$$

where $\hat{\mathbf{z}}$ is a unit vector along the z axis. Poisson brackets between components of $\mathbf{L}(u)$ at different values of u can be evaluated using Eq. (7.5).

$$\left\{L^a(v), L^b(w)\right\} = \varepsilon_{abc}\frac{L^c(v) - L^c(w)}{v - w} \tag{7.7}$$

(Relations (7.7) hold for each term in (7.6) separately; all terms Poisson-commute with each other). It follows from Eq. (7.7) that the lengths of the Lax vector at different values of u Poisson-commute:

$$\left\{\mathbf{L}^2(v), \mathbf{L}^2(w)\right\} = 0 \tag{7.8}$$

The scalar function $\mathbf{L}^2(u)$ can be represented in the form

$$\mathbf{L}^2(u) = \frac{1}{g^2} + \sum_{j=0}^{n-1}\left(\frac{2H_j}{u - \epsilon_j} + \frac{\mathbf{s}_j^2}{(u - \epsilon_j)^2}\right) \tag{7.9}$$

where

$$H_j = \sum_{k=0}^{n-1}{}' \frac{\mathbf{s}_j \cdot \mathbf{s}_k}{\epsilon_j - \epsilon_k} - \frac{s_j^z}{g} \tag{7.10}$$

Since Eq. (7.8) holds for any v and w, all H_j Poisson-commute with each other. Therefore, each H_j, as well as any algebraic combination of H_j, defines a classical model[27] that has n degrees of freedom (n classical spins) and n integrals of motion (including itself) and thus is integrable in the usual sense[28]. Note that the sum of H_j is proportional to the z-component of the total spin $\mathbf{J}$, therefore J_z is conserved by all H_j and their combinations. Moreover, the following identity follows from Eqs. (7.4,7.10)

$$H_{BCS} = -g\sum_j \epsilon_j H_j + \text{const} \tag{7.11}$$

This implies that the classical BCS model (7.4) Poisson-commutes with all H_j's and thus is also integrable. Equations (7.10) and (7.11) can be straightforwardly quantized by replacing $\mathbf{s}_j \to \hat{\mathbf{K}}_j$. The resulting operators $\hat{H}_j$ all pairwise commute, thus showing the integrability of quantum models (7.1) and (7.2).

To obtain the general solution for the mean-field dynamics of the BCS model (7.1), we follow the method of Ref. [29] and introduce $n-1$ *separation* variables u_k as zeros of $L_-(u) = L_x(u) - iL_y(u)$, i.e. $\sum_j s_j^-/(u_k - \epsilon_j) = 0$.

Equations of motion for the variables u_k are[30]

$$\dot{u}_k = 2i\sqrt{Q_{2n}(u_k)}\prod_{m\neq k}(u_k - u_m)^{-1} \tag{7.12}$$

where $Q_{2n}(u)$ is the *spectral polynomial* defined as

$$Q_{2n}(u) = g^2\mathbf{L}^2(u)\prod_j (u-\epsilon_j)^2 \tag{7.13}$$

By Eq. (7.9), the coefficients of $Q_{2n}(u)$ depend only on the integrals of motion H_j.

Eqs. (7.12) constitute the well-known Jacobi's inversion problem solvable in terms of hyperelliptic theta functions[31]. Here we outline the final answer, the details will be reported elsewhere[30]. Klenian σ- and ζ-functions of *genus* G (in our case $G = n-1$) are defined as

$$\begin{aligned} &\zeta_l(\mathbf{x}) = \frac{\partial \ln\sigma(\mathbf{x})}{\partial x_l} \quad \sigma(\mathbf{x}) = \sum_{\mathbf{m}\in Z^G} \exp\left[S_{\mathbf{m}}(x)/2\right] \\ &S_{\mathbf{m}}(x) = \mathbf{x}\cdot\eta\omega^{-1}\mathbf{x} + 2i\pi(\mathbf{m}\cdot\tau\mathbf{m} + \omega^{-1}\mathbf{x}\cdot\mathbf{m}) \end{aligned} \tag{7.14}$$

where the sum is over all G-dimensional integer vectors $\mathbf{m}$, $\tau = \omega'\omega^{-1}$, and ω, ω', and η are $G\times G$ matrices of periods (see below). The solution is

$$s_j^-(t) = \langle \hat{c}_{j\downarrow}(t)\hat{c}_{j\uparrow}(t)\rangle = J_-(t) r(\epsilon_j, t)\prod_{k\neq j}\frac{\epsilon_j}{\epsilon_j-\epsilon_k} \tag{7.15}$$

$$\Delta(t) = gJ_-(t) = g\sum_j s_j^-(t) = c_n e^{-i\beta t}\frac{\sigma(\mathbf{x}+\mathbf{d})}{\sigma(\mathbf{x}-\mathbf{d})} \tag{7.16}$$

Here $\mathbf{x}^T = i(c_1,\ldots,c_{n-2}, 2t+c_{n-1})$; $\mathbf{d}$ is a vector of constants; $\beta = gJ_z + \sum_j \epsilon_j$; $c_1,\ldots,c_n$ are constants fixed by the initial conditions, and

$$r(u,t) = 1 - \sum_{k=1}^{n-1}(\zeta_k(\mathbf{x}+\mathbf{d}) - \zeta_k(\mathbf{x}-\mathbf{d}) + a_k)u^{k-n} \tag{7.17}$$

Constants a_k, the matrices of periods, constant vector $\mathbf{d}$, are all uniquely determined[32] by the spectral polynomial $Q_{2n}(u)$, i.e. by integrals of motion.

The evolution of $\mathbf{s}_j(t) = \langle\hat{\mathbf{K}}_j(t)\rangle$ described by the general solution is typical of an integrable system[28]. It is characterized by n frequencies, which in our case can be determined[30] in terms of integrals of motion, and are typically incommensurate. Note that $|\Delta(t)|$ contains only $n-1$ frequencies. The typical dynamics is stable against perturbations destroying integrability[28].

Now let us discuss some particular solutions. There are two types of equilibrium states that play an important role in the dynamics. In *normal* states all spins are parallel to the z-axis, $2\mathbf{s}_j^z = \pm 1$. Since $2\mathbf{s}_j = \langle\hat{n}_j\rangle - 1$, these states correspond to the ground state and excitations of the single-particle part of the Hamiltonian (7.1) (Fermi gas). They are stationary within the mean-field dynamics (7.3). For a finite system, they are non-stationary for the quantum Hamiltonian (7.1) and their short time dynamics is entirely driven by quantum corrections (cf. Refs. [33, 34]).

The second type of equilibrium states are *anomalous* ones, which correspond to the BCS ground state and excitations. These states are obtained by aligning each spin in (7.4) self-consistently along the effective magnetic field acting on it. The self-consistency condition is the BCS gap equation. As $\mathbf{s}_j = \langle\hat{\mathbf{K}}_j\rangle$, one can obtain the BCS wave-function and energy spectrum from anomalous equilibrium configurations of classical spins $\mathbf{s}_j$.

It turns out that equilibrium states are a part of a more general scheme when the dynamics of n spins degenerates to that of $m < n$ *collective* spins (*m-spin solutions*) governed by the same Hamiltonian (7.4) only with m spins and new parameters μ_j instead of ϵ_j. Normal and anomalous states correspond to 0- and 1-spin solutions, respectively. To construct m-spin

solutions one has to take the Lax-vector (7.6) to be proportional to that of a system with m spins $\mathbf{t}_k$, $\mathbf{L}(u) = [1 + \sum_j b_j/(u - \epsilon_j)]\mathbf{L_t}(u)$, where b_j are time-independent constants, and $\mathbf{L_t}(u) = -\hat{\mathbf{z}}/g + \sum_k \mathbf{t}_k/(u - \mu_k)$. Then, $2(n - m)$ of $2n$, typically distinct, roots of the spectral polynomial $Q_{2n}(u)$ become doubly degenerate and $n - m$ separation variables u_k are frozen in these double roots, which automatically solves the equations of motion for these $n - m$ variables. The dynamics is obtained by replacing $n \to m$ and $\epsilon_k \to \mu_k$ in Eqs. (7.14–7.17) and is characterized by $m < n$ typically incommensurate frequencies. For $m = 2$ the solution is in terms of hyperelliptic functions of genus $G = m - 1 = 1$, i.e. in terms of ordinary elliptic functions.

Now let us discuss the connection of our results with the previous work. The solutions for the mean field BCS dynamics obtained in Ref. [15] are 2-spin solutions in the above classification. They were used in Ref. [15] to describe the evolution beginning from a state infinitesimally close to the normal ground state. In our view, the dynamics in the vicinity of this state can have additional features and deserves further analysis.

The 2-spin solutions resemble the TDGL approach in that they describe the dynamics of all pairs in terms of only two collective degrees of freedom resulting in large amplitude single frequency (periodic) oscillations of the order parameter magnitude $|\Delta(t)|$. Mathematically, they lie on a 1d curve of points in a multi-dimensional (infinite-dimensional in the thermodynamic limit) space of possible values of integrals of motion. The situation with other few spin solutions is similar[35]. In contrast, the general solution we obtained here *typically* has a large (infinite in the thermodynamic limit) number of incommensurate frequencies and a substantially reduced amplitude. The difference between the general and few spin solutions is clear in a linear analysis[11, 12] around the BCS ground state that displays normal modes with frequencies $\omega_k = 2\sqrt{\epsilon_k^2 + \Delta_0^2}$, where ϵ_k are single-particle energies and Δ_0 is the equilibrium order parameter. In the linear regime, the general solution becomes an arbitrary superposition of all normal modes, while few spin solutions single out all, but few modes. For example, 2-spin solutions of Ref. [15] correspond to a single normal mode with a frequency $2\Delta_0$.

In conclusion, we have obtained the explicit general solution for the mean-field dynamics of the BCS paired state and discussed a number of special cases including two types of equilibrium states and few spin solutions. A still open problem is to fully analyze the solution in the thermodynamic limit. It is also desirable to better understand the dynamics in the vicinity of normal states where quantum effects become important. Finally, it is interesting to identify experimental setups where peculiar features of the nonequilibrium Cooper pairing in the nonadiabatic regime can be observed such as e.g. cold Fermi gases.

We are grateful to I. Aleiner, V. Falko, L. Glazman, L. Levitov, A. Millis, A. Polyakov, and O. Tsyplyatyev for stimulating discussions. This research was supported by NSF DMR 0210575 and by ARO/ARDA (DAAD19-02-1-0039).

Note Added. Recently, we became aware of a publication[36] that is in agreement with some of our conclusions – that the initial dynamics of the normal ground state is driven by quantum corrections and that the system can reach a steady state at large times.

8 Pure Goldstone mode in the quench dynamics of a confined ultracold Fermi gas in the BCS-BEC crossover regime by Kettmann et al.

Abstract

We present a numerical study of the dynamic response of a confined superfluid Fermi gas to a rapid change of the scattering length (i.e., an interaction quench). Based on a fully

microscopic time-dependent density-matrix approach within the full Bogoliubov-de Gennes formalism that includes a 3D harmonic confinement we simulate and identify the emergence of a Goldstone mode of the BCS gap in a cigar-shaped ^{6}Li gas. By analyzing this Goldstone mode over a wide range of parameters, we show that its excitation spectrum is gapless and that its main frequency is not fixed by the trapping potential but that it is determined by the details of the quench. Thus, we report the emergence of a pure Goldstone mode of the BCS gap that –in contrast to situations in many previous studies– maintains its gapless excitation spectrum predicted by the Goldstone theorem. Furthermore, we observe that the size-dependent superfluid resonances resulting from the atypical BCS-BEC crossover have a direct impact on this Goldstone mode. Finally, we find that the interaction quench-induced Goldstone mode leads to a low-frequency in-phase oscillation of the single-particle occupations with complete inversion of the lowest-lying single-particle states which could provide a convenient experimental access to the pure gapless Goldstone mode.

8.1 Conclusion

In conlusion, we have calculated the dynamics of a confined ultracold ^{6}Li gas at $T = 0$ induced by an interaction quench on the BCS side of the BCS-BEC crossover. We used a full dynamical BdG approach to set up and solve the equations of motion for the single-particle occupations and coherences. In doing so, we have shown that the interaction quench excites a low-energy linear dynamics of the complex phase of the BCS gap, i.e., a Goldstone mode. We have analyzed this Goldstone mode over a wide range of parameters showing that its excitation spectrum is gapless and that its main frequency is not fixed by the trap frequencies but that it is determined by the details of the quench. Furthermore, we found that the atypical BCS-BEC crossover leads to resonances in the gapless Goldstone mode. Finally, we investigated the impact of the gapless Goldstone mode on the single-particle occupations. We have shown that it leads to an in-phase oscillation of the whole single-particle spectrum with a full inversion of the lowest-lying single-particle states which could provide an experimental access to the gapless homogeneous Goldstone mode.

8.2 Introduction

Due to their unique controllability ultracold Fermi gases provide an ideal system to test concepts of many-particle physics as well as particle theory. Adjustable interparticle interactions provide the possibility to explore both the regime of weak attractive interactions where a superfluid Bardeen Cooper Schrieffer (BCS) phase emerges as well as the regime of weak repulsive interactions which lead to the formation of a Bose-Einstein condensate (BEC). Both regimes are connected by a smooth BCS-BEC crossover with strong interparticle interactions including a point of unitarity where the coupling strength diverges [Giorgini *et al.*(2008), Bloch *et al.*(2008)]. Furthermore, the emergence of a BCS phase is associated with a spontaneously broken $U(1)$ symmetry which makes ultracold Fermi gases a convenient candidate to study the fundamental concept of spontaneous symmetry breaking (SSB) [Weinberg(1996)].

Spontaneously broken gauge symmetries and the resulting two types of fundamental collective excitations –gapped amplitude/Higgs modes and gapless phase/Goldstone modes (see Fig. 8.1)– are of fundamental interest for several fields of physics like condensed matter and particle physics. Probably the most prominent application of the concept of SSB is the Higgs mechanism in particle physics [Higgs(1964)]. In condensed matter physics SSB occurs in several systems, for example in ferromagnets (see, e.g., [Burgess(2000)]), superfluid ^{3}He [Paulson *et al.*(1973), Lawson *et al.*(1973)] and BCS superconductors [Anderson(1958), Weinberg(1996)]. In these cases, the fundamental excitations –known as magnons (i.e., spin waves), second sound (i.e., heat waves) and plasmons– correspond to the Goldstone modes resulting from SSB.

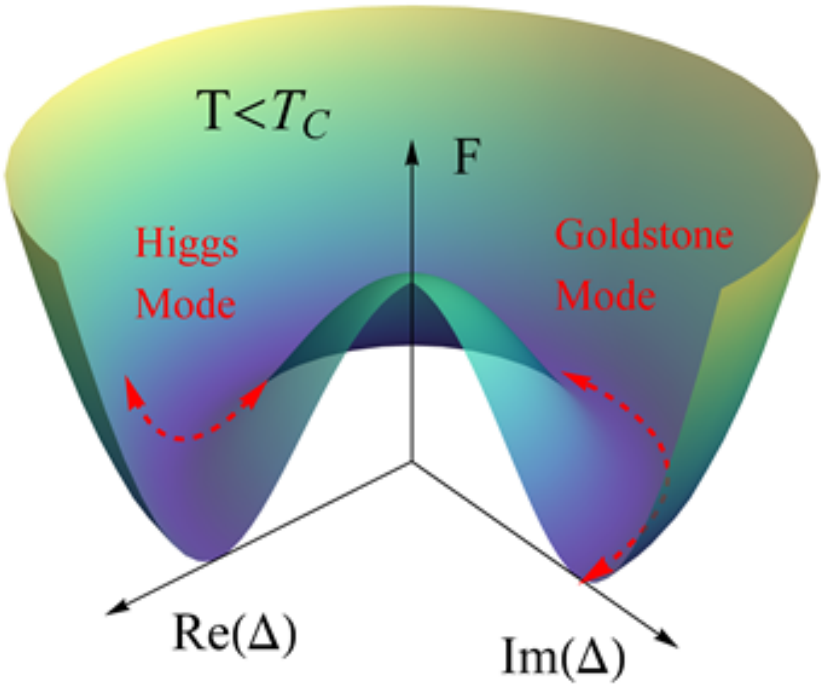

Figure 8.1: (color online) Ginzburg-Landau free energy of a BCS phase of a homogeneous Fermi gas for $T < T_C$ (schematic). The rotational $U(1)$ symmetry is broken, when the gap Δ of the system gains a certain phase inside the rim of the potential. The resulting excitation modes are the Higgs-amplitude mode and the Goldstone mode, i.e., a phase oscillation of the gap.

In the field of ultracold Fermi gases the Higgs and the Goldstone mode have received great attention over the past years. The Higgs mode, i.e., the amplitude oscillation of the BCS gap, is difficult to address in experiment since it does not couple directly to external probes [Pekker and Varma(2015)]. This is why measurements of the Higgs mode have only recently been achieved for lattice superfluids [Bissbort *et al.*(2011), Endres *et al.*(2012)] (in the case of BCS superconductors an experimental access has been found via THz spectroscopy [Matsunaga *et al.*(2013), Matsunaga *et al.*(2014)]), while several theoretical studies on the Higgs mode have been reported [Barankov *et al.*(2004), Barankov and Levitov(2006), Yuzbashyan *et al.*(2006), Dzero *et al.*(2007), Scott *et al.*(2012), Bruun(2014), Hannibal *et al.*(2015)]. In contrast, the Goldstone mode, i.e., the oscillation of the complex phase of the BCS gap, has been intensively studied both theoretically and experimentally (see, e.g., [Kinast *et al.*(2004a), Kinast *et al.*(2004b), Bartenstein *et al.*(2004), Altmeyer *et al.*(2007a), Altmeyer *et al.*(2007b), Riedl *et al.*(2008), Baranov and Petrov(2000), Bruun and Mottelson(2001), Bruun(2002), Hu *et al.*(2004), Heiselberg(2004), Stringari(2004), Grasso *et al.*(2005), Korolyuk *et al.*(2011)]).

However, most previous studies were based on the fact that the Goldstone mode couples to the real-space dynamics of the Fermi gas. Therefore, it can be excited by inducing a collective oscillation of the trapped cloud, which can be achieved, e.g., by various schemes of confinement change or by optical excitation. The dynamics in the Goldstone mode is then directly reflected in the collective oscillation of the cloud and can be observed via the latter. However, a coupling to the real-space oscillation of the cloud implies a coupling to the trapping potential. I.e., in the previous studies the frequency of the Goldstone mode was fixed by the frequencies of the trap which stands in direct contrast to the Goldstone theorem predicting a gapless excitation spectrum of the phase mode. Thus, the observation of the gapless phase mode resulting from the Goldstone theorem was so far obstructed by the coupling to the trapping potential via the collective oscillation of the cloud.

In contrast, we report the emergence of a pure Goldstone mode in the dynamics of a trapped ultracold Fermi gas by showing that its original gapless excitation spectrum can be recovered

by exciting the cloud via an interaction quench. To this end, we observe that the frequency of the interaction quench-induced phase mode can be tuned over a wide range from zero to finite values by adjusting the details of the quench. We explain this by the circumstance that the excited Goldstone mode is homogeneous, i.e., that it does not introduce any phase gradients, and that it therefore does not couple to the trapping potential.

To do so, we study the dynamics of the BCS gap of a confined ultracold ^{6}Li gas at $T = 0$ on the BCS side of the BCS-BEC crossover [i.e., the Fermi wave vector k_F times the scattering length a is given by $0 > 1/(k_F a) > -1$] as well as in the BCS regime [i.e., $-1 > 1/(k_F a)$]. We calculate the dynamics of the Bogoliubov quasiparticles in the framework of the Bogoliubov-de Gennes (BdG) formalism and by that the dynamics of the BCS gap. The investigated system is in the low-density regime, i.e., we use a short-range s-wave interaction between particles with opposite spin. The confinement is modeled by a cigar-shaped 3D harmonic potential, which in good approximation describes the standard laser confinement used in experiment [Bloch *et al.*(2008)]. The system is excited by an instantaneous interaction quench, i.e., a rapid change of the interparticle interaction strength. This can experimentally be achieved, e.g., by an optical control of a Feshbach resonance [Clark *et al.*(2015)].

Our work is structured as follows. In section 8.3 we present the formalism we used within the context of this work, i.e., a full BdG approach as well as its simplification via the Anderson approximation. We will derive the equations of motion for the quasiparticle expectation values which allow for a calculation of the phase dynamics of the BCS gap. In section 9.4 we present the results obtained by the full BdG approach and show that they are well reproduced by Anderson's approximate solution. Based on the latter we will analyze the effect of the excitation parameters and of the trapping frequencies on the interaction-quench-induced Goldstone mode as well as the impact of this Goldstone mode on an experimentally accessible quantity, i.e., the single-particle excitations of the cloud. Finally, we conclude and summarize our findings in section 9.1.

8.3 Theoretical approach

To calculate the ground state as well as the dynamical properties of a BCS condensate in a trap we start from the Bogoliubov-de Gennes (BdG) Hamiltonian [De Gennes(1989), Datta and Bagwell(1999)]:

$$\begin{aligned} H_{BdG} = &\int \Psi_\uparrow^\dagger(\mathbf{r}) H_0 \Psi_\uparrow(\mathbf{r})\, \mathrm{d}^3 r + \int \Psi_\downarrow^\dagger(\mathbf{r}) H_0 \Psi_\downarrow(\mathbf{r})\, \mathrm{d}^3 r \\ &+ \int \left[\Delta(\mathbf{r}) \Psi_\uparrow^\dagger(\mathbf{r}) \Psi_\downarrow^\dagger(\mathbf{r}) + \Delta^*(\mathbf{r}) \Psi_\downarrow(\mathbf{r}) \Psi_\uparrow(\mathbf{r})\right] \mathrm{d}^3 r. \end{aligned} \tag{8.1}$$

Here the field operators $\Psi_\sigma^{(\dagger)}(\mathbf{r})$ describe the annihilation (creation) of Fermions –in this case atoms of ^{6}Li– with spin σ at the position $\mathbf{r}$ and the BCS gap is given by

$$\Delta(\mathbf{r}) = -g \left\langle \Psi_\downarrow(\mathbf{r}) \Psi_\uparrow(\mathbf{r}) \right\rangle . \tag{8.2}$$

The interaction strength $g = -\frac{4\pi\hbar^2 a}{m}$ is determined by the s-wave scattering length a and the mass of the particles m. The 3D harmonic trapping potential $V(\mathbf{r})$ is included in the one-particle Hamiltonian $H_0 = \frac{p^2}{2m} + V(\mathbf{r}) - \mu$ with the chemical potential μ, where we set the trapping frequencies to $f_x = f_y =: f_\perp \gg f_\parallel := f_z$, i.e., a cigar-shaped trap.
In the following, we will show how to diagonalize Eq. (8.1) and thus obtain its eigenstates and energies which describe the single-particle excitations of the BCS condensate.

8.3.1 The BdG ground state

To calculate the ground-state properties of the BCS condensate it is instructive to write the eigenvalue equation corresponding to Eq. (8.1) as the BdG equation [De Gennes(1989)]

$$\begin{pmatrix} H_0 & \Delta(\mathbf{r}) \\ \Delta^*(\mathbf{r}) & -H_0^* \end{pmatrix} \begin{pmatrix} u_M(\mathbf{r}) \\ v_M(\mathbf{r}) \end{pmatrix} = E_M \begin{pmatrix} u_M(\mathbf{r}) \\ v_M(\mathbf{r}) \end{pmatrix}. \tag{8.3}$$

This equation has the form of a one-particle Schrödinger equation[1], which implies that H_{BdG} describes non-interacting quasiparticles, i.e., the single-particle excitations of the BCS condensate. Therefore, Eq. (9.3) can be diagonalized which yields the corresponding single-particle wave functions $[u_M(\mathbf{r}), v_M(\mathbf{r})]$ and energies E_M. However, before we do so, we want to state that the single-particle states divide into two branches (one of positive energies $E_M = E_{m\alpha} > 0$ and one of negative energies $E_M = E_{m\beta} = -E_{m\alpha}$) that can be expressed by one another [Datta and Bagwell(1999)]. Accordingly, we simplify our formalism by writing the corresponding expressions –whenever possible– solely in terms of the positive-energy states and by dropping the index α. I.e., in the following we set $[u_m(\mathbf{r}), v_m(\mathbf{r})] := [u_{m\alpha}(\mathbf{r}), v_{m\alpha}(\mathbf{r})]$ and $E_m := E_{m\alpha}$. Furthermore, we transform into the excitation picture, i.e., we flip the β-branch $[(m\beta) \to (mb)]$ and leave the α-branch unchanged $[(m\alpha) = (ma)]$. This yields one twofold degenerate branch with $E_m = E_{ma} = E_{mb}$. The corresponding creation operators read

$$\gamma_{ma}^\dagger = \int \left[u_m(\mathbf{r}) \Psi_\uparrow^\dagger(\mathbf{r}) + v_m(\mathbf{r}) \Psi_\downarrow(\mathbf{r}) \right] \mathrm{d}^3 r \tag{8.4}$$

$$\gamma_{mb}^\dagger = \int \left[u_m(\mathbf{r}) \Psi_\downarrow^\dagger(\mathbf{r}) - v_m(\mathbf{r}) \Psi_\uparrow(\mathbf{r}) \right] \mathrm{d}^3 r. \tag{8.5}$$

We solve the BdG equation by expressing the single-particle states $[u_M(\mathbf{r}), v_M(\mathbf{r})]$ in terms of the bare atomic states, i.e., the eigenstates of the harmonic trap $\phi_i(\mathbf{r})$,

$$u_M(\mathbf{r}) = \sum_{i=1}^{N} u_M^{(i)} \phi_i(\mathbf{r}) \tag{8.6}$$

$$v_M(\mathbf{r}) = \sum_{i=1}^{N} v_M^{(i)} \phi_i(\mathbf{r}), \tag{8.7}$$

with $M \in \{ma, mb\}$. Here, we restrict the sum to atomic states from a window of width $\Delta\epsilon \sim 1\mu$ around the chemical potential (i.e., $0.5\mu < \epsilon < 1.5\mu$) to reduce the numerical effort[2]. Inserting this in the BdG equation, multipliying by $\phi_m(\mathbf{r})$ and integrating over $\mathbf{r}$ yields:

$$\begin{pmatrix} \epsilon_1 - \mu & 0 & \cdots & 0 & (\Delta)_{11} & \cdots & & (\Delta)_{1N} \\ 0 & \epsilon_2 - \mu & \ddots & \vdots & \vdots & \ddots & & \vdots \\ \vdots & \ddots & \ddots & 0 & & & & \\ 0 & \cdots & 0 & \epsilon_N - \mu & (\Delta)_{N1} & \cdots & & (\Delta)_{NN} \\ (\Delta)_{11}^* & \cdots & & (\Delta)_{1N}^* & -\epsilon_1 + \mu & 0 & \cdots & 0 \\ \vdots & \ddots & & \vdots & 0 & -\epsilon_2 + \mu & \ddots & \vdots \\ & & & & \vdots & \ddots & \ddots & 0 \\ (\Delta)_{N1}^* & \cdots & & (\Delta)_{NN}^* & 0 & \cdots & 0 & -\epsilon_N + \mu \end{pmatrix} \begin{pmatrix} u_M^{(1)} \\ u_M^{(2)} \\ \vdots \\ u_M^{(N)} \\ v_M^{(1)} \\ v_M^{(2)} \\ \vdots \\ v_M^{(N)} \end{pmatrix} = E_M \begin{pmatrix} u_M^{(1)} \\ u_M^{(2)} \\ \vdots \\ u_M^{(N)} \\ v_M^{(1)} \\ v_M^{(2)} \\ \vdots \\ v_M^{(N)} \end{pmatrix}, \tag{8.8}$$

[1] To be precise, the many-body nature of the BCS pairing is included in Eq. (9.3) via the self-consistent calculation of the BCS gap $\Delta(\mathbf{r})$ (see below).

[2] We have checked that the qualitative features investigated in this work are independent from the size of this window. However, the features shift quantitatively, e.g., the gaps and frequencies shift to larger values when increasing the window size.

with $(\Delta)_{mn} := \int \mathrm{d}^3 r \phi_m^*(\mathbf{r})\Delta(\mathbf{r})\phi_n(\mathbf{r})$.[3] However, the BCS gap can be expressed in terms of the Bogoliubov transformation [Eqs. (8.4) and (8.5)] which yields

$$\begin{aligned}\Delta(\mathbf{r}) = -g\sum_{m,n} & v_m^*(\mathbf{r})u_n(\mathbf{r})\left\langle \gamma_{ma}^\dagger \gamma_{na}\right\rangle \\ & + u_m(\mathbf{r})u_n(\mathbf{r})\left\langle \gamma_{mb}\gamma_{na}\right\rangle \\ & - v_m^*(\mathbf{r})v_n^*(\mathbf{r})\left\langle \gamma_{ma}^\dagger\gamma_{nb}^\dagger\right\rangle \\ & + u_m(\mathbf{r})v_n^*(\mathbf{r})\left[\left\langle \gamma_{nb}^\dagger\gamma_{mb}\right\rangle - \delta_{mn}\right],\end{aligned} \tag{8.9}$$

and for the ground-state gap

$$\Delta_{\mathrm{GS}}(\mathbf{r}) = g\sum_m u_m(\mathbf{r})v_m^*(\mathbf{r}). \tag{8.10}$$

Therefore, a diagonalization of Eq. (8.8) requires a self-consistent treatment together with Eq. (8.10). In doing so, we set the chemical potential $\mu = E_F$ with E_F the Fermi energy of the bare atomic system, i.e., we assume that the chemical potential is not effected by the BCS pairing. Strictly speaking this assumption is only valid in the deep BCS regime. However, our numerical data on the basis of the Anderson approximation (see section 8.3.3) show that it has no qualitative effect on the features studied in this work.

A final remark to Eq. (8.10): In the presented form the gap equation exhibits an ultraviolet-divergence, i.e., –strictly speaking– Eq. (8.10) needs to be regularized to ensure the convergence of the sum over the BdG eigenstates [Bloch *et al.*(2008)]. However, in our case we restrict those sums to a rather narrow energy range around the Fermi level (see above) and this numerical cutoff remedies the need for a further regularization. This will be different in the calculations based on the Anderson approximation, as will be discussed below.

8.3.2 Quench dynamics

To calculate the dynamics of the BCS condensate we make use of the Bogoliubov transformation Eqs. (8.4) and (8.5). The quasiparticles resulting from that transformation are the single-particle excitations of the BCS phase, which are created, when the system is perturbed. All dynamical quantities investigated in the context of this work can be expressed in terms of expectation values of these quasiparticles. Therefore, we use Heisenberg's equation of motion for the quasiparticle operators to numerically calculate the dynamics of the quasiparticle expectation values.

To this end, we express the BdG Hamiltonian in terms of the single-particle operators for a general nonequilibrium situation where $\Delta(\mathbf{r},t) \neq \Delta_{\mathrm{GS}}(\mathbf{r})$, i.e., where the current value of the gap differs from the ground-state value $\Delta_{\mathrm{GS}}(\mathbf{r})$. Thus, inserting Eqs. (8.4) and (8.5) into Eq. (8.1) where $\Delta = \Delta(\mathbf{r},t) \neq \Delta_{\mathrm{GS}}(\mathbf{r})$ and identifiying Δ_{GS} via Eq. (8.10) yields

$$\begin{aligned}H_{\mathrm{BdG}} = & \sum_m E_{ma}\left(\gamma_{ma}^\dagger\gamma_{ma} + \gamma_{mb}^\dagger\gamma_{mb} - 1\right) \\ & + \sum_{m,n}\left[(\Delta - \Delta_{\mathrm{GS}})_{u_m^* v_n} + (\Delta^* - \Delta_{\mathrm{GS}}^*)_{v_m^* u_n}\right]\gamma_{ma}^\dagger\gamma_{na} \\ & + \sum_{m,n}\left[(\Delta - \Delta_{\mathrm{GS}})_{u_m^* u_n^*} - (\Delta^* - \Delta_{\mathrm{GS}}^*)_{v_m^* v_n^*}\right]\gamma_{ma}^\dagger\gamma_{nb}^\dagger\end{aligned}$$

[3] To calculate matrix elements of the form $\int \mathrm{d}^3 r \phi_m(\mathbf{r})\phi_n(\mathbf{r})\phi_k(\mathbf{r})\phi_l(\mathbf{r})$ we used an analytical expression derived in [Lord(1949)].

$$
\begin{aligned}
&- \sum_{m,n} \Big[(\Delta - \Delta_{\mathrm{GS}})_{v_m v_n} - (\Delta^* - \Delta^*_{\mathrm{GS}})_{u_m u_n} \Big] \gamma_{mb} \gamma_{na} \\
&+ \sum_{m,n} \Big[(\Delta - \Delta_{\mathrm{GS}})_{v_m u_n^*} + (\Delta^* - \Delta^*_{\mathrm{GS}})_{u_m v_n^*} \Big] \gamma^\dagger_{mb} \gamma_{nb} \\
&- \sum_{m,n} \Big[(\Delta - \Delta_{\mathrm{GS}})_{v_m u_n^*} + (\Delta^* - \Delta^*_{\mathrm{GS}})_{u_m v_n^*} \Big] ,
\end{aligned} \tag{8.11}
$$

with

$$
\begin{aligned}
(\Delta - \Delta_{\mathrm{GS}})_{u_m v_n} :=& \\
&\int \mathrm{d}^3 r u^*_m(\mathbf{r}) \big[\Delta(\mathbf{r}, t) - \Delta_{\mathrm{GS}}(\mathbf{r}) \big] v_n(\mathbf{r}).
\end{aligned} \tag{8.12}
$$

We insert this into Heisenberg's equation of motion

$$
\frac{d}{dt} A_H = \frac{i}{\hbar} \left[H_H, A_H \right] + \left(\frac{\partial}{\partial t} A \right)_H , \tag{8.13}
$$

where A_H is the corresponding operator in the Heisenberg picture and $\left(\frac{\partial}{\partial t} A \right)_H = 0$ for the quasiparticle operators since all our calculations are performed with fixed basis states $[u_m(\mathbf{r}), v_m(\mathbf{r})]$. For the required single-particle expectation values this yields the following equations of motion:

$$
\begin{aligned}
i\hbar \frac{d}{dt} \langle \gamma^\dagger_{ma} \gamma_{na} \rangle = &-(E_m - E_n) \langle \gamma^\dagger_{ma} \gamma_{na} \rangle + \sum_l \Big(\\
&- \Big[(\Delta - \Delta_{\mathrm{GS}})_{u_l^* v_m} + (\Delta^* - \Delta^*_{\mathrm{GS}})_{v_l^* u_m} \Big] \langle \gamma^\dagger_{la} \gamma_{na} \rangle + \Big[(\Delta - \Delta_{\mathrm{GS}})_{u_n^* v_l} + (\Delta^* - \Delta^*_{\mathrm{GS}})_{v_n^* u_l} \Big] \langle \gamma^\dagger_{ma} \gamma_{la} \rangle \\
&+ \Big[(\Delta - \Delta_{\mathrm{GS}})_{u_n^* u_l^*} - (\Delta^* - \Delta^*_{\mathrm{GS}})_{v_n^* v_l^*} \Big] \langle \gamma^\dagger_{ma} \gamma^\dagger_{lb} \rangle - \big[- (\Delta - \Delta_{\mathrm{GS}})_{v_l v_m} + (\Delta^* - \Delta^*_{\mathrm{GS}})_{u_l u_m} \big] \langle \gamma_{lb} \gamma_{na} \rangle \Big)
\end{aligned} \tag{8.14}
$$

$$
\begin{aligned}
i\hbar \frac{d}{dt} \langle \gamma^\dagger_{mb} \gamma_{nb} \rangle = &-(E_m - E_n) \langle \gamma^\dagger_{mb} \gamma_{nb} \rangle + \sum_l \Big(\\
&- \Big[(\Delta - \Delta_{\mathrm{GS}})_{u_l^* v_m} + (\Delta^* - \Delta^*_{\mathrm{GS}})_{v_l^* u_m} \Big] \langle \gamma^\dagger_{lb} \gamma_{nb} \rangle + \Big[(\Delta - \Delta_{\mathrm{GS}})_{u_n^* v_l} + (\Delta^* - \Delta^*_{\mathrm{GS}})_{v_n^* u_l} \Big] \langle \gamma^\dagger_{mb} \gamma_{lb} \rangle \\
&+ \Big[(\Delta - \Delta_{\mathrm{GS}})_{u_n^* u_l^*} - (\Delta^* - \Delta^*_{\mathrm{GS}})_{v_n^* v_l^*} \Big] \langle \gamma^\dagger_{la} \gamma^\dagger_{mb} \rangle - \big[- (\Delta - \Delta_{\mathrm{GS}})_{v_l v_m} + (\Delta^* - \Delta^*_{\mathrm{GS}})_{u_l u_m} \big] \langle \gamma_{nb} \gamma_{la} \rangle \Big)
\end{aligned} \tag{8.15}
$$

$$
\begin{aligned}
i\hbar \frac{d}{dt} \langle \gamma_{mb} \gamma_{na} \rangle = -i\hbar \frac{d}{dt} \Big(\langle \gamma^\dagger_{na} \gamma^\dagger_{mb} \rangle \Big)^* = &(E_m + E_n) \langle \gamma_{mb} \gamma_{na} \rangle + \sum_l \Big(\\
&\Big[(\Delta - \Delta_{\mathrm{GS}})_{u_n^* v_l} + (\Delta^* - \Delta^*_{\mathrm{GS}})_{v_n^* u_l} \Big] \langle \gamma_{mb} \gamma_{la} \rangle + \Big[(\Delta - \Delta_{\mathrm{GS}})_{u_n^* u_l^*} - (\Delta^* - \Delta^*_{\mathrm{GS}})_{v_n^* v_l^*} \Big] \Big(\delta_{ml} - \langle \gamma^\dagger_{lb} \gamma_m \\
&- \Big[(\Delta - \Delta_{\mathrm{GS}})_{u_l^* u_m^*} - (\Delta^* - \Delta^*_{\mathrm{GS}})_{v_l^* v_m^*} \Big] \langle \gamma^\dagger_{la} \gamma_{na} \rangle + \Big[- (\Delta - \Delta_{\mathrm{GS}})_{v_l u_m^*} + (\Delta^* - \Delta^*_{\mathrm{GS}})_{u_l v_m^*} \Big] \langle \gamma_{lb} \gamma_{na} \rangle \Big).
\end{aligned} \tag{8.16}
$$

We solve these nonlinearly coupled equations of motion for the initial value problem defined by an instantaneous interaction quench. I.e., we start from the ground state corresponding

to a scattering length a_i and instantaneously switch to a different value[4] $a_i \to a_f$. Therefore, during the quench at the time $t = 0$ the system has no time to relax to the new ground state corresponding to a_f but it remains in the old ground state corresponding to a_i. I.e., all quasiparticle expectation values of the form $\langle \gamma_M^\dagger \gamma_{M'} \rangle$ and $\langle \gamma_M \gamma_{M'} \rangle$ with $M \in \{ma, mb\}$ and $M' \in \{m'a, m'b\}$ which correspond to the old ground state vanish for $t = 0$. With this in mind, we invert the Bogoliubov transformation for the operators γ_M in the old basis before the quench and insert the resulting expressions for Ψ_σ and $\Psi_\sigma^\dagger$ into the quasiparticle operators in the new basis after the quench [Eqs. (8.4) and (8.5)]. This yields the initial values for the dynamics

$$\langle \gamma_{ma}^\dagger \gamma_{na} \rangle|_{t=0} = \sum_k \int \mathrm{d}^3 r \Big[v_m(\mathbf{r}) \tilde{u}_k(\mathbf{r}) - u_m(\mathbf{r}) \tilde{v}_k(\mathbf{r}) \Big] \cdot \int \mathrm{d}^3 r' \Big[v_n^*(\mathbf{r}') \tilde{u}_k^*(\mathbf{r}') - u_n^*(\mathbf{r}') \tilde{v}_k^*(\mathbf{r}') \Big] \tag{8.17}$$

$$\langle \gamma_{ma}^\dagger \gamma_{nb}^\dagger \rangle|_{t=0} = \sum_k \int \mathrm{d}^3 r \Big[v_m(\mathbf{r}) \tilde{u}_k(\mathbf{r}) - u_m(\mathbf{r}) \tilde{v}_k(\mathbf{r}) \Big] \cdot \int \mathrm{d}^3 r' \Big[v_n(\mathbf{r}') \tilde{v}_k^*(\mathbf{r}') + u_n(\mathbf{r}') \tilde{u}_k^*(\mathbf{r}') \Big] \tag{8.18}$$

$$\langle \gamma_{mb} \gamma_{na} \rangle|_{t=0} = \Big(\langle \gamma_{na}^\dagger \gamma_{mb}^\dagger \rangle|_{t=0} \Big)^* \tag{8.19}$$

$$\langle \gamma_{mb}^\dagger \gamma_{nb} \rangle|_{t=0} = -\sum_k \int \mathrm{d}^3 r \Big[v_m^*(\mathbf{r}) \tilde{v}_k(\mathbf{r}) + u_m^*(\mathbf{r}) \tilde{u}_k(\mathbf{r}) \Big] \cdot \int \mathrm{d}^3 r' \Big[v_n(\mathbf{r}') \tilde{v}_k^*(\mathbf{r}') + u_n(\mathbf{r}') \tilde{u}_k^*(\mathbf{r}') \Big] + \delta_{mn}, \tag{8.20}$$

where $\tilde{u}_m$ and $\tilde{v}_m$ refer to the single-particle states before the quench and u_m and v_m to those after the quench.

With Eqs. (8.17)-(8.20) we can numerically integrate the equations of motion and thus calculate the gap dynamics for a gas of ^{6}Li in a 3D harmonic trap via Eq. (9.14). In section 8.4.1 we will present the corresponding results for the phase dynamics of the gap. However, before that we introduce Anderson's approximation which we will use to perform elaborate parameter scans and to calculate the gap dynamics for systems with rather large particle number that are numerically too complex to address within the full BdG approach. In doing so, we will restrict our explanations to the main aspects of the approximation. A detailed description of the corresponding formalism with all expressions derived from the above can be found in our previous work [Hannibal *et al.*(2015)].

8.3.3 Anderson's Approximation

In Anderson approximation the expansion of the quasiparticle wave function in Eqs. (8.6) and (8.7) is truncated such that $u_m(\mathbf{r}) = u_m \phi_m(\mathbf{r})$ and $v_m(\mathbf{r}) = v_m \phi_m(\mathbf{r})$. This strongly simplifies the formalism presented above. For the ground-state properties the diagonalization of Eq. (8.8) directly yields

$$E_m = \sqrt{(\varepsilon_m - \mu)^2 + (\Delta_{mm}^{\mathrm{GS}})^2} \tag{8.21}$$

[4] This assumption of an instantaneous quench is valid, since the experimentally achieved quench times ∼ns are way below the timescales of the gap dynamics ∼ms.

and

$$u_m = \sqrt{\frac{1}{2}\left(1 + \frac{\varepsilon_m - \mu}{E_m}\right)} \qquad v_m = \sqrt{\frac{1}{2}\left(1 - \frac{\varepsilon_m - \mu}{E_m}\right)}. \tag{8.22}$$

which –in combination with Eq. (8.10)– leads to a BCS-like selfconsistency equation, that we solve numerically. In doing so, we use much larger energy windows in the sum over the states as compared to the full BdG approach since the numerical effort is strongly reduced in the case of the Anderson approximation. Thereby, we employ the regularization scheme introduced in [Hannibal *et al.*(2015)]. Only when directly comparing the full BdG equations with the Anderson approximation (Sec. 8.4.1) we use the same cutoffs in both calculations to improve the comparability of the respective calculations.

For the dynamical situation we furthermore assume that $(\Delta - \Delta_{\mathrm{GS}})_{x_m y_n} = (\Delta - \Delta_{\mathrm{GS}})_{x_m y_n} \delta_{mn}$ with $x_m, y_m \in \{u_m, v_m\}$, i.e., that the main implications of the Anderson approximation $\Delta^{\mathrm{GS}}_{mn} = \Delta^{\mathrm{GS}}_{mn}\delta_{mn}$ holds for the dynamical situation as well. That leads to a great simplification of the equations of motion.

However, strictly speaking Anderson's approximation is only valid if $\Delta^{\mathrm{GS}}_{mn} \ll \delta\varepsilon$ with $\delta\varepsilon$ the level spacing of the harmonic eigenenergies. In general, this only holds for weak coupling, i.e., deep in the BCS regime, and/or for strong confinements and thus large level spacing. Nevertheless, our numerical data show that the approximation reproduces all the main features investigated in this work even for moderate confinements in the BCS-BEC crossover regime (cf. section 8.4.1).

8.4 Results

In the following, we investigate the phase dynamics of the spatially averaged BCS gap[5]

$$\bar{\Delta}(t) = \frac{1}{V}\int \mathrm{d}^3 r \Delta(\mathbf{r}, t) \tag{8.23}$$

for an ultracold gas of ^{6}Li in a cigar-shaped harmonic trap. We use $V = l_x l_y l_z$ with l_α being the oscillator length in direction α as a normalization volume. We excite the system by interaction quenches $a_i \to a_f$.

In section 8.4.1 we will identify the emergence of a Goldstone mode in the phase dynamics of the BCS gap with one dominant low-frequency contribution. Furthermore, we will show that the results obtained within the Anderson approximation are in good agreement with the full BdG solution. In section 8.4.2 we will analyze this Goldstone mode over a wide range of parameters and we will show that its excitation spectrum is gapless and that its main frequency is not determined by the trap parameters but by the details of the excitation.

In section 8.4.3 we will investigate the influence of the confinement parameters on the phase dynamics and by that the effect of the superfluid resonances found in [Shanenko *et al.*(2012)]. Furthermore, in section 8.4.4 we will evaluate the impact of the interaction quench-induced Goldstone mode on the single-particle excitations of the cloud which could provide an experimental access to the gapless phase mode.

8.4.1 Phase dynamics of the gap

Figure 8.2 shows the dynamics of the phase $\varphi = \arg(\bar{\Delta})$ of the spatially averaged BCS gap for a system with $f_\perp = 1\,\mathrm{kHz}$ and $f_\parallel = 96\,\mathrm{Hz}$ excited by quenches with the strength $\delta\,[1/(k_F a)] = 1/(k_F a_f) - 1/(k_F a_i) = -0.1$ at different positions in the BCS-BEC crossover. The particle number is set to $N_P = 120$ and the expansion of the single-particle wave functions

[5] In our case the phase of the gap φ is nearly homogeneous (see below), i.e., $\bar{\varphi} \approx \varphi(\mathbf{r})$.

in Eqs. (8.6) and (8.7) is restricted to atomic states from a window of width $\Delta\epsilon := 0.92E_F$ around the chemical potential (i.e., $\mu - 0.46E_F \leq \varepsilon \leq \mu + 0.46E_F$). This is the limitation of our current numerical setup for the full BdG approach.

The solid lines in Fig. 8.2 show the data obtained by the full equations of motion (8.14) - (8.16). First of all, one clearly observes that –for all quenches– the phase dynamics of the gap is strongly dominated by a linear decrease in time. Therefore, after the quench the system performes a constant phase "motion" of the gap which nicely corresponds to the simplified picture of a Mexican-hat potential introduced in Fig. 8.1: The potential is flat inside the rim which implies a constant phase velocity, i.e., a steady oscillation inside the rim where the frequency of the latter –i.e., the frequency of the Goldstone mode– is defined by the time-averaged slope $f_G := \frac{1}{2\pi}\frac{\Delta\varphi}{\Delta t}$ where Δt is large compared to the intrinsic time scales of the system.[6] The corresponding values are given by $f_G = 1.6\,\mathrm{Hz}$ for the weakest coupling strength and $f_G = 21.9\,\mathrm{Hz}$ for $1/(k_F a_f) = -0.9$ and $f_G = 118.7\,\mathrm{Hz}$ for $1/(k_F a_f) = -0.5$ (for illustrative purposes the curves for the two weaker coupling strengths are scaled by a factor 3 and 10, respectively). Thus, the interaction quench-induced "phase velocity" strongly increases when approaching the unitary point $1/(k_F a) = 0$.

Furthermore, a closer look at Fig. 8.2 reveals that a higher-frequency oscillation exists on top of the linear contribution. This contribution is strongest for the system with $1/(k_F a_f) = -1.4$ and much weaker –and thus not directly visible in Fig. 8.2– for the stronger-coupling cases. A more detailed analysis shows that the corresponding frequencies again increase when approaching the unitary point, i.e., this dynamics is fast for large and slow for small coupling strengths. Nevertheless, the corresponding range of frequencies coincides with that from the spectrum of the Higgs mode. This indicates that the Higgs and the Goldstone mode are weakly coupled, where we observe that the influence of the Higgs mode increases when approaching the BCS limit $1/(k_F a) \ll -1$ and when increasing the modulus of quench strength $|\delta\,[1/(k_F a)]\,|$. However, the Higgs mode was extensively studied in [Hannibal *et al.*(2015)]. Therefore, in this work we will not go into details about these contributions.

[6] We want to remark that the appearance of a Goldstone mode with a fixed frequency is similar to the case of the AC Josephson effect. There, a difference in the chemical potentials μ_i on the two sides of a Josephson junction leads to the emergence of a Goldstone mode with the frequency given by $f_G \sim (\mu_2 - \mu_1)$ [Pekker and Varma(2015)]. In contrast, in our case the Goldstone mode is driven by the quench which drives the system instantaneously from an equilibrium into a non-equilibrium state.

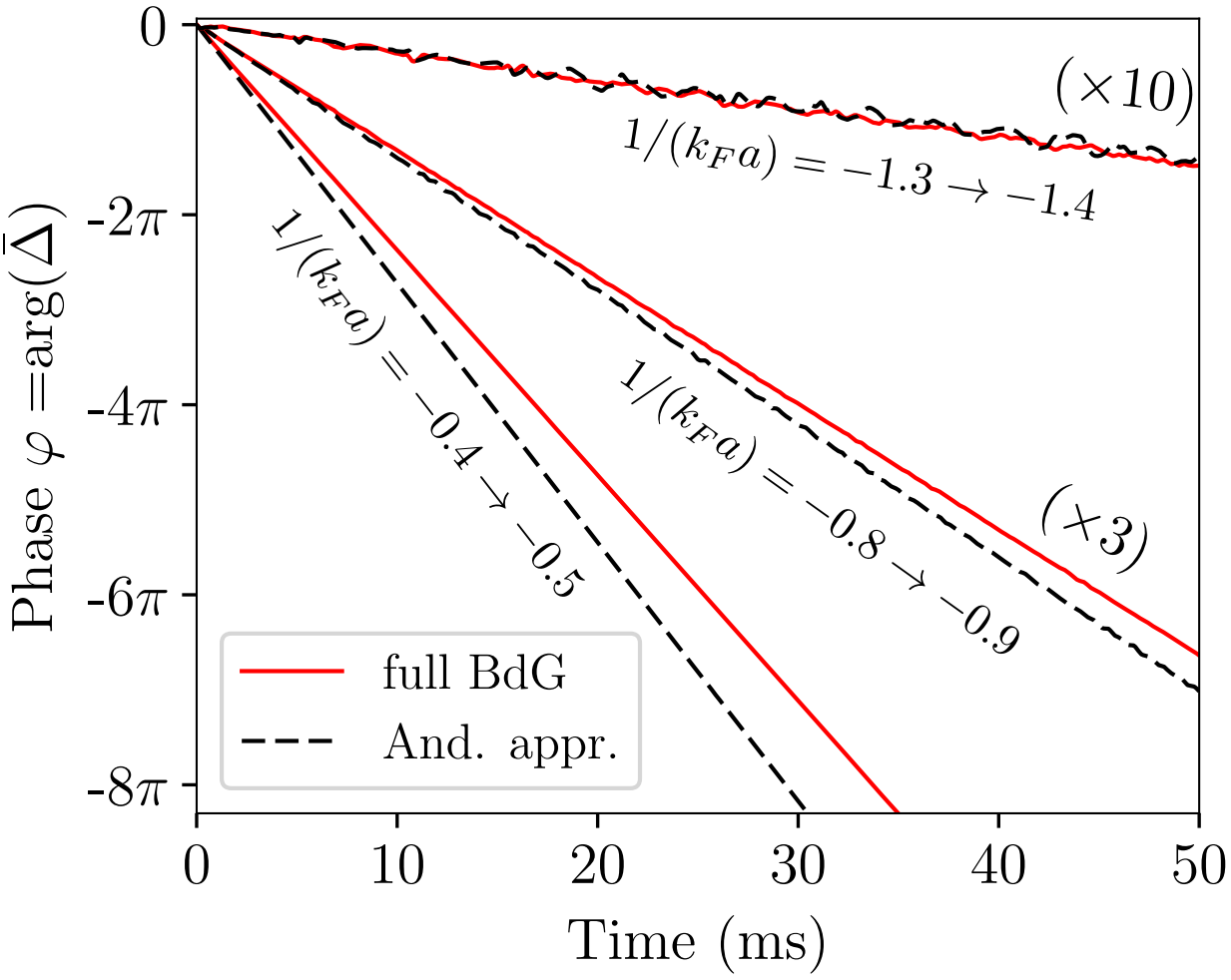

Figure 8.2: (color online) Phase dynamics for the full BdG solution (solid lines) and the Anderson approximate solution (dashed lines) for $\delta\,[1/(k_F a)] = -0.1$ and different final coupling strengths: $1/(k_F a_f) = -0.5$, $1/(k_F a_f) = -0.9$ (scaled by a factor of 3) and $1/(k_F a_f) = -1.4$ (scaled by a factor of 10); parameters: $f_\parallel = 96\,\mathrm{Hz}$, $f_\perp = 1\,\mathrm{kHz}$, $N_P = 120$.

The dashed lines in Fig. 8.2 show the Anderson approximate solution corresponding to section 8.3.3 (note that in order to improve the comparability here we have used an ungregularized Anderson solution with the same cutoff as in the calculations without Anderson approximation). One can see that the approximate solution gives an overall good qualitative agreement with the full dynamics: It shows the same linear decrease in time with a –in the stronger coupling cases not directly visible– higher-frequency contribution on top. Again, the slow linear decrease corresponds to the Goldstone mode while the higher-frequency component results from the coupling to the Higgs mode[7]. However, one can observe as well that the quantitative deviations between the full and the approximate solution increase with increasing coupling strength: While –considering that the corresponding curves in Fig. 8.2 are scaled by a factor of 10– the frequency of the Goldstone mode, i.e., the slope of the linear contribution, matches very well for the case of $1/(k_F a_f) = -1.4$ the deviation of the two solutions becomes rather significant when increasing the coupling strength.

[7]The agreement of both solutions with respect to the Higgs mode may not look very convincing. However, already rather small deviations in the spectral composition of the Higgs mode result in large deviations in the time domain at larger times. I.e., the qualitative agreement of both solutions is in indeed good.

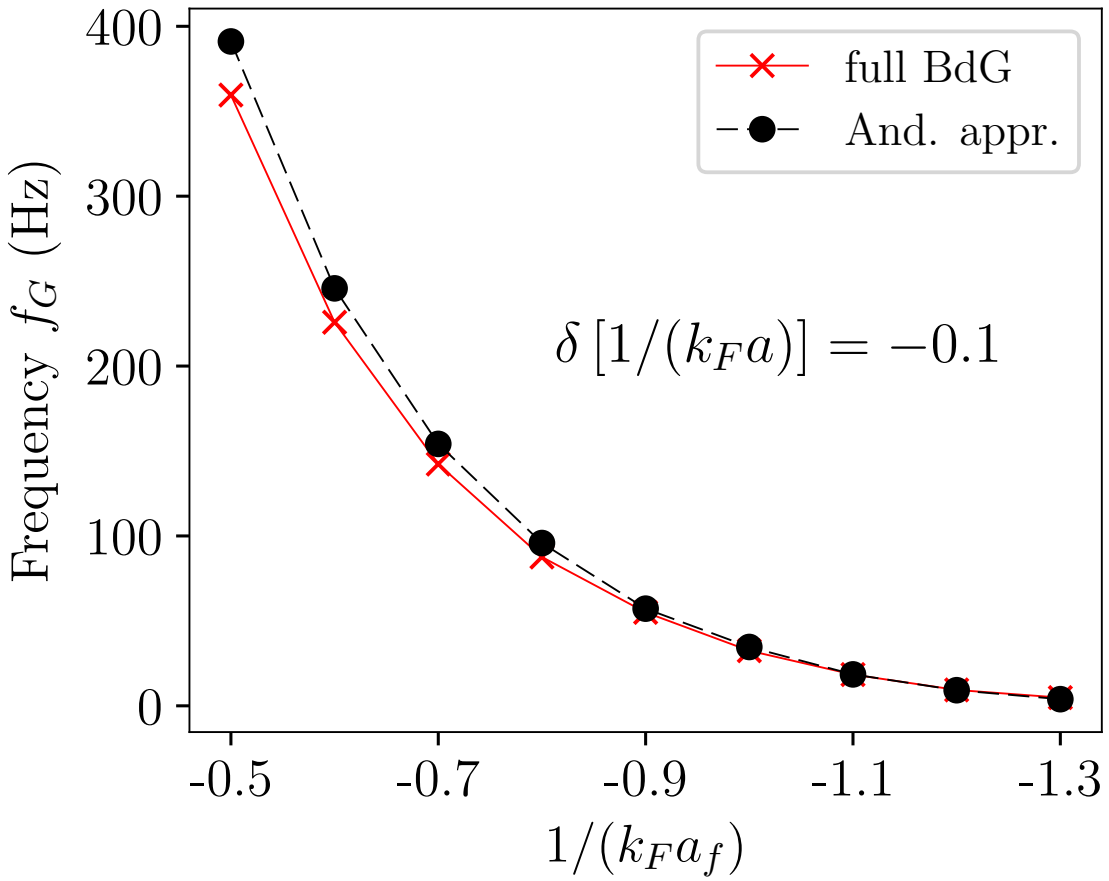

Figure 8.3: (color online) Frequency of the Goldstone mode resulting from the full BdG solution (solid line) and from Anderson's approximate solution (dashed line) for the same system as in Fig. 8.2 but varying $1/(k_F a_f)$ (to reduce the numerical effort we set $\Delta\epsilon = 0.58 E_F$).

This is illustrated in Fig. 8.3. There, the frequencies of the Goldstone mode resulting from the full and from the approximate solution are shown for a fixed quench strength $\delta\,[1/(k_F a)] = -0.1$ and varying $1/(k_F a_f)$. One can clearly observe that the approximate solution reproduces well the qualitative trend, i.e., an overall increase of the frequency of the Goldstone mode when approaching the unitary point. Indeed, when entering the BCS regime even the quantitative values match very well. However, one can see as well, that the deviation between both solutions increases with increasing coupling strength and becomes rather large in the crossover regime. This indicates that Anderson's approximation tends to break down –as expected– when approaching the unitary point.

Nevertheless, we want to emphasize that all features in the phase dynamics investigated in this work are fully reproduced by the Anderson approximation. Solely the shift in frequency between the full and the approximate solution increases with increasing coupling strength. Therefore, all following calculations of this work are performed in Anderson approximation which allows for a drastical reduction of computational effort and thus for a detailed investigation of parameter dependencies and of larger systems at all. In doing so, from now on all sums will be restricted to states from a window of size $2E_F$ around the Fermi level instead of $0.92E_F$ as before to ensure a better quantitative convergence of the obtained frequencies (cf. [Hannibal *et al.*(2015)]).

Continuing in Anderson approximation we will now investigate the phase dynamics in closer detail, i.e., we will analyze the influence of the external parameters on the frequency f_G of the Goldstone mode and we will point out by which quantities it is determined. To do so, we will

first investigate the influence of the coupling strength and of the details of the quench. In section 8.4.3 we will focus on the effect of the confinement.

8.4.2 Influence of the quench

Figure 8.2 already suggests that the frequency of the Goldstone mode f_G depends on the details of the quench instead of being fixed by the external parameters of the cloud. The phase dynamics changes from a very slow decrease for the system in the BCS regime with $1/(k_F a_f) = -1.4$ to a rather fast decrease in the crossover regime with $1/(k_F a_f) = -0.5$. However, in Fig. 8.2 the quench strength by means of $\delta\,[1/(k_F a)]$ was kept fixed. Only the position in the BCS-BEC crossover was varied. Accordingly, we will in the following investigate the influence of the quench strength on the phase dynamics for one particular final coupling strength $1/(k_F a_f)$ in Fig. 8.4 and for a wider range of $1/(k_F a_f)$ in Fig. 8.5. In doing so, we will show, that the excitation spectrum of the interaction quench-induced Goldstone mode is gapless, i.e., it is a Goldstone mode in the original sense of the Goldstone theorem. Furthermore, we will show that its frequency can be adjusted by changing the details of the quench and that it is determined by the initial values of the dynamics and by the gap of the system after the quench.

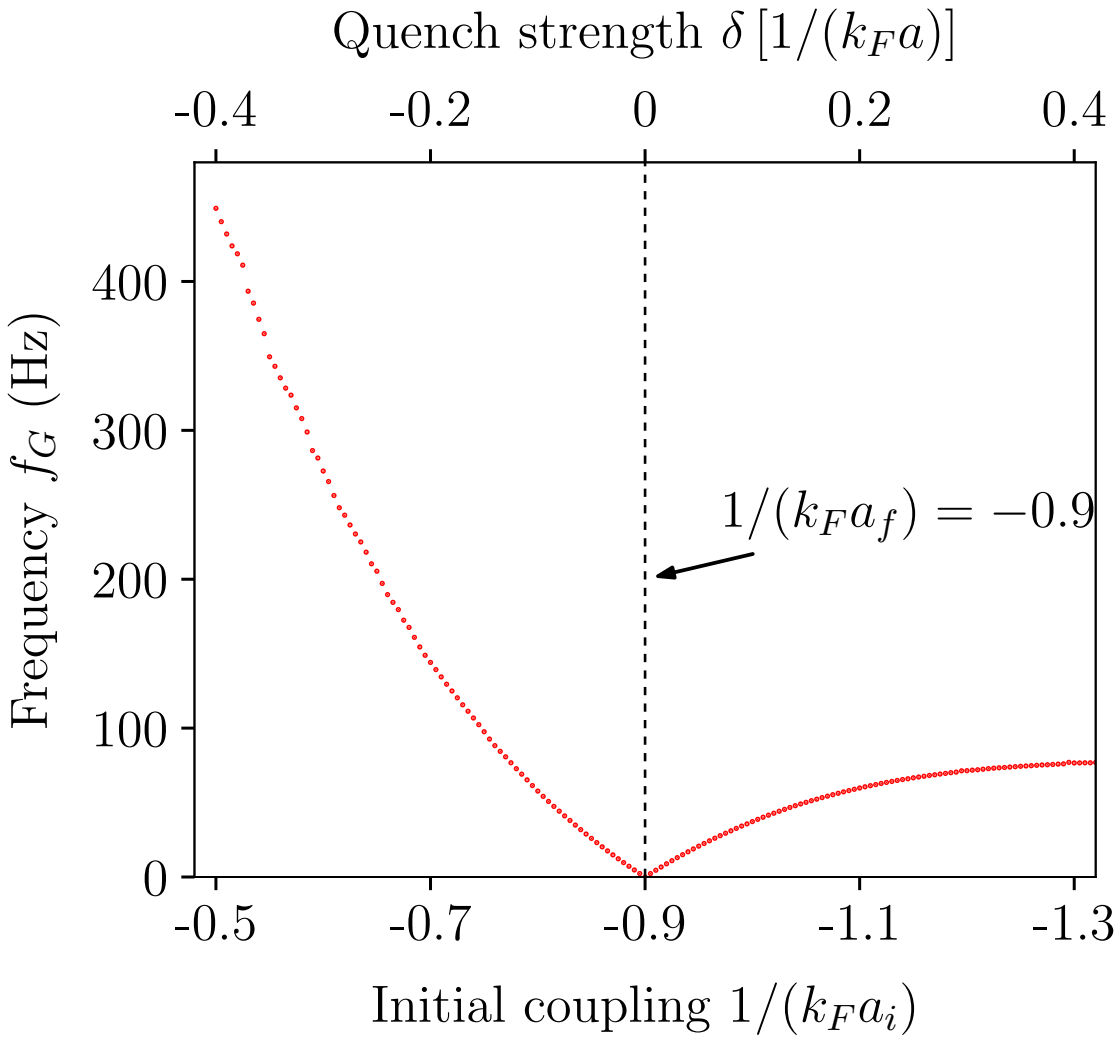

Figure 8.4: (color online) Frequency of the Goldstone mode f_G for quenches with varying strength to $1/(k_F a_f) = -0.9$; parameters: $f_\parallel = 96\,\mathrm{Hz}$, $f_\perp = 1\,\mathrm{kHz}$, $N = 1000$.

Figure 8.4 shows the frequency of the Goldstone mode for a system with $1/(k_F a_f) = -0.9$ in the same trap as in Fig. 8.2 but –since we now apply Anderson's approximation– for a larger particle number[8] of $N_P = 1000$. The initial coupling strength $1/(k_F a_i)$ is varied, i.e., the dependence of f_G on the quench strength is shown.

First of all, Fig. 8.4 demonstrates that the phase dynamics strongly depends on the quench strength: When approaching $1/(k_F a_i) = 1/(k_F a_f) = -0.9$, i.e., the point of quench strength $\delta\,[1/(k_F a)] = 0$, from either side [from larger or smaller values of $1/(k_F a_i)$] the frequency of the Goldstone mode continuously decreases to zero. Thus, the frequency of the Goldstone mode decreases with decreasing (modulus of the) quench strength and continuously vanishes for $\delta\,[1/(k_F a)] \to 0$. This implies that the excitation spectrum of the interaction quench-induced phase mode is indeed gapless as stated above.

Furthermore, we observe that the dependence of f_G on the quench strength in Fig. 8.4 is asymmetric: Negative quenches with $\delta\,[1/(k_F a)] < 0$, i.e., those on the left hand side of Fig. 8.4, lead to a stronger increase in f_G and thus to larger frequencies than positive quenches. This asymmetry is linked to the fact that the same excitation strength in terms of $1/(k_F a)$, i.e., the same $|\delta\,[1/(k_F a)]\,|$, results in different actual changes in the scattering length $|\delta a| = |a_f - a_i|$ depending on the position of the initial system in the crossover. Hence, negative quenches lead to much larger changes in the scattering length $|\delta a|$ –and therefore in the gap– than positive quenches. As we will show later on, this results in larger f_G. However, before we do so, we will demonstrate that the features found above hold for a wide range of quenches in the BCS-BEC crossover. Indeed, our numerical data indicate that the above found nature of the phase dynamics holds for all moderate quenches on the BCS side of the BCS-BEC crossover, i.e., for all quenches that can be associated with the phase II of the quantum quench phase diagram introduced in [Yuzbashyan *et al.*(2015)]. For quenches exceeding this range, the phase dynamics tends to become irregular. In particular, strong negative quenches which lead to a dynamical vanishing of the gap in the Higgs mode (phase I) exhibit a persistent but very irregular phase dynamics which makes the definition of a frequency of the Goldstone mode arbitrary. However, in this work we restrict ourselves to the investigation of the regular phase dynamics in the gapless Golstone mode, i.e., to quenches in the phase II.

To this end, Fig. 8.5 shows the dependence of f_G on the quench strength for varying $1/(k_F a_f)$, i.e., each horizontal line in Fig. 8.5 corresponds to a plot like in Fig. 8.4 but for a different coupling strength.

[8] With our current numerical setup we can calculate the dynamics of single systems for up to $N_P \sim 10^4$ particles. However, there are no qualitative changes in the gap dynamics when increasing the particle number, i.e., here we restrict ourselves to rather small N_P to reduce the numerical effort.

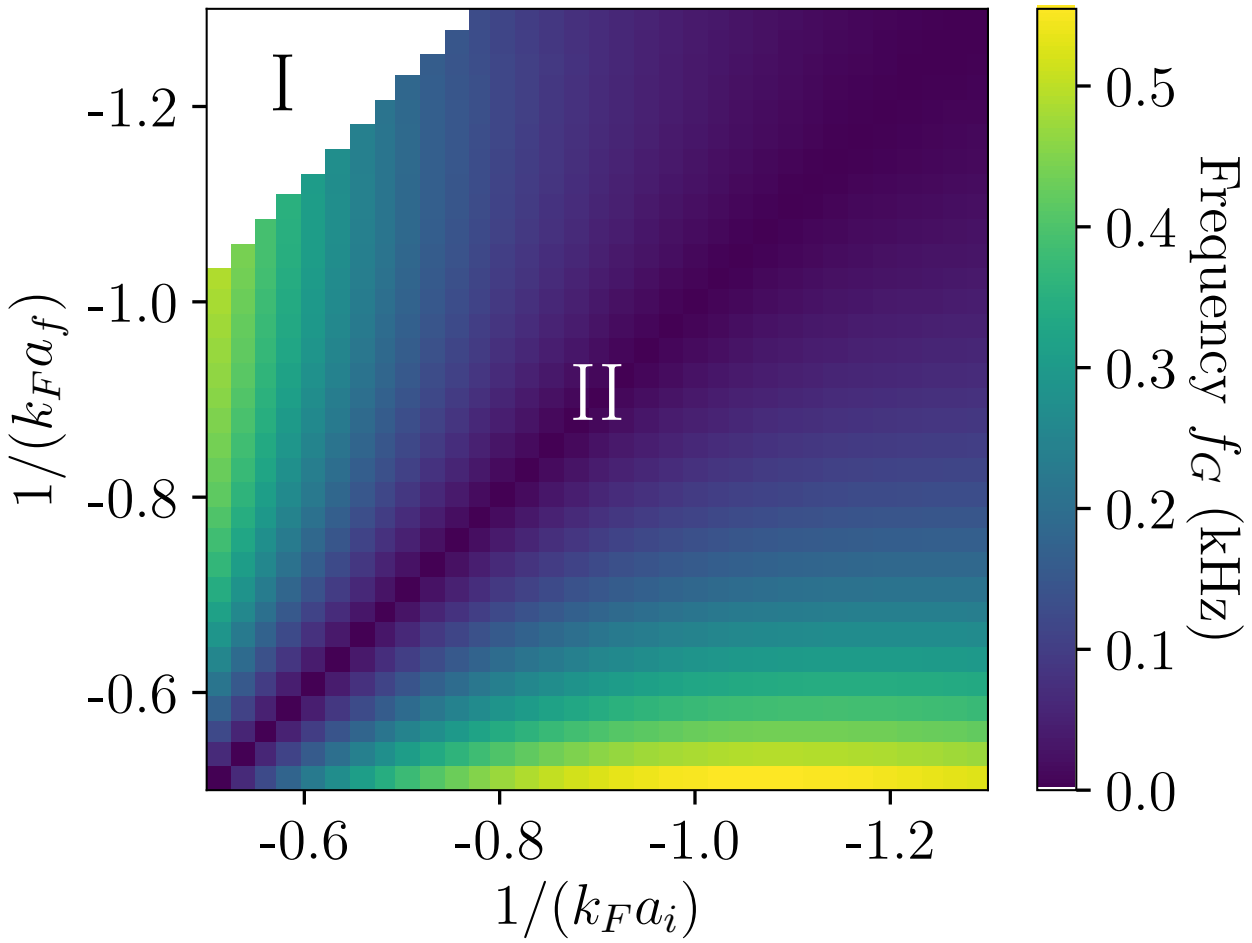

Figure 8.5: (color online) Frequency of the Goldstone mode f_G for different excitations $1/(k_F a_i) \to 1/(k_F a_f)$ corresponding to phase II of the quantum quench phase diagram (see main text); quenches corresponding to phase I are not shown; parameters: $f_\parallel = 96\,\mathrm{Hz}$, $f_\perp = 1\,\mathrm{kHz}$, $N = 1000$.

Indeed, one observes on the basis of Fig. 8.5 that the nature of the Goldstone mode described above holds for all phase II quenches investigated here (we omit the quenches in the upper left corner corresponding to phase I). For each horizontal line in Fig. 8.5 we see a decrease of f_G with decreasing modulus of the quench strength $|\delta\,[1/(k_F a)]\,|$ as found above with a continously vanishing Goldstone mode when approaching $1/(k_F a_i) = 1/(k_F a_f)$. However, furthermore one can see, that the frequency of the Goldstone mode also depends on the vertical position of the quench in Fig. 8.5: It is largest for quenches at the bottom, i.e., for systems with large coupling strength. In fact, one can observe that quenches with the same $|\delta\,[1/(k_F a)]\,|$ but opposite directions, e.g., those correspoding to the points $[1/(k_F a_i), 1/(k_F a_f)] = (-1.0, -0.5)$ and $[1/(k_F a_i), 1/(k_F a_f)] = (-0.5, -1.0)$ lead to significantly different f_G. This indicates that f_G depends not only on the quench strength but also on the coupling strength of the system after the quench, i.e., a stronger coupling results in a larger f_G. In the following, we will explain both these features –the dependence on the quench strength and the dependence on the final coupling strength– by taking into account that the only parameters of the dynamics affected by the quench are the initial values of the excitation and the gap after the quench. We will isolate the effects of both quantities on the basis of Fig. 8.5 and Eqs. (8.17)-(8.20).

To do so, we at first want to state that the frequency of the Goldstone mode depends linearly on the initial values of the dynamics which in Anderson approximation read (cf. [Hannibal

et al.(2015)] and Eqs. (8.17)-(8.20))

$$\begin{aligned}\left\langle \gamma^\dagger_{ma}\gamma_{ma}\right\rangle\big|_{t=0} &= (v_m\tilde{u}_m - u_m\tilde{v}_m)^2 =: x^{(0)}_m \\ \left\langle \gamma^\dagger_{ma}\gamma^\dagger_{mb}\right\rangle\big|_{t=0} &= (v_m\tilde{u}_m - u_m\tilde{v}_m)\,(v_m\tilde{v}_m + u_m\tilde{u}_m) \\ &=: y^{(0)}_m, \end{aligned} \tag{8.24}$$

with $\tilde{u}_m$ and $\tilde{v}_m$ (u_m and v_m) being the Anderson amplitudes before (after) the quench [see Eq. (8.22)]. Indeed, our numerical data show that by artificially multiplying these initial values by a factor k the frequency f_G increases by the same factor[9], i.e.,

$$f_G\left(k\cdot\{x^{(0)}_m, y^{(0)}_m\}\right) = k f_G\left(\{x^{(0)}_m, y^{(0)}_m\}\right).$$

This means that –whatever the actual system parameters (a_f, N_P, $f_\parallel$, $f_\perp$) are– the frequency of the Goldstone mode can be tuned by adjusting the initial values of the dynamics. As Eqs. (8.22) and (8.24) imply, the latter depend on the gaps of the system before and after the quench which are defined by the quench.

A detailed evaluation of Eqs. (8.24) shows that the initial values are large when the difference between the gaps before and after the quench and thus between the amplitudes $(\tilde{u}_m, \tilde{v}_m)$ and (u_m, v_m) is large. This is the case for strong quenches, i.e., strong quenches result in large initial values which well coincides with the above findings for f_G. However, Eqs. (8.24) also show that the amplitude of the initial excitation is independent from the quench direction. When changing the quench direction, i.e., when interchanging $(\tilde{u}_m, \tilde{v}_m) \Leftrightarrow (u_m, v_m)$ in Eqs. (8.24), only the sign of the anomalous initial values $\left\langle \gamma^\dagger_{ma}\gamma^\dagger_{mb}\right\rangle\big|_{t=0}$ changes. Therefore, the initial values for quenches with the same $|\delta\,[1/(k_F a)]\,|$ but opposite directions have the same strength but –as observed above– the frequency is larger for the respective positive quench to the stronger coupling $1/(k_F a_f)$. This indicates that the frequency of the Goldstone mode also depends on the actual coupling strength of the system after the quench.

We can conclude the results of this paragraph: The excitation spectrum of the Goldstone mode of the BCS gap of a 3D confined ultracold Fermi gas excited by an interaction quench is gapless and the frequency of the Goldstone mode can be tuned in a wide range by adjusting the strength of the quench. Again, this coincides with the simplified picture of Fig. 8.1: However small the quench-induced initial "momentum" of the phase dynamics might be, it results in a constant "phase motion" inside the rim. This is –in simple words– the consequence of the Goldstone theorem, which therefore can well be observed in the dynamics after an interaction quench.

However, the fact that in our case the Goldstone mode is gapless and that its frequency can be adjusted by the strength of the excitation stands in contrast to the experimental and theoretical findings of Refs. [Kinast *et al.*(2004a), Kinast *et al.*(2004b), Bartenstein *et al.*(2004), Altmeyer *et al.*(2007a), Altmeyer *et al.*(2007b), Riedl *et al.*(2008), Baranov and Petrov(2000), Bruun and Mottelson(2001), Bruun(2002), Hu *et al.*(2004), Heiselberg(2004), Stringari(2004), Grasso *et al.*(2005), Korolyuk *et al.*(2011)]. There, the frequency of the phase dynamics was found to be fixed by the frequencies of the trapping potential. Nevertheless, this discrepancy can be explained by the circumstance that in the previous works the dynamics was induced by spatially inhomogeneous perturbations of the cloud, e.g., by confinement quenches or optical excitations. Such a spatial perturbation creates a motion of the superfluid in the trap with a time-dependent verlocity v_s. This directly induces a dynamics of the phase of the gap via [Giorgini *et al.*(2008)]

$$\mathbf{v_s} = \frac{\hbar}{2m}\nabla\arg\big[\Delta(\mathbf{r},t)\big]. \tag{8.25}$$

[9] For the situation of strong interactions and strong quenches even an analytical expression can be found: $\omega_G = 2\pi f_G \approx \mathrm{Im}(\frac{d}{dt}\bar{\Delta})|_{t=0}/\bar{\Delta}_{\mathrm{GS}}$.

On the one hand, this means that –whenever a superfluid velocity v_s is excited– the real-space dynamics is directly linked to a dynamics in the Goldstone mode. In this sense, the latter can be observed through the motion of the cloud. On the other hand, the trapping potential governs the real-space dynamics of the cloud. Therefore, a direct coupling of the Goldstone mode to the real-space dynamics implies that the trap imprints its frequencies on the Goldstone mode. For inhomogeneous excitations f_G is thus pushed to the trap frequencies as found in the previous works.[10]

In our case the excitation is spatially homogeneous and does not –as our numerical data confirm– produce any significant phase gradients. Therefore, no real-space dynamics of the cloud is induced by the interaction quench which implies that the phase dynamics does not couple to the trap. Accordingly, the excitation spectrum of this *homogeneous* Goldstone mode remains gapless. In this sense the interaction quench-induced Goldstone mode remains pure.

8.4.3 Impact of the superfluid resonances

In this section we want to study the influence of the confinement on the frequency of the gapless Goldstone mode and by that the impact of the size-dependend superfluid resonances theoretically predicted in [Shanenko *et al.*(2012)]. To do so, we will investigate the dependence of the phase dynamics on the trapping frequency in x-y direction $f_\perp$ for a system with fixed $f_\parallel = 96\,\mathrm{Hz}$, $N_P = 1000$ atoms in the trap and a quench given by $1/(k_F a) = -0.8 \to -0.9$. The complementary situation, i.e., a fixed $f_\perp$ with varying $f_\parallel$ produces the same effects. Therefore, the influence of $f_\parallel$ will not be investigated separately.

Figure 8.6 shows the frequency of the gapless Goldstone mode for the above system over a wide range of $f_\perp$. One can see, that –on top of a global increasing trend[11]– f_G exhibits a series of local maxima for different values of $f_\perp$. The distance of the maxima increases with increasing $f_\perp$ while at the same time the maxima become more pronounced. I.e., the maxima in f_G occur less frequent but more pronounced when approaching higher values of $f_\perp$.

Furthermore, the dashed lines in Fig. 8.6 indicate the positions of integer system parameter $S = \mu/\hbar\omega_\perp$ with $\omega_\perp = 2\pi f_\perp$. These positions indicate trap parameters where the minimum of an atomic subband crosses the chemical potential (for a detailed description of the band structure see section 8.4.4). To be precise: The distance between two atomic subbands is $\hbar\omega_\perp$ and the minimum of the lowest subband is at $\varepsilon = \hbar\omega_\perp$. Therefore, the integer part of S is the number of subbands that have a minimum below/at the chemical potential, i.e., the number of subbands crossing the chemical potential. One can see that every resonance closely follows such a point of integer system parameter S.

An explanation for this behavior can be given on the basis of the atypical BCS-BEC crossover [Shanenko *et al.*(2012)]: On the one hand, the atomic states closest to the chemical potential contribute strongest to the pairing. On the other hand, the states with the lowest quantum numbers m_z which are located at the subband minima exhibit the strongest interaction matrix elements [Hannibal *et al.*(2015)]. Therefore, each time an atomic subband crosses the chemical potential ($S = 1, 2, 3, ..$) the pairing is enhanced and the system is shifted towards the unitary point. Following section 8.3.2, this results in a larger frequency of the gapless Goldstone mode.

However, the decrease of the impact of the resonances for increasing system parameter reflects the circumstance that for large S several subbands contribute to the pairing while only a small fraction of the corresponding atomic states exhibits an enhanced coupling due to the resonance. Thus, for increasing S the influence of the resonant states on the overall coupling

[10] Actually, both manifestations of the Goldstone mode –the gapped inhomogeneous and the gapless one– may exist at the same time depending on the nature of the excitation.

[11] This global increase is due to the circumstance that the density of the condensate and thus the gap increases when $f_\perp$ is increased with fixed $f_\parallel$ and N_P.

decreases.

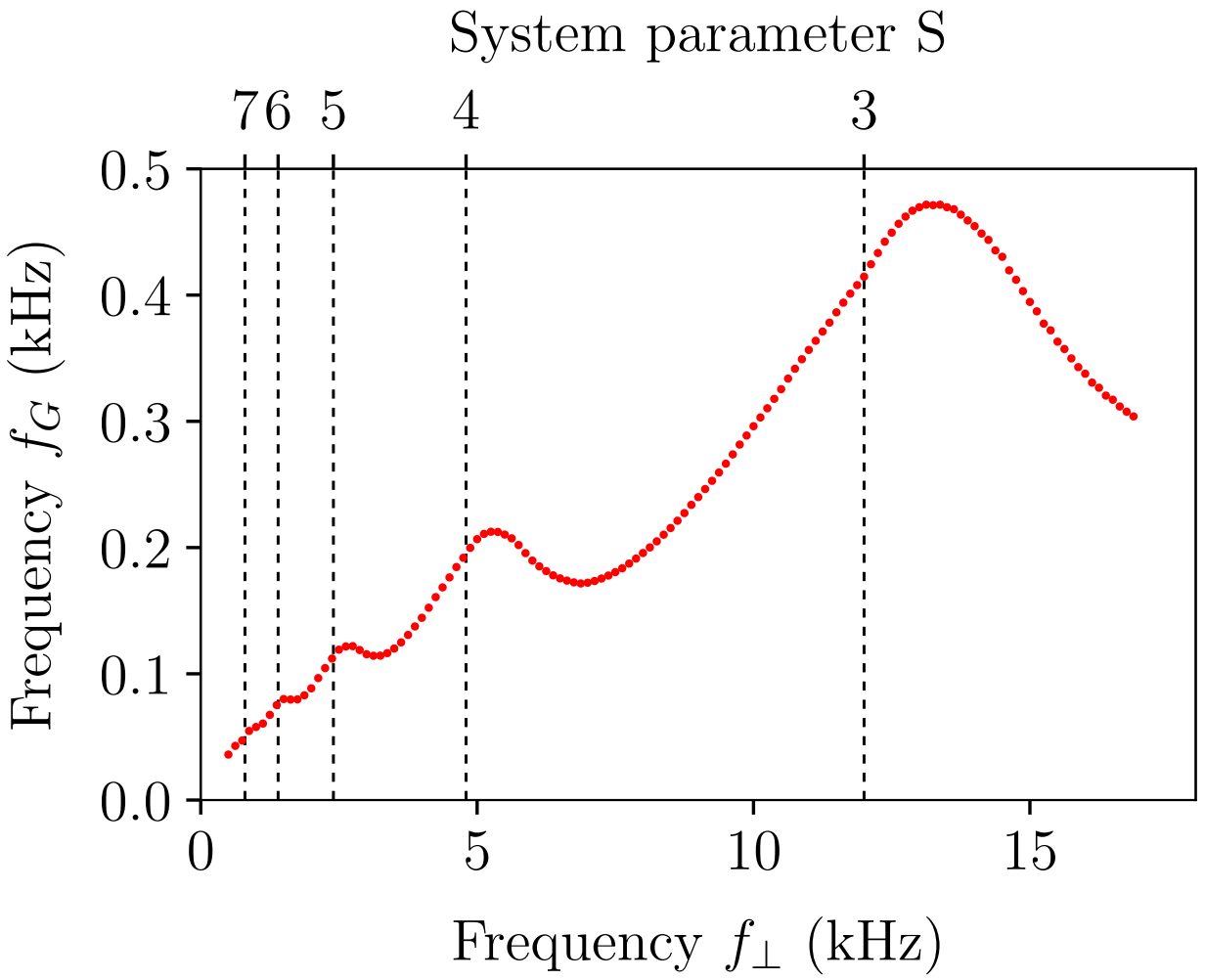

Figure 8.6: (color online) Frequency of the gapless Goldstone mode f_G for fixed $f_\parallel = 96\,\mathrm{Hz}$, $N_P = 1000$ and $1/(k_F a) = -0.8 \to -0.9$; upper label: system paramter $S = \mu/\hbar\omega_\perp$.

8.4.4 Goldstone mode in the single-particle excitations

In this section we study the impact of the phase dynamics of the BCS gap on an experimentally more relevant physical quantity, the single-particle excitations of the condensate. An experimental investigation of the single-particle excitations has already been reported in [Stewart *et al.*(2008)] via RF-spectroscopy. Thus, they could provide a convenient access to the quench dynamics investigated here. Indeed, we will show that the gapless Goldstone mode is directly visible in the dynamics of the single-particle occupations and that it leads to a full inversion of the lowest-lying single-particle states. We will demonstrate this by investigating the effect of the phase dynamics on individual occupations as well as on the whole single-particle band structure.

In doing so, we focus on a cloud with the confinement frequencies given by $f_\parallel = 56\,\mathrm{Hz}$ and $f_\perp = 4\,\mathrm{kHz}$, with $N_P = 1700$ atoms in the trap and with an excitation of $1/(k_F a) = -0.8 \to -0.9$. For such a cigar-shaped trap the atomic energies $\varepsilon_{m_x,m_y,m_z} := \varepsilon_m$ are strongly separated with respect to m_x and m_y and comparatively dense with respect to m_z, i.e., they form subbands. The single-particle energies of Eq. (8.21) inherit this band structure which can be seen in Fig. 8.7.

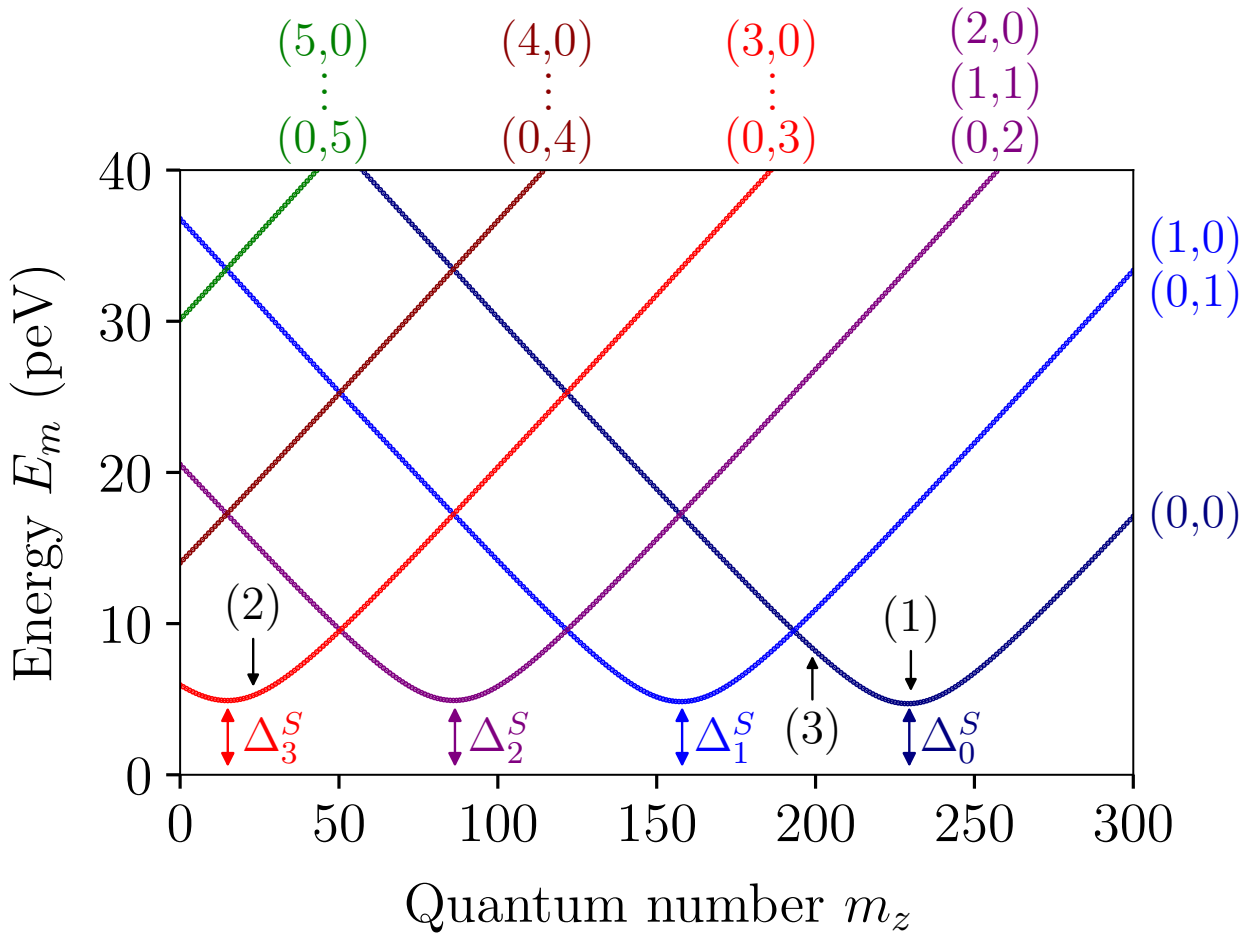

Figure 8.7: (color online) Single-particle energies for a strongly confined Fermi gas in a BCS phase with four atomic subbands crossing the chemical potential; Δ_i^S denotes the gap of the subbands with $m_x + m_y = i$ and (m_x, m_y) denotes the subband index (see main text); the marked states (1), (2), (3) are discussed below; parameters: $f_\parallel = 56\,\mathrm{Hz}$, $f_\perp = 4\,\mathrm{kHz}$, $N = 1700$ and $1/(k_F a) = -0.9$.

There, a plot of the single-particle energies against the quantum number m_z is shown for the system introduced above. One clearly observes several subbands each of which corresponds to certain sets of quantum numbers (m_x, m_y), where –due to the cylindrical symmetry of the system– each subband is $2(m_x+m_y+1)$ fold degenerate (the factor 2 results from the degeneracy of the two single-particle branches corresponding to the two spin configurations)[12]. Furthermore, the four subbands with the lowest sets of quantum numbers (m_x, m_y) show minima when the corresponding atomic subbands cross the chemical potential, i.e., at different values for m_z. The states located at the minima thus lie in close vicinity to the chemical potential and contribute strongly to the BCS pairing (the expectation values $\Delta_{mm}^{\mathrm{GS}}$ corresponding to these states, i.e., the subband gaps, will be denoted as Δ_i^S with $i = m_x + m_y$ being the subband index; see Fig. 8.7). The higher atomic subbands with $m_x + m_y \geq 4$ do not cross the chemical potential. The corresponding single-particle subbands therefore do not exhibit any minima.

Since the single-particle operators corresponding to the energies of Fig. 8.7 –i.e., those

[12] Actually, subbands with different and not just interchanged quantum numbers (m_x, m_y) are not exactly degenerate due to slightly different subband gaps Δ_m^S (on the order of 0.1 peV for the investigated systems). For example: The subbands $(0, 3)$ and $(3, 0)$ are exactly degenerate, whereas the subbands $(0, 3)$ and $(1, 2)$ are split by $\sim 0.5\,\mathrm{peV}$. However, in the presented plots and with the assumed experimental accuracy this splitting is not resolved.

of Eqs. (8.4) and (8.5)– are defined in the excitation picture all energy states of Fig. 8.7 are not occupied in the ground state before the quench. But, during the temporal evolution following the quench occupations of the order of 1 are created. We will show this explicitly for three particular single-particle states [marked as (1), (2) and (3) in Fig. 8.7], one close to the minimum of the subband (1,2) ($E_m = 5.2\,\mathrm{peV}$), one at the minimum of the subband (0,0) ($E_m = 4.7\,\mathrm{peV}$) and one at a higher energy in the subband (0,0) ($E_m = 8.4\,\mathrm{peV}$). Furthermore, we will identify the gapless Goldstone mode of the BCS gap in the corresponding dynamics.

The dynamics of the three single-particle occupations is shown in Fig. 8.8 (a) for the first 20 ms after the quench. We clearly observe that all occupations oscillate in phase with one dominant low frequency. The states (1) (blue line) and (2) (red line) have a large amplitude of the order of 1 while the amplitude of state (3) (green line) is much smaller. Furthermore, the three occupations each exhibit an individual weak higher-frequency component which has the largest frequency for the state (3) of high energy. However, we find that the amplitude of the higher-frequency component increases with decreasing the scattering length, i.e., when entering the BCS regime with $1/(k_F a) < -1$.

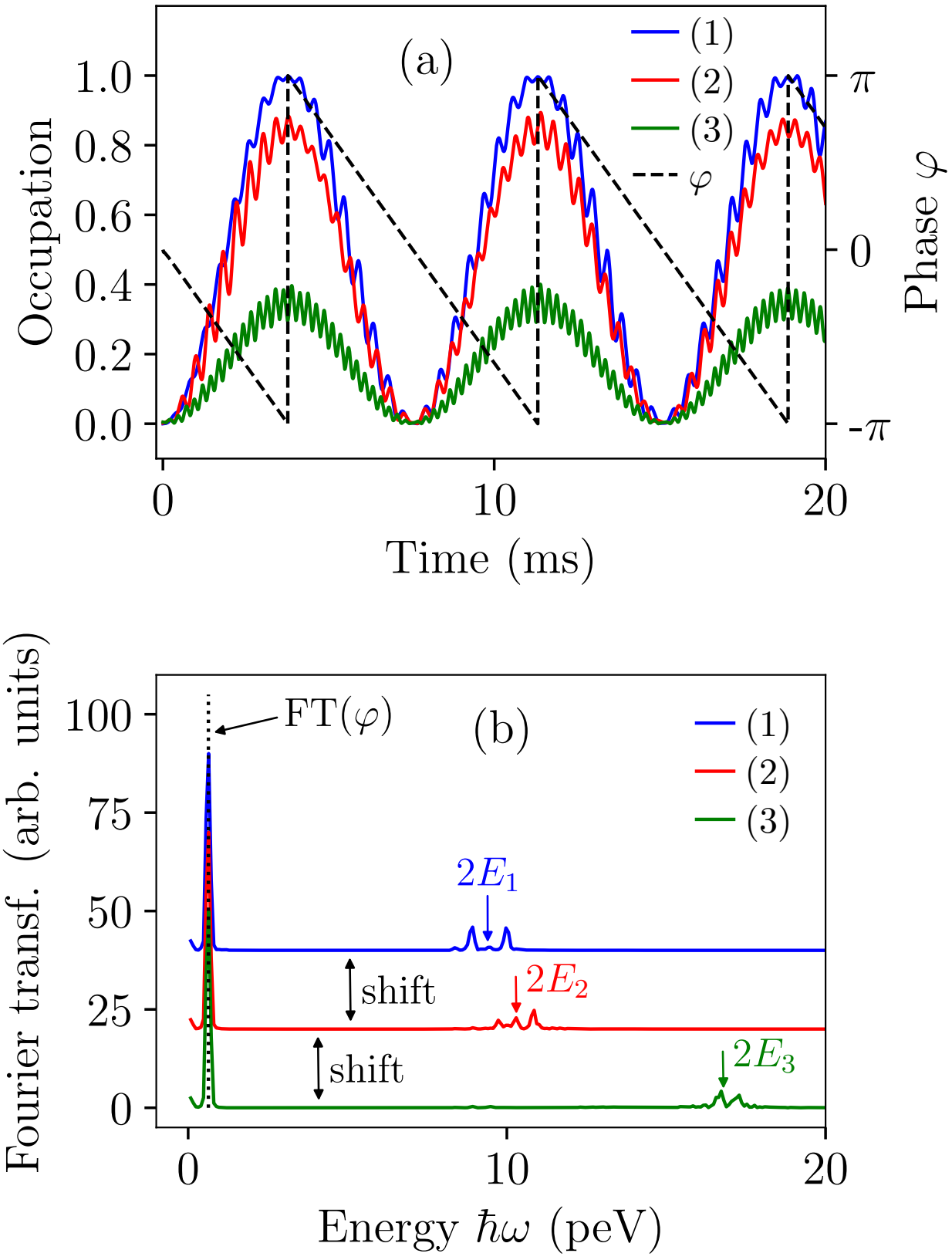

Figure 8.8: (color online) (a) Dynamics of three particular single-particle occupations, one state of higher energy (3) and two from subband minima (1), (2) (see Fig. 8.7). (b) Fourier transform of the functions in (a).

A comparison of the single-particle dynamics with the dynamics of the phase of the gap [Fig. 8.8 (a); dashed line] shows that the dominant low oscillation frequency originates from

the Goldstone mode of the gap: The phase of the gap shows the same linear dynamics as in section 8.3.2 with a rate corresponding to the low-frequency part of the single-particle occupations. Thus, the gapless Goldstone mode is directly visible in the excitation dynamics of the condensate.

To investigate the single-particle dynamics in closer detail, Figure 8.8 (b) shows the Fourier spectrum of the data of Fig. 8.8 (a). Again, we observe that the dominant low frequencies of the occupations and the phase of the BCS gap exactly match. But, the origin of the higher frequencies in the excitation dynamics can now be seen as well: Besides the dominant low-frequency components each spectrum exhibits a series of weak peaks at approximately twice the energy of the corresponding single-particle state. I.e., the higher-frequency components result from an eigenoscillation of the single-particle occupations. In Ref. [Hannibal *et al.*(2015)] a sum of all eigenoscillations was shown to result in the Higgs mode of the gap. The higher-frequency components can thus be understood as fragments of the Higgs mode of the BCS gap.

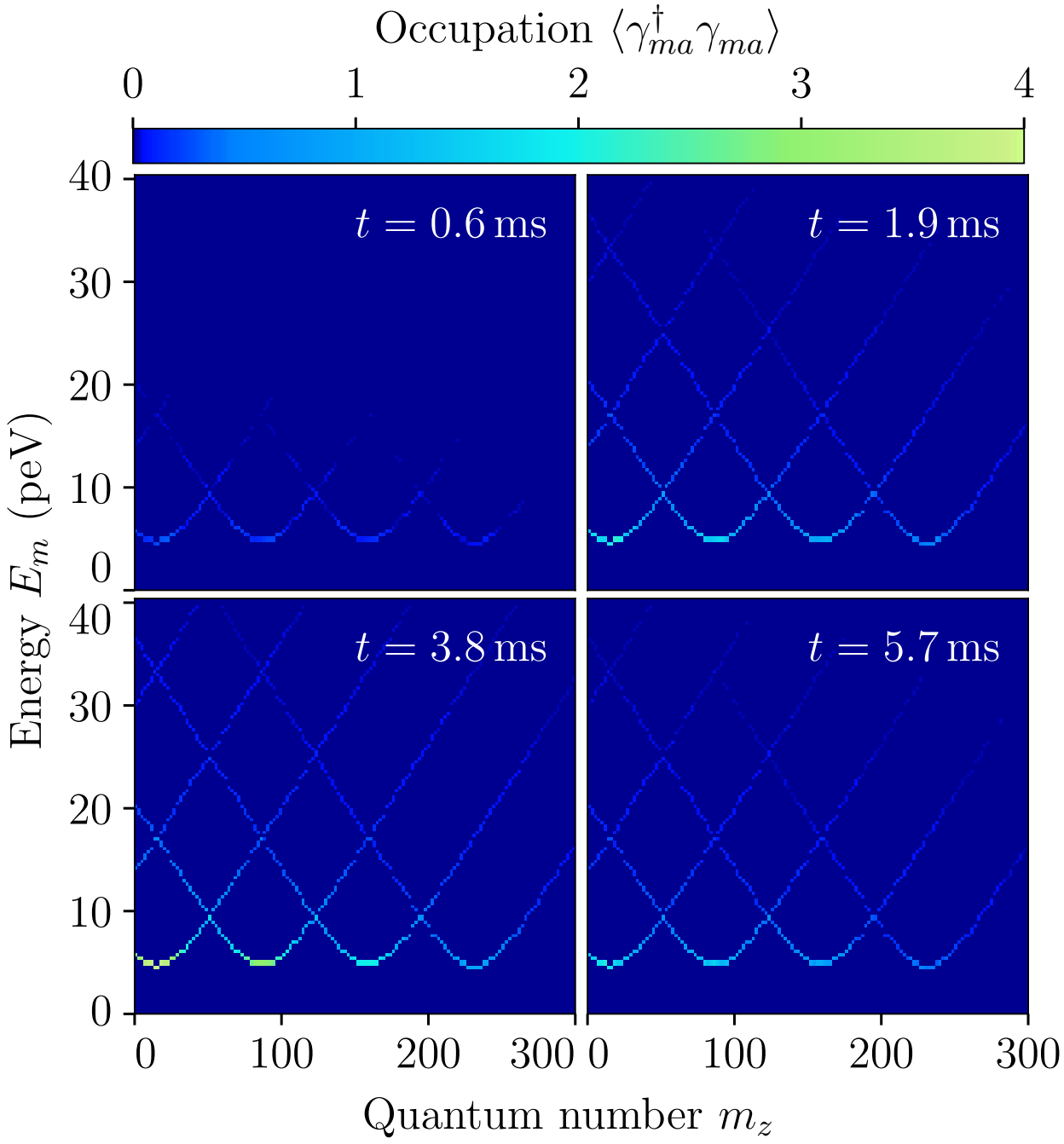

Figure 8.9: (color online) Single-particle occupations at different times after the interaction quench; parameters: See Fig. 8.7.

At last, –to analyze the impact of the gapless Goldstone mode on the whole single-particle spectrum– Figure 8.9 shows snapshots of the single-particle occupations plotted against the quantum number m_z and the excitation energy E_m, like they could be measured by angle- and momentum-resolved RF spectroscopy [Stewart *et al.*(2008)], for a series of time steps after the quench. The first snapshot corresponds to the time $t = 0.6\,\mathrm{ms}$ and thus directly follows the quench. Here, the excitations are rather weak and can hardly be seen. However, going on in time we observe that all occupations increase in phase until the time $t = 3.8\,\mathrm{ms}$, where the maximum occupation of all states is reached. Afterwards the occupations decrease until the initial situation is reached again. Thus, Fig. 8.9 is an illustration of the in-phase oscillation of all single-particle occupations due to the gapless Goldstone mode.

In addition, –neglecting the contributions from the eigenoscillation– the snapshot for $t =$

3.8 ms provides a map of the amplitude of the single-particle oscillations since here the dominant low-frequency part of all occupations exhibits its maximum value. On the basis of this amplitude map one observes, that the amplitude distribution shows a resonance behaviour: The amplitude is largest for states with low quantum number m_z and low energy E_m and decreases with increasing values of m_z and E_m. In fact, directly at the minimum of the subbands with $m_x + m_y = 3$ the oscillation amplitude is 4, decreasing by 1 for every next lower subband $m_x + m_y$. However, this dependence is due to the $(m_x + m_y + 1)$-fold degeneracy of the subbands (only the particle-like excitations of the single-particle branch a are shown). I.e., the oscillation amplitude of each individual single-particle occupation at a subband minimum is 1. Thus, the single-particle occupations at the subband minima exhibit a full inversion.

Concluding this section we can thus state: We have shown that the gapless Goldstone mode of an interaction-quenched ultracold Fermi gas directly couples to the single-particle occupations and leads to a full inversion of the lowest-lying states. An experimental access to the dynamical single-particle occupations would thus allow for a direct observation of the massless Goldstone Boson predicted by the Goldstone theorem. However, we want to remark that an application of RF-spectroscopy –a state-of-the-art experimental access to the single-particle excitations [Stewart *et al.*(2008), Stewart *et al.*(2010)]– to the dynamical situation is restricted to the observation of the inhomogeneous phase dynamics. It turns out that it does not contain any signature of the gapless homogeneous Goldstone mode (see appendix). Therefore, at least a modification of this experimental technique would be required to observe the gapless Goldstone mode via the single-particle excitations.

8.5 Gapless Goldstone mode and RF spectroscopy

One way to study the single-particle occupations in experiment is RF spectroscopy as was shown in Ref. [Stewart *et al.*(2008)]. There, a first direct measurement of the single-particle excitations via RF spectroscopy was achieved for a thermal superfluid gas of ultracold ^{40}K in the BCS-BEC crossover. An application of RF spectroscopy to the dynamical situation could thus allow for a direct observation of the Goldstone mode without coupling it to the trap. This could be achieved, e.g., via a pump-probe like experimental setup: By introducing a delay time t between the quench (the "pump pulse") and the actual RF measurement (the "probe pulse") a time-resolved single-particle spectrum like in Fig. 8.9 could be obtained. However, in the following we will show that RF signals give a direct measurement of the single-particle occupations only if no single-particle coherences are present. In contrast, we will demonstrate that –for our case of a coherent evolution of the condensate– the single-particle coherences cancel the signature of the gapless Goldstone mode in the RF signal and thus prohibit its direct observation via RF spectroscopy.

The basic principle of RF spectroscopy applied to ultracold Fermi gases is to optically excite the atoms from one of the two hyperfine states of the condensate, i.e., the state denoted as $|k\uparrow\rangle$, to a third hyperfine state which is not involved in the BCS pairing (following Ref. [Ketterle and Zwierlein(2008)] we will denote this state as $|k\sigma\rangle$ with $\sigma = 3$; depending on the atom species used the actual spin of the corresponding hyperfine state will be different though). Then, the resulting occupations of the third hyperfine state can be used –at least in the absence of coherences between the single-particle states– as a direct measure of the corresponding single-particle occupations (see below and [Ketterle and Zwierlein(2008)]).

As stated above, an RF excitation results in a simultaneous spin flip of all atoms in the cloud which is described by the operator [Ketterle and Zwierlein(2008)]

$$\hat{V} = V_0 \sum_k \left(c^\dagger_{k3} c_{k\uparrow} + c^\dagger_{k\uparrow} c_{k3} \right), \tag{8.26}$$

with $c^\dagger_{k\sigma}$ ($c_{k\sigma}$) creating (annihilating) one atom in the state with quantum number k and spin index $\sigma \in \{\uparrow, \downarrow, 3\}$. Here, we assume the excitation to be orthogonal with respect to the quantum number k, i.e., we only consider transitions $|k\uparrow\rangle \to |k'3\rangle$ with $k = k'$. Strictly speaking this applies only to very large systems where k corresponds to the wave number and if we furthermore assume $\hbar k_{RF} \ll \hbar k$, i.e., that the momentum of the photons is much smaller than the momentum of the atoms. However, in Anderson Approximation transitions with $k \neq k'$ do not contribute to the RF signal since all nondiagonal single-particle expectation values vanish (see below). Thus, we can apply Eq. (8.26) to our current situation.

Following [Ketterle and Zwierlein(2008)], we use

$$c_{k\uparrow} = u_k \gamma^\dagger_{ka} - v_k \gamma_{kb} \tag{8.27}$$

and we furthermore assume the third hyperfine state to be initially empty, i.e., $c_{k3}|\Psi(t)\rangle = 0$ with $|\Psi(t)\rangle$ the state of the condensate before the RF pulse. This yields:

$$\hat{V} = V_0 \sum_k c^\dagger_{k3} \left(u_k \gamma^\dagger_{ka} - v_k \gamma_{kb} \right). \tag{8.28}$$

Therefore, the RF excitation transfers single atoms to the state $|k3\rangle$ by creating a quasiparticle in the single-particle state ka and destroying one in state kb. However, we are interested in the occupations of state $|k3\rangle$ after the excitation, i.e., we have to investigate the transitions governed by the matrix elements

$$M_k = \langle f|V|\Psi(t)\rangle, \tag{8.29}$$

where $|\Psi(t)\rangle = |\gamma(t)\rangle|0\rangle_3$ is composed of the quasiparticle contribution $|\gamma(t)\rangle$ and the vacuum of the third hyperfine state $|0\rangle_3$. Since the exact quasiparticle configuration after the RF pulse is not relevant, the final state of the transition $|f\rangle$ needs to take into account all possible end states for the quasiparticles, i.e.,

$$|f\rangle = \sum_{k'} \left(u_{k'} \gamma^\dagger_{k'a} - v_{k'} \gamma_{k'b} \right) |\gamma(t)\rangle |k3\rangle. \tag{8.30}$$

Inserting this into Eq. (8.29) and keeping in mind that in Anderson approximation $\langle \gamma^\dagger_{ma/b} \gamma_{na/b} \rangle = \langle \gamma^\dagger_{ma} \gamma^\dagger_{nb} \rangle = 0$ for $m \neq n$ and that $\langle \gamma^\dagger_{ma} \gamma_{ma} \rangle = \langle \gamma^\dagger_{mb} \gamma_{mb} \rangle$ [Hannibal *et al.*(2015)] we obtain

$$M_k \sim (u_k^2 - v_k^2) \langle \gamma^\dagger_{ka} \gamma_{ka} \rangle - 2 u_k v_k \mathrm{Re} \left(\langle \gamma^\dagger_{ka} \gamma^\dagger_{kb} \rangle \right) + v_k^2. \tag{8.31}$$

Therefore, the population in the state $|k3\rangle$ created by the RF pulse is a direct measure of the single-particle occupations if the single-particle coherences $\langle \gamma^\dagger_{ka} \gamma^\dagger_{kb} \rangle$ vanish. This is the case for every thermal state of the condensate. I.e., –in that case– a momentum- and energy-resolved measurement of the occupation of the third hyperfine state maps the single-particle band structure (cf. [Stewart *et al.*(2008)]).

However, if single-particle coherences are present, they may interfere with the signal from the occupations and prohibit an observation of the latter. This is the case for our situation as can be seen by calculating M_k directly from Eq. (8.26) The quasiparticle part of the transition matrix elements M_k is basically given by the occupation of the atomic state $|k\uparrow\rangle$, i.e.,

$$M_k \sim \langle c^\dagger_{k\uparrow} c_{k\uparrow} \rangle \tag{8.32}$$

Therefore, the overall transition matrix element considering all transtitions to the third hyperfine state yields

$$M_{\text{total}} \sim \sum_k \langle c^\dagger_{k\uparrow} c_{k\uparrow} \rangle = N_{P\uparrow}. \tag{8.33}$$

However, $N_{P\uparrow}$ is a conserved quantity during the free quench dynamics, i.e., during the dynamics before the RF pulse. Therefore, M_{total} and thus the overall RF-induced occupations of the third hyperfine state do not depend on the actual time of the RF measurement. This implies that the contribution from the Goldstone mode in the occupations has to be canceled out by a corresponding contribution in the single-particle coherences since all single-paricle occupations oscillate in phase with respect to the gapless Goldstone mode. Therefore, every individual M_k is a constant with respect to the Goldstone mode. In that sense, particle conservation prohibits an observation of the gapless Goldstone mode via RF spectroscopy.

Indeed, our numerical data confirm that the contribution of the single-particle coherences to Eq. (8.31) exactly cancels out the signal of the Goldstone mode from the single-particle occupations. This confirms that the Goldstone mode in the present form is not visible via RF spectroscopy.

However, the same applies to the real-space dynamics of the condensate: For the same reasons as stated above the gapless homogeneous Goldstone mode is not visible in the atomic density $\rho(\mathbf{r},t)$ of the cloud. With Eqs. (8.4)-(8.5) one directly obtains

$$\begin{aligned}\rho(\mathbf{r},t) &= \sum_\sigma \langle \hat{\Psi}_\sigma^\dagger(\mathbf{r},t)\hat{\Psi}_\sigma(\mathbf{r},t)\rangle \\ &= 2\sum_k \big[(u_k^2 - v_k^2)\langle \gamma_{ka}^\dagger \gamma_{ka}\rangle \\ &\qquad - 2u_k v_k \mathrm{Re}\left(\langle \gamma_{ka}^\dagger \gamma_{kb}^\dagger\rangle\right) + v_k^2\big]|\varphi_k(\mathbf{r})|^2, \end{aligned} \tag{8.34}$$

which has the same structure as Eq. (8.31). Therefore, the gapless homogeneous Goldstone mode does not couple to the real-space dynamics of the cloud as already stated in section 8.3.2. However, the resemblence of Eqs. (8.34) and (8.31) also implies that the Goldstone mode is visible in the RF signal for the case of inhomogeneous excitations. There, the symmetry between the single-particle excitations and coherences preventing the gapless homogeneous Goldstone mode from observation must be broken to allow for a collective oscillation of the cloud. Therefore, we state that in our case of a homogeneous excitation the Goldstone mode is visible neither in the single-particle excitations nor in the real-space dynamics of the cloud. But, for the same reason it must be visible in both quantities for the case of inhomogeneous excitations.

9 Dynamical vanishing of the order parameter in a confined Bardeen-Cooper-Schrieffer Fermi gas after an interaction quench by Hannibal et al.

Abstract

We present a numerical study of the Higgs mode in an ultracold confined Fermi gas after an interaction quench and find a dynamical vanishing of the superfluid order parameter. Our calculations are done within a microscopic density-matrix approach in the Bogoliubov-de Gennes framework which takes the three-dimensional cigar-shaped confinement explicitly into account. In this framework, we study the amplitude mode of the order parameter after interaction quenches starting on the BCS side of the BEC-BCS crossover close to the transition and ending in the BCS regime. We demonstrate the emergence of a dynamically vanishing superfluid order parameter in the spatiotemporal dynamics in a three-dimensional trap. Further, we show that the signal averaged over the whole trap mirrors the spatiotemporal behavior and allows us to systematically study the effects of the system size and aspect ratio on the observed dynamics. Our analysis enables us to

connect the confinement-induced modifications of the dynamics to the pairing properties of the system. Finally, we demonstrate that the signature of the Higgs mode is contained in the dynamical signal of the condensate fraction, which, therefore, might provide a new experimental access to the nonadiabatic regime of the Higgs mode.

9.1 Conclusion

In this paper, we have presented a numerical study of the dynamical vanishing of the order parameter in a cigar-shaped ultracold Fermi gas in the framework of the fully microscopic BdG equations. We have calculated the spatiotemporal dynamics of the order parameter after an interaction quench. We have observed a rapid initial decay as well as a revival which both affect the whole trap. Thus, both can be characterized by the spatially averaged gap. Whereas, after the initial decay we find an oscillation of the order parameter in the longitudinal direction of the harmonic trap which is not seen in the average value due to the continuity equation.

Exploiting the spatially averaged order parameter, we have demonstrated that the dynamical vanishing in inhomogeneous systems is robust with respect to the size and aspect ratio of the system while modifications to this vanishing arise from the finite size due to the trap potential. The occurrence of a vanishing order parameter predicted in the homogeneous case is maintained but the precise onset of the vanishing is altered by the pairing properties in the trap. We find that the pairing strength, characterized by the gap at the chemical potential or equivalently by the smallest BdG eigenenergies, increases with the aspect ratio as $r^{2/3}/\tau_{\mathrm{trap}}$ and with the particle number as $N^{1/3}$.

We have found that the transition to a vanishing order parameter in a cigar-shaped ultracold Fermi gas is determined by two criteria which both need to be fulfilled and which depend contrarily on the aspect ratio of the trap. For small aspect ratios the position of the transition is determined by the initial decay rate which needs to be sufficiently fast compared to the characteristic time scale of the trap. In this case we observe that the quench strength necessary for the transition decreases with increasing aspect ratio. However, for smaller quench strengths and larger aspect ratios the signature of the linear Higgs mode from "phase II" becomes more prominent which prevents a vanishing to be visible. Then, the transition is determined by the linear Higgs mode which leads to an increasing transition quench strength with increasing aspect ratio.

Furthermore, we have shown that the condensate fraction on the BCS side of the BCS-BEC crossover can be a suitable measure to access the Higgs mode in such a cigar-shaped ultracold Fermi gas. Nevertheless, we also find that the condensate fraction will reduce the amplitude of the signal compared to the order parameter and does not mirror the Higgs mode exactly. We expect that this does not introduce new effects but will rather only lead to a shift of the observed transition.

9.2 Introduction

Due to a remarkable control over many relevant system parameters which, in most cases, can be tuned at will, ultracold quantum gases are an ideal testbed for many-body theories and for concepts known from solid-state theory. These include, e.g., lattice symmetries [Bloch *et al.*(2008)], topological properties [Goldman et al.(2016)], spin-orbit coupling [Galitski and Spielman(2013), Wu et al.(2016)], and non-homogeneous superconductivity [Liao et al.(2010)]. For these reasons ultracold Fermi gases have received great attention both from an experimental and from a theoretical point of view [Bloch *et al.*(2008), Giorgini *et al.*(2008)].

Using a Feshbach resonance [Chin et al.(2010)] to adjust the interaction strength a Bardeen-Cooper-Schrieffer (BCS) superfluid state of Cooper pairs has been achieved for small attractive interactions, whereas in the limit of large interactions between the fermions repulsive bosonic

dimers form and a Bose Einstein condensate (BEC) of the latter has been observed [Regal et al.(2004)]. Those two limiting superfluid states are connected by the BCS-BEC crossover featuring strong interactions and unitary properties [Zwerger(2011)].

The implementation of ultracold Fermi gases always requires an external confinement, e.g., optical traps. The control of this external confinement on the one hand provides means for the outstanding control over the system [Bloch *et al.*(2008), Grimm et al.(2000)]. On the other hand, this implies a finite system size which can have a major impact on the physics of a superfluid system. The pairing properties strongly depend on the structure of the energy spectrum of the system and, hence, on the dimensionality of the system. Theoretical studies predict an atypical BCS-BEC crossover due to confinement effects [Shanenko *et al.*(2012)].

Recently, efforts have been devoted to the non-equilibrium properties of the superfluid state [Polkovnikov et al.(2011), Yin and Radzihovsky(2013), Yin and Radzihovsky(2016)]. Due to the spontaneously broken U(1) symmetry two fundamental modes of the complex order parameter evolve: the (massive Higgs) amplitude mode and the (massless Goldstone) phase mode. The observation of the collective Higgs excitation in a system with spontaneous symmetry breaking (SSB) is of fundamental importance to gain a better understanding of the physical system at hand, as was recently demonstrated in the case of the standard model of particle physics [Collaboration(2012)].

The first evidence of the Higgs mode was reported by Raman scattering in a superconducting charge density wave compound [Sooryakumar and Klein(1980), Littlewood and Varma(1981)]. Furthermore, in ultracold gases the Higgs mode has been observed in the spectral response of a 2D optical lattice excited by an amplitude modulation of the lattice [Endres et al.(2012)]. A time-resolved observation of the nonadiabatic regime of the Higgs mode [Papenkort et al.(2007), Papenkort et al.(2008)], as has been achieved in a superconducting NbN film [Matsunaga *et al.*(2014), Matsunaga et al.(2013), Matsunaga and Shimano(2012)], is still pending for ultracold gases. In order to reach the nonadiabatic regime the challenging implementation of an interaction quench has been proposed to be done either by an RF flip of one species of the condensate (cf. [Fröhlich et al.(2011)]), which leads, in the vicinity of a Feshbach resonance, to the desired almost instantaneous change of the scattering length. Alternatively the quench could be implemented by an optical control of the interaction in quantum gases [Clark et al.(2015)]. However, there are several theoretical studies addressing an ultracold Fermi gas after an interaction quench [Yuzbashyan *et al.*(2015), Yuzbashyan et al.(2006), Yuzbashyan and Dzero(2006), Yuzbashyan et al.(2005), Barankov and Levitov(2006), Bruun et al.(1999), Bruun(2014), Scott *et al.*(2012), Hannibal et al.(2015)]. In the case of a homogeneous system three dynamical phases depending on the excitation condition have been predicted analytically [Yuzbashyan *et al.*(2015)]. They include persistent oscillations of the BCS gap ("phase III"), damped oscillations with inverse square root decay ("phase II") and a dynamical vanishing of the order parameter ("phase I"). Previous studies in confined systems focused on the damped oscillations and showed that for superconducting BCS nanowires the decay exponent is changed from $-1/2$ to $-3/4$ due to quantum size resonances [Zachmann et al.(2013)], while for even tighter confined superconducting nanorods the decaying oscillation becomes irregular [Kettmann et al.(2017)]. In a BCS Fermi gas confined in a box with periodic boundary conditions in two dimensions and a harmonic confinement in the third dimension the inverse square-root decay has been confirmed [Scott *et al.*(2012)] and for a three-dimensional harmonic confinement an additional fragmentation of the damped oscillations has been predicted [Hannibal et al.(2015)].

In this paper we show that the dynamical vanishing of the superfluid order parameter, i.e., phase I, also emerges in a Fermi gas confined in a three dimensional harmonic trapping potential after an interaction quench. The emergence of phase I has not only been shown in ultracold Fermi gases but also in BCS superconductors [Papenkort et al.(2009), Chou et al.(2017)]. Here, we analyze the transition to a dynamically vanishing order parameter in dependence of the

confinement properties. To this end, we present a numerical study based on the previously published microscopic density matrix approach within the Bogoliubov-de Gennes framework [Hannibal et al.(2015)]. This allows for a full microscopic and coherent quantum mechanical treatment of the system and provides access to the spatiotemporal dynamics of the order parameter as well as to the condensate fraction which is a possible experimental candidate to carry the signature of the Higgs mode.

This paper is organized as follows. In Sec. 9.3 we will give a short summary of the used theoretical model, while Sec. 9.4 is devoted to the results of our numerical calculations. We start by discussing the spatiotemporal dynamics of the order parameter in Sec. 9.4.1. In the next step, we will give a detailed analysis of the dynamical vanishing in a cigar-shaped trap in Secs. 9.4.2 and 9.4.3 based on the spatially averaged order parameter. In Secs. 9.4.4 and 9.4.5 we will provide extrapolations to typical experimental particle numbers. Finally, in Sec. 9.4.6 we present the dynamics of the condensate fraction after an interaction quench. In Sec. 9.1 we will briefly summarize our findings.

9.3 Theoretical Model

We employ the Bogoliubov-de Gennes (BdG) formalism [Hannibal et al.(2015), Datta and Bagwell(1999), De Gennes(1989)] to calculate the dynamics of the superfluid order parameter $\Delta(\mathbf{r},t)$ of an ultracold Fermi gas confined in an axially symmetric harmonic trapping potential after an interaction quench. In this section, we provide a short summary of the most essential aspects of the used formalism and the relevant system parameters. For a comprehensive discussion of the formalism we refer the reader to our previous work [Hannibal et al.(2015)].

We consider the gas to be composed of fermionic ^{6}Li atoms in two different internal spin states (labeled by $\uparrow$ and $\downarrow$) with equal particle numbers $N_\uparrow = N_\downarrow = N/2$. The atoms in the two spin states interact via a contact interaction with $V_{\text{contact}} = (4\pi\hbar^2 a/m)\,\delta(\mathbf{r_1}-\mathbf{r_2}) = g\,\delta(\mathbf{r_1}-\mathbf{r_2})$, where m is the mass of a ^{6}Li atom and $a<0$ is the scattering length. Hence we only consider systems on the BCS side of the BEC-BCS crossover.

We use a cigar-shaped harmonic confinement potential given by $V_{\text{conf}} = \frac{1}{2}m\omega_\perp^2(x^2+y^2) + \frac{1}{2}m\omega_\parallel^2 z^2$, where $\omega_\perp$ ($\omega_\parallel$) is the radial (longitudinal) confinement frequency, respectively. We denote the eigenfunctions of the confinement potential by $\langle\hat{r}|k\rangle = \phi_k(\mathbf{r})$ and the equidistant single-particle energies of the confinement potential are labeled by ξ_k, where we use the tuple $k=(k_x,k_y,k_z)$ with $k_i \in \{0,1,2,..\}$. In this paper, we consider elongated traps characterized by an aspect ratio of the cloud $r = \omega_\perp/\omega_\parallel \gg 1$. In such a geometry one-dimensional subbands form resulting in quantum size oscillations in the case of small particle numbers [Shanenko *et al.*(2012), Hannibal et al.(2015)]. In order to characterize the number and positions of these subbands it is instructive to introduce the subband parameter $s = E_F/(\hbar\omega_\perp)$ where the Fermi energy E_F is given by the chemical potential in the non-interacting case. That is, for a system with $s=j$, where $j\in\mathbb{N}$, the minimum of subband j is located at the Fermi energy. The choice $s=j+0.5$ implies that the physics of the system are not dominated by a single band and the effects of the quantum size resonances are negligible also in small systems (cf. [Hannibal et al.(2015)]).

In order to describe the system, we use the introduced contact interaction and confinement potential and we obtain the BdG Hamiltonian with the BCS-like mean-field approximation

$$\begin{aligned} H_{\text{BdG}} = &\sum_\sigma \int d^3r\, \Psi_\sigma^\dagger(\mathbf{r}) H_0 \Psi_\sigma(\mathbf{r}) \\ &+ \int d^3r\, \Delta^*(\mathbf{r})\Psi_\downarrow(\mathbf{r})\Psi_\uparrow(\mathbf{r}) + h.c.\,, \end{aligned} \tag{9.1}$$

where H_0 is the single-particle Hamiltonian. By doing so we introduce the superfluid spatially dependent order parameter

$$\Delta(\mathbf{r}) = g \left\langle \Psi_\downarrow(\mathbf{r}) \Psi_\uparrow(\mathbf{r}) \right\rangle . \tag{9.2}$$

Here, $\Psi_\sigma(\mathbf{r})$ is the field operator annihilating an atom with spin σ at position $\mathbf{r}$. The corresponding eigenvalue problem to the Hamiltonian in Eq. (9.1) is the BdG equation which reads

$$\begin{pmatrix} H_0 & \Delta(\mathbf{r}) \\ \Delta^*(\mathbf{r}) & -H_0^* \end{pmatrix} \begin{pmatrix} u_K(\mathbf{r}) \\ v_K(\mathbf{r}) \end{pmatrix} = E_K \begin{pmatrix} u_K(\mathbf{r}) \\ v_K(\mathbf{r}) \end{pmatrix} . \tag{9.3}$$

The solution of this equation yields two branches (labeled by $K \to ka$ and $K \to kb$) for the eigenenergies and eigenfunctions which result from the two spin species. However, the eigenenergies and eigenfunctions can be expressed by one another [Datta and Bagwell(1999)]. Therefore, we drop the index a/b wherever possible and imply thereby the use of the states and energies corresponding to branch a.

Since the BdG equation has the form of a one-particle Schrödinger equation we use the BdG wave functions to introduce Bogoliubov's quasiparticles which diagonalize H_{BdG}. The transformation reads

$$\begin{aligned} \gamma_{ka}^\dagger &= \int u_k(\mathbf{r}) \Psi_\uparrow^\dagger(\mathbf{r}) + v_k(\mathbf{r}) \Psi_\downarrow(\mathbf{r}) \, d^3r \\ \gamma_{kb}^\dagger &= \int u_k(\mathbf{r}) \Psi_\downarrow^\dagger(\mathbf{r}) - v_k(\mathbf{r}) \Psi_\uparrow(\mathbf{r}) \, d^3r. \end{aligned} \tag{9.4}$$

In order to obtain the solution of the BdG equation we make use of Anderson's approximation [Anderson(1959)], i.e., we assume the BdG wave functions to be proportional to the bare atomic wave functions with $u_k(\mathbf{r}) = u_k \phi_k(\mathbf{r})$ and $v_k(\mathbf{r}) = v_k \phi_k(\mathbf{r})$. This yields the BdG eigenenergies

$$E_k = \sqrt{(\xi_k - \mu)^2 + \Delta_k^2} \tag{9.5}$$

and BdG coefficients

$$u_k = \sqrt{\frac{1}{2}\left(1 + \frac{\xi_k - \mu}{E_k}\right)} \quad v_k = \sqrt{\frac{1}{2}\left(1 - \frac{\xi_k - \mu}{E_k}\right)} \tag{9.6}$$

where $\Delta_k = \langle k | \Delta(\mathbf{r}) | k \rangle$. Exploiting this solution and substituting Bogoliubov's quasiparticles in the definition of the order parameter in Eq. (9.2) we obtain the well-known self-consistency equations for the order parameter and the chemical potential μ in the ground state of the system at $T = 0\,\mathrm{K}$. They read

$$\Delta_k = -\frac{1}{2} \sum_{k'} V_{kk'} \frac{\Delta_{k'}}{E_{k'}} \chi_{k'} \tag{9.7}$$

$$N = 2 \sum_k \left(1 - \frac{\xi_k - \mu}{E_k}\right), \tag{9.8}$$

where we have used $V_{kk'} = g \int d^3r \, |\phi_k(\mathbf{r})|^2 \, |\phi_{k'}(\mathbf{r})|^2$. The self-consistent solution Δ_k of these equations characterizes the pairing properties in the ground state of the system, where the pairing takes place predominantly in an interval around the chemical potential as known from bulk BCS theory. The factor $\chi_{k'} = (1 - E_{k'}/\xi_{k'})$ in Eq. (10.36) regularizes the well-known ultraviolet divergence of the contact interaction [Bruun et al.(1999), Bruun and Heiselberg(2002), Shanenko *et al.*(2012)]. This regularization is introduced into all terms which result from summations over states k. Additionally, the numerically necessary cutoff is chosen such that all physical effects are qualitatively correctly accounted for.

In order to excite the nonadiabatic dynamics of the system we implement an interaction quench, i.e., an instantaneous change of the scattering length a, which leaves the particle density $n(\mathbf{r}) = n_\uparrow(\mathbf{r}) + n_\downarrow(\mathbf{r}) = 2\left\langle \Psi_\uparrow^\dagger \Psi_\uparrow \right\rangle$ unchanged. In doing so, only occupations $x_{kl} = \left\langle \gamma_{ka}^\dagger \gamma_{la} \right\rangle = \left\langle \gamma_{kb}^\dagger \gamma_{lb} \right\rangle$ and coherences $y_{kl} = \left\langle \gamma_{ka}^\dagger \gamma_{lb}^\dagger \right\rangle = \left\langle \gamma_{lb} \gamma_{ka} \right\rangle^*$ which are diagonal in terms of the quasiparticles, i.e., $x_{kl} = x_k\,\delta_{kl}$ and $y_{kl} = y_k\,\delta_{kl}$, are excited.

In the next step, we utilize Heisenberg's equations of motion in order to obtain equations of motion for the occupations x_k and coherences y_k of the density matrix. For our dynamical calculations we choose a time-independent basis, i.e., the basis given by the final system (u_m,v_m). This leads to a time-dependent Hamiltonian and the appearance of terms specifying the deviation between the dynamical gap Δ and the ground-state value Δ_{GS}. The obtained equations of motion read

$$i\hbar \frac{d}{dt} x_k = a_k y_k^* - a_k^* y_k \tag{9.9}$$

$$i\hbar \frac{d}{dt} y_k = -2\, E_k^{(\mathrm{ren})} y_k + a_k\,(1 - 2x_k)\,, \tag{9.10}$$

where

$$E_k^{(\mathrm{ren})} = E_k + 2\,u_k v_k \mathrm{Re}\left[(\Delta - \Delta_{\mathrm{GS}})_{\mathrm{k}}\right] \tag{9.11}$$

$$a_k = v_k^2 (\Delta - \Delta_{GS})_k - u_k^2 (\Delta - \Delta_{GS})_k^* \tag{9.12}$$

and the deviation of the current gap is given by

$$(\Delta - \Delta_{GS})_k = -\sum_l \left[2 v_l u_l x_l + u_l^2 y_l^* - v_l^2 y_l\right] V_{kl} \chi_l. \tag{9.13}$$

Here, χ_l regularizes this term in analogy to Eq. (10.36). We solve these equations of motion numerically with the Runge-Kutta-Fehlberg method which provides good numerical stability for all investigated sets of parameters.

Finally, we invert Bogoliubov's transformation and we arrive at the space- and time-dependent order parameter in terms of the quasiparticles which reads

$$\Delta(\mathbf{r},t) = g \sum_k 2\, v_k(\mathbf{r}) u_k(\mathbf{r}) \left(x_k(t) - \frac{1}{2}\right) + u_k^2(\mathbf{r})\, y_k^*(t) - v_k^2(\mathbf{r})\, y_k(t). \tag{9.14}$$

9.4 Results

In this section, we will first discuss the full spatiotemporal dynamics of the modulus of the order parameter $|\Delta(\mathbf{r},t)|$ and in the next step we turn to the temporal evolution of the modulus of the spatially averaged order parameter given by

$$\overline{\Delta}(t) = \left| \frac{1}{V} \int d^3 r \Delta(r,t) \right|, \tag{9.15}$$

where the volume $V = (\hbar/m)^{3/2} \omega_\perp^{-1} \omega_\parallel^{-1/2} = l_\perp^2 l_\parallel$ is determined by the harmonic trapping frequencies. This quantity will enable us to carry out a systematic study of the obtained dynamics in dependence on the trap parameters.

In this paper, we investigate interaction quenches for which the initial ground state, characterized by $1/(k_F a_i)$ and the ground-state gap $\overline{\Delta}_i$, is situated in the crossover regime of the

BEC-BCS crossover and the final ground state $[1/(k_F a_f), \overline{\Delta}_f]$, is situated deep in the BCS regime. Here, we assume the well-known dispersion relation of the homogeneous Fermi gas in order to obtain the Fermi wave vector k_F. Throughout the paper we choose $1/(k_F a_f) = -1.45$ and characterize the strength of the quench by the initial coupling parameter $1/(k_F a_i)$. We note that it would also be possible to characterize the quench strength by $\overline{\Delta}_f/\overline{\Delta}_i$ in analogy to [Yuzbashyan *et al.*(2015)]. However, with the introduced regularization $\overline{\Delta}_f/\overline{\Delta}_i$ converges much slower than Δ_k when increasing the numerical cutoff. Since Δ_k determines the main properties of the system in our formalism it is sufficient to choose the numerical cutoff according to Δ_k, which substantially reduces the numerical effort. Bearing this in mind, we characterize the quench strength by $1/(k_F a_i)$, which is independent of the numerical cutoff. In the case of a homogeneous system a study of similar quenches has been done before and our quenches here are connected to the emergence of phase I [Yuzbashyan *et al.*(2015), Yuzbashyan and Dzero(2006)].

9.4.1 Spatiotemporal dynamics

In this section, we will investigate the spatiotemporal dynamics of the order parameter. To this end, we keep here, and in Secs. 9.4.2 and 9.4.3, the subband parameter $s = 3.5$ fixed. Furthermore, we choose $\omega_\parallel = 2\pi \cdot 120\,\mathrm{Hz}$, which then determines together with a given aspect ratio r and subband parameter s the transverse trapping frequency $\omega_\perp$ and the particle number N.

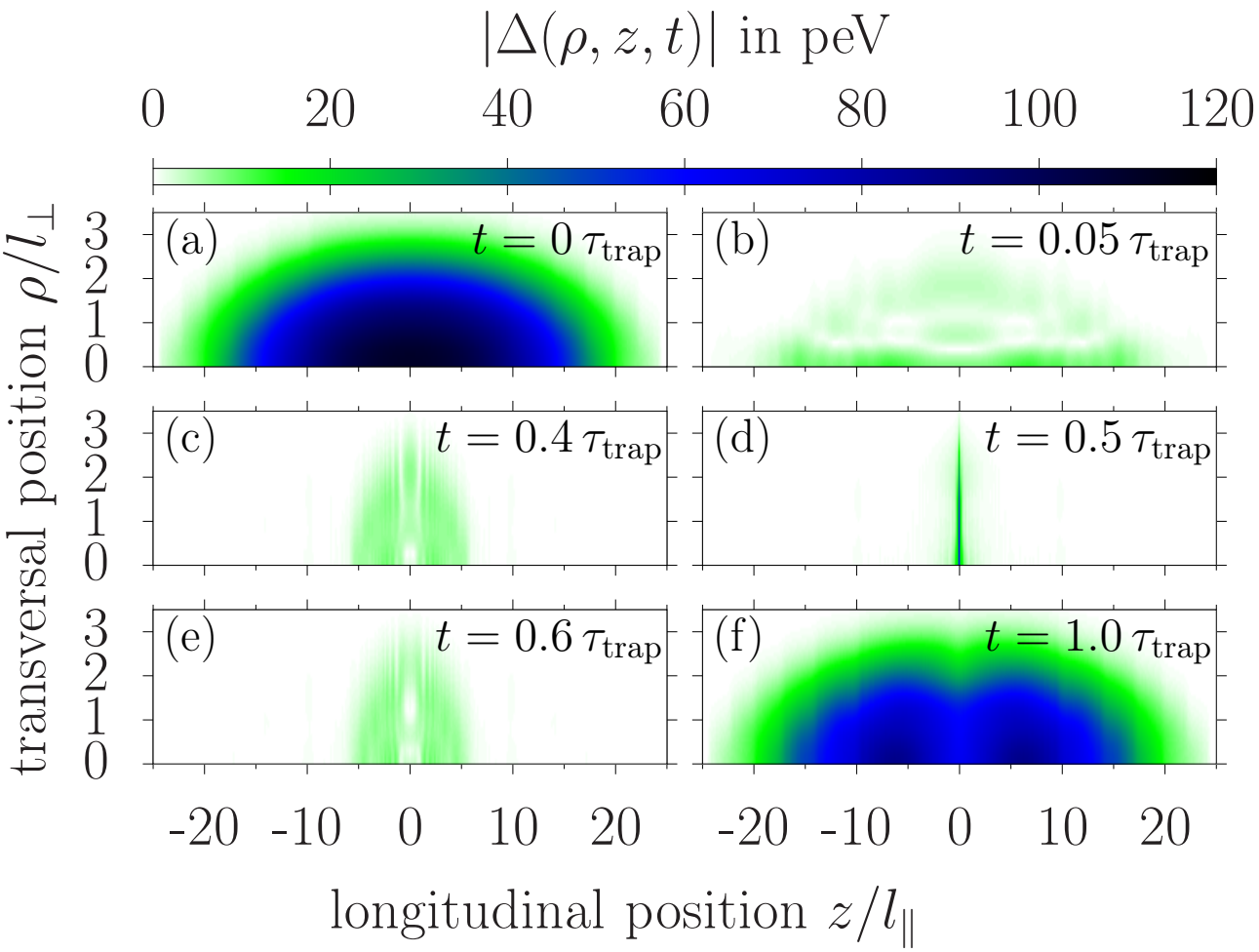

Figure 9.1: Spatiotemporal dynamics of the modulus of the order parameter after a sudden change of the scattering length from $1/(k_F a_i) = -0.4$ to $1/(k_F a_f) = -1.45$ and an aspect ratio of $r = 50$, where $\tau_{\mathrm{trap}} = h/\delta E = 1/(2f_\parallel)$ is the characteristic time scale of the trap [Hannibal et al.(2015)].

In Fig. 9.1 we show the spatially dependent modulus of the order parameter $|\Delta(\mathbf{r},t)|$ at six different times after an excitation by an interaction quench. Figure 9.1(a) shows the initial spatial distribution of the gap at $t = 0$ after the instantaneous quench, i.e., the excitations introduced by the quench are already included. We find a symmetrical distribution which features a maximum in the center of the trap. After $t = 0.05\tau_{\mathrm{trap}}$, we obtain a rapid decay of the order parameter of approximately one order of magnitude which affects the whole trap (cf. Fig. 9.1(b)). In addition, we find that the relative suppression of the order parameter with respect to the ground-state value of the final system is strongest in the center of the trap. Subsequently, we find that the remaining condensate moves towards the center of the trap where the distribution of the order parameter becomes very narrow with a large amplitude at $t = 0.5\tau_{\mathrm{trap}}$ (cf. Fig. 9.1(d)). Comparing Figs. 9.1(c) and (e), which are almost identical, we see that this behavior occurs oscillatory and we find that the frequency is given by $f_{\mathrm{collapse}} = 2f_{\parallel}$. Finally, in Fig. 9.1(f) we see a revival of the order parameter at $t = \tau_{\mathrm{trap}}$, which shows two maxima located symmetric to the center of the trap.

Overall, from Fig. 9.1 we extract two effects. The first one is characterized by the rapid initial decay of the order parameter and the revival after τ_{trap}. The initial distribution of $|\Delta(\mathbf{r}, t = 0)|$ is set by the ground-state order parameter of the initial system while at the time of the revival we see that the order parameter shows two maxima which result from –as our data shows– the spatial profile of the order parameter in the final system. The second effect is an oscillation taking place in the remaining superfluid after the initial decay. We see from our data that the suppression of the order parameter with respect to the ground-state value is strongest in the center of the trap. This causes the superfluid to start oscillating in the harmonic trap by moving towards the center. An analysis of the complex phase of the order parameter $\Phi(\mathbf{r},t)$ shows that this oscillation fulfills the general relation between the superfluid velocity and the gradient of the phase, i.e., $v_s = \hbar/m\,\nabla\Phi(\mathbf{r},t)$. This implies that the order parameter obeys a continuity equation and, hence, this oscillation will not be visible in the spatially averaged order parameter, as we will see in the next section.

Before we proceed, we point out that during the dynamics the average occupation number of the fermionic atoms stays smeared out around the chemical potential and the coherences y_k of the density matrix stay finite, indicating the existence of pair correlations at all times. In equilibrium these properties are directly linked to a superfluid behavior of the system. In a dynamical situation these properties are typically related to a superfluid behavior of the system even in the case of a vanishing order parameter as was also pointed out in Ref. [Yuzbashyan and Dzero(2006)].

In the following, we will systematically analyze the dynamical vanishing of the order parameter in a harmonic trap. To this end, we will discuss the modulus of the order parameter averaged over the trap. First, we will show that this is a suitable quantity to characterize the dynamical vanishing. Further, we will investigate its dependence on the aspect ratio r of the trap for small systems with fixed parameter s. In the next step we will show how the results scale for a larger system and, finally, we will present the dynamics of the condensate fraction for larger systems after the same type of quench.

9.4.2 Dynamical vanishing in the spatially averaged order parameter

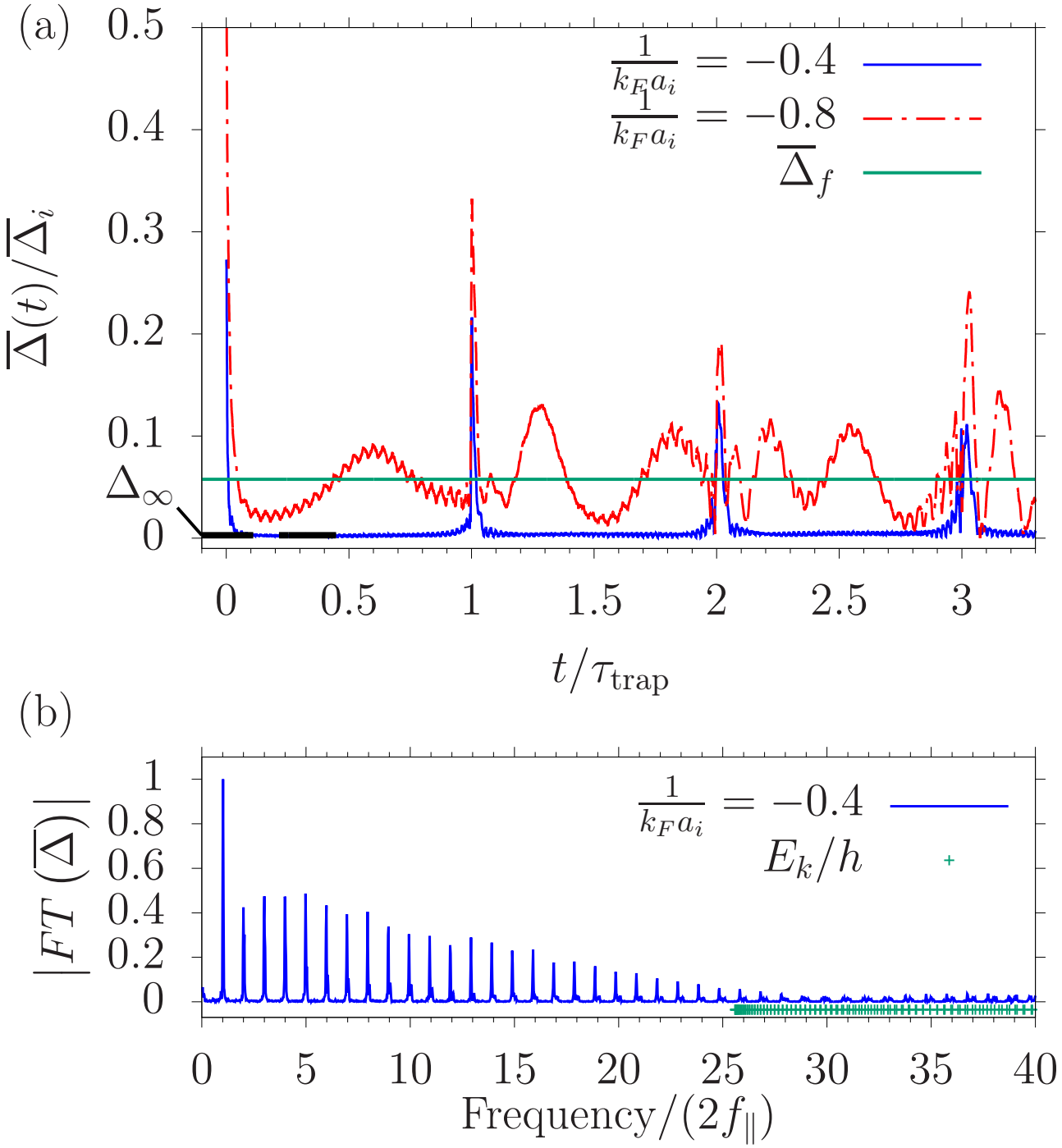

Figure 9.2: (a) Dynamics of the spatially averaged gap after a sudden change of the scattering length from $1/(k_F a_i) = -0.4$ (blue solid line) and $1/(k_F a_i) = -0.8$ (red dash-dotted line) to $1/(k_F a_f) = -1.45$ and an aspect ratio of $r = 50$. The gap is normalized to the spatially averaged ground-state gap of the system before the quench $\overline{\Delta}_i$. $\overline{\Delta}_f$ is the spatially averaged ground-state gap of the final system and Δ_∞ marks the height of the plateau for $1/(k_F a_i) = -0.4$; (b) Fourier transform of the gap dynamics with $1/(k_F a_i) = -0.4$ and the BdG eigenenergies E_k.

Figure 9.2(a) shows the dynamics of the modulus of the spatially averaged order parameter in a system with $r = 50$ after quenches with $1/(k_F a_i) = -0.4$ (blue solid curve) and $1/(k_F a_i) =$

-0.8 (red dash-dotted curve). After the stronger quench (i.e., $1/(k_F a_i) = -0.4$, being identical to Fig. 9.1) a decay of the modulus of the order parameter to a value which is much smaller than the ground-state value of the final system $\overline{\Delta}_f$ (solid green line) is seen. Following this decay a plateau evolves where the averaged value of the height of the plateau is labeled by Δ_∞. Although the height of the plateau is very small compared to $\overline{\Delta}_f$ there are still some oscillations with the transverse confinement frequency $\omega_\perp$ visible. Since we cannot expect an exact vanishing of our numerical solution of a nondissipative model, we will, nevertheless, refer to such a behavior as dynamical vanishing of the gap. A technical discussion of the classifications of the numerical solutions is provided in the Appendix. Overall, our definition of the dynamical vanishing of the gap is in close analogy to what has been labeled phase I in a homogeneous system [Yuzbashyan *et al.*(2015)].

Additionally, in contrast to the homogeneous system, there are pronounced spikes visible at τ_{trap}. These result from the rephasing of the oscillators, i.e., the quasiparticle occupations and coherences, with equidistant energies spaced by $\delta E = 2hf_\parallel$ that contribute to the dynamics. Therefore, the time is given by $\tau_{\mathrm{trap}} = h/\delta E = 1/(2f_\parallel)$ as has been discussed for the dynamics dominated by a dephasing of these oscillators, also labeled by phase II [Hannibal et al.(2015), Yuzbashyan *et al.*(2015)].

In comparison to the spatiotemporal dynamics in Fig. 9.1 we find that $\overline{\Delta}(t)$ precisely maps the rapid decay and the revival of the order parameter. As expected the oscillations towards the center of the trap are not visible; instead we observe an oscillation with the transverse confinement frequency. In general, this oscillation is also visible in $\Delta(\mathbf{r})$. However, it is not visible in Fig. 9.1 due to the temporal spacing of frames since $f_\perp \gg f_\parallel$. Thus, we establish that $\overline{\Delta}(t)$ is suitable to analyze both the initial decay and the evolution of a plateau in the dynamics of the order parameter in a cigar-shaped trap.

The weaker quench, i.e., $1/(k_F a_i) = -0.8$, belongs to phase II and shows an oscillation around a non-vanishing average, slightly smaller than $\overline{\Delta}_f$. The higher-frequency parts are given by the transverse trapping energy $\hbar\omega_\perp$. For an exhaustive discussion of phase II in an inhomogeneous system we refer the reader to our previous publication [Hannibal et al.(2015)]. In addition, comparing the two quenches we see that a larger quench leads to a faster initial decay of the order parameter which we will come back to later.

In order to gain further insight into the dynamics we show the Fourier transform of the dynamically vanishing amplitude of the order parameter in Fig. 9.2(b). We observe a spectrum with equidistant Fourier components spaced by $2f_\parallel$ which decay with increasing energy. The equidistant peaks evolve as a result of a nonlinear behavior of the equations of motion. While for a small quench, i.e., in the linear phase II, the Fourier components are given by the BdG quasiparticle energies (green dots) the frequencies for a large quench are given by the difference between the energies of the quasiparticle states contributing to the dynamics. To be precise, each occupation and coherence oscillates dominantly with a frequency given by twice the difference between the corresponding single-particle energy and the chemical potential μ. Since the final system is located in the BCS regime, i.e., $\mu \approx E_F$, this difference is always a multiple of $\hbar\omega_\parallel$. Overall, we obtain in phase I a spectrum with equidistant peaks dominated by non-linear effects. We refer to such a spectrum as "quasi-ungapped" spectrum, since the gap of the spectrum is given by the energy spacing of the equidistant peaks which is much smaller than the quasiparticle gap of the ground state.

In such a case of an equidistant quasi-ungapped spectrum a Fourier series directly connects the initial decay in the time domain with the width of the distribution of the frequency components. We label this width by β and determine it by an exponential fit in the time domain, which we discuss in the Appendix. In frequency space a physical understanding of the width of the decay can be obtained when considering the BCS pairing properties: Cooper pairing of atoms takes place in an interval around the chemical potential determined by the BdG wave

functions. From the solution of the BdG equation we see that the width of this interval is determined by the gap Δ_k of state k at the chemical potential μ. Further, the pairing strength continuously decreases in the given interval with increasing distance to the chemical potential due to the form of the BdG wave functions. This implies that the amplitude of the oscillation of the occupations and coherences decays with increasing distance to the chemical potential. Therefore, considering Eq. (9.14) also the Fourier coefficients of the dynamical vanishing gap decay with increasing energy over a width determined by Δ_k.

Overall, we find that the width β is connected to the pairing properties at the chemical potential which can be characterized by the smallest BdG eigenenergy E_{min}, since $\xi_k \approx \mu$ at the chemical potential. Hence, we obtain that $\beta \propto E_{\mathrm{min}}$ for the dynamical vanishing of phase I. We have confirmed numerically that there is no additional dependence on the aspect ratio, i.e., for a given E_{min} β is identical for any aspect ratio r.

Summarizing, from Fig. 9.2 we have extracted the relevant physical properties to understand the dynamical vanishing in an inhomogeneous system. We have shown that the dynamics has a nonlinear character and we have related the dynamical behavior to the ground-state properties of the final system for a given quench strength and aspect ratio. We have shown that for a given quench the initial decay characterized by β is proportional to the pairing properties in the final state, i.e., E_{min} which, thus, will be an important variable for the subsequent analysis. With this fundamental understanding we now turn to the transition between the two different "phases" and investigate the impact of different aspect ratios.

9.4.3 Impact of the aspect ratio

In the following we will systematically investigate the impact of the aspect ratio of the cloud on the emergence of a dynamical vanishing of the spatially averaged order parameter. We will first establish numerical criteria necessary for the analysis and then evaluate the dynamics for various aspect ratios and again connect the observed behavior to the ground-state pairing properties characterized by E_{min}.

For the subsequent analysis of the dynamical vanishing of the order parameter Δ_∞ will be the central quantity. We obtain Δ_∞ from our numerical data by fitting an exponential decay $f(t) = \exp(-\beta t) + \alpha$ in the beginning and by checking whether a flat plateau evolves afterwards. For this we require β to be large enough (criterion A) and an oscillatory behavior to be nonvisible in the subsequent dynamics (criterion B). If a plateau is identified we take Δ_∞ as the height of this plateau otherwise Δ_∞ is the arithmetic mean over the whole calculation time. A discussion of details and implications of our numerical procedure is provided in the Appendix.

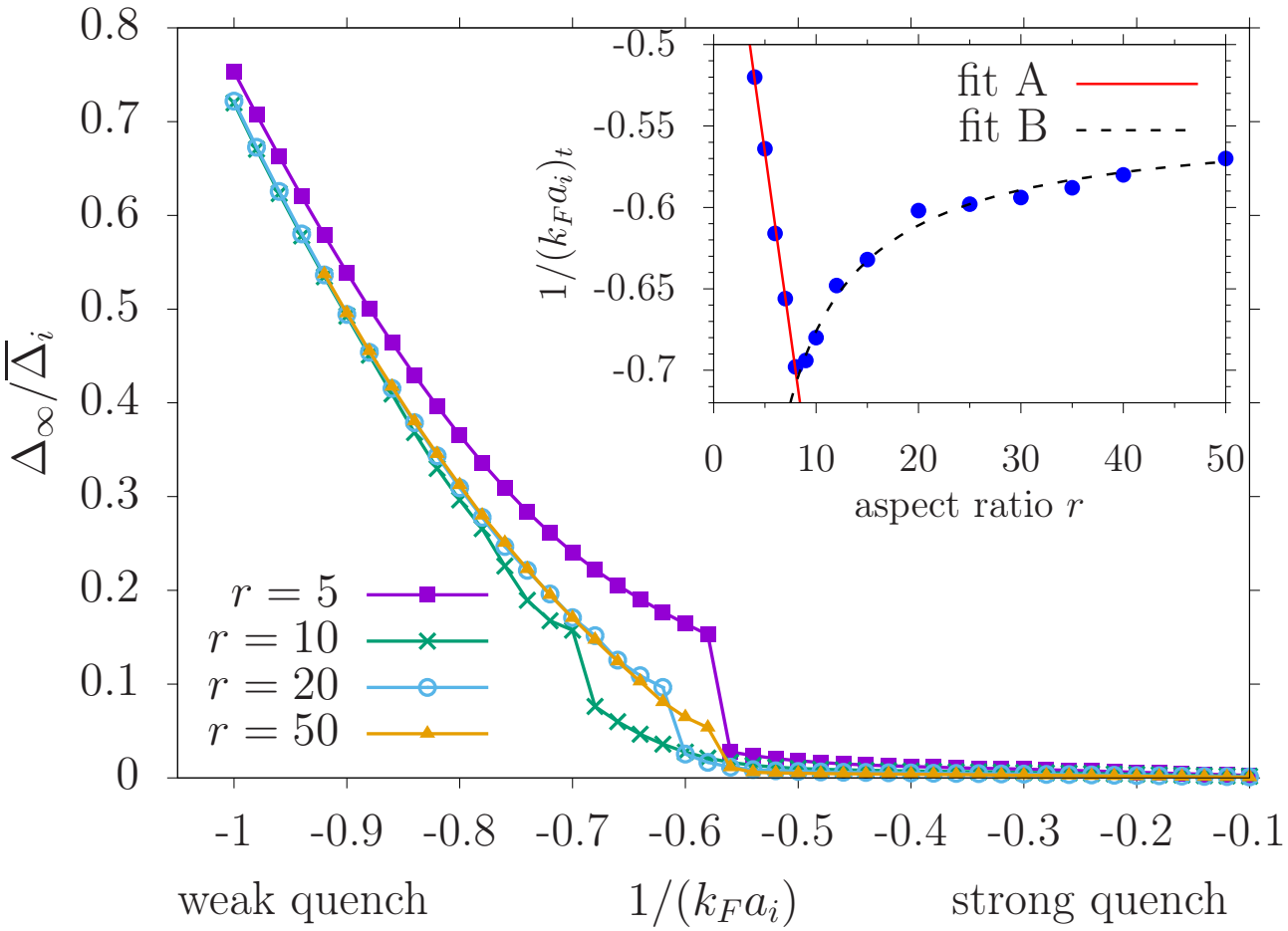

Figure 9.3: Δ_∞ normalized to the ground-state gap of the initial system $\overline{\Delta}_i$ for different quenches with $1/(k_F a_f) = -1.45$ and aspect ratios r. Inset: quench parameter $1/(k_F a_i)_t$ at the transition to the dynamical vanishing vs. the aspect ratio r. The red solid line (fit A) shows a linear fit to data for $r \leq 8$ and the black dashed line (fit B) is an inverse proportional fit to data for $r \geq 9$.

In the following, we carry out an analysis of Δ_∞ for a range of quenches which all end at the same $1/(k_F a_f) = -1.45$ where we vary the aspect ratio of the systems and keep the parameters $s = 3.5$ and $\omega_\parallel = 2\pi \cdot 120\,\mathrm{Hz}$ fixed. In Fig. 9.3 we show results for four different aspect ratios which represent the effects obtained from our numerical data. For small quenches, i.e., small $1/(k_F a_i)$, we find a decreasing of Δ_∞ with increasing quench strength, i.e., larger $1/(k_F a_i)$, as has been predicted before [Yuzbashyan *et al.*(2015), Scott *et al.*(2012)]. Increasing the quench strength further, we observe a drop in Δ_∞ where the position of this visible drop is altered depending on the aspect ratio. The drop implies that the specified conditions for a vanishing order parameter are met and Δ_∞ is taken as the height of the identified plateau. Furthermore, we see that the height of the obtained plateau continuously tends to zero where it almost coincides for all aspect ratios. In the following, we will investigate the dependence of the drop on the aspect ratio which marks the transition to a vanishing order parameter.

For $r = 5$ (purple boxes) we find a distinct drop at $1/(k_F a_i)_t \approx -0.56$ to a plateau with a small height. When increasing the aspect ratio to $r = 10$ (green crosses) we observe that the transition to a plateau behavior is shifted to smaller quench strength, i.e., $1/(k_F a_i)_t \approx -0.69$. At the same time the height of the plateau after the transition is increased. In contrast, increasing the aspect ratio even further to $r = 20$ (blue circles) and $r = 50$ (orange triangles) leads to a reversal in the shift of the necessary quench strength for the transition. For $r = 50$ it is given by $1/(k_F a_i)_t \approx -0.56$, while the height of the plateau is reduced, since it is determined by the same curve for all aspect ratios which is set by the nonlinear behavior of the equations

of motion.

In order to investigate the shifts of the transition to a dynamical vanishing in more detail, we plot the initial coupling parameter at the transition point $1/(k_F a_i)_t$ in dependence of the aspect ratio in the inset of Fig. 9.3. For small aspect ratios $r \leq 8$ we find that $1/(k_F a_i)_t$ decreases linearly which is illustrated by the linear fit A. In contrast, for $r \geq 9$ the transition quench strength increases again and shows an $a/r + b$ (fit B) dependence, where $b \approx -0.55$ is in agreement with the maximum value of $1/(k_F a_i)_t$ in the main part of Fig. 9.3. It provides a limit of the quench strength necessary for aspect ratios $r \geq 50$. In the following, we will investigate these two confinement-induced shifts of the critical value of the quench strength characterized by $1/(k_F a_i)$, responsible for the transition to the dynamical vanishing. To this end, we will analyze the dominant energy and, hence, time scales of the system. This includes the dependence of the initial decay constant β, which turns out to control the behavior according to fit A, as well as the period of the Higgs mode in phase II, which will control the emergence of a dynamical vanishing and the visibility of a plateau in the range of aspect ratios where fit B applies.

In order to observe a vanishing of the order parameter the initial decay needs to be sufficiently fast compared to the trap time τ_{trap} (cf. criterion A). Therefore, we start by investigating the initial decay characterized by β with respect to the trap time τ_{trap} in dependence of the initial coupling $1/(k_F a_i)$ and the aspect ratio r. Figure 9.4 shows $\beta\tau_{\text{trap}}$ for a range of different quenches which are identical to those in Fig. 9.3. We find a nonlinear increase of the initial decay rate with an increased quench strength for all aspect ratios. That is, a stronger quench leads to a faster decay as expected for our initial value problem: the initially excited occupations and coherences depend on the order parameter in the initial system. Since we keep the final system identical the initial system for a larger quench is located closer to the BCS-BEC crossover and, hence, features a larger gap. This leads to a wider pairing interval determined by the BdG coefficients u_m, v_m and, therefore, to larger initial values which are distributed over a wider range of energies. This carries over to the spectral properties of the dynamics and thus leads to a larger β and, hence, a faster initial decay. Therefore, we establish the criterion $\beta\tau_{\text{trap}} > 10$ as a necessary condition for the vanishing to occur, as discussed in the Appendix.

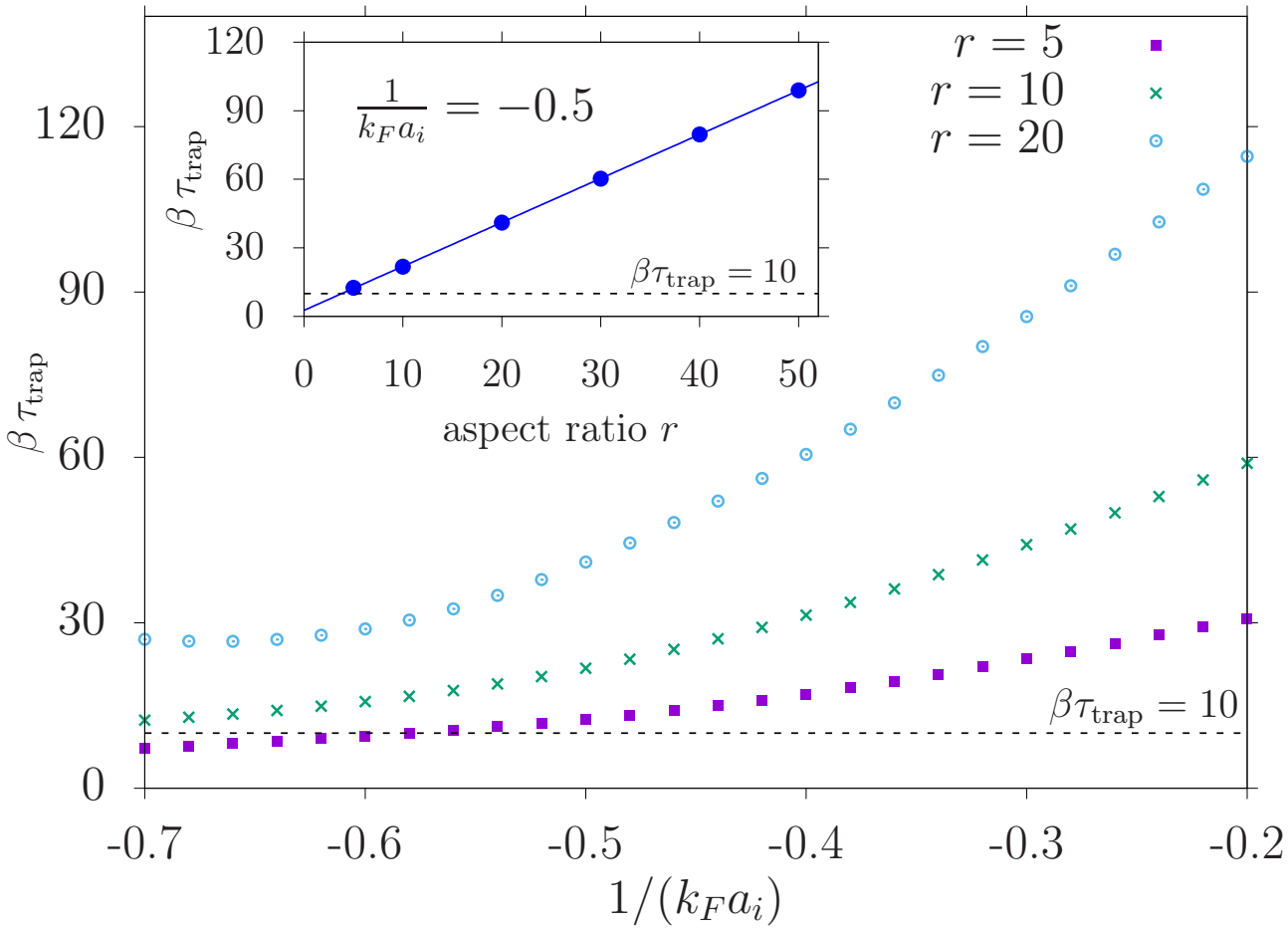

Figure 9.4: Time scale of the initial decay with respect to the trap time $\beta\tau_{\mathrm{trap}}$ for various quenches to $1/(k_F a_f) = -1.45$ and $\omega_{\parallel} = \text{const.}$ for $r = 5, 10$ and 20. Inset: $\beta\tau_{\mathrm{trap}}$ vs. the aspect ratio r at fixed quench conditions; the dashed black line marks the condition $\beta\tau_{\mathrm{trap}} = 10$ in either figure.

In the case of a system with an aspect ratio of $r = 5$ this criterion is met for $1/(k_F a_i) > -0.56$. This matches with the onset of the dynamical vanishing as seen in Fig. 9.3 and applies to all systems which show the behavior of fit A. The linear behavior of fit A is inherited from the linear dependence of $\beta\tau_{\mathrm{trap}}$ on the aspect ratio which we show in the inset of Fig. 9.4 at a fixed quench strength. Here, the solid blue line is a linear fit to the data points. Since the dependence of $\beta\tau_{\mathrm{trap}}$ on the quench strength is rather small in the range of the shift of $1/(k_F a_i)_t$ in Fig. 9.3 the dependence of $1/(k_F a_i)_t$ on r is dominated by the dependence of $\beta\tau_{\mathrm{trap}}$ on the aspect ratio which results in the observed linear dependence of fit A due to criterion A.

In contrast, for the other shown aspect ratios in Fig. 9.4 ($r = 10, 20$) the condition $\beta\tau_{\mathrm{trap}} > 10$ is fulfilled for any quench strength with $1/(k_F a_i) > -0.7$. Nevertheless, in comparison with Fig. 9.3 one finds that this does not necessarily lead to a dynamical vanishing of the gap. Furthermore, in the inset of Fig. 9.3 we found a different dependence of $1/(k_F a_i)_t$ on the aspect ratio r for these systems. This suggests that a different effect, which turns out to be connected to criterion B, is responsible for the transition point to the dynamical vanishing. Since these systems are located at the transition between phase I and phase II we go back to a system from phase II [cf. red dash-dotted line in Fig. 9.2(a)] and discuss the dependence of the relevant energy scale on the aspect ratio in this phase.

If the period of the Higgs mode T_{Higgs} is large compared to the trap time, i.e., $T_{\mathrm{Higgs}}/\tau_{\mathrm{trap}} \gg 1$, a plateau after the initial decay can become visible (cf. Fig. 9.7 in the Appendix). Additionally to the criterion A of a fast initial decay, characterized by $\beta\tau_{\mathrm{trap}}$, we require the features of the linear Higgs mode of phase II to be non-visible in the dynamics. This is expressed through

the condition $T_{\mathrm{Higgs}}/\tau_{\mathrm{trap}} \gg 1$ (criterion B). If this second condition is not met, we observe an oscillation of the spatially averaged order parameter around the mean value Δ_∞ even if the initial decay is sufficiently fast.

In order to determine the period of the linear Higgs mode we consider the dominant energy scale in phase II which is given by the main frequency of the amplitude (Higgs) mode f_{Higgs}. Previous studies [Hannibal et al.(2015), Yuzbashyan *et al.*(2015)] showed that f_{Higgs} depends on the quench strength: in the case of a very small quench f_{Higgs} is given by $2E_{\mathrm{min}}$. Further, for all quenches from "phase II" f_{Higgs} is closely connected to the mean value Δ_∞ of the oscillations [13]. Therefore, f_{Higgs} decreases with increasing excitation strength as can be seen from Fig. 9.3. However, the decrease of Δ_∞ occurs in the same manner for all aspect ratios and, hence, does not introduce a significant dependence of f_{Higgs} on the aspect ratio. As a result, the dependence of f_{Higgs} on the aspect ratio is in good approximation solely inherited from the dependence of E_{min} on the aspect ratio.

We investigate this dependence in the following sections and find that the minimal quasiparticle energy E_{min} increases with the aspect ratio. Therefore, the period of the Higgs mode T_{Higgs} decreases with increasing aspect ratio and it turns out that this decrease is in good agreement with the $1/r$ behavior of fit B in the inset of Fig. 9.3, which we will come back to in Sec. 9.4.5. Hence now the transition is determined by the criterion B.

Summarizing, we have analyzed the confinement-induced effects on the continuous transition to the dynamical vanishing of the order parameter in a cigar-shaped ultracold Fermi gas. Exploiting our introduced classification, we have formulated two criteria which need to be fulfilled in order to observe a dynamical vanishing characterized by the emergence of a plateau. These two criteria depend contrarily on the aspect ratio and, hence, we distinguish the following two cases. For small aspect ratios $r \lesssim 8$ the transition is determined by the initial decay constant $\beta \propto E_{\mathrm{min}}$. This leads to a linear shift of the transition in dependence of the order parameter according to fit A. For larger aspect ratios $r \gtrsim 9$ (fit B) the transition is determined by the period of the Higgs mode where again the relevant dependence is solely given by E_{min}. Since we have shown that both criteria depend on E_{min} we will provide a more general study of this key variable in the next sections.

9.4.4 Scaling properties

In this section we will consider the dependence of E_{min} on the aspect ratio r in a more general situation where the aspect ratio $r = \omega_\perp/\omega_\parallel$ is changed as $r \to \lambda r$, where we now keep a fixed particle number of $N = 1000$ as opposed to the parameter s. In order to achieve this scaling of the aspect ratio r we consider three possible options which are shown in Table 1. For each option we numerically calculate E_{min}, E_F, and β and extract the scaling behavior by fits analog to those in the inset of Fig. 9.4.

Option one is to keep $\omega_\parallel$ fixed, which is similar to the previous method but now we keep the particle number N fixed, option two ensures a constant $\omega_\perp$, while option three leaves the volume of the trap unchanged. Strictly speaking, all scaling possibilities could already be deduced from options one and two but we add option three for illustration. Table 1 lists the exponents p of the corresponding dependence of $E_{\mathrm{min}}\tau_{\mathrm{trap}} \to \lambda^p E_{\mathrm{min}}\tau_{\mathrm{trap}}$ for each option.

Our numerical study shows that the scaling of both $\beta\tau_{\mathrm{trap}}$ and $E_{\mathrm{min}}\tau_{\mathrm{trap}}$ is –independent of the way in which the scaling of the aspect ratio r is performed– proportional to $\lambda^{2/3}$. The scaling of $E_{\mathrm{min}}\tau_{\mathrm{trap}}$ follows directly from the gap equation (10.36): we consider Δ_k to be located at the bottom of a subband, i.e., $\xi_k \approx \mu$, and omit the term introduced for regularization. Then, according to Eq. (9.5) $\Delta_k/E_k \approx 1$ holds true and the effect of the scaling is determined by

[13] In the homogeneous dynamical BCS theory both the frequency of the oscillations and the average value is given by the gap.

way of scaling	$\omega_\parallel$	$\omega_\perp$	τ_{trap}	E_F	$E_{\text{min}}\tau_{\text{trap}}$
1: $\omega_\parallel = \text{const}$	0	1	0	2/3	2/3
2: $\omega_\perp = \text{const}$	-1	0	1	-1/3	2/3
3: $\text{Vol} = \text{const}$	-2/3	1/3	2/3	0	2/3

Table 1: Scaling exponents p of λ for the relevant quantities of a cigar-shaped cloud when scaling the aspect ratio as $r \to \lambda r$ and fixed particle number N.

$V_{kk'} \propto a\,\omega_\perp \omega_\parallel^{1/2}$. Bearing in mind, that we keep $1/(k_F a)$ fixed which implies a scaling of the scattering length as $a \propto k_F^{-1} \propto E_F^{-1/2} \propto V^{-1/3}$, this yields in all three options $E_{\text{min}}\tau_{\text{trap}} \propto \lambda^{2/3}$, as one can deduce from Table 1. Additionally, this also implies $\beta\tau_{\text{trap}} \propto \lambda^{2/3}$, since $\beta \propto E_{\text{min}}$ as argued in Sec. 9.4.2.

However, we point out that from the inset of Fig. 9.4 we find a different scaling of $\beta\tau_{\text{trap}}$ which can be explained by the fact that the particle number is changed when keeping the parameter s = const. If we keep s = const. and scale the aspect ratio as $r \to \lambda r$ we find from our analysis that $N \to \lambda N$ and, hence, $E_F \to \lambda E_F$. However, in order to generalize our previous findings to any scaling of the aspect ratio thus to experimentally more relevant systems in a cigar-shaped trap, we will discuss the behavior for larger particle numbers in the next subsection.

9.4.5 Large system

We will now consider a cloud of ^{6}Li atoms in a cigar-shaped trap with larger particle numbers and calculate the smallest BdG quasiparticle energy E_{min} of the system. As argued above the relevant time scales of the dynamics are set by this pairing property for a fixed quench. Hence, in this section we extend our systematic analysis to much larger particle numbers up to $N \sim 10^5$ by only calculating the ground-state properties of the given system. A full dynamical calculation of these systems is not possible due to numerical constraints.

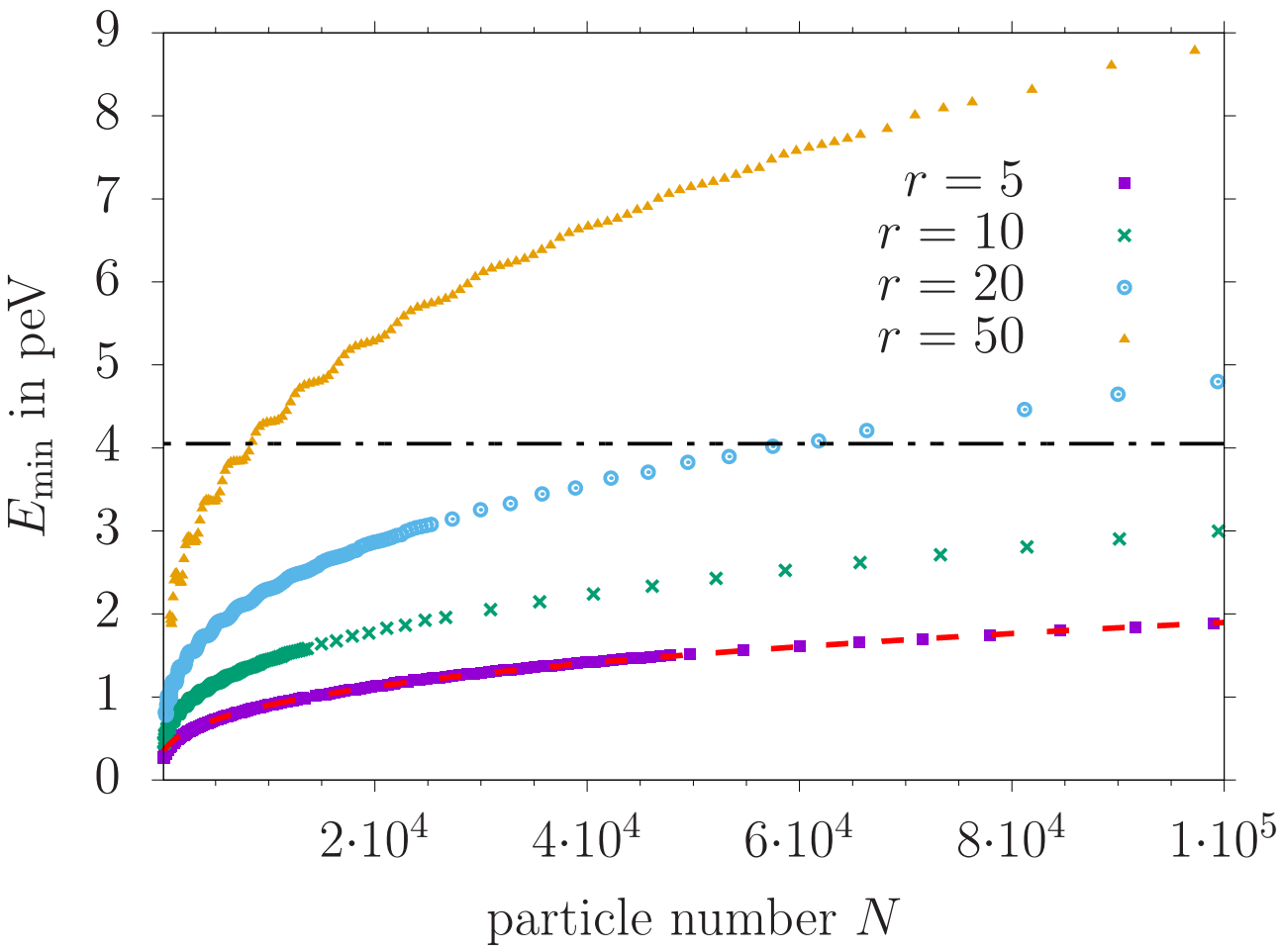

Figure 9.5: Minimal BdG quasiparticle energy E_{min} for various aspect ratios in dependence of the particle number N. The red dashed line is a fit $E_{\mathrm{min}} = a\,N^{1/3} + b$ to the data for $r = 5$ and the dash-dotted black line is the value of E_{min} for $N = 1 \cdot 10^6$ obtained from the fit.

Figure 9.5 shows the increase of the smallest BdG eigenenergy E_{min} in dependence of the particle number N, where the aspect ratio is scaled such that $\omega_{\parallel} = \text{const.}$. The dashed red line shows a fit $E_{\mathrm{min}} = a\,N^{1/3} + b$ for an aspect ratio $r = 5$ and the oscillations visible for small particle numbers are the aforementioned quantum size oscillations [Shanenko *et al.*(2012)], which can be neglected for the general analysis of the scaling in this paper. Overall, we extract from our numerical data that $E_{\mathrm{min}} \propto N^{1/3}$ for all aspect ratios r which also implies that $\beta \propto N^{1/3}$.

With this result, we now go back to the case discussed in Sec. 9.4.3 where the parameters s and $\omega_{\parallel}$ are fixed which implies that the particle number scales with $N \propto r$. Combining the general scaling properties of $E_{\mathrm{min}}\tau_{\mathrm{trap}} \propto r^{2/3}$ in Table 1 with the dependence on the particle number yields $T_{\mathrm{Higgs}} \propto 1/f_{\mathrm{Higgs}} \propto 1/E_{\mathrm{min}} \propto 1/r$ and $\beta \propto E_{\mathrm{min}} \propto r$. This is in good agreement with the inset of Fig. 9.3 and the inset of Fig. 9.4, respectively.

Furthermore, the black dash-dotted line shows the value of E_{min} for $N = 1 \cdot 10^6$ as obtained from the shown fit. From the intersections with the black dash-dotted line obtained in Fig. 9.5 we can choose system parameters with rather small particle numbers which resemble closely the situation in a system with a far larger particle number but smaller aspect ratio. In the next section we present the calculation of the condensate fraction for a system with $r = 50$ and $N = 8428$ for this reason.

9.4.6 Condensate fraction

We obtain the condensate fraction of the system following the usual definition of the condensate fraction c of the order parameter [Leggett(2006)], which yields

$$c = \frac{V}{Ng^2} \int d^3r \, |\Delta(\mathbf{r})|^2 \,, \tag{9.16}$$

where V is the volume, N the particle number, and g the interaction strength. In Fig. 9.6 the dynamics of the condensate fraction and the modulus of the averaged gap is shown for a system with an aspect ratio of $r = 50$ and a particle number $N = 8428$. This is the system that energetically resembles a system with an aspect ratio of $r = 5$ and a particle number of $N = 1 \cdot 10^6$.

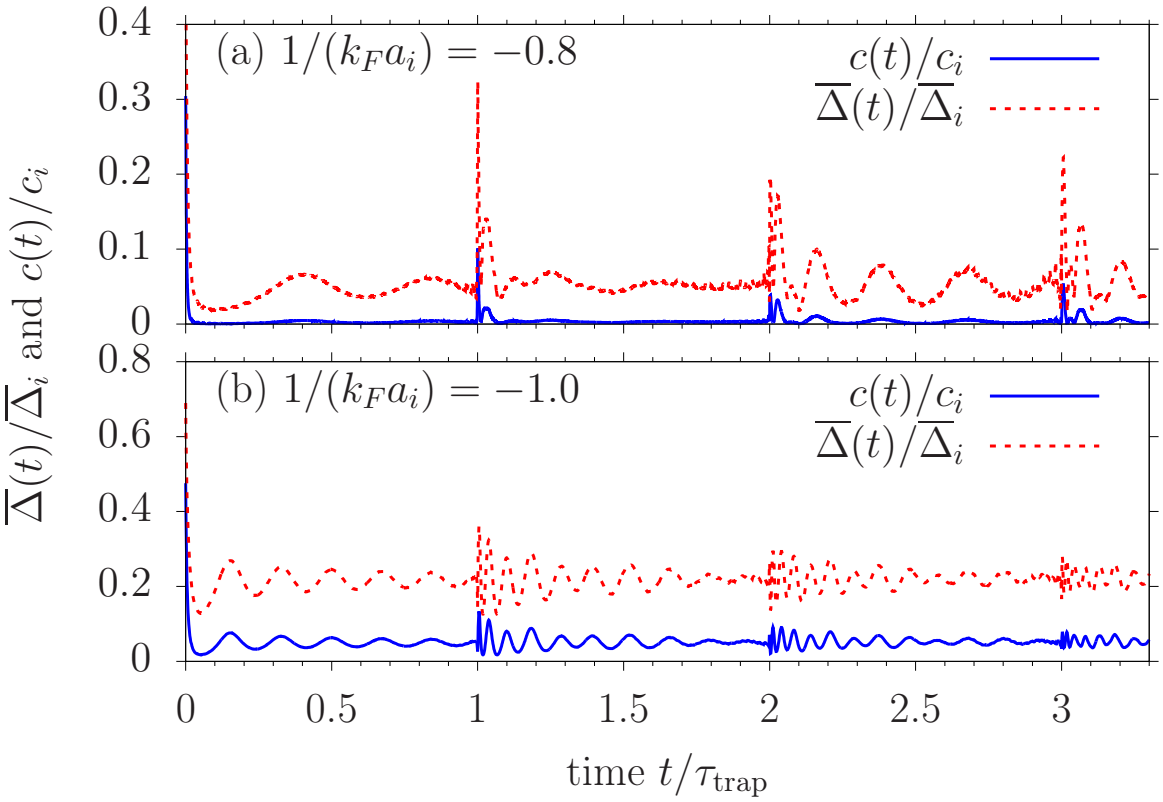

Figure 9.6: Condensate fraction (blue solid line) and modulus of averaged order parameter (red dashed line) after a quench to $1/(k_F a_f) = -1.45$ from (a) $1/(k_F a_i) = -0.8$ and from (b) $1/(k_F a_i) = -1.0$, with an aspect ratio $r = 50$, and a particle number $N = 8428$. The data is normalized to the ground-state value of the initial system c_i and $\overline{\Delta}_i$, respectively.

From Fig. 9.6(a) it becomes apparent that the visibility of the signature of the Higgs mode is reduced in the signal of the condensate fraction due to the quadratic dependence on the order parameter. While the signal still contains all frequencies inherited from the Higgs mode, the amplitude of these oscillations is barely visible and the resulting dynamics of the condensate fractions fulfills all requirements to be identified as vanishing. In the case of a smaller quench, i.e., further away from the transition, the signal of the condensate fraction is large enough to maintain the visibility of the Higgs mode, i.e., its shape and, hence, main frequency, as is shown in Fig. 9.6(b).

Overall, the condensate fraction could provide a measure to detect amplitude oscillations of the superfluid gap in an ultracold Fermi gas. However, due to the quadratic dependence on the gap the condensate fraction is already for rather small quenches reduced to $\lesssim 10\%$ of the

initial condensate fraction. This can make it challenging to detect oscillations in a time-resolved manner. Further, when analyzing the transition to a vanishing order parameter this will lead to observing a shift of the transition to smaller quench strength. However, we expect the finite-size effects to be qualitatively identical for the condensate fraction as previously discussed for the modulus of the spatially averaged order parameter since all main frequencies are inherited.

9.5 Fitting procedure

In this Appendix we discuss our fitting routine in order to obtain Δ_∞ in "phase I" and "phase II" from our numerical data $\overline{\Delta}(t)$.

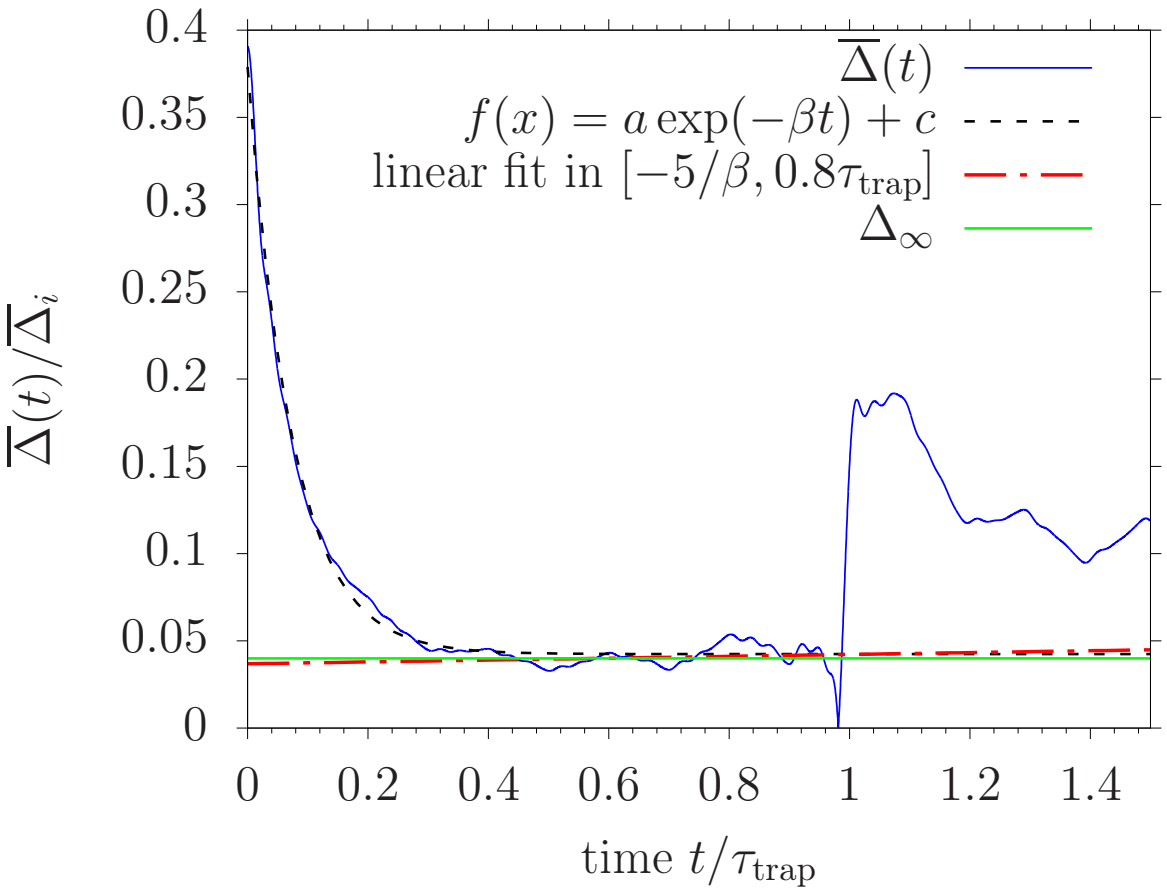

Figure 9.7: Exemplary illustration of our fitting routines in order to obtain Δ_∞ for a system with $r = 10$ and a quench with $1/(k_F a_i) = -0.66$. In this system we find a plateau behavior before τ_{trap}, which is characterized by the non-vanishing mean value of the plateau.

In Fig. 9.7 we show the results of the fitting routines carried out for an exemplary case of $r = 10$ and $1/(k_F a_i) = -0.66$, i.e., a system with a plateau with a non-vanishing height (cf. Fig. 9.3). First, we fit $f(t) = a\exp(-\beta t) + c$ to our data (black dotted line) and check whether $\beta\,\tau_{\text{trap}}/2 > 5$ holds true. If that is the case the initial decay is fast enough that at $t = 0.5\tau_{\text{trap}}$ the amplitude of the oscillations described by an exponential decay contributes with less than 1% to the total signal and a plateau can become visible before τ_{trap} as shown in Fig. 9.7.

Since the exponential fit is only carried out for the initial decay the offset does not identify the visibility of a plateau correctly in the transition between the two phases. Therefore, if $\beta\,\tau_{\text{trap}}/2 > 5$ is fulfilled, we carry out a linear fit from $5/\beta$ to $0.8\,\tau_{\text{trap}}$ and require the relative incline to be less than 10%. If these criteria are met we find a plateau and choose Δ_∞ to be the mean value for $5/\beta \leq t \leq 0.8\,\tau_{\text{trap}}$; otherwise, we take Δ_∞ as the arithmetic mean over the whole calculation time. The lower bound of the interval is motivated by the initial exponential

decay while the upper bound ensures that the emergence of the peak at τ_{trap} does not hinder a detection of a visible plateau. A linear fit is necessary to rule out oscillatory behavior as, for example, seen in the red dash-dotted line in Fig. 9.2. This routine enables us to systematically distinguish between the dynamical vanishing of the gap including the height of the plateau and linear dephasing dynamics of "phase II".

In mean-field theory a phase transition is obtained in the thermodynamic limit, which has previously been done on the case of the homogeneous system [Yuzbashyan *et al.*(2015)]. In order to investigate the confinement-induced effects to the dynamics in such an ultracold Fermi gas the thermodynamic limit is not suitable. This directly implies that the transition between the "phase I" and "phase II" takes place continuously in the inhomogeneous system. The above introduced classification quantifies the effects of the two "phases" and, hence, enables us to investigate the effects of the aspect ratio to this continuous transition. Although the criteria are well motivated from our observations of the dynamical behavior the exact numerical values for each criteria are within a reasonable range arbitrarily. However, changing the criteria within a reasonable range does not have a qualitative effect on the results presented in this paper. Solely, small quantitative changes such as slightly shifted transition points to the vanishing regime or heights of the plateau occur.

10 Observing Dynamical Phases of BCS Superconductors in a Cavity QED Simulator by Young et al.

Abstract

In conventional Bardeen-Cooper-Schrieffer (BCS) superconductors [Bardeen *et al.*(1957)], electrons with opposite momenta bind into Cooper pairs due to an attractive interaction mediated by phonons in the material.

While superconductivity naturally emerges at thermal equilibrium, it can also emerge out of equilibrium when the system's parameters are abruptly changed [Yuzbashyan *et al.*(2006), Barankov and Levitov(2006), Yuzbashyan and Dzero(2006), Gurarie and Radzihovsky(2007), 36, 93, Yuzbashyan *et al.*(2015)].

The resulting out-of-equilibrium phases are predicted to occur in real materials and ultracold fermionic atoms but have not yet all been directly observed.

(I thought, they have been observed, no?)

Here we realise an alternate way to generate the proposed dynamical phases using cavity quantum electrodynamics (cavity QED).

Our system encodes the presence or absence of a Cooper pair in a long-lived electronic transition in ^{88}Sr atoms coupled to an optical cavity and represents interactions between electrons as photon-mediated interactions through the cavity [Lewis-Swan *et al.*(2021), Kelly *et al.*(2022)].

(how???)

To fully explore the phase diagram, we manipulate the ratio between the single-particle dispersion and the interactions after a quench and perform real-time tracking of subsequent dynamics of the superconducting order parameter using non-destructive measurements.

We observe regimes where the order parameter decays to zero (phase I) [Barankov and Levitov(2006), Yuzbashyan and Dzero(2006)], assumes a non-equilibrium steady-state value (phase II) [Barankov and Levitov(2006), Yuzbashyan *et al.*(2006)], or exhibits persistent oscillations (phase III) [Barankov and Levitov(2006), Yuzbashyan *et al.*(2006)].

This opens up exciting prospects for quantum simulation, including the potential to engineer unconventional superconductors and to probe beyond mean-field effects like the spectral form factor [Stewart(2017), Sato and Ando(2017)], and for increasing coherence time for quantum sensing.

(which prospects? beyond mean-field effects???)

Conclusion

The demonstrated capability to emulate dynamical phases of superconductors in optical cavities opens exciting prospects for quantum simulation. For example, it will be interesting to see if our cavity simulator can engineer and probe topological superfluid phases [93, Black-Schaffer(2012), Nandkishore *et al.*(2012), Kiesel *et al.*(2012), Kiesel *et al.*(2013), Fischer *et al.*(2014), Shankar *et al.*(2022)]

(topological superfluid phases???)

and understand competing superconducting orders [Laughlin(1998), Balatsky *et al.*(2006)] in a single system

(competing superconducting orders ????),

or else enable simulation of superfluidity in phenomena relevant to high energy physics [Schäfer and Teaney(2009), Pehlivan *et al.*(2011)].

10.1 Introduction

Quantum simulation offers a path to understand a broad range of phenomena, from high-temperature superconductivity and correlated quantum magnetism in condensed matter physics [Zhou *et al.*(2021)] to quarks and gluons in nuclei and matter under extreme conditions [Shuryak(2017)], as well as the black hole information paradox in gravitational physics [Harlow(2016)].

(interesting, but it is not related to the topic)

A fascinating and promising case is the prethermal dynamical phases [Marino *et al.*(2022)] predicted to emerge from quenches of superconductors and superfluids [Yuzbashyan *et al.*(2006), Barankov and Levitov(2006), Yuzbashyan and Dzero(2006), Gurarie and Radzihovsky(2007), 36, 93, Yuzbashyan *et al.*(2015), Volkov,Kogan (1973), Yuzbashyan *et al.*(2005), Barankov *et al.*(2004), Yuzbashyan(2008), Foster *et al.*(2014), Collado *et al.*(2023)], systems that feature Cooper pairing of electrons or neutral fermions.

(just a collection of relevant citations)

While there has been great progress in pump-probe experiments of superconductors to induce such fast quenches using THz technology, and signs of phases I and II have been observed, the intense pulses couple nonlinearly to the Cooper pairs in the superconductor and complicate a clean observation of the dynamical phases [Mansart *et al.*(2013), Matsunaga *et al.*(2013), Matsunaga *et al.*(2014)].

(I'll read it, I don't know yet, why is it so?)

For these reasons, the realisation of fermionic superfluids in ultracold atomic gases [Randeria and Taylor(2014)] has generated great excitement [Yuzbashyan *et al.*(2006), Barankov and Levitov(2006), Yuzbashyan and Dzero(2006), Gurarie and Radzihovsky(2007), 36, 93, Yuzbashyan *et al.*(2015)]; however, to date observations have been limited to spectroscopic signatures rather than the full time dynamics [Behrle *et al.*(2018)].

(spectroscopic signatures ???)

In neither system has a systematic scan of the dynamical phase diagram been performed, and in fact phase III has not been observed.

(dynamical phase diagram ????)

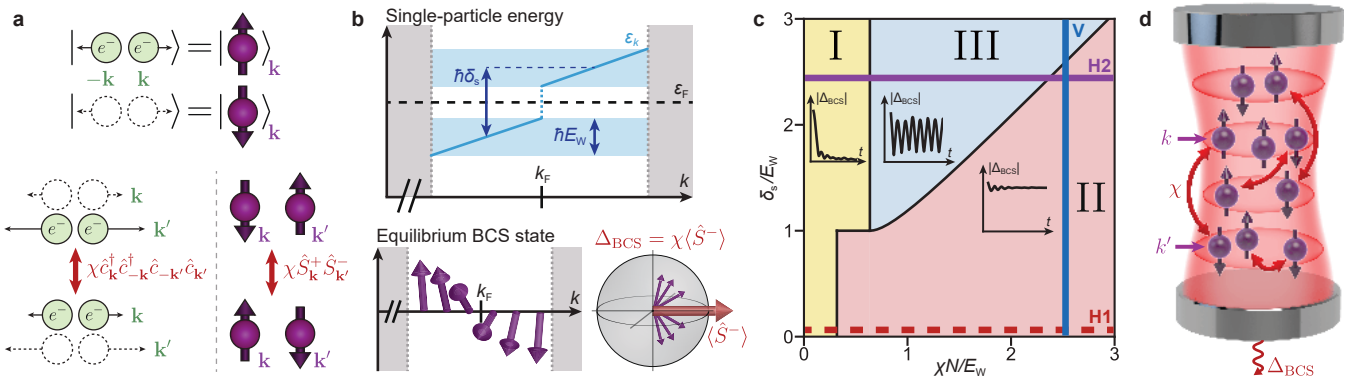

Figure 10.1: **Engineering BCS dynamical phases. a**, The Anderson pseudospin mapping encodes the presence and absence of a Cooper pair as the up and down states of a spin-1/2 system, respectively. Under this mapping, the attractive interaction $\chi\hat{c}^\dagger_{\mathbf{k}}\hat{c}^\dagger_{-\mathbf{k}}\hat{c}_{-\mathbf{k}'}\hat{c}_{\mathbf{k}'}$ between electrons is equivalent to an all-to-all exchange interaction $\chi\hat{S}^+_{\mathbf{k}}\hat{S}^-_{\mathbf{k}'}$ between pseudospins. **b**, Model parameters. The top plot shows the effective dispersion relation near the Fermi surface engineered in our system as a function of parameters δ_s and E_W, controlled using AC Stark shifts. The bottom plot visualises the ground state of a BCS superconductor using Anderson pseudospins. Near the Fermi momentum, the pseudospins develop a phase-coherent superposition at a scale set by a nonzero BCS pairing gap Δ_{BCS}. This gap is self-consistently defined from the spin coherence as shown on the Bloch sphere. **c**, Dynamical phase diagram. The three dynamical phases can be realised by varying parameters χN, δ_s, and E_W. Representative dynamics of the BCS order parameter $|\Delta_{BCS}|$ for each phase are shown as insets. We explore cut H1 (dashed line) in Fig. 10.2 using a single ensemble of atoms and cuts V and H2 (solid lines) in Figs. 10.3 and 10.4 using two separately controlled sub-ensembles. **d**, Cavity QED implementation of the BCS interaction. Coupling many strontium atoms to a detuned optical cavity generates infinite-range spin-exchange interactions mediated by a virtual exchange of cavity photons. This interaction also causes a field proportional to Δ_{BCS} to leak out of the cavity, providing a real-time probe of the dynamics.

Here, we take a step forward towards this challenge by using internal electronic states to encode effective Cooper pairs. (I have no idea what is meant here)

At the heart of this implementation is the Anderson pseudospin mapping [Anderson(1958)] by which the presence or absence of Cooper pairs in a momentum mode is encoded in a pseudo spin-1/2 system. We simulate Anderson pseudospins using a long-lived electronic transition in ^{88}Sr with interactions between the spins mediated by a high finesse optical cavity. (how????)

As proposed in Refs. [Lewis-Swan *et al.*(2021), Kelly *et al.*(2022)], the scattering between Cooper pairs in condensed matter systems can be engineered in our system via the exchange of photons through the cavity (see Fig. 10.1**d**).

(read their article, tell why it can be so??? I have no idea now)

In this way, the dynamics of a collection of interacting spin-1/2 systems maps onto the low-energy physics of a superconductor or superfluid.

We probe all three dynamical phases (phases I, II, and III) predicted to exist in BCS superconductors

(where was this prediction made???)

by utilising the high degree of control and flexibility in state initialisation, interaction control, and non-destructive measurements available when coupling long-lived atoms to an optical cavity. Behaviours intrinsic to phase I (normal phase) and phase II (finite steady-state superconductivity) have previously been observed in spin systems realized in optical cavities

[Davis *et al.*(2020), Norcia *et al.*(2018a)] and in two-level atoms interacting via collisions [Allred *et al.*(2002), Kleine *et al.*(2008), Deutsch *et al.*(2010), Smale *et al.*(2019)].

We build on this work by clarifying the connection between these dynamical phases from the BCS model and the physics of many-body gap protection in spin systems.

(what is the second, gap protection??)

Our results also provide the first demonstration of phase III (a self-generated Floquet phase featuring persistent oscillations of the order parameter), which is predicted to dynamically emerge in superconductors via quenches from weak to strong interactions [Barankov and Levitov(2006), Yuzbashyan *et al.*(2015)]. In our system, we instead engineer this phase using flexible control of the single-particle dispersion [Lewis-Swan *et al.*(2021), Collado *et al.*(2023)] (to understand it, I would need to read these articles), dynamically resembling the low-energy condition of a BCS superconductor.

For all experiments, we perform real-time tracking of the superconducting order parameter, enabling fast readout of the dynamics.

10.2 Experimental setup and model system

To realise dynamical phases of the BCS model, we laser cool an ensemble of $N = 10^5 - 10^6$ ^{88}Sr atoms and trap them inside a $\lambda_L = 813$ nm 1D optical lattice supported by a high-finesse optical cavity.

(what is an optical lattice?)

A spin-1/2 system is encoded in the electronic ground state $|\downarrow\rangle = |^1S_0, m_J = 0\rangle$ and a long-lived optical excited state $|\uparrow\rangle = |^3P_1, m_J = 0\rangle$.

Along this transition, we define spin operators $\hat{S}_k^- = |\downarrow\rangle\langle\uparrow|_k$ and $\hat{S}_k^z = (|\uparrow\rangle\langle\uparrow|_k - |\downarrow\rangle\langle\downarrow|_k)/2$ for single atoms with labels $k \in \{1, ..., N\}$, as well as the collective lowering operator $\hat{S}^- = \sum_k \hat{S}_k^-$ and raising operator $\hat{S}^+ = (\hat{S}^-)^\dagger$.

Assuming homogeneous atom-light coupling in the cavity and unitary dynamics, our system can be described by the Hamiltonian

$$\hat{H} = \hbar\chi\hat{S}^+\hat{S}^- + \sum_k \varepsilon_k \hat{S}_k^z. \tag{10.1}$$

The first term represents an infinite-range spin-exchange interaction described by a frequency scale χ [Norcia *et al.*(2018a)], realised using the collective coupling between the atomic ensemble and a detuned optical cavity mode.

(why????? what is the meaning of these spins?? need to study [Norcia *et al.*(2018a)])

Inhomogeneous atom-light coupling and dissipative processes (including, foremost, single-particle spontaneous decay) are present in the current implementation but do not largely change the qualitative behaviour of the targeted dynamical phases under our experimental conditions (see Methods). Previously, we have characterised this interaction [Norcia *et al.*(2018a)] and studied collective dynamics by applying an external drive [Muniz *et al.*(2020)]. In this work, we go beyond the fully collective manifold by engineering a spread in single-particle energies $\varepsilon_k = \hbar\omega_k$ using applied AC Stark shifts ω_k [Baghdad *et al.*(2023), Sauerwein *et al.*(2023)]. These shifts form the second term in the Hamiltonian and compete with the spin-exchange interaction.

Equation (10.1) is the so-called Richardson-Gaudin spin model [Richardson and Sherman(1964), Gaudin(1976)], which describes the low-energy physics of

Bardeen-Cooper-Schrieffer (BCS) superfluids and superconductors using the Anderson pseudospin mapping [Anderson(1958)].

(read their paper!!??)

This mapping relates the presence (or absence) of a Cooper pair formed by a pair of electrons with momenta $\pm\mathbf{k}$ to a spin-up (or down) at momentum $\mathbf{k}$, as shown in Fig. 10.1**a**. Correspondingly, annihilating a Cooper pair maps to a spin lowering operator by the relation $\hat{S}^-_{\mathbf{k}} := \hat{c}_{\mathbf{k}}\hat{c}_{-\mathbf{k}}$, where $\hat{c}_{\pm\mathbf{k}}$ are fermionic annihilation operators. Similarly, the spin operator $2\hat{S}^z_{\mathbf{k}} + 1 := \hat{c}^\dagger_{\mathbf{k}}\hat{c}_{\mathbf{k}} + \hat{c}^\dagger_{-\mathbf{k}}\hat{c}_{-\mathbf{k}}$ counts the number of electrons with momentum $\mathbf{k}$ or $-\mathbf{k}$. Our cavity system therefore manifestly implements a BCS superconductor if one identifies the label k of an atom in the cavity with the momentum $\mathbf{k}$ of the electrons in a Cooper pair. In this way, the first term in Eq. (10.1) is equivalent to the attractive interaction between electrons in the superconductor, and the second term can be associated with the kinetic energy or dispersion relation of the electrons. Note that the BCS model, described by Eq. (10.1), only accounts for the zero momentum collective excitations present in conventional superfluids and superconductors [Anderson(1958)].

The BCS order parameter in the Anderson mapping is defined by $\Delta_{\mathrm{BCS}} = \chi\langle\sum_{\mathbf{k}} \hat{c}_{\mathbf{k}}\hat{c}_{-\mathbf{k}}\rangle = \chi\langle\hat{S}^-\rangle$, as depicted in Fig. 10.1**b**.

In equilibrium, it plays the role of the BCS pairing gap, which energetically favours many-body states where the electrons arrange in a coherent superposition between Cooper pairs and holes for states close to the Fermi energy.

Away from equilibrium, Δ_{BCS} is also predicted to characterise the three dynamical phases (I, II, and III) that arise after quenches in superconductors and superfluids [Marino *et al.*(2022)].

(so they don't call it the gap??? what then do they mean by the "dynamical phase"??)

Such dynamical phases represent distinct regimes of dynamical behaviour that arise after a sudden perturbation of a control parameter in a closed many-body system.

They are described using a time-averaged or steady-state order parameter that demonstrates non-analytic behaviour at the boundary between phases.

(a very unclear sentence. regimes use some secret steady-state order parameter? what is it??)

In particular, the BCS model is predicted to exhibit second-order dynamical phase transitions.

(what is it??)

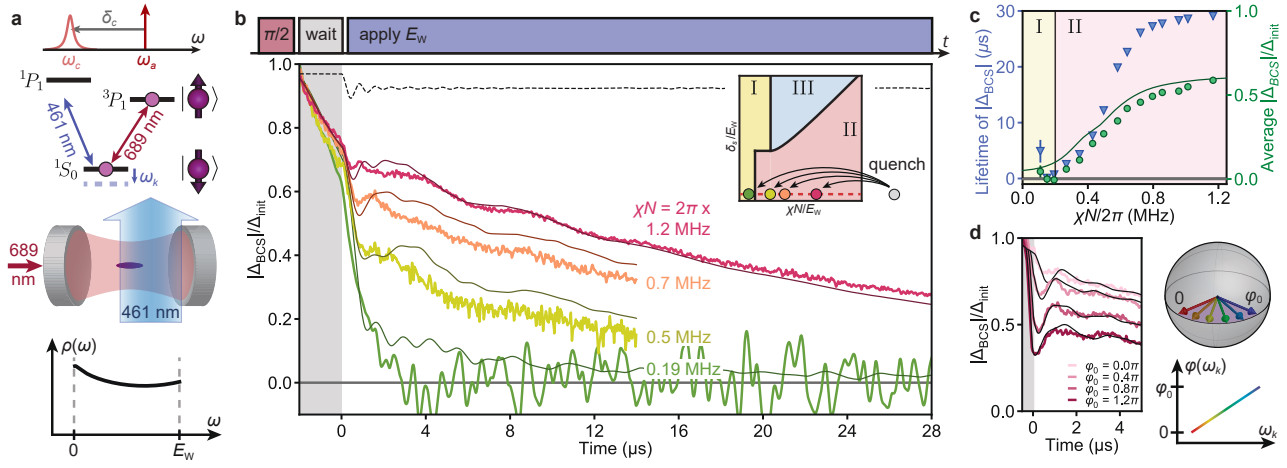

Figure 10.2: **Phase I to phase II transition.**

Explanation of 10.2. **a**, Tuning the single-particle dispersion. We shine an off-resonant 461 nm beam onto the atoms from outside the cavity. This generates a distribution of AC

Stark shifts representing a roughly uniform density of states $\rho(\omega)$ (bottom plot). **b**, Probing phase I and phase II. We perform a rapid $\pi/2$ pulse to prepare a highly coherent initial state, wait for 2 μs, quench to a variable $\chi N/E_{\mathrm{W}}$ with $\delta_{\mathrm{s}} = 0$, and then let the system evolve. The inset shows the explored parameter cut and identifies post-quench $\chi N/E_{\mathrm{W}}$ values with coloured dots. The main plot shows experimental time traces of $|\Delta_{\mathrm{BCS}}|$ (coloured curves) accompanied by numerical simulations (darker lines). Two curves are extended to demonstrate long-time coherence protection, with the $\chi N/2\pi = 0.19$ MHz trace smoothed for clarity. For $\chi N/2\pi = 1.2$ MHz, we show an ideal simulation neglecting dissipation and motional effects (dashed line), which exhibits transient Higgs oscillations. Hints of these oscillations are present in experimental data with additional damping. **c**, Characterising the phase transition. Blue triangles show the fitted coherence time of $|\Delta_{\mathrm{BCS}}|$ from $t = 1$ μs to 30 μs. Green circles show the time-averaged $|\Delta_{\mathrm{BCS}}|$ between $t = 3$ μs and 8 μs, with the dark green line representing numerical simulations. In all cases, we identify a phase transition at $\chi N/2\pi = 0.2$ MHz. Error bars in all plots represent the s.e.m. of boostrap resamplings on experimental shots. **d**, Varying initial conditions. Before $t = 0$, we shine a high-intensity 461 nm beam within 300 ns, engineering an initial phase spread $\varphi(\omega_k) \in [0, \varphi_0]$ depicted on the Bloch sphere. The phase $\varphi(\omega_k)$ applied to atom k is proportional to the post-quench frequency shift ω_k. Traces represent different φ_0 and show enhanced oscillations with increasing φ_0.

Phase I is characterised by a steady state with a vanishing order parameter $|\Delta_{\mathrm{BCS}}(t)| \to 0$ at long times. Phase II exhibits a steady state with a constant nonzero order parameter $\Delta_\infty := \lim_{t\to\infty} |\Delta_{\mathrm{BCS}}(t)| > 0$. Finally, phase III features oscillations in $|\Delta_{\mathrm{BCS}}(t)|$ that persist to long times, realising a Floquet superfluid despite not being periodically driven [Foster *et al.*(2014), 93, Yuzbashyan *et al.*(2015), 36]. The long-time behaviour of these dynamical phases admits a simpler description in terms of the Lax-reduced Hamiltonian, which is an effective Hamiltonian taking the same form of Eq. (10.1) but with rescaled parameters and a reduced number of spins [Yuzbashyan *et al.*(2015), Marino *et al.*(2022)]. Under this formulation, phases I, II, and III emerge when the Lax-reduced Hamiltonian describes effective zero-spin, one-spin, and two-spin systems respectively.

Inspired by the Lax-reduced Hamiltonian, and in order to explore all three dynamical phases, we engineer two sub-ensembles of atoms with separate control over energy shifts within each sub-ensemble. For practical convenience, we introduce experimental control in the form of an overall frequency splitting δ_{s} between two sub-ensembles and an effective frequency width E_{W} of each sub-ensemble to engineer a tunable dispersion relation ε_k as in Fig. 10.1**b**. Phase I and phase II can also be observed using a single ensemble of atoms as shown in Fig. 10.2. Both experimental setups can nonetheless be described by a common phase diagram as shown in Fig. 10.1**c**.

We initialise all the atoms in the $|\downarrow\rangle$ state and then apply a coherent $\pi/2$ pulse through the cavity in 100 ns such that $\Omega \gg \chi N$, where Ω is the pulse Rabi frequency and χN is the characteristic interaction strength for an ensemble of N atoms. This establishes a large BCS order parameter Δ_{BCS} on a timescale faster than any other relevant dynamics, mimicking the ground state of a Hamiltonian with an infinite interaction strength χ. We then quench the system by rapidly turning on ε_k, which sets a finite ratio $\chi N/E_{\mathrm{W}}$ and a variable $\delta_{\mathrm{s}}/E_{\mathrm{W}}$, allowing us to explore the dynamical phase diagram shown in Fig. 10.1**c**.

We measure both the pre- and post-quench dynamics of $|\Delta_{\mathrm{BCS}}|$ by monitoring light emitted by the atoms into the cavity as a function of time (see Fig. 10.1**d**).

This light arises from a superradiance process which is suppressed when the cavity resonance is detuned from the atomic transition frequency by much more than κ, the cavity power decay linewidth [Weiner *et al.*(2012), Bohnet *et al.*(2013), Norcia *et al.*(2016)].

(what it the superradiance? what is going on in the cited articles??)

In this limit, the established cavity field adiabatically follows $\langle \hat{S}^- \rangle$, which is proportional to Δ_{BCS}. By measuring the leakage of light from the cavity in heterodyne with a local oscillator, we therefore obtain a real-time probe of Δ_{BCS}.

(how is it???)

Importantly, at the chosen detuning this probe is quasi-nondestructive, since only a small fraction of the atoms emit light over relevant timescales. In plots of $|\Delta_{\mathrm{BCS}}|$ over time, we normalise traces to the initial gap size Δ_{init} measured right after the $\pi/2$ pulse.

10.3 Phase I to phase II

We probe the phase I to phase II transition by varying the ratio $\chi N/E_{\mathrm{W}}$ between the interaction strength and the width of the single-particle energy distribution. As shown in Fig. 10.2**a**, we shine an off-resonant 461 nm beam onto a single atomic ensemble from the side of the cavity that generates a distribution of AC Stark shifts with a spread E_{W}. Careful shaping of the 461 nm beam allows us to realise a roughly flat density of states (see Methods), resulting in a setup consistent with the $\delta_{\mathrm{s}} = 0$ line in Fig. 10.1**c** (see Supplemental Online Material). After the initial $\pi/2$ pulse, we wait for 2 μs to let transient dynamics settle and then turn on the 461 nm beam to quench on $E_{\mathrm{W}}/2\pi = 0.83$ MHz from an initial value $E_{\mathrm{W}}^{(0)}/2\pi \ll 0.1$ MHz. The beam exhibits a rise time of roughly 50 ns, much faster than the relevant dynamics. To scan across the phase diagram in the inset of Fig. 10.2**b**, we vary the interaction strength χN between shots by changing the atom number N.

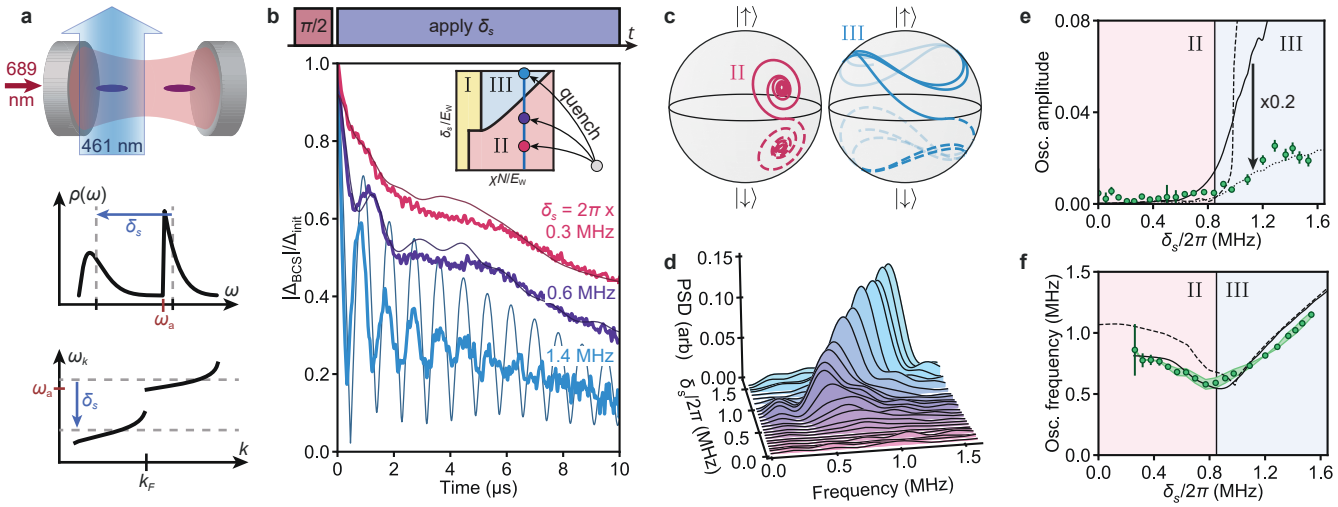

Figure 10.3: **Phase II to phase III transition.** **a**, Engineering a bimodal energy distribution. We prepare two atomic clouds with centres separated by 3 mm and shine an off-resonant 461 nm beam centred on one cloud. This generates a density of states $\rho(\omega)$ (middle plot), equivalent to a dispersion relation $\varepsilon_k = \hbar\omega_k$ (bottom plot). **b**, Probing phase II and phase III. We prepare the same initial state as in Fig. 10.2**b** with a $\pi/2$ pulse, quench to a finite δ_s/E_W, and then let the system evolve. The inset shows the explored parameter cut and identifies post-quench δ_s/E_W values with coloured dots. As before, coloured traces represent experimental time traces of $|\Delta_{BCS}|$, and darker lines represent numerical simulations. **c**, Ideal simulations of mean-field trajectories for the two sub-ensembles (solid and dashed curves) in phase II (magenta) and phase III (blue). The trajectories are projected onto the surface of the Bloch sphere for visual clarity. **d**, Fourier response of $|\Delta_{BCS}|^2$ for different δ_s, plotted as power spectra of the dynamics from $t = 0.5$ μs to 4 μs after subtracting slow-moving behaviour. **e**, Average oscillation amplitude between $t = 3$ μs and 8 μs. For the remaining plots, dashed lines represent ideal simulations (ignoring dissipation or motional effects), and solid dark lines correspond to full simulations. The additional dotted line represents numerical simulations rescaled by $\times 0.2$, plotted to show similar trend behaviour between experimental data and simulations. We identify a phase transition around $\delta_s/2\pi = 0.85$ MHz. **f**, Oscillation frequency of $|\Delta_{BCS}|$, measured using power spectra calculated in (**d**). We correct for systematics inferred from our data analysis and assume this correction has an uncertainty of 100%, shown by the green band. The phase transition point observed in data in panels (**e**) and (**f**) agrees well with simulations.

As shown in Fig. 10.2**b** and **c**, we observe two distinct dynamical behaviours corresponding to phases I and II, signalled by the decay rate of $|\Delta_{BCS}|$. For experiments with sufficiently small χN, such as $\chi N/2\pi = 0.19$ MHz, $|\Delta_{BCS}|$ decays with a $1/e$ coherence time of 0.9 ± 0.1 μs. This coherence time is consistent with single-particle dephasing of $\langle \hat{S}^- \rangle$ set by the energy spread $\hbar E_W$ and is nearly constant throughout this regime. We identify the fast decay of $|\Delta_{BCS}|$ as an experimental signature of phase I. For larger interaction strengths, we observe a rapid increase in coherence time up to a maximum of 29 μs when $\chi N/2\pi = 1.2$ MHz; this constitutes an improvement of more than a factor of 30. We identify this extended coherence time regime as phase II. The residual decay of $|\Delta_{BCS}|$ in this regime can be attributed to intrinsic dissipative processes including spontaneous emission, off-resonant superradiant emission, and scattering of 461 nm light [Norcia *et al.*(2016), Norcia *et al.*(2018a)], which set a maximum predicted coherence time of 29 μs (see Methods). All experimental observations (coloured traces) are in good agreement with numerical simulations based on experimental conditions (dark lines—see Methods).

Due to the separation of timescales in the decay of $|\Delta_{\mathrm{BCS}}|$, we are able to determine the boundary between phase I and phase II in our experiment by calculating the average $|\Delta_{\mathrm{BCS}}|$ in a time window from 3 μs to 8 μs as a function of χN (see Fig. 10.2**c**). In this analysis, phase I features a vanishing average $|\Delta_{\mathrm{BCS}}|$, while phase II sees a nonzero $|\Delta_{\mathrm{BCS}}|$ that increases with χN. The sharp rise of average $|\Delta_{\mathrm{BCS}}|$ around $\chi N/2\pi = 0.2$ MHz indicates a dynamical phase transition, which agrees with the point predicted by numerical simulations. In a spin-model picture, the BCS pairing gap corresponds to the energy gap between collective angular momentum states, which exists due to the spin-exchange interaction $\chi\hat{S}^{+}\hat{S}^{-}$ [Rey *et al.*(2008)]. Phase II corresponds to the parameter region where such interactions are sufficiently strong to protect against single-particle dephasing. As a result, the observed transition directly relates to previous experiments exploring coherence protection in other systems [Davis *et al.*(2020), Norcia *et al.*(2018a), Smale *et al.*(2019), Deutsch *et al.*(2010), Kleine *et al.*(2008), Allred *et al.*(2002)].

In BCS superconductors, the excitation of a Higgs mode is predicted to occur in phase II. This mode can be characterised by a collective damped oscillation of the order parameter $|\Delta_{\mathrm{BCS}}|$ with a characteristic frequency of $2\Delta_{\infty}$ [Yuzbashyan *et al.*(2015)]. We observe hints of Higgs oscillations by comparing the experimental trace of $|\Delta_{\mathrm{BCS}}|$ at $\chi N/2\pi = 1.2$ MHz (red curve in Fig. 10.2**b**) with the dissipation-free simulation (dashed line in Fig. 10.2**b**) and noticing that the first dip in the experimental trace coincides with the first cycle of Higgs oscillations (see Methods). The size of this feature can be increased experimentally by engineering an initial phase spread $\varphi(\omega_k) \in [0, \varphi_0]$ between atoms which is correlated with the post-quench frequency shifts ω_k of the atoms, as shown in Fig. 10.2**d**. The initial state with a nonzero opening angle φ_0 shares qualitative features with the BCS ground state at finite χ up to a $\pi/2$ rotation on the Bloch sphere [Lewis-Swan *et al.*(2021)], in contrast to the initial state mimicking the BCS ground state with infinite χ in Fig. 10.2**b**.

10.4 Phase II to phase III

We probe the phase II to phase III transition using a vertical cut through the dynamical phase diagram. To realise this, we introduce an energy splitting $\hbar\delta_{\mathrm{s}}$ between two individually addressable clouds of atoms along the cavity axis using AC Stark shifts from our 461 nm beam, as shown in Fig. 10.3**a**. In combination with a background energy spread $\hbar E_{\mathrm{W}}$ associated with lattice shifts (see Methods), this produces a bimodal density of states and a dispersion relation similar to the one proposed in Fig. 10.1**b**. As before, we begin the experiment with a highly coherent state and with $\delta_{\mathrm{s}} = 0$. Then, we quench on a nonzero δ_{s} and let the system evolve. Between shots, we scan δ_{s} while fixing $\chi N/2\pi = 0.9$ MHz and $E_{\mathrm{W}}/2\pi \approx 0.34$ MHz to explore the vertical cut.

The resulting dynamics show a marked change in the dynamical evolution of $|\Delta_{\mathrm{BCS}}|$ over the scan as shown in Fig. 10.3**b**, which we attribute to a transition between phase II and phase III dynamics. For small δ_{s}, we either see Higgs-like oscillations which are damped after 3 μs (the trace where $\delta_{\mathrm{s}}/2\pi = 0.6$ MHz) or, for very small splittings, no oscillations resolvable above the noise floor ($\delta_{\mathrm{s}}/2\pi = 0.3$ MHz). We associate this regime with phase II since it overlaps with the previously observed phase II dynamics in parameter space. For larger δ_{s}, curves instead show large-amplitude oscillations that persist for more than 5 μs ($\delta_{\mathrm{s}}/2\pi = 1.4$ MHz). We identify the long-lived oscillations in this parameter regime as an experimental signature of phase III.

Intuitively, we can understand the difference between the two phases by identifying the two sub-ensembles of atoms with two Bloch vectors (see Fig. 10.3**c**). In phase II, a finite δ_{s} causes the Bloch vectors to precess in different directions, but the dominant scale χN locks them together to form the solid and dashed magenta orbits. In the presence of a finite E_{W}, the orbits decay, but the Bloch vectors maintain phase coherence. On the other hand, in phase III δ_{s} is large enough that the two Bloch vectors accrue an unbounded relative phase, as in the blue

orbits. The presence of interactions locks each sub-ensemble separately against a finite E_{W}, leading to persistent oscillations. This effective beating of two large spins in a macroscopic array of spin-1/2 particles is truly an interaction-driven effect since the interactions are strong enough to lock the spins within each sub-ensemble but not strong enough to lock both sub-ensembles together. In our implementation of phase III, the bimodal distribution allows us to dynamically separate the Bloch vectors of the two sub-ensembles, instead of starting with an already split distribution like in weakly interacting BCS ground states featuring a sharp Fermi edge. Despite their qualitative differences, these two situations can be dynamically connected (see Methods).

We can experimentally define a boundary between phase II and phase III using the separation of timescales observed for oscillations in $|\Delta_{\mathrm{BCS}}|$. Fig. 10.3**e** shows the average oscillation amplitude in a time window from $t = 3$ μs to 8 μs. In this analysis, we observe a sharp rise in oscillation amplitude at $\delta_{\mathrm{s}}/2\pi = 0.85$ MHz $\approx \chi N/2\pi$ as we increase δ_{s}, which we identify as a dynamical phase transition. Numerical simulations plotted in Fig. 10.3**e** agree fairly well with data in capturing trend behaviour and estimating the phase transition point. However, we see a discrepancy in the absolute size of the observed and predicted oscillation amplitudes. We attribute this to an extra dephasing mechanism (likely residual motional effects) in our system or other imperfections in the experimental sequence not captured by the theory model.

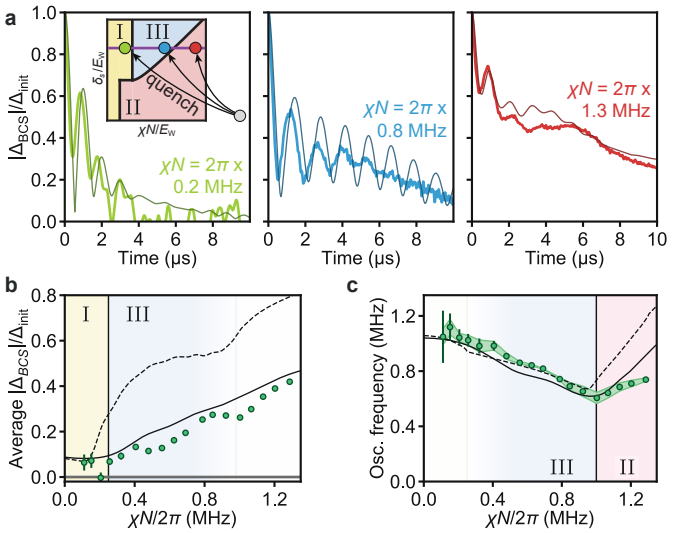

Figure 10.4: **Scan across three dynamical phases. a**, Probing phase I, II and III dynamics using time traces of $|\Delta_{\mathrm{BCS}}|$. Quenches are performed in the same manner as in Fig. 10.3**b**, except between shots we hold post-quench values of δ_{s} fixed and vary χN instead. The inset shows the explored cut through the phase diagram and identifies final $\chi N/E_{\mathrm{W}}$ values with green (phase I), blue (phase III), and red (phase II) dots. The $\chi N/2\pi = 0.2$ MHz trace is smoothed for clarity. **b**, Time average of $|\Delta_{\mathrm{BCS}}|$ in a bin from $t = 3$ μs to 8 μs vs. interaction strength. The experimental data shows signatures of a phase I to phase III transition at $\chi N/2\pi = 0.25$ MHz. **c**, Oscillation frequency of $|\Delta_{\mathrm{BCS}}|$ vs. interaction strength in a bin from $t = 0.5$ μs to 4 μs. Again, we correct for systematics inferred from our data analysis and assume this correction has an uncertainty of 100%, shown by the green band. This data identifies a phase III to phase II transition at $\chi N/2\pi = 1.0$ MHz. Experimental data and transitions in both plots are consistent with numerical simulations.

We verify the location of the phase II to phase III transition using the short-time oscillation frequency (from $t = 0.5$ μs to 4 μs) as an additional experimental signature. As can be seen in the Fourier responses in Fig. 10.3**d** and quantified in Fig. 10.3**f**, the oscillation frequency exhibits a dip vs. δ_{s} at the previously-identified phase boundary. This dip is present in roughly

the same location for experiment and theory and is expected to coincide with the phase II to phase III transition (see Supplemental Online Material).

10.5 Scan across three dynamical phases

Finally, we observe all three dynamical phases in a single cut through parameter space, as shown in Fig. 10.4**a**. We run the same experimental sequence described in Fig. 10.3, but instead scan χN between shots with $\delta_s/2\pi = 1.1$ MHz and $E_W/2\pi = 0.46$ MHz fixed. This allows us to probe phase I, phase III and then phase II by increasing atom number N.

Using order parameters established in Figs. 10.2 and 10.3, we determine boundaries between the three phases. As shown in Fig. 10.4**b**, the long-time average of $|\Delta_{BCS}|$ rises suddenly around $\chi N/2\pi = 0.25$ MHz in both data and simulations. This transition marks the boundary between phase I and phase III. Additionally, at $\chi N/2\pi = 1.0$ MHz we observe a dip in the short-time oscillation frequency of $|\Delta_{BCS}|$ (Fig. 10.4**c**), marking a transition between phase III and phase II. For this scan, we do not use the long-time oscillation amplitude as an order parameter due to poor signal-to-noise for smaller values of χN.

10.6 Methods

10.6.1 Experimental setup: phase I to phase II transition

To explore the phase diagram cut in Fig. 10.2, we first load $10^5 - 10^6$ ^{88}Sr atoms from a magneto-optical trap into an 813 nm optical lattice supported by a high-finesse optical cavity, similar to previous experiments [Norcia *et al.*(2016), Norcia *et al.*(2018b), Norcia *et al.*(2018a), Muniz *et al.*(2020)]. The resulting atomic cloud has a temperature of roughly 15 μK, resulting in a Gaussian distribution transverse to the cavity axis with standard deviation $\sigma_y = \sigma_z = 16$ μm (coordinates defined in Extended Data Fig. 10.1**a**). Further, the cloud is extended over thousands of lattice sites, forming a distribution along the cavity axis with a standard deviation $\sigma_x = 430$ μm. We measure an axial trapping frequency of $\omega_x/2\pi = 165$ kHz, giving a Lamb-Dicke parameter of $\eta = 0.17$ for excitation with 689 nm light. At the measured temperature, $\eta^2(2\bar{n}+1) = 0.11 \ll 1$, placing the atoms in the Lamb-Dicke regime. We set a quantisation axis along $\hat{y}$ with a 2.4 G magnetic field and tune the lattice polarisation to a "magic angle" relative to this axis, such that the differential lattice shift between ground ($|^1S_0\rangle$) and excited ($|^3P_1, m_J = 0\rangle$) states vanishes [Muniz *et al.*(2020)]. Using piezoelectric actuators, we stabilise the cavity length to set the closest TEM_{00} resonance to be 51 MHz red-detuned from the atomic transition.

After loading into the lattice, we initialise the atoms with a $\hat{y}$-polarised drive through the cavity which is nominally resonant with the atomic transition. Because the drive is far off-resonance from the cavity (which has linewidth $\kappa/2\pi = 153$ kHz at 689 nm), the induced Rabi frequency is somewhat suppressed. Nonetheless, we find that roughly 5 mW of power before the cavity is sufficient to drive the atoms with a $\pi/2$ pulse in 100 ns. We allow the atoms to settle for 2 μs in order to distinguish the desired physics from transient dynamics observed after state initialisation, which we attribute to undesired excitation of sideband transitions. We then shine a 461 nm beam from the side of the cavity along the $\hat{y}$ direction, detuned from the $|^1S_0\rangle - |^1P_1\rangle$ transition by more than 10 GHz, in order to induce AC Stark shifts on the ground state. The beam has waists $(w_x, w_z) = (1030\ \mu\text{m}, 75\ \mu\text{m})$ along the $\hat{x}$ and $\hat{z}$ directions at the plane of the atoms, and its centre is displaced from the centre of the atomic cloud by $x_0 = 580$ μm along the cavity axis. From these dimensions, we calculate an atomic density of states $\rho(\omega)$ as a function of frequency shift which is roughly uniform between 0 and a maximum shift $\hbar E_W$. We estimate

that for the power and detuning used in this cut, the 461 nm beam scatters off the atoms with an average rate of $R_{\mathrm{sc}}/2\pi = 1.3$ kHz, roughly a factor of six smaller than $\gamma/2\pi = 7.5$ kHz, the spontaneous emission rate. Combined with collective emission from the atoms as described in the Readout section of the Methods, these dissipation processes set a maximum predicted coherence time in the system of 29 μs.

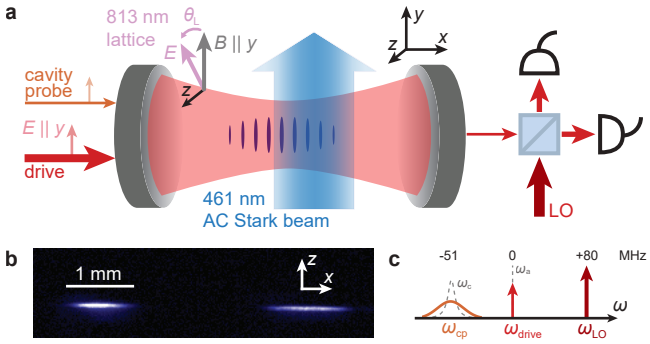

Extended Data Fig. 10.1: **Experimental configuration.** **a**, Detailed diagram of the cavity and all relevant beams. A magnetic field along $\hat{y}$ sets the quantisation axis. The 813 nm optical lattice supported by the cavity has a tunable linear polarisation. We drive a $\pi/2$ pulse with a beam polarised along $\hat{y}$ through the cavity, and during the experiment we probe the cavity resonance frequency using a second $\hat{y}$-polarised beam to measure atom number. A 461 nm beam far-detuned from the $|^1S_0\rangle - |^1P_1\rangle$ transition shines on the atoms from the side of the cavity, inducing AC Stark shifts. We probe signals transmitted through the cavity using a balanced heterodyne detector. **b**, Fluorescence image of the two atomic clouds used when scanning through phase III in Figs. 10.3 and 10.4. **c**, Frequency landscape of 689 nm beams. The atomic drive frequency ω_{drive} is resonant with the atomic transition. The cavity probe frequency ω_{cp} is nominally centred with the cavity resonance frequency, 51 MHz red-detuned from the atomic transition. The local oscillator used in heterodyne detection has frequency ω_{LO} and is 80 MHz blue-detuned from the atomic transition.

10.6.2 Experimental setup: cuts through phase III

For the two cuts through phase III described in Figs. 10.3 and 10.4, we load the atoms in two clouds separated by 3 mm, as shown in Extended Data Fig. 10.1**b**. The left cloud has an extent described by standard deviations $(\sigma_x, \sigma_z) = (200\ \mu\mathrm{m}, 16\ \mu\mathrm{m})$. The right cloud has a similar extent along σ_z but is broader along the cavity axis. We tune the lattice polarisation to point along $\hat{z}$, which breaks the magic angle condition and introduces a differential trap depth between ground and excited states of 0.47 MHz for atoms experiencing peak lattice intensity. Due to their finite temperature, the atoms experience a spread in lattice intensities which leads to an inhomogeneous trap depth. We estimate the induced distribution of energy shifts by assuming the atoms occupy a 2D Gaussian distribution radially with standard deviation $\sigma_y = \sigma_z = 16\ \mu$m, compared to the lattice waist $w_y = w_z = 80\ \mu$m. This produces a peaked distribution equivalent to the narrow peak in Fig. 10.3**a**.

In these experiments, we perform a $\pi/2$ pulse as before and then immediately shine a 461 nm beam centred on the left ("bright") atomic cloud. Unlike in the previous cut, we do not wait for transient dynamics to settle after state initialisation, for the sake of simplicity. We do not see major differences between observed and expected behaviour when omitting the wait period. The beam has waists $(w_x, w_z) = (1700\ \mu\mathrm{m}, 80\ \mu\mathrm{m})$. We install a beam block just before the chamber that clips the beam tail that would otherwise hit the right ("dark") atomic cloud. The 3 mm separation between clouds is sufficiently large to ensure the beam does not significantly diffract around the beam block. The beam shifts the mean energy of the bright

cloud away from that of the dark cloud, introducing a tunable δ_s. While nominally, we hold E_W fixed while scanning δ_s to explore the phase II to phase III transition, in reality the finite size of the blue beam introduces an additional contribution to E_W on the bright cloud. As δ_s increases, therefore, both the size and shape of the single-particle energy distribution changes. We calculate E_W in a consistent manner by estimating the standard deviation of the bright cloud distribution and matching the result to a uniform distribution with the same standard deviation (see Supplemental Online Material). In the main text, we report the value of E_W obtained at the phase transition point for the phase II to phase III transition. As we increase the 461 nm beam power, the atoms also scatter more blue photons. At the largest applied AC Stark shift, we estimate that the bright cloud experiences a scattering rate of $R_{sc}/2\pi = 3.4$ kHz, resulting in lower coherence times for traces with large δ_s. However, this excess decoherence does not bias our measurements of oscillation amplitude and frequency at times $t \leq 8$ μs.

10.6.3 Readout

After initialisation in all experiments, the atomic ensemble establishes a small electric field inside the cavity which adiabatically follows $\langle \hat{S}^- \rangle$ [Norcia *et al.*(2018a)]. Assuming homogeneous atom-light coupling (see next section for modifications due to inhomogeneous coupling), the complex amplitude of the electric field leaking out of the cavity is given by

$$\alpha_{out}(t) = -\frac{g}{\delta_c}\sqrt{\kappa_m}\langle \hat{S}^-(t) \rangle, \tag{10.2}$$

where α_{out} has units of $\sqrt{\text{photons/s}}$. Here, $2g/2\pi = 10.6$ kHz is the single-photon Rabi frequency for an atom maximally coupled to the cavity, $\delta_c/2\pi = (\omega_c - \omega_a)/2\pi = -51$ MHz is the detuning between the cavity resonance frequency ω_c and the atomic transition frequency ω_a, and $\kappa_m/2\pi = 41$ kHz is the rate at which photons incident on the cavity mirror are transmitted. α_{out} is a form of dissipation in the system equivalent to superradiance in a detuned cavity limit. Over the region of parameter space explored in this work, we estimate that the dissipation rate never exceeds $\gamma_{SR}/2\pi = 2.3$ kHz. We measure the detuned superradiant light as it leaks out of the cavity using balanced heterodyne detection, providing us with a real-time probe of $\langle \hat{S}^- \rangle \propto \Delta_{BCS}$. In plots of $|\Delta_{BCS}|$ in the main text, we calculate the square magnitude of this quantity and average over 400-1600 shots of the experiment, taken within 2-10 minutes. We then perform background subtraction to remove vacuum noise power from the heterodyne signal. Finally, we take a signed square root of the result to return an estimate of $|\Delta_{BCS}|$ which averages to zero in the absence of a real signal. This explains why some traces dip below zero despite representing a nonnegative quantity.

Additionally, the cavity experiences a (dispersive) shift in its resonance frequency proportional to the number of atoms. We use this fact to measure atom number by sending a pulsed probe tone through the cavity and measuring the frequency shift using the transmitted light. Since this light is spectrally resolved from the light emitted by the atoms, we are able to measure both signals independently on our heterodyne detector. The different optical frequencies involved in the heterodyne beat are compared in Extended Data Fig. 10.1**c**.

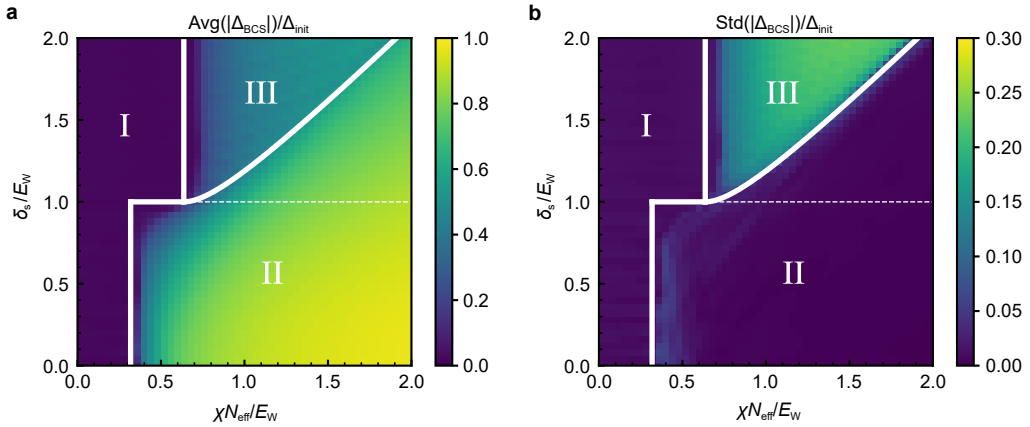

Extended Data Fig. 10.2: **Numerical simulation of the dynamical phase diagram based on Eq. (10.3).** We identify the dynamical phases based on the long-time average (**a**) and the long-time standard deviation (**b**) of $|\Delta_{\mathrm{BCS}}(t)|$, normalised by its initial value $\Delta_{\mathrm{init}} \equiv |\Delta_{\mathrm{BCS}}(0)|$. The white solid lines mark the corresponding dynamical phase boundaries, analytically derived from Eq. (10.1), which agree with the numerical results based on Eq. (10.3). The white dashed lines mark an extra dynamical phase transition that only exists for Eq. (10.1).

10.6.4 Dynamical phase diagram

The unitary dynamics of our system is modelled by an effective atom-only Hamiltonian, given by

$$\hat{H} = \hbar\chi \sum_{jk} \zeta_j \zeta_k \hat{S}_j^+ \hat{S}_k^- + \sum_k \varepsilon_k \hat{S}_k^z, \tag{10.3}$$

where $\hat{S}_k^{+,-}, \hat{S}_k^{x,y,z}$ are the standard spin-1/2 operators on atom k. We define $\chi = -g^2\delta_c/(\delta_c^2 + \kappa^2/4)$, where g and δ_c are as defined in the previous section, and κ is the cavity linewidth. The spatial dependence of the interaction term is characterised by $\zeta_j = \cos(j\phi)$ with $\phi = \pi\lambda_L/\lambda_c$, which arises because the lattice wavelength $\lambda_L = 813$ nm is incommensurate with the cavity wavelength $\lambda_c = 689$ nm. In contrast to Eq. (10.1), Eq. (10.3) becomes non-integrable due to the inhomogeneity in the interaction term. Nevertheless, as shown in Extended Data Fig. 10.2, Eq. (10.3) leads to a similar dynamical phase diagram as Eq. (10.1) if we

1. Use a generalised superconducting order parameter $\Delta_{\mathrm{BCS}} = \chi \sum_k \zeta_k \langle \hat{S}_k^- \rangle$;

2. Interpret the $\pi/2$-pulse as a pulse along the cavity axis under the Hamiltonian $\hat{H}_{\mathrm{drive}} = \hbar\Omega \sum_k \zeta_k S_k^y$ that generates the maximum possible $|\Delta_{\mathrm{BCS}}|$, which occurs when $\Omega t = 0.586\pi$;

3. Replace the atomic number N by an effective atom number $N_{\mathrm{eff}} = N/2$, such that χN_{eff} represents the averaged interaction strength of Eq. (10.3).

We can still measure the generalised order parameter Δ_{BCS} using the field leaking out of the cavity as in the previous section, since with inhomogeneous coupling the transmitted field takes the form $\alpha_{\mathrm{out}}(t) = -\frac{g}{\delta_c}\sqrt{\kappa_m} \sum_k \zeta_k \langle \hat{S}_k^-(t) \rangle \propto \Delta_{\mathrm{BCS}}$. The dynamical phase diagram in Extended Data Fig. 10.2 is numerically calculated based on unitary evolution under Eq. (10.3), with a single-particle dispersion $\varepsilon_k/\hbar$ sampled from a uniform distribution in the frequency range $[-\delta_s/2 - E_W/2, -\delta_s/2 + E_W/2]$ and $[\delta_s/2 - E_W/2, \delta_s/2 + E_W/2]$. There χN corresponds to the averaged interaction strength of Eq. (10.3). We identify the dynamical phases based on

the long-time average of $|\Delta_{\mathrm{BCS}}|$, given by

$$\mathrm{Avg}(|\Delta_{\mathrm{BCS}}|) = \lim_{T\to\infty} \frac{1}{T} \int_0^T |\Delta_{\mathrm{BCS}}(t)| dt, \tag{10.4}$$

as well as the long-time oscillation amplitude of $|\Delta_{\mathrm{BCS}}|$. Since the oscillations in $|\Delta_{\mathrm{BCS}}|$ might deviate from a sinusoidal form, for theoretical simulations it is easier to use the standard deviation as a measure of the oscillation amplitude:

$$\begin{aligned} &\mathrm{Std}(|\Delta_{\mathrm{BCS}}|) \\ &= \left[\lim_{T\to\infty} \frac{1}{T} \int_0^T \Big(|\Delta_{\mathrm{BCS}}(t)| - \mathrm{Avg}(|\Delta_{\mathrm{BCS}}|) \Big)^2 dt \right]^{1/2}. \end{aligned} \tag{10.5}$$

When comparing to experimental data, we measure oscillation amplitude using the Fourier spectrum because technical noise in the experiment contributes to the standard deviation of the time traces (see Fig. 10.3**d**). The dynamical phases can be characterised in theoretical simulations by

- Phase I: $\mathrm{Avg}(|\Delta_{\mathrm{BCS}}|) = 0$, $\mathrm{Std}(|\Delta_{\mathrm{BCS}}|) = 0$.
- Phase II: $\mathrm{Avg}(|\Delta_{\mathrm{BCS}}|) > 0$, $\mathrm{Std}(|\Delta_{\mathrm{BCS}}|) = 0$.
- Phase III: $\mathrm{Avg}(|\Delta_{\mathrm{BCS}}|) > 0$, $\mathrm{Std}(|\Delta_{\mathrm{BCS}}|) > 0$.

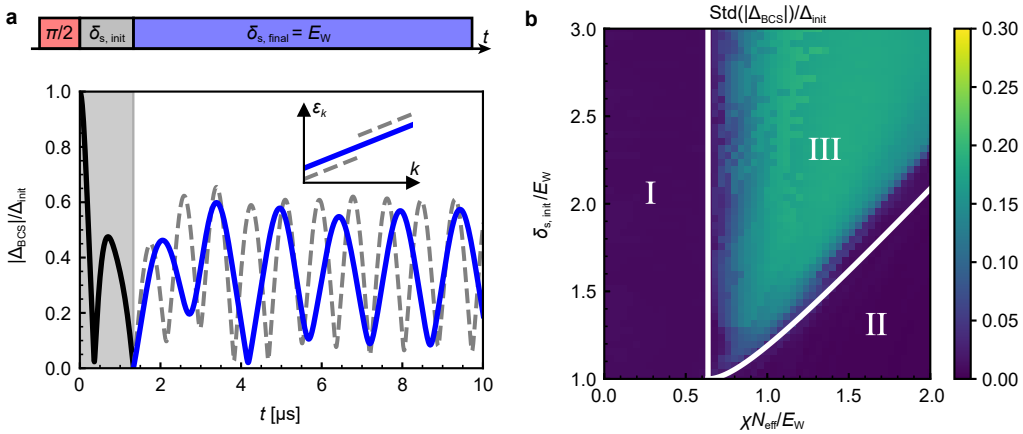

Extended Data Fig. 10.3: **Alternative approach for phase III. a**, Simulation of an alternative experimental sequence. As described by the timing sequence at the top, we simulate an experiment that prepares the initial state using a $\pi/2$ pulse, lets the system evolve under a bimodal distribution of single-particle energy (see the inset) until $|\Delta_{\mathrm{BCS}}|$ reaches its minimum value, and then quenches the system back to a continuous distribution of single-particle energies (see the inset). The theoretically predicted time trace of $|\Delta_{\mathrm{BCS}}|$ with $\chi N/E_{\mathrm{W}} = 1.0$ and $\delta_{\mathrm{s,init}}/E_{\mathrm{W}} = 1.6$ is shown at the bottom. The blue (grey dashed) line shows phase III dynamics under a continuous (bimodal) distribution. **b**, Long-time standard deviation of $|\Delta_{\mathrm{BCS}}(t)|$ after quenching to the continuous distribution shown in **a**. The white lines are dynamical phase boundaries for bimodal distributions (see Extended Data Fig. 10.2). Nearly all the choices of parameter for phase III using bimodal distributions can lead to phase III behaviours after quenching to the continuous distribution.

The dynamical phase boundaries (white solid lines) in Extended Data Fig. 10.2 are analytically calculated using a Lax analysis applied to Eq. (10.1), similar to the one discussed in [Lewis-Swan *et al.*(2021), Marino *et al.*(2022)], and take the following form (see Supplemental Online Material for a detailed derivation):

- Phase I to phase II:

$$\begin{aligned} &\frac{\chi N}{E_{\mathrm{W}}} = \frac{1}{\pi} \quad \text{with} \quad \frac{\delta_{\mathrm{s}}}{E_{\mathrm{W}}} \in [0,1], \\ &\frac{\delta_{\mathrm{s}}}{E_{\mathrm{W}}} = 1 \quad \text{with} \quad \frac{\chi N}{E_{\mathrm{W}}} \in \left[\frac{1}{\pi}, \frac{2}{\pi}\right]. \end{aligned} \tag{10.6}$$

- Phase I to phase III:

$$\frac{\chi N}{E_{\mathrm{W}}} = \frac{2}{\pi} \quad \text{with} \quad \frac{\delta_{\mathrm{s}}}{E_{\mathrm{W}}} > 1. \tag{10.7}$$

- Phase II to phase III:

$$\frac{\delta_s}{E_{\mathrm{W}}} = \csc\left(\frac{E_{\mathrm{W}}}{\chi N}\right) \quad \text{with} \quad \frac{\chi N}{E_{\mathrm{W}}} > \frac{2}{\pi}. \tag{10.8}$$

The analytical results agree with the numerical simulations for Eq. (10.3). The only difference is that Eq. (10.1) predicts an extra dynamical phase transition marked by the white dashed line. The dynamical phase boundaries shown in Fig. 10.1**c** are constructed by the analytical formulas above.

10.6.5 Phase III dynamics: the case of a continuous single-particle dispersion

In this manuscript, we generate phase III using a bimodal single-particle dispersion, represented with idealized assumptions by Fig. 10.1**b** and with actual experimental conditions by Fig. 10.3**a**. Here we show that this experimentally convenient approach generates similar phase III dynamics to the one obtained in the case of a continuous dispersion but with different initial conditions.

This is done by the protocol shown in Extended Data Fig. 10.3**a**, which uses a bimodal distribution ($\delta_{\mathrm{s,init}} > E_{\mathrm{W}}$) just to generate a state with minimum $|\Delta_{\mathrm{BCS}}|$. At this point the system's dispersion is restored to be continuous by setting $\delta_{\mathrm{s,final}} = E_{\mathrm{W}}$. This approach more closely resembles the phase III quench discussed in actual BCS superconductors, where phase III is observed by quenching from a state with weak BCS paring gap $|\Delta_{\mathrm{BCS}}|$ to one with a strong pairing gap [Yuzbashyan *et al.*(2015)]. Numerical simulations based on Eq. (10.3) show that nearly all choices of parameters that lead to phase III using a bimodal distribution also lead to phase III dynamics when quenching to a continuous distribution. The only exception is a small parameter regime close to the boundary between phase III and phase II (see Extended Data Fig. 10.3**b**). Note that here we use definitions for Δ_{BCS}, the $\pi/2$ pulse, and χN which correspond to Eq. (10.3), as explained in the previous section.

10.6.6 Numerical simulations

The black dashed lines in Figs. 10.2, 10.3, and 10.4 are computed from unitary evolution under Eq. (10.3) using a single-particle dispersion ε_k, sampled from the experimentally engineered distribution.

The black solid lines in the same figures are obtained by adding dissipative processes and axial motion to Eq. (10.3). The system dynamics is described by the following master equation for the density matrix $\hat{\rho}$:

$$\frac{d\hat{\rho}}{dt} = -\frac{i}{\hbar}[\hat{H}, \hat{\rho}] + \mathcal{L}(\hat{L}_c)[\hat{\rho}] + \sum_k \mathcal{L}(\hat{L}_{s,k})[\hat{\rho}] + \sum_k \mathcal{L}(\hat{L}_{\mathrm{el},k})[\hat{\rho}]. \tag{10.9}$$

The Lindblad superoperator takes the form $\mathcal{L}(\hat{L})[\hat{\rho}] = \hat{L}\hat{\rho}\hat{L}^\dagger - \frac{1}{2}(\hat{L}^\dagger\hat{L}\hat{\rho} + \hat{\rho}\hat{L}^\dagger\hat{L})$. Superradiance through the cavity is described by the jump operator

$$\hat{L}_c = \sqrt{\Gamma}\sum_k \zeta_k \hat{S}_k^-, \tag{10.10}$$

where $\Gamma = \chi\kappa/\delta_c$. Spontaneous emission from the atomic excited state is described by the jump operator

$$\hat{L}_{s,k} = \sqrt{\gamma}\hat{S}_k^-, \tag{10.11}$$

where $\gamma/2\pi = 7.5$ kHz is the spontaneous emission rate out of $^3P_1$. Single-particle decoherence is described by the jump operator

$$\hat{L}_{\mathrm{el},k} = \sqrt{2\gamma_{\mathrm{el}}}\hat{S}_k^z, \tag{10.12}$$

where γ_{el} is a fitting parameter taking into account free space scattering from the AC Stark shift beam, as well as other decoherence processes in the experiment (see Supplemental Online Material). These are the dominant dissipative processes in our system.

The axial trapping frequency of the lattice is 165 kHz and is therefore smaller than the spin-exchange interaction rate χN for most of the experiments. As a consequence, in contrast to the idealised model where atoms are assumed to be frozen, motional processes need to be accounted for, even though they are suppressed in the Lamb-Dicke regime. As shown in the Supplemental Online Material, axial motion can lead to a faster damping rate of $|\Delta_{\mathrm{BCS}}|$ oscillations. The predicted dynamical phase boundaries are nevertheless unaffected by the axial motion.

All the numerical simulations are computed using the mean-field approximation, which replaces the operators $\hat{S}_k^{x,y,z}$ by their expectation values $\langle\hat{S}_k^{x,y,z}\rangle$ in the Heisenberg equation of motion. The mean-field treatment of the BCS model is predicted to be exact in the thermodynamic limit due to the infinite-range nature of the interactions [Yuzbashyan *et al.*(2015)]. The atom number for numerical simulation is set to 5000 for the ideal conditions and 2000 for actual experimental conditions. We rescale χ to match χN with experimental values.

[H]

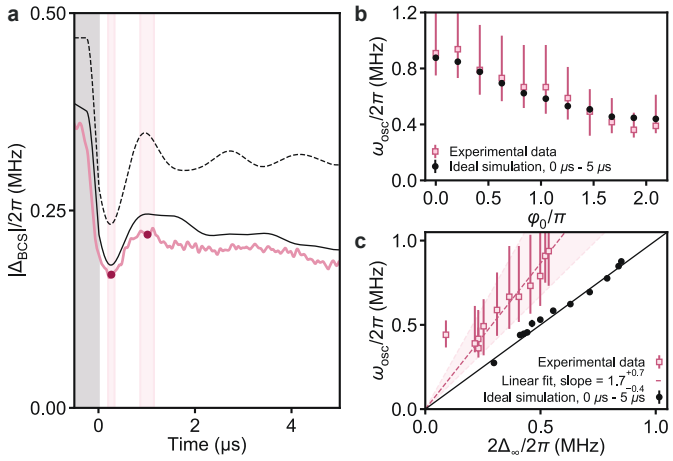

Extended Data Fig. 10.4: **Collective scaling in damped phase II oscillations.** **a**, Time dynamics of $|\Delta_{\mathrm{BCS}}|$ measured after engineering an initial phase spread over $[0, \varphi_0]$ where $\varphi_0 = 0.8\pi$ as in Fig. 2**d**, plotted in absolute frequency units (pink trace). The solid black curve represents a numerical simulation of the full system, whereas the dashed curve represents an ideal simulation neglecting dissipation and motional effects. We obtain a crude estimate of oscillation frequency in the experimental data by fitting a trough and peak to smoothed data (after subtracting slow-moving behaviour) within the first couple μs (magenta points), using these points to infer a half period of oscillation, and with uncertainties determined using a 90% amplitude threshold (pink bands). **b**, Comparing oscillation frequency estimates of experimental data (pink squares) with those of ideal simulations (black dots) for different φ_0. Theory oscillation frequencies are calculated using a Fourier transform from $t = 0$ μs to $t = 5$ μs. Error bars for experimental data are set by the minimum and maximum frequencies implied by uncertainties in the half period shown in **a**. The two frequency estimates agree within error bars. **c**, Collective scaling of oscillation frequency. For each φ_0 measured in the experiment, we plot the oscillation frequency against the long-time BCS gap Δ_∞, calculated at $t = 18$ μs for ideal simulations and at $t = 3$ μs for experimental data. The solid black line is defined by $\omega_{\mathrm{osc}} = 2\Delta_\infty$, demonstrating the expected scaling for Higgs oscillations. The dashed pink line represents a linear fit to the experimental data. The pink band shows the uncertainty in the slope assuming correlated error in ω_{osc}, such that its bounds are defined by linear fits to the data assuming maximum and minimum values for ω_{osc} as defined by the error bars.

10.6.7 Higgs-like behaviour in short-time phase II dynamics

When quenching into phase II, we observe highly damped oscillations in $|\Delta_{\mathrm{BCS}}|$, reminiscent of the Higgs oscillations predicted to arise in this regime of the BCS model. Here, we analyse traces from Fig. 10.2**d**, in which we engineer a variable phase spread $\varphi(\omega_k) \in [0, \varphi_0]$ before quenching into phase II, to study this potential connection.

In the BCS model, Higgs oscillations can be characterised by their frequency, which should scale with the long-time BCS order parameter Δ_∞ as $\omega_{\mathrm{osc}} = 2\Delta_\infty$ [Yuzbashyan *et al.*(2015)]. We confirm this scaling in theory by measuring the oscillation frequency from $t = 0$ μs to $t = 5$ μs in idealised numerical simulations ignoring dissipation and motional effects (black dashed line in Extended Data Fig. 10.4**a**). For different values of the phase spread extent φ_0, the system reaches its steady state at a different long-time BCS gap Δ_∞. By parametrically plotting the oscillation frequency vs. $2\Delta_\infty$ as a function of φ_0 in panel **c**, we observe the expected scaling.

As discussed in the main text, oscillations in $|\Delta_{\mathrm{BCS}}|$ are consistently smaller and decay more quickly in experiment than in theory. Nonetheless, we obtain a crude estimate of the experimental oscillation frequency by measuring a half period from the first trough and peak

of $|\Delta_{\mathrm{BCS}}(t)|$, as shown in panel **a**. In panel **b**, we compare the frequency in experimental data to that of ideal simulations for different φ_0 and show that the frequencies agree within error bars. This suggests that the transient dynamics observed in $|\Delta_{\mathrm{BCS}}|$ are related to the Higgs oscillations present in theory.

Although the experimental oscillation frequency agrees with simulations, the steady-state order parameter Δ_∞ is much smaller, as can be seen in Extended Data Fig. 10.4**a**. As a result, the measured frequencies scale linearly with Δ_∞ but with a different prefactor. In panel **c**, we fit a linear relation of $\omega_{\mathrm{osc}} = (1.7^{+0.7}_{-0.4}) \times 2\Delta_\infty$ to the data, where the slope uncertainty bounds are calculated assuming errors in ω_{osc} are perfectly correlated. Most of the reduction in Δ_∞ can be captured in theory by considering dissipation and motional effects (solid black trace). We see an additional small difference in $|\Delta_{\mathrm{BCS}}|$ between full numerical simulations and experimental data, which we attribute to drifts in experimental alignments and calibration factors over time. This difference is not apparent in Fig. 10.2**d** because we plot $|\Delta_{\mathrm{BCS}}|$ in normalised units.

10.7 Dynamical phase diagram

In this section, we perform detailed analysis of the dynamical phase diagram shown in Fig. 1**c** in the main text. We start from analytic calculation in the case of homogeneous couplings, and then generalize to the case of inhomogeneous couplings. Finally we discuss the application of our findings to experimental conditions.

10.7.1 Homogeneous model

First we discuss the dynamical phases for the BCS Hamiltonian with homogeneous couplings,

$$\hat{H} = \hbar\chi \hat{S}^+ \hat{S}^- + \sum_k \varepsilon_k \hat{S}^z_k. \tag{10.13}$$

We will set $\hbar = 1$. As shown in Ref. [Yuzbashyan *et al.*(2015), Lewis-Swan *et al.*(2021)], the dynamical phases can be determined using a mean-field Lax vector analysis. The Lax vector is defined as $\vec{L}(u) = L^x(u)\hat{x} + L^y(u)\hat{y} + L^z(u)\hat{z}$ with components,

$$L^x(u) = \sum_k \frac{S^x_k(0)}{u - \varepsilon_k/2}, \quad L^y(u) = \sum_k \frac{S^y_k(0)}{u - \varepsilon_k/2}, \quad L^z(u) = -\frac{1}{\chi} - \sum_i \frac{S^z_k(0)}{u - \varepsilon_k/2}, \tag{10.14}$$

where $S^{x,y,z}_k(0)$ are the expectation value of operators $\hat{S}^{x,y,z}_k$ in the initial state.

Here we consider the initial state as $S^x_k(0) = 1/2$, $S^y_k(0) = S^z_k(0) = 0$, and ε_k is chosen from a uniform distribution in the frequency range $[-\delta_{\mathrm{s}}/2 - E_{\mathrm{W}}/2, -\delta_{\mathrm{s}}/2 + E_{\mathrm{W}}/2]$ and $[\delta_{\mathrm{s}}/2 - E_{\mathrm{W}}/2, \delta_{\mathrm{s}}/2 + E_{\mathrm{W}}/2]$. In this case, the mean-field Lax vector takes the following form:

$$\begin{aligned}
\chi L^x(u) &\approx \frac{\chi N}{2}\left[\frac{1}{2E_{\mathrm{W}}}\int_{-\delta_{\mathrm{s}}/2-E_{\mathrm{W}}/2}^{-\delta_{\mathrm{s}}/2+E_{\mathrm{W}}/2}\frac{dx}{u - x/2} + \frac{1}{2E_{\mathrm{W}}}\int_{\delta_{\mathrm{s}}/2-E_{\mathrm{W}}/2}^{\delta_{\mathrm{s}}/2+E_{\mathrm{W}}/2}\frac{dx}{u - x/2}\right] \\
&= \frac{\chi N}{2E_{\mathrm{W}}}\left[\ln\left(u + \frac{\delta_{\mathrm{s}}}{4} + \frac{E_{\mathrm{W}}}{4}\right) - \ln\left(u + \frac{\delta_{\mathrm{s}}}{4} - \frac{E_{\mathrm{W}}}{4}\right) + \ln\left(u - \frac{\delta_{\mathrm{s}}}{4} + \frac{E_{\mathrm{W}}}{4}\right) - \ln\left(u - \frac{\delta_{\mathrm{s}}}{4} - \frac{E_{\mathrm{W}}}{4}\right)\right], \\
&\chi L^y(u) = 0, \\
&\chi L^z(u) = -1.
\end{aligned} \tag{10.15}$$

Note that $\ln z$ in the complex plane is a multivalued function. Here we take the principal value $\ln z = \ln|z| + i\mathrm{Arg}(z)$, where $\mathrm{Arg}(z)$ is the argument of z restricted in the interval $(-\pi, \pi]$. Directly combining the logarithm functions might lead to moving out of the principal branch.

One can define the dynamical phases based on the number of complex roots of equation $\vec{L}(u)\cdot\vec{L}(u)=0$: Phase I has zero complex roots, phase II has a pair of complex roots, phase III has two pairs of complex roots. Whether the complex roots have non-zero or vanishing real parts could be used for further separation of the phases. In our case, the equation $\vec{L}(u)\cdot\vec{L}(u)=0$ takes the following form,

$$\frac{\chi N}{2E_{\mathrm{W}}}\left[\ln\left(u+\frac{\delta_{\mathrm{s}}}{4}+\frac{E_{\mathrm{W}}}{4}\right)-\ln\left(u+\frac{\delta_{\mathrm{s}}}{4}-\frac{E_{\mathrm{W}}}{4}\right)+\ln\left(u-\frac{\delta_{\mathrm{s}}}{4}+\frac{E_{\mathrm{W}}}{4}\right)-\ln\left(u-\frac{\delta_{\mathrm{s}}}{4}-\frac{E_{\mathrm{W}}}{4}\right)\right]=\pm i. \tag{10.16}$$

We find four dynamical phases based on analyzing the roots of Eq. (10.16):

- Phase I: No complex roots, which exist in the regime

$$\frac{\delta_{\mathrm{s}}}{E_{\mathrm{W}}}<1,\quad \frac{\chi N}{E_{\mathrm{W}}}<\frac{1}{\pi}\qquad\text{or}\qquad \frac{\delta_{\mathrm{s}}}{E_{\mathrm{W}}}>1,\quad \frac{\chi N}{E_{\mathrm{W}}}<\frac{2}{\pi}. \tag{10.17}$$

- Phase II: A pair of complex roots,

$$\frac{u}{E_{\mathrm{W}}}=\pm\frac{i}{4}\left[\cot\left(\frac{E_{\mathrm{W}}}{\chi N}\right)+\sqrt{\csc^2\left(\frac{E_{\mathrm{W}}}{\chi N}\right)-\frac{\delta_s^2}{E_{\mathrm{W}}^2}}\right], \tag{10.18}$$

  which exist in the regime

$$\frac{\delta_{\mathrm{s}}}{E_{\mathrm{W}}}<1,\quad \frac{\chi N}{E_{\mathrm{W}}}>\frac{1}{\pi}. \tag{10.19}$$

- Phase IIIa: Two pairs of complex roots with vanishing real parts,

$$\frac{u_1}{E_{\mathrm{W}}}=\pm\frac{i}{4}\left[\cot\left(\frac{E_{\mathrm{W}}}{\chi N}\right)+\sqrt{\csc^2\left(\frac{E_{\mathrm{W}}}{\chi N}\right)-\frac{\delta_s^2}{E_{\mathrm{W}}^2}}\right],\quad \frac{u_2}{E_{\mathrm{W}}}=\pm\frac{i}{4}\left[\cot\left(\frac{E_{\mathrm{W}}}{\chi N}\right)-\sqrt{\csc^2\left(\frac{E_{\mathrm{W}}}{\chi N}\right)-\frac{\delta_s^2}{E_{\mathrm{W}}^2}}\right], \tag{10.20}$$

  which exist in the regime

$$\frac{\delta_{\mathrm{s}}}{E_{\mathrm{W}}}>1,\quad \frac{\chi N}{E_{\mathrm{W}}}>\frac{2}{\pi},\quad \frac{\delta_{\mathrm{s}}}{E_{\mathrm{W}}}<\csc\left(\frac{E_{\mathrm{W}}}{\chi N}\right). \tag{10.21}$$

  In phase IIIa, the order parameter, Δ_{BCS} oscillates around a non-zero value (non-ZOPA) as pointed out in Ref. [Collado *et al.*(2023), Lewis-Swan *et al.*(2021)].

- Phase IIIb: Two pairs of complex roots with non-zero real parts,

$$\frac{u_1}{E_{\mathrm{W}}}=\frac{1}{4}\left[\sqrt{\delta_s'^2-\csc^2\left(\frac{1}{\chi' N}\right)}\pm i\cot\left(\frac{1}{\chi' N}\right)\right],\quad \frac{u_2}{E_{\mathrm{W}}}=\frac{1}{4}\left[-\sqrt{\delta_s'^2-\csc^2\left(\frac{1}{\chi' N}\right)}\pm i\cot\left(\frac{1}{\chi' N}\right)\right], \tag{10.22}$$

  which exist in the regime

$$\frac{\delta_{\mathrm{s}}}{E_{\mathrm{W}}}>1,\quad \frac{\chi N}{E_{\mathrm{W}}}>\frac{2}{\pi},\quad \frac{\delta_{\mathrm{s}}}{E_{\mathrm{W}}}>\csc\left(\frac{E_{\mathrm{W}}}{\chi N}\right). \tag{10.23}$$

  In phase IIIb, Δ_{BCS} oscillates with zero order parameter average (ZOPA) as explained in Ref. [Collado *et al.*(2023), Lewis-Swan *et al.*(2021)].

The dynamical phases derived from the Lax analysis above are supported by numerical evidences, as shown in Fig. 10.5**a** and Fig. 10.5**b**. We numerically solve the dynamics of $\Delta_{\mathrm{BCS}} = \chi\langle\hat{S}^{-}\rangle$ under Eq. (10.13) based on mean field approximation, and then identify dynamical phases based on long-time average of $|\Delta_{\mathrm{BCS}}|$,

$$\mathrm{Avg}(|\Delta_{\mathrm{BCS}}|) = \lim_{T\to\infty}\frac{1}{T}\int_0^T |\Delta_{\mathrm{BCS}}(t)|dt, \tag{10.24}$$

and long-time oscillation amplitude of $|\Delta_{\mathrm{BCS}}|$. Since the oscillations in $|\Delta_{\mathrm{BCS}}|$ might deviates from a sinusoidal form, it is easier to use the standard deviation as a measure of the oscillation amplitude,

$$\mathrm{Std}(|\Delta_{\mathrm{BCS}}|) = \left[\lim_{T\to\infty}\frac{1}{T}\int_0^T \Big(|\Delta_{\mathrm{BCS}}(t)| - \mathrm{Avg}(|\Delta_{\mathrm{BCS}}|)\Big)^2 dt\right]^{1/2}, \tag{10.25}$$

although experimentally it's better to use the peak of Fourier spectrum to suppress the noise (see Fig. 3**d** in the main text). The dynamical phases can be characterized by

- Phase I: $\mathrm{Avg}(|\Delta_{\mathrm{BCS}}|) = 0$, $\mathrm{Std}(|\Delta_{\mathrm{BCS}}|) = 0$.
- Phase II: $\mathrm{Avg}(|\Delta_{\mathrm{BCS}}|) > 0$, $\mathrm{Std}(|\Delta_{\mathrm{BCS}}|) = 0$.
- Phase III: $\mathrm{Avg}(|\Delta_{\mathrm{BCS}}|) > 0$, $\mathrm{Std}(|\Delta_{\mathrm{BCS}}|) > 0$.

Since ε_k is chosen from a distribution with particle-hole symmetry (symmetric about 0), Δ_{BCS} becomes a real number in this case. One can further separate phase IIIa and phase IIIb by the behavior of Δ_{BCS} shown in Fig. 10.5**e** and Fig. 10.5**f**.

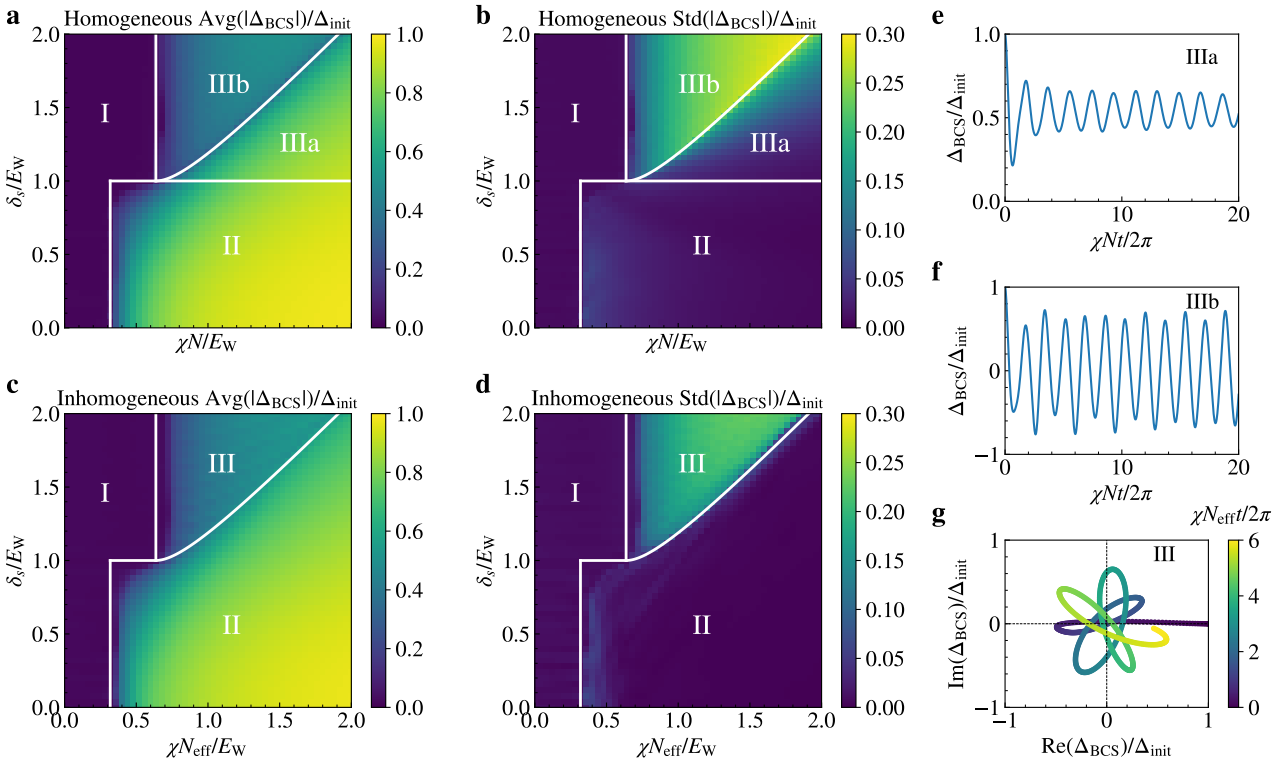

Extended Data Fig. 10.5: **Dynamical phase diagrams.** **a** and **b**, Dynamical phase diagram of the homogeneous model normalized by $\Delta_{\text{init}}/\chi N = 1/2$, where Δ_{init} is the initial value of $|\Delta_{\text{BCS}}|$. The white lines are the dynamical critical points derived from the Lax analysis. **c** and **d**, Dynamical phase diagram of the inhomogeneous model normalized by $\Delta_{\text{init}}/\chi N_{\text{eff}} = \mathcal{J}_1(\Omega\tau)$. The white lines are the same as the homogeneous model. **e**, Time evolution of Δ_{BCS} at $\delta_{\text{s}}/E_{\text{W}} = 1.1$, $\chi N/E_{\text{W}} = 1.0$ under the homogeneous model (phase IIIa). **f**, Time evolution of Δ_{BCS} at $\delta_{\text{s}}/E_{\text{W}} = 1.6$, $\chi N/E_{\text{W}} = 1.0$ under the homogeneous model (phase IIIb). **g**, Time evolution of Δ_{BCS} at $\delta_{\text{s}}/E_{\text{W}} = 1.6$, $\chi N/E_{\text{W}} = 1.0$ under the inhomogeneous model (phase III).

10.7.2 Inhomogeneous model

Here we discuss the dynamical phases for the BCS Hamiltonian with inhomogeneous coupling,

$$\hat{H} = \hbar\chi \sum_{jk} \zeta_j \zeta_k \hat{S}_j^+ \hat{S}_k^- + \sum_k \varepsilon_k \hat{S}_k^z, \tag{10.26}$$

where ζ_k is generated by random sampling of $\cos(x)$, with x chosen from a uniform distribution in the interval $[0, 2\pi)$. Similar to the homogeneous model, $\varepsilon_k/\hbar$ is still chosen from a uniform distribution in the frequency range $[-\delta_{\text{s}}/2 - E_{\text{W}}/2, -\delta_{\text{s}}/2 + E_{\text{W}}/2]$ and $[\delta_{\text{s}}/2 - E_{\text{W}}/2, \delta_{\text{s}}/2 + E_{\text{W}}/2]$. In this case, we explore the dynamical phases numerically since the Lax analysis is not applicable. As shown in Fig. 10.7**c** and Fig. 10.7**d**, one can obtain similar dynamical phases as the homogeneous model: Phase I remains the same, Phase IIIa merges into Phase II, and Phase IIIb becomes the new Phase III. The phase boundary can be roughly captured by the analytical solution of the homogeneous model. Note that χN_{eff} is the averaged interaction strength in the inhomogeneous case, where $N_{\text{eff}} = N/2$. The superconducting order parameter is defined as $\Delta_{\text{BCS}} = \chi \sum_k \zeta_k \langle \hat{S}_k^- \rangle$. The initial condition is chosen as the maximum $|\Delta_{\text{BCS}}|$ one can achieved by an external drive along the cavity axis, $\hat{H}_{\text{drive}} = \Omega \sum_k \zeta_k \hat{S}_k^y$. Assuming the initial state can be prepared by applying $\hat{H}_{\text{drive}}$ for a time τ, we have

$$\frac{\Delta_{\text{init}}}{\chi N_{\text{eff}}} \approx \frac{1}{2\pi} \int_0^{2\pi} dx \cos(x) \sin(\Omega\tau \cos(x)) = \mathcal{J}_1(\Omega\tau), \tag{10.27}$$

where $\mathcal{J}_n$ is the Bessel function of the first-kind, and the maximum of $\mathcal{J}_1(\Omega\tau)$ can be achieved at $\Omega\tau = 0.586\pi$. It is worth to mention that $\Delta_{\rm BCS}$ is a real number initially, but it becomes a complex number during the time evolution, as shown in Fig. 10.7**g**.

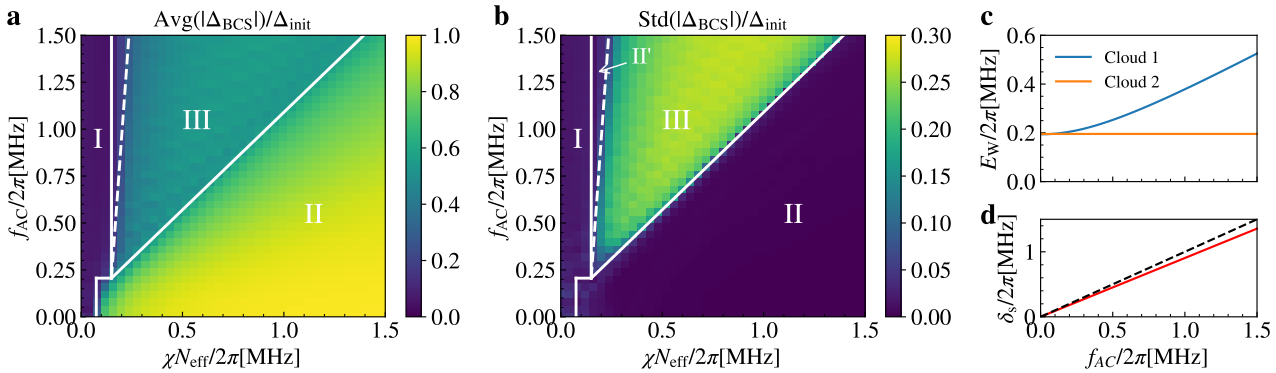

Extended Data Fig. 10.6: **Experimental control of dynamical phases.** **a** and **b**, Dynamical phase diagram for the experiment with two atomic ensembles, in terms of averaged spin-exchange interaction strength $\chi N_{\rm eff}$ and peak AC Stark shift $f_{\rm AC}$. The white lines show the predicted dynamical phase boundaries to guide the eye. The white dashed line marks a small region of phase II' due to the imbalance of $E_{\rm W}$ for the two atomic ensembles. **c**, $E_{\rm W}$ as a function of peak AC Stark shift $f_{\rm AC}$, with AC Stark shift applying to atomic cloud 1. **d**, $\delta_{\rm s}$ as a function of peak AC Stark shift $f_{\rm AC}$ (red line). The dashed line marks the place where $\delta_{\rm s} = f_{\rm AC}$.

10.7.3 Experimental control of dynamical phases

Here we elaborate on the experimental implementation of the Hamiltonian Eq. (10.26). As discussed in the previous section, we would like to approximately engineer single-particle energies $\varepsilon_k/\hbar$ sampled from a uniform distribution in the frequency range $[-\delta_{\rm s}/2 - E_{\rm W}/2, -\delta_{\rm s}/2 + E_{\rm W}/2]$ and $[\delta_{\rm s}/2 - E_{\rm W}/2, \delta_{\rm s}/2 + E_{\rm W}/2]$. The two different experimental schemes used in the main text to explore the energy distribution are summarized in the following table:

	Description	Approx. $\varepsilon_k/\hbar$
Scheme I (Fig. 2, main text)	1) Single atomic cloud 2) AC Stark shift	$[-\tilde{E}_{\rm W}/2, \tilde{E}_{\rm W}/2]$
Scheme II (Fig. 3, 4, main text)	1) Two atomic clouds 2) AC Stark shift to cloud 1	Cloud 1: $[-\delta_{\rm s}/2 - E_{\rm W}/2, -\delta_{\rm s}/2 + E_{\rm W}/2]$ Cloud 2: $[+\delta_{\rm s}/2 - E_{\rm W}/2, +\delta_{\rm s}/2 + E_{\rm W}/2]$

The first scheme is used to probe the phase I to phase II transition. We use a single atomic ensemble and apply an AC Stark shift beam with a gradient to approximately engineer $\varepsilon_k/\hbar$ from a uniform distribution $[-\tilde{E}_{\rm W}/2, \tilde{E}_{\rm W}/2]$, as discussed in the Methods. As shown in Fig. 2**a** in the main text, the distribution of atomic frequencies is not exactly uniform, so we calculate the variance of the frequency distribution experimentally. Theoretically we assign a spread $\tilde{E}_{\rm W}$ such that the uniform distibution over $[-\tilde{E}_{\rm W}/2, \tilde{E}_{\rm W}/2]$ matches the measured experimental variance. We use this scheme to probe the dynamical phase diagram at $\delta_{\rm s} = 0$ (see Fig. 1**c** in the main text).

It is worth mentioning that the uniform distribution $[-\tilde{E}_{\rm W}/2, \tilde{E}_{\rm W}/2]$ can be interpreted in two different ways: 1) $\delta_{\rm s} = 0$ and $E_{\rm W} = \tilde{E}_{\rm W}$; 2) $\delta_{\rm s} = E_{\rm W} = \tilde{E}_{\rm W}/2$. Here we prefer the

first interpretation $\delta_s = 0$ because in this scheme we only have a single control parameter (the strength of AC Stark shift beam). Additionally, the line $\delta_s = E_W$ in the dynamical phase diagram has an implication that a small perturbation of δ_s can generate a gap in atomic frequency, which is prohibited under this mapping between experimental controls and the model parameters.

In the second scheme that probes transitions into phase III, we use two atomic ensembles and apply an AC Stark shift beam (peak AC Stark shift f_{AC}) to the first ensemble to generate a frequency splitting δ_s between the two ensembles. In contrast to the first scheme, as discussed in the Methods, here we instead use the differential lattice light shifts to engineer a frequency spread E_W for each ensemble. As shown in Fig. 3**a** in the main text, in this case we define δ_s as the mean frequency difference between the two ensembles, and E_W as the width of a uniform distribution generating the same variance.

It is worth mentioning that the Gaussian profile of the AC Stark shift beam leads to an increase in E_W for the first atomic ensemble, as well as a reduction of the expected splitting of the two ensembles $\delta_s < f_{AC}$, as shown in Fig. 10.6**c** and **d**. Using experimental parameters, we get the dynamical phase diagram as depicted in Fig. 10.6**a** and **b**. The imbalance of E_W for the two atomic ensembles can lead to a small region of phase II' marked by the white dashed line. This occurs because the spin-exchange interaction is able to lock the ensemble with smaller E_W, while the ensemble with larger E_W remains unlocked, which leads to $|\Delta_{BCS}|$ approaching a small but nonzero constant value. In the experiment, due to other dissipative processes and reduced signal-to-noise ratio for small χN, we do not observe a difference between phase I and phase II'. This is the cause of a small discrepancy between theory and experiment in Fig. 4**b** in the main text in identifying the position of the phase transition.

10.8 Short-time signatures of dynamical phases

In this section, we discuss the properties of the dynamical phases using short-time observables, since dissipative processes and noise in the experiment lead to difficulties in measuring long-time observables. In the following, we show that phase I can be characterized by the fast decay of $|\Delta_{BCS}|$, phase II can be characterized by Higgs oscillations. We further show that the phase II to phase III transition can be captured by the dip in the short-time oscillation frequency of $|\Delta_{BCS}|$. Finally, we provide an explanation of the frequency dip using an analytical solution of the two-spin BCS model.

10.8.1 Phase I: fast decay

In phase I, the single-particle energy term $\sum_k \varepsilon_k \hat{S}_k^z$ dominates over the spin-exchange interaction. To leading order, one can calculate $|\Delta_{BCS}|$ in the homogeneous model by dropping the interaction term, which gives

$$\begin{aligned}\frac{|\Delta_{BCS}|}{\chi N} &\approx \frac{1}{2N}\left|\sum_k e^{-i\varepsilon_k t/\hbar}\right| = \frac{1}{2}\left|\frac{1}{2E_W}\int_{-\delta_s/2-E_W/2}^{-\delta_s/2+E_W/2} e^{-ixt}dx + \frac{1}{2E_W}\int_{\delta_s/2-E_W/2}^{\delta_s/2+E_W/2} e^{-ixt}dx\right| \\ &= \frac{1}{2}\left|\cos\left(\frac{\delta_s}{2}\right)\right| \cdot \left|\frac{\sin(E_W t/2)}{E_W t/2}\right|.\end{aligned} \tag{10.28}$$

The decay profile of $|\Delta_{BCS}|$ is set by a sinc function with a $1/e$ coherence time t satisfying $E_W t/2\pi \approx 0.7$. For the inhomogeneous model a similar fast decay time scale of the order of $E_W t/2\pi \sim 1$ can be derived. As shown in Fig. 2**b** in the main text, we observe fast decay of $|\Delta_{BCS}|$ within 1 μs in phase I. The decay time scale for the other dynamical phases can be more than 10 times longer.

10.8.2 Phase II: Higgs oscillation

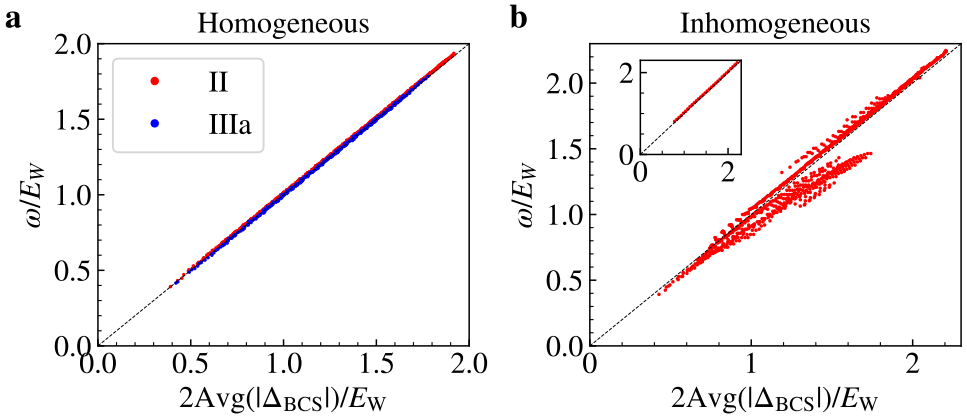

Extended Data Fig. 10.7: **Relation between oscillation frequency and averaged order parameter in Higgs oscillations.** **a**, Homogeneous model where each point is a choice of $(\chi N, \delta_s)$ in phase II (red) and phase IIIa (blue). The dashed line represents $\omega = 2\mathrm{Avg}(|\Delta_{\mathrm{BCS}}|)$. **b**, Inhomogeneous model where each point is a choice of $(\chi N_{\mathrm{eff}}, \delta_s)$ in phase II. The inset shows the points with $\delta_s = 0$.

Higgs oscillation, generated by collective excitation of the Higgs mode in BCS superconductor, is characterized by the oscillation of $|\Delta_{\mathrm{BCS}}|$ at frequency $\omega = 2\mathrm{Avg}(|\Delta_{\mathrm{BCS}}|)$ [Yuzbashyan *et al.*(2015)]. For the homogeneous model (see Fig. 10.7**a**), we numerically confirmed this relation for all the points in phase II and phase IIIa. For the inhomogeneous model (see Fig. 10.7**b**), this relation is approximately satisfied in phase II. In experiment, we observe hints of Higgs oscillation (see Fig. 2 in the main text), which can be ideally described by the inhomogeneous model with $\delta_s = 0$ (see the inset in Fig. 10.7**b**).

10.8.3 Transition to phase III: frequency dip

In the main text, we discuss a way to understand the phase II to phase III transition by visualising the two atomic ensembles as two large spins. For the inhomogeneous model, phase II exists in the small δ_s regime, where the two spins lock to each other and form a single large spin through spin-exchange interactions. In this case the many-body gap protection leads to the damped oscillations observed in phase II. Increasing δ_s in phase II leads to the reduction of the many-body gap, and hence to a decrease of the corresponding oscillation frequency. Phase III exists in the large δ_s regime, where the spin locking occurs separately in each ensemble, and the two large spin are instead precessing around each other, with a rate set by the splitting δ_s and the spin-exchange interaction. Increasing δ_s in phase III leads to a speed up of the oscillation frequency. Therefore one expects the existence of a frequency dip separating between phase II and phase III. Indeed as shown in Fig. 10.8**c** and **d**, we find good agreement between the frequency dip and the corresponding dynamical critical point. For small δ_s, the oscillation frequency approaches the Higgs oscillation frequency discussed in the previous subsection. For large δ_s, the oscillation frequency approaches δ_s. The reduction of oscillation frequency compared to δ_s indicates many-body effects in phase III. It's worth to mention that in contrast to the inhomogeneous model, the frequency dip indicates the phase IIIa to phase IIIb transition for the homogeneous model.

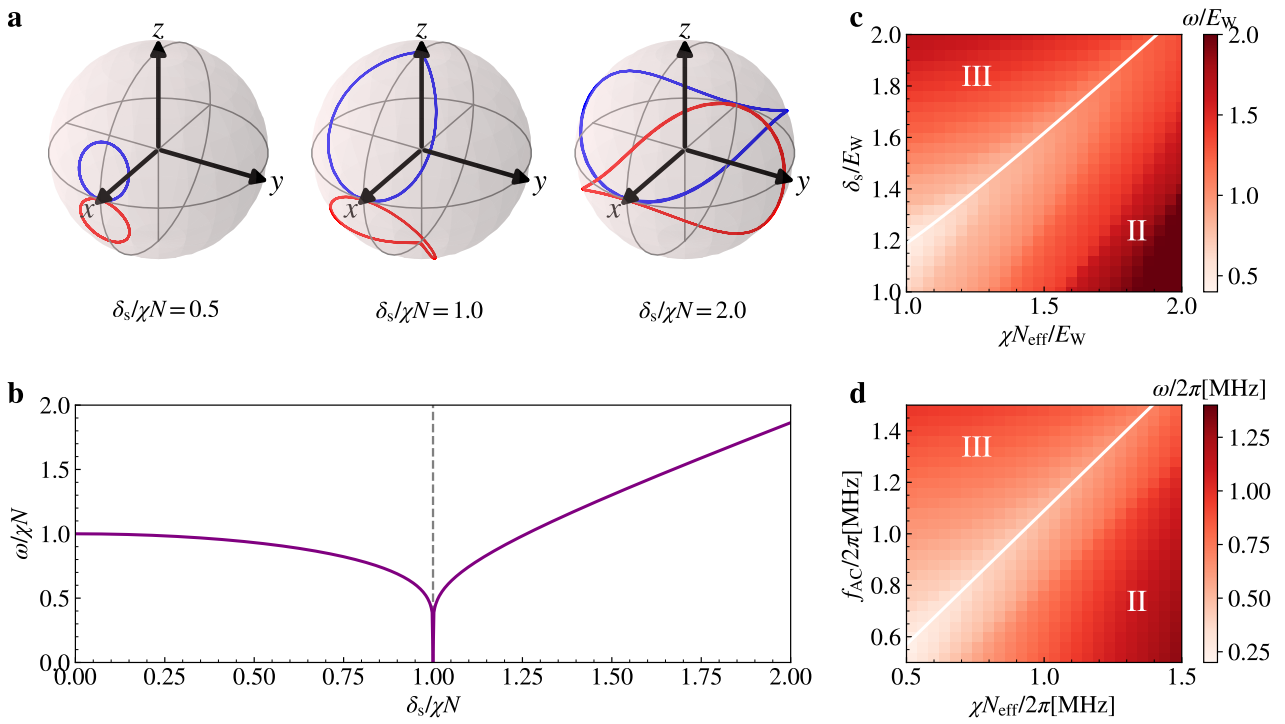

Extended Data Fig. 10.8: **Frequency dip as a signature of the phase II to phase III transition.** **a**, Mean field trajectories of the two large spin model evolving under Eq. (10.29). From left to right, Bloch spheres display trajectories with $\delta_s/(\chi N) = 0.5, 1$, and 2 respectively. **b**, Oscillation frequency of $|\Delta_{BCS}|$ in the two-spin BCS model Eq. (10.29) as a function of $\delta_s/\chi N$. The frequency dip at $\delta_s/\chi N = 1$ marks the dynamical phase transition point. **c**, Short-time frequency ω of the dynamics under inhomogeneous atom-light coupling (see Eq. (3) in the Methods). The white line marks the phase II to phase III transition, the same boundary as shown in Extended Data Fig. 2 from the Methods. **d**, Short-time frequency ω of the dynamics using experimental control parameters. The white line marks the phase II to phase III transition and represents the same boundary as in Fig. 10.6. The frequency dips match the dynamical critical points for both cases.

10.8.4 Frequency dip in the two-spin BCS model

Here we use the analytical mean field solution of the BCS Hamiltonian with two large spins ($S = N/4$ for each spin) to understand the frequency dip discussed above. In this case, the Hamiltonian simplifies to

$$\hat{H}/\hbar = \chi \hat{S}^+ \hat{S}^- + \frac{\delta_s}{2}\hat{S}_1^z - \frac{\delta_s}{2}\hat{S}_2^z, \tag{10.29}$$

where $\hat{S}^\pm = \hat{S}_1^\pm + \hat{S}_2^\pm$. The mean field equations of motion for the Hamiltonian above can then be written as

$$\begin{aligned} &\frac{d}{dt}S_1^x = 2\chi S^y S_1^z - \frac{\delta_s}{2}S_1^y, \quad \frac{d}{dt}S_1^y = -2\chi S^x S_1^z + \frac{\delta_s}{2}S_1^x, \quad \frac{d}{dt}S_1^z = -2\chi(S_2^y S_1^x - S_2^x S_1^y), \\ &\frac{d}{dt}S_2^x = 2\chi S^y S_2^z + \frac{\delta_s}{2}S_2^y, \quad \frac{d}{dt}S_2^y = -2\chi S^x S_2^z - \frac{\delta_s}{2}S_2^x, \quad \frac{d}{dt}S_2^z = -2\chi(S_1^y S_2^x - S_1^x S_2^y). \end{aligned} \tag{10.30}$$

The spin components without the hat represent the expectation value of the corresponding spin operators.

In the following, we assume an initial state satisfying $S_1^x = S_2^x = N/4$, $S_1^y = S_2^y = S_1^z = S_2^z = 0$. The conserved quantities of the two-spin BCS model are the total magnetisation

$$S^z = S_1^z + S_2^z = 0, \tag{10.31}$$

the total energy

$$E/\hbar = \chi S^+S^- + \frac{\delta_s}{2}S_1^z - \frac{\delta_s}{2}S_2^z = \chi\left(\frac{N}{2}\right)^2, \tag{10.32}$$

as well as the spin length of each of the large spins, $(S_1^x)^2 + (S_1^y)^2 + (S_1^z)^2 = (N/4)^2$, $(S_2^x)^2 + (S_2^y)^2 + (S_2^z)^2 = (N/4)^2$. Using these conserved quantities, one can derive from the mean field equations in Eq. (10.30) an equation of motion for the BCS order parameter, $\Delta_{\mathrm{BCS}} = \chi S^-$. To simplify the notation, we define $\Delta \equiv |\Delta_{\mathrm{BCS}}|/\chi N$, i.e. $\Delta^2 = S^+S^-/N^2$. From Eq. (10.31) and Eq. (10.32), we obtain

$$\frac{d}{dt}\Delta^2 = -\frac{\delta_s}{\chi N^2}\frac{d}{dt}S_1^z = \frac{2\delta_s}{N^2}(S_2^yS_1^x - S_2^xS_1^y), \tag{10.33}$$

which leads to

$$\begin{aligned}\frac{d^2}{dt^2}\Delta^2 &= \frac{2\delta_s}{N^2}\left(S_1^x\frac{d}{dt}S_2^y + S_2^y\frac{d}{dt}S_1^x - S_1^y\frac{d}{dt}S_2^x - S_2^x\frac{d}{dt}S_1^y\right)\\ &= 4\delta_s\chi\Delta^2S_1^z - \frac{2\delta_s^2}{N^2}(S_1^xS_2^x + S_1^yS_2^y).\end{aligned} \tag{10.34}$$

From the above conserved quantities, we can create the equivalent expressions $\delta_s S_1^z = -\chi N^2(\Delta^2 - 1/4)$, $2(S_1^xS_2^x + S_1^yS_2^y) = N^2\Delta^2 - 2\times(N/4)^2 + 2(S_1^z)^2$. Plugging these into the equation of motion gives

$$\frac{d^2}{dt^2}\Delta^2 = -6(\chi N)^2(\Delta^2)^2 + \left(2(\chi N)^2 - \delta_s^2\right)\Delta^2 + \frac{\delta_s^2 - (\chi N)^2}{8}. \tag{10.35}$$

The equation above can be further simplified to

$$\frac{1}{2}\left(\frac{d}{dt}\Delta\right)^2 + V(\Delta) = 0, \tag{10.36}$$

where

$$V(\Delta) = \frac{1}{2}(\chi N)^2\left(\Delta^2 - \frac{1}{4}\right)\left(\Delta^2 - \frac{1-(\delta_s/\chi N)^2}{4}\right), \tag{10.37}$$

with an initial condition $\Delta = 1/2$. Eq. (10.36) can be understood as a classical particle with position Δ oscillating in the potential $V(\Delta)$. For $\delta_s < \chi N$, we find Δ oscillating between $\Delta_{\max} = 1/2$ and $\Delta_{\min} = \sqrt{1-(\delta_s/\chi N)^2}/2$. This is equivalent to phase II in the cases of many spins with inhomogeneous atom-light couplings, because all the oscillations damp in the large χN limit. For $\delta_s > \chi N$, we find Δ oscillating between $\Delta_{\max} = 1/2$ and $\Delta_{\min} = 0$, since the definition of Δ requires $\Delta \geq 0$. This is equivalent to phase III in the cases of many spins because the phase connects to single-particle oscillations in the large δ_s limit. Therefore, a dynamical phase transition occurs at $\delta_s/\chi N = 1$, which is equivalent to the phase II to phase III transition in the many-spin system.

The analytical solution of Eq. (10.36) can be written in terms of Jacobian elliptic funtions dn and cn:

$$\Delta(t) = \begin{cases} \frac{1}{2}\mathrm{dn}\left(\frac{1}{2}\chi N t\middle|(\delta_s/\chi N)^2\right) & \text{if } \delta_s < \chi N \\ \\ \frac{1}{2}\left|\mathrm{cn}\left(\frac{1}{2}\delta_s t\middle|(\chi N/\delta_s)^2\right)\right| & \text{if } \delta_s > \chi N \end{cases}. \tag{10.38}$$

The frequency of $\Delta(t)$ can be written in terms of the complete elliptic integral of the first kind $K(k^2)$:

$$\frac{\omega}{\chi N} = \begin{cases} \dfrac{\pi}{2K\Big((\delta_s/\chi N)^2\Big)} & \text{if } \delta_s < \chi N \\ \dfrac{\delta_s}{\chi N}\dfrac{\pi}{2K\Big((\chi N/\delta_s)^2\Big)} & \text{if } \delta_s > \chi N \end{cases}. \tag{10.39}$$

The mean-field trajectories on the Bloch sphere are shown in Fig. 10.8**a**, and the oscillation frequency Eq. (10.39) is shown in Fig. 10.8**b**. The dynamical phase transition can also be understood from the mean field trajectories. For $\delta_s < \chi N$, the two large spins lock to each other and oscillate near the x axis of the Bloch sphere. For $\delta_s > \chi N$, the two large spins are unlocked and precess around the whole Bloch sphere. Near the dynamical critical point, the mean field trajectories are close to the north pole or south pole of the Bloch sphere, which leads to a slow down of the oscillations because they approach stable fixed points of the Hamiltonian.

10.9 Axial Motion

In this section, we elaborate on how to take into account axial motion present in the experimental system. Similar discussions can be found in Ref. [Muniz *et al.*(2020)]. We start with the one-dimensional Hamiltonian of our cavity QED system with two internal atomic levels ($|\uparrow\rangle$ and $|\downarrow\rangle$), given by

$$\begin{aligned}\hat{H} = &\sum_{\sigma=\{\uparrow,\downarrow\}} \int dx\ \hat{\psi}^\dagger_\sigma(x)\left[\frac{\hat{p}^2}{2M} + V_0\sin^2(k_L x)\right]\hat{\psi}_\sigma(x) + \int dx\ \hat{\psi}^\dagger_\uparrow(x)\Big[\hbar\omega_0 + U_{ac}(x)\Big]\hat{\psi}_\uparrow(x) \\ &+ \hbar g_c \int dx\ \cos(k_c x)\Big[\hat{\psi}^\dagger_\uparrow(x)\hat{\psi}_\downarrow(x)\hat{a} + \hat{a}^\dagger\hat{\psi}^\dagger_\downarrow(x)\hat{\psi}_\uparrow(x)\Big] + \hbar\omega_c\hat{a}^\dagger\hat{a},\end{aligned} \tag{10.40}$$

where $k_L = 2\pi/\lambda_L$ is the wavenumber of the lattice beams ($\lambda_L = 813$nm), k_c is the wavenumber of the cavity mode ($\lambda_c = 689$nm), ω_0 is the atomic transition frequency between $|\uparrow\rangle$ and $|\downarrow\rangle$ states, $U_{ac}(x)$ is the AC Stark shift applied to the atoms (including the differential light shift from the lattice beams and the transverse AC Stark shift beam), and ω_c is the frequency of cavity resonance.

Since the atoms are trapped in an optical lattice with lattice depth on the order of $10^3 E_R$, we can approximate each lattice site as an harmonic trap with axial trapping frequency $\hbar\omega_T = \sqrt{4V_0E_R}$, where $E_R = \hbar^2k_L^2/2M$ is the lattice recoil energy. We also ignore tunnelling processes between lattice sites. In this case, one can expand the atomic field operator in terms of lattice site index j and harmonic oscillator levels n:

$$\hat{\psi}_\sigma(x) = \sum_{jn}\hat{c}_{jn,\sigma}\phi_n(x - ja_L). \tag{10.41}$$

Here, $a_L = \lambda_L/2$ is the lattice spacing, and ϕ_n is the harmonic oscillator wave function for mode n, given by

$$\phi_n(x) = \frac{1}{\sqrt{2^n n!}}\left(\frac{M\omega_T}{\pi\hbar}\right)^{1/4} \mathrm{e}^{-M\omega_T x^2/2\hbar} H_n\left(\sqrt{\frac{M\omega_T}{\hbar}}x\right) \tag{10.42}$$

where $H_n(x)$ are the Hermite polynomials. Plugging this expansion into the Hamiltonian and transforming to the rotating frame of the atoms, we obtain

$$\hat{H}/\hbar = \sum_{jn\sigma} n\omega_T\hat{c}^\dagger_{jn,\sigma}\hat{c}_{jn,\sigma} + \sum_{jn}\varepsilon_{jn}\hat{c}^\dagger_{jn,\uparrow}\hat{c}_{jn,\uparrow} + g_c\sum_{jnm}\zeta^{nm}_j(\hat{c}^\dagger_{jn,\uparrow}\hat{c}_{jm,\downarrow}\hat{a} + \hat{a}^\dagger\hat{c}^\dagger_{jm,\downarrow}\hat{c}_{jn,\uparrow}) + \delta_c\hat{a}^\dagger\hat{a} \tag{10.43}$$

where $\delta_c = \omega_c - \omega_a$. For simplicity, we assume $U_{ac}(x)$ is either small or slowly varying in space and thus does not change the trap geometry. This term gives rise to an inhomogeneous transition frequency $\varepsilon_{jn} = \int dx U_{ac}(x)[\phi_n(x - ja_L)]^2/\hbar$. We calculate ζ_j^{nm} in the following way:

$$\begin{aligned}\zeta_j^{nm} &= \int dx\ \cos(k_c x)\phi_n(x - ja_L)\phi_m(x - ja_L) = \int dx\ \cos(k_c x + k_c j a_L)\phi_n(x)\phi_m(x) \\ &= \cos(j\varphi)\int dx\ \cos(k_c x)\phi_n(x)\phi_m(x) - \sin(j\varphi)\int dx\ \sin(k_c x)\phi_n(x)\phi_m(x) \\ &= \cos(j\varphi)\,\mathrm{Re}\left[(i\eta)^s e^{-\eta^2/2}\sqrt{\frac{n_<!}{n_>!}}L_{n_<}^s(\eta^2)\right] - \sin(j\varphi)\,\mathrm{Im}\left[(i\eta)^s e^{-\eta^2/2}\sqrt{\frac{n_<!}{n_>!}}L_{n_<}^s(\eta^2)\right].\end{aligned} \tag{10.44}$$

where $\varphi = \pi k_L/k_c$, $s = |n - m|$, $n_< = \min(n, m)$, $n_> = \max(n, m)$, $L_n^\alpha(x)$ are the generalised Laguerre polynomials, and $\eta = k_c\sqrt{\hbar/2M\omega_T}$ is the Lamb-Dicke parameter. In our case $\omega_T/2\pi = 165$ kHz, implying that $\eta = 0.17$. This places us in the Lamb-Dicke regime where ζ_j^{nm} is negligible for $|n - m| > 1$. It can be convenient to rewrite the Hamiltonian in terms of operators $\hat{S}^j_{n\sigma,m\sigma'} = \hat{c}^\dagger_{jn,\sigma}\hat{c}_{jm,\sigma'}$, resulting in the following form:

$$\hat{H}/\hbar = \sum_{jn\sigma} n\omega_T \hat{S}^j_{n\sigma,n\sigma} + \sum_{jn}\varepsilon_{jn}\hat{S}^j_{n\uparrow,n\uparrow} + g_c\sum_{jnm}\zeta_j^{nm}(\hat{S}^j_{n\uparrow,m\downarrow}\hat{a} + \hat{a}^\dagger\hat{S}^j_{m\downarrow,n\uparrow}) + \delta_c\hat{a}^\dagger\hat{a}. \tag{10.45}$$

In addition to the Hamiltonian dynamics, we also consider dissipation processes such as cavity loss with a rate $\kappa/2\pi = 153$ kHz, as well as spontaneous emission with a rate $\gamma/2\pi = 7.5$ kHz. The full dynamics of this open system can be described by the following Lindblad master equation:

$$\frac{\mathrm{d}}{\mathrm{d}t}\hat{\rho} = -\frac{i}{\hbar}[\hat{H}, \hat{\rho}] + \left[\hat{L}_{\mathrm{cav}}\hat{\rho}\hat{L}^\dagger_{\mathrm{cav}} - \frac{1}{2}\{\hat{L}^\dagger_{\mathrm{cav}}\hat{L}_{\mathrm{cav}}, \hat{\rho}\}\right] + \sum_{jn}\left[\hat{L}_{j,n}\hat{\rho}\hat{L}^\dagger_{j,n} - \frac{1}{2}\{\hat{L}^\dagger_{j,n}\hat{L}_{j,n}, \hat{\rho}\}\right], \tag{10.46}$$

where the jump operator for cavity loss is given by $\hat{L}_{\mathrm{cav}} = \sqrt{\kappa}\hat{a}$, and the single-particle jump operators for spontaneous emission are given by $\hat{L}_{j,n} = \sqrt{\gamma}\hat{S}^j_{n\downarrow,n\uparrow}$. Here, we assume that spontaneous emission is in the Lamb-Dicke regime.

In the experiment, δ_c is the largest frequency scale ($\delta_c \gg g_c\sqrt{N}, \kappa$), so we can adiabatically eliminate the cavity photons [Reiter and Sørensen(2012)] and obtain the following effective atom-only master equation:

$$\frac{\mathrm{d}}{\mathrm{d}t}\hat{\rho} = -\frac{i}{\hbar}[\hat{H}_{\mathrm{eff}}, \hat{\rho}] + \left[\hat{L}_{\mathrm{col}}\hat{\rho}\hat{L}^\dagger_{\mathrm{col}} - \frac{1}{2}\{\hat{L}^\dagger_{\mathrm{col}}\hat{L}_{\mathrm{col}}, \hat{\rho}\}\right] + \sum_{jn}\left[\hat{L}_{j,n}\hat{\rho}\hat{L}^\dagger_{j,n} - \frac{1}{2}\{\hat{L}^\dagger_{j,n}\hat{L}_{j,n}, \hat{\rho}\}\right]. \tag{10.47}$$

Here, the effective Hamiltonian is given by

$$\hat{H}_{\mathrm{eff}}/\hbar = \sum_{jn\sigma} n\omega_T\hat{S}^j_{n\sigma,n\sigma} + \sum_{jn}\varepsilon_{jn}\hat{S}^j_{n\uparrow,n\uparrow} + \chi\sum_{jnm}\sum_{kpq}\zeta_j^{nm}\zeta_k^{pq}\hat{S}^j_{n\uparrow,m\downarrow}\hat{S}^k_{p\downarrow,q\uparrow}, \tag{10.48}$$

and effective collective jump operator generating superradiant decay takes the form

$$\hat{L}_{\mathrm{col}} = \sqrt{\Gamma}\sum_{jnm}\zeta_j^{nm}\hat{S}^j_{m\downarrow,n\uparrow}, \tag{10.49}$$

where $\chi = -g_c^2\delta_c/(\delta_c^2 + \kappa^2/4)$ and $\Gamma = g_c^2\kappa/(\delta_c^2 + \kappa^2/4)$. The equivalent superconducting order parameter takes the following form:

$$\Delta_{\mathrm{BCS}} = \chi\sum_{kpq}\zeta_k^{pq}\langle\hat{S}^k_{p\downarrow,q\uparrow}\rangle. \tag{10.50}$$

One can recover the inhomogeneous model discussed in the previous section by removing the axial harmonic oscillator level labels.

Similarly, the Hamiltonian for initial state preparation takes the form

$$\hat{H}_{\text{drive}}/\hbar = \sum_{jn\sigma} n\omega_T \hat{S}^j_{n\sigma,n\sigma} + \frac{1}{2}\sum_{jnm} \zeta_j^{nm}(\Omega \hat{S}^j_{n\uparrow,m\downarrow} + \Omega^* \hat{S}^j_{m\downarrow,n\uparrow}). \tag{10.51}$$

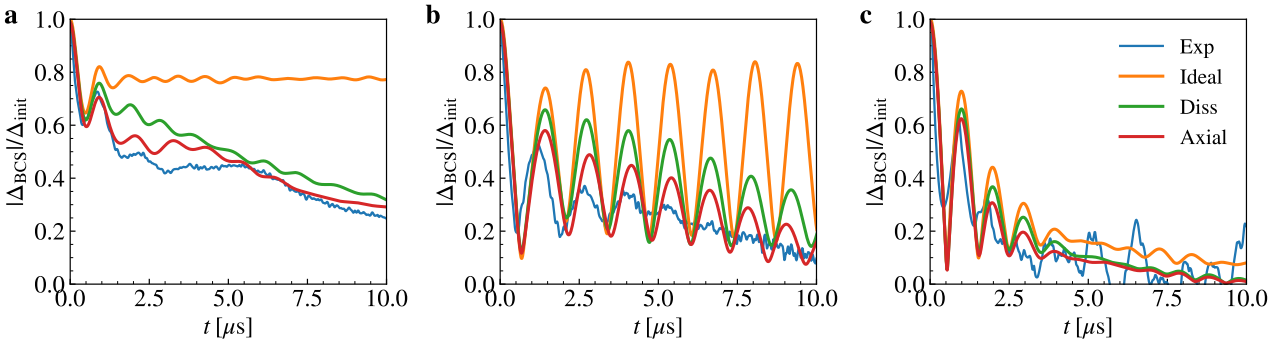

Extended Data Fig. 10.9: **Understanding experimental results with axial motion effects.** **a** Example phase II traces with $\chi N/2\pi = 1.29$MHz, $f_{\text{AC}}/2\pi = 1.1$MHz. **b** Example phase III traces with $\chi N/2\pi = 0.79$MHz, $f_{\text{AC}}/2\pi = 1.1$MHz. **c** Example phase I traces with $\chi N/2\pi = 0.15$MHz, $f_{\text{AC}}/2\pi = 1.1$MHz. The blue points are experimental data, the orange lines represent numerical simulations under ideal conditions (see Eq. (3) in the Methods), the green lines include dissipative processes on top of the ideal simulations, and the red lines consider both dissipative processes and axial motion effects.

In numerical simulations, we perform a mean-field approximation, which replaces the operators $\hat{S}^j_{p\sigma,q\sigma'}$ by their expectation values $\langle \hat{S}^j_{p\sigma,q\sigma'} \rangle$ in the Heisenberg equation of motion. We perform a random sampling of the axial harmonic oscillator mode n for each atom based on a thermal distribution of 15 μK, and we only include the modes n and $n \pm 1$ into our calculation due to the Lamb-Dicke parameter. The atom number in our simulations is set to 2000; to match χN to experimental values, we rescale χ accordingly. We also empirically take into account two additional dissipation processes to quantitatively capture the behavior of $|\Delta_{\text{BCS}}|$ at longer time scales. The first is a single-particle decoherence between electronic states, described by the jump operators $\hat{L}^{\text{el}}_{j,\sigma} = \sqrt{\gamma_{\text{el}}} \sum_n \hat{S}^j_{n\sigma,n\sigma}$ with $\gamma_{\text{el}}/2\pi < 1$kHz for Fig. 2 starting from $t = 0\mu$s, and by $\gamma_{\text{el}}/2\pi = 0.0036(f_{\text{AC}}/2\pi) + 4$kHz for Fig. 3 and Fig. 4 in the main text. The second is a single-particle decoherence between motional states, described by the jump operators $\hat{L}^{\text{mo}}_{j,n} = \sqrt{\gamma_{\text{mo}}} \sum_\sigma \hat{S}^j_{n\sigma,n\sigma}$ with $\gamma_{\text{mo}}/2\pi = 15$kHz.

Some example traces including axial motion effects are depicted in Fig. 10.9. Generally speaking, accounting for these effects allows us to more accurately predict features present in the experimentally measured evolution of $|\Delta_{\text{BCS}}|$, at the same time leaving the predicted dynamical phase boundaries unchanged. As shown in Fig. 10.9a, including axial motion effects in phase II traces allows us to capture the faster damping rate of the Higgs oscillations, as well as a slow oscillation in $|\Delta_{\text{BCS}}|$ at the axial trapping frequency. Likewise, as shown in Fig. 10.9b, including axial motion effects in phase III traces allows us to capture the faster damping rate of the oscillations in $|\Delta_{\text{BCS}}|$, although the observed damping rate is still faster than the rate predicted by theory. Finally, as shown in Fig. 10.9c, all the theory simulations of phase I dynamics are similar to the simulation under ideal conditions, indicating that axial motion does not play an significant role in this regime.

11 Higgs mode in a strongly interacting fermionic superfluid by Behrle, Harrison et al.

11.0.1 Main theory

Higgs and Goldstone modes are possible collective modes of an order parameter upon spontaneously breaking a continuous symmetry. Whereas the low-energy Goldstone (phase) mode is always stable, additional symmetries are required to prevent the Higgs (amplitude) mode from rapidly decaying into low-energy excitations. In high-energy physics, where the Higgs boson[1] has been found after a decades-long search, the stability is ensured by Lorentz invariance. In the realm of condensed–matter physics, particle–hole symmetry can play this role[2] and a Higgs mode has been observed in weakly-interacting superconductors[3, 4, 5]. However, whether the Higgs mode is also stable for strongly-correlated superconductors in which particle–hole symmetry is not precisely fulfilled or whether this mode becomes overdamped has been subject of numerous discussions[6, 7, 8, 9, 10, 11]. Experimental evidence is still lacking, in particular owing to the difficulty to excite the Higgs mode directly. Here, we observe the Higgs mode in a strongly-interacting superfluid Fermi gas. By inducing a periodic modulation of the amplitude of the superconducting order parameter Δ, we observe an excitation resonance at frequency $2\Delta/h$. For strong coupling, the peak width broadens and eventually the mode disappears when the Cooper pairs turn into tightly bound dimers signalling the eventual instability of the Higgs mode.

Spontaneous symmetry breaking occurs when an equilibrium state exhibits a lower symmetry than the corresponding Hamiltonian describing the system. The system then spontaneously picks one of the energetically degenerate choices of the order parameter and due to the specific energy landscape this process is accompanied by new collective modes. The typical picture, which exemplifies spontaneous symmetry breaking, uses a Mexican-hat shaped energy potential (see Figure 1a) that suggests the emergence of two distinct collective modes: the gapless "Goldstone mode", which is associated with long-wavelength phase fluctuations of the order parameter, and an orthogonal gapped mode, the "Higgs mode", which describes amplitude modulations of the order parameter. While Goldstone modes, such as phonons, appear necessarily when continuous symmetries are broken, stable Higgs modes are scarce, since decay channels might be present. The best-known example of a Higgs mode appears in the Standard Model of particle physics where this mode gives elementary particles their mass [1].

In the non-relativistic low-energy regime usually encountered in condensed-matter physics, the existence of a stable Higgs mode cannot be taken for granted[6]. However, under certain conditions, other symmetries, such as particle-hole symmetry, can play the role of Lorentz invariance and induce a stable Higgs mode. A notable example of a low-energy particle-hole symmetric theory hosting a stable Higgs mode is the famous Bardeen-Cooper-Schrieffer (BCS) Hamiltonian describing weakly interacting superconductors [2, 12]. Evidence for the Higgs mode has been found in conventional BCS superconductors [3, 4, 5]. However, experimental detections have been solely indirect as the Higgs mode does not couple directly to electromagnetic fields owing to the gauge invariance required for its existence. The far-reaching importance of the Higgs mode is further illustrated by its observation in a variety of specially tuned systems such as antiferromagnets [13], liquid ^{3}He [14], ultracold bosonic atoms near the superfluid/Mott-insulator transition [15, 16], spinor Bose gases [17], and Bose gases strongly coupled to optical fields [18]. In contrast, weakly-interacting Bose-Einstein condensates do not exhibit a stable Higgs mode [6, 10, 11].

In recent years, research has focused on advanced materials exhibiting superconductivity far beyond the conventional BCS description, such as cuprates, pnictides, and the unitary Fermi

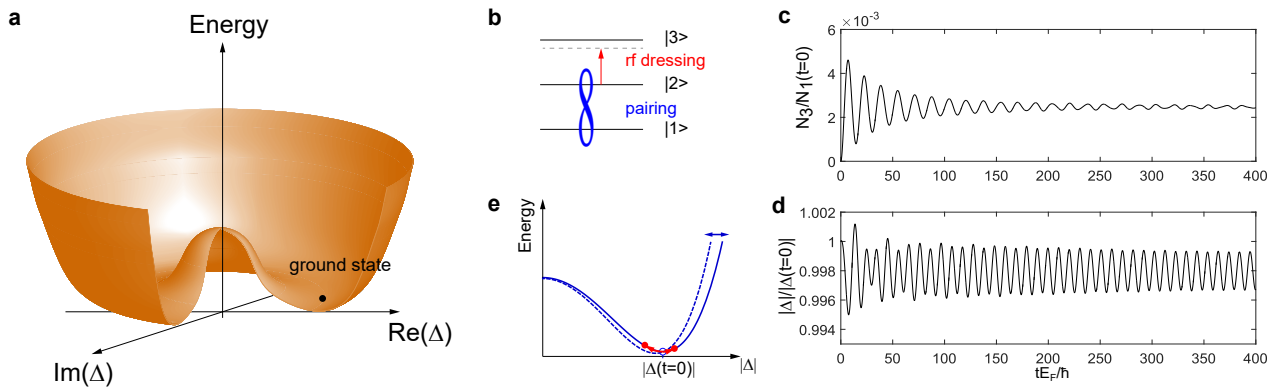

Figure 11.1: Principle of the Higgs mode excitation. (a) Mexican hat potential of the free energy as a function of real and imaginary part of the complex order parameter Δ. The equilibrium state order parameter takes spontaneously one of the values at the energy minima. (b) We employ radiofrequency dressing of the paired superfluid by off-resonant coupling to an unoccupied state $|3\rangle$. This results in a periodic modulation of both the occupation of the state $|3\rangle$ (c) and the superconducting gap (d). Shown are numerical simulations for a coupling constant $1/(k_F a) = -0.6704$, $\hbar\Omega_R = 0.0353 E_F$ and $\hbar\delta = -0.3247 E_F$. (e) By adjusting the modulation frequency, we achieve an excitation of the Higgs mode in the Mexican hat.

gas. Many of these materials are characterized by strong fermionic correlations. Even though in this context the existence of a Higgs mode has been the topic of theoretical debates [7, 8, 9, 10, 11], experimental evidence for the Higgs mode in systems exhibiting strong correlations between fermions is still absent.

Here, we spectroscopically excite the Higgs mode in a superfluid Fermi gas in the crossover between a weakly-interacting BCS superfluid and a Bose-Einstein condensate (BEC) of strongly-coupled dimers (Fig. 1). We induce a periodic modulation of the amplitude of the superconducting order parameter Δ and find an excitation resonance near twice the superconducting gap value. On the BCS side, the spectroscopic feature agrees with the theoretical expectation of the Higgs mode. On the BEC side of the crossover, we find strong broadening beyond the predictions of BCS theory and, eventually, the disappearance of the mode as predicted for a weakly-interacting BEC [6, 10, 11].

Our measurements are conducted in an ultracold quantum gas of $\sim 4 \times 10^6$ ^{6}Li atoms prepared in a balanced mixture of the two lowest hyperfine states $|1\rangle$ and $|2\rangle$ of the electronic ground state. The gas is trapped in a harmonic potential with frequencies of $(\omega_x, \omega_y, \omega_z) = 2\pi \times (91, 151, 235)$ Hz and is subjected to a homogeneous magnetic field, which is varied in the range of $740 - 1000$ G in order to tune the s-wave scattering length a near the Feshbach resonance located at 834 G. This results in an adjustment of the interaction parameter of the gas in the range of $-0.8 \lesssim 1/(k_F a) \lesssim 1$, i.e. across the whole BCS/BEC crossover. The Fermi energy in the center of the gas is $E_F \simeq h \times (34 \pm 3)$ kHz at each of the considered interaction strengths and sets the Fermi wave vector $k_F = \sqrt{8\pi^2 m E_F/h^2}$, where m denotes the mass of the atom and h is Planck's constant.

Excitation of the Higgs mode requires a scheme which couples to the amplitude of the order parameter rather than creating phase fluctuations or strong single-particle excitations. Previous theoretical proposals[19, 8, 20] for exciting the Higgs mode in ultracold Fermi gases have focused on a modulation of the interaction parameter $1/(k_F a)$, however, experimentally only single-particle excitations have been observed from such a modulation[21]. We have developed a novel excitation scheme employing a radiofrequency (rf) field dressing the state $|2\rangle$ with the initially unoccupied hyperfine state $|3\rangle$ thereby modulating the pairing between the $|1\rangle$ and $|2\rangle$ states, see Figure 1b and c. Previous experiments investigating ultracold gases with rf

spectroscopy[22, 23, 24, 25] have focused on studying single-particle excitations. To this end, there, the duration of the rf pulse τ had been chosen shorter than the inverse of the Rabi frequency Ω_R, such that the spectra could be interpreted in the weak-excitation limit using Fermi's golden rule. In contrast, here, we employ an rf drive far red-detuned from single-particle resonances in the interacting many-body system and in the long-pulse limit $\Omega_R\tau \gg 1$, in order to couple to the amplitude of the order parameter. To illustrate this, consider first an isolated two-level system of the $|2\rangle$ and the $|3\rangle$ state coupled by a Rabi frequency Ω_R with detuning δ from the resonance. The occupation probability of the atoms in the $|2\rangle$ state is $p_{|2\rangle} = 1 - \Omega_R^2/{\Omega'_R}^2 \sin^2(\Omega'_R t/2)$, i.e. the continuous rf dressing leads to a time-periodic modulation of the occupation of the $|2\rangle$-state with the effective Rabi frequency $\Omega'_R = \sqrt{\Omega_R^2 + \delta^2}$.

In the many-body problem of the BCS/BEC crossover, the situation is complicated by the dispersion of the (quasi-) particles and the presence of interactions. In particular, a continuum of excitations typically occurs above the energy of the lowest single-particle excitation to state $|3\rangle$ (see Figure 2a). Deep in the BCS regime, the continuum of excitations is related to the different momentum states and the excitation scheme can be approximated by coupling each occupied momentum state of the BCS quasi-particles in level $|2\rangle$ to the corresponding momentum state in state $|3\rangle$ since the rf dressing transfers negligible momentum. The effective Rabi frequency $\Omega'_{R,k} = \sqrt{\Omega_R^2 + \delta_k^2}$ and therefore the excitation probability becomes momentum dependent by the many-body detuning $\hbar\delta_k = \hbar\delta - E_k - \xi_k$, where ξ_k is the single-particle dispersion, and $E_k = \sqrt{\xi_k^2 + |\Delta|^2}$ is the quasi-particle dispersion and Δ is the s-wave superconducting order parameter. A red-detuned rf drive, as employed here, avoids resonant coupling to the single-particle excitations, however, still modulates off-resonantly the occupation of the excited states as shown in Figure 2b.

The off-resonant periodic modulation of the occupation of the state $|2\rangle$ with controllable frequency $\Omega'_{R,k}$ induces a modulation of the amplitude of the order parameter $|\Delta|$ (Fig. 1e, for details see Methods) and hence couples directly to the Higgs mode. To illustrate this mechanism, we numerically solve the minimal set of coupled equations of motion describing the evolution of the order parameter in the presence of an rf coupling to state $|3\rangle$ (see Methods and Supplementary Figure). We see that the Fourier spectrum of $|\Delta|$ for one modulation frequency displays – aside from a response corresponding to the modulation frequencies $\Omega'_{R,k}$ – a sharp peak at the gap value $2|\Delta|$, see Figure 2d. By the momentum-resolved representation (Figure 2c) we identify this peak to be dominated by the Higgs excitation with a momentum-independent dispersion. The amplitude of the latter is maximum when the averaged effective drive frequency $\hbar\bar{\Omega}_{mod} \approx 2|\Delta|$ in accordance with its expected frequency. The Higgs mode is a collective mode of the system and even for the harmonically trapped gas exhibits a unique frequency. Numerical studies in the BCS limit have shown that in harmonically trapped systems, the Higgs mode should occur at the frequency of twice the superconducting gap evaluated at the maximum density of the gas [8, 26, 27, 28, 29] and hence we use this as our reference for the value of the gap in order to compare with theory and other experiments.

In the experiment, we search for the Higgs mode by measuring the energy absorption spectrum of the fermionic superfluid in the $|1, 2\rangle$ states for different interactions. Using Ω_R and δ as adjustable parameters, we dress the $|2\rangle$ state by the $|3\rangle$ state with adjustable modulation frequency given by the effective Rabi frequency. We choose a drive frequency in the single–particle excitation gap. For our experiments we measure the modulation frequency Ω_{mod} and amplitude α of the time-dependent population of the $|3\rangle$ state (for calibration, see Methods and Supplementary Figure). We then use a constant excitation amplitude $p_{|3\rangle} \simeq 0.5\%$ and apply the modulation for a fixed period of 30 ms. After the excitation we conduct a rapid magnetic field sweep onto the molecular side of the Feshbach resonance and convert Cooper pairs into dimers and measure the condensate fraction of the molecular condensate in time-of-flight imaging. The change in the condensate fraction provides us with a sensitive measure of

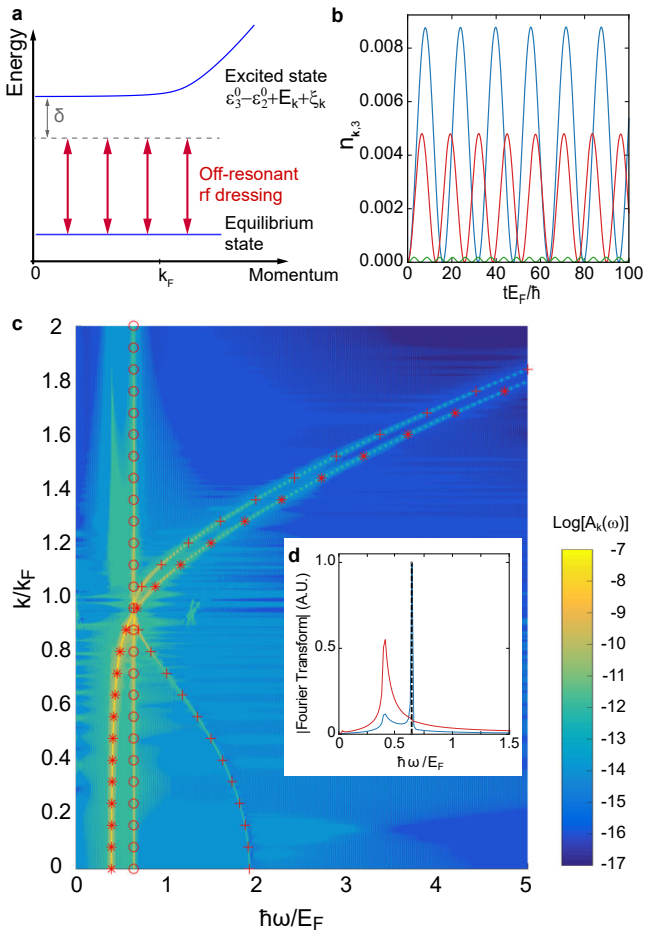

Figure 11.2: Illustration of the excitation scheme for one modulation frequency. (a) The radiofrequency field is red-detuned from the single-particle excitation of the interacting system. It creates an off-resonant excitation to the state $|3\rangle$ with a varying detuning for different momenta. (b) Time-evolution of the momentum-resolved occupation of the $|3\rangle$ state with momentum $\boldsymbol{k}$ for a fixed value of $\frac{1}{k_F a} = -0.63$, a Rabi frequency $\hbar\Omega_R = 0.038E_F$, and a detuning $\hbar\delta = -0.34E_F$. Blue: $|\boldsymbol{k}|/k_F = 0$, red: $|\boldsymbol{k}|/k_F = 0.8$, green: $|\boldsymbol{k}|/k_F = 1.1$. (c) Spectral weight of the momentum-resolved gap $A_{\mathbf{k}}(\omega)$ (see Methods). The circles indicate the Higgs mode, the stars mark the response to the modulation frequency and the crosses indicate the quasiparticle excitations at $2E_k$. The position of the star at $k = 0$ approximately represents the effective modulation frequency for the chosen parameters. (d) Fourier spectra (momentum integrated) of the occupation of the $|3\rangle$ state (red) and $|\Delta|$ (blue). The dashed line is the expected location of the Higgs mode at $2|\Delta|$. Subplots b, c, and d are for the same driving and detuning parameters.

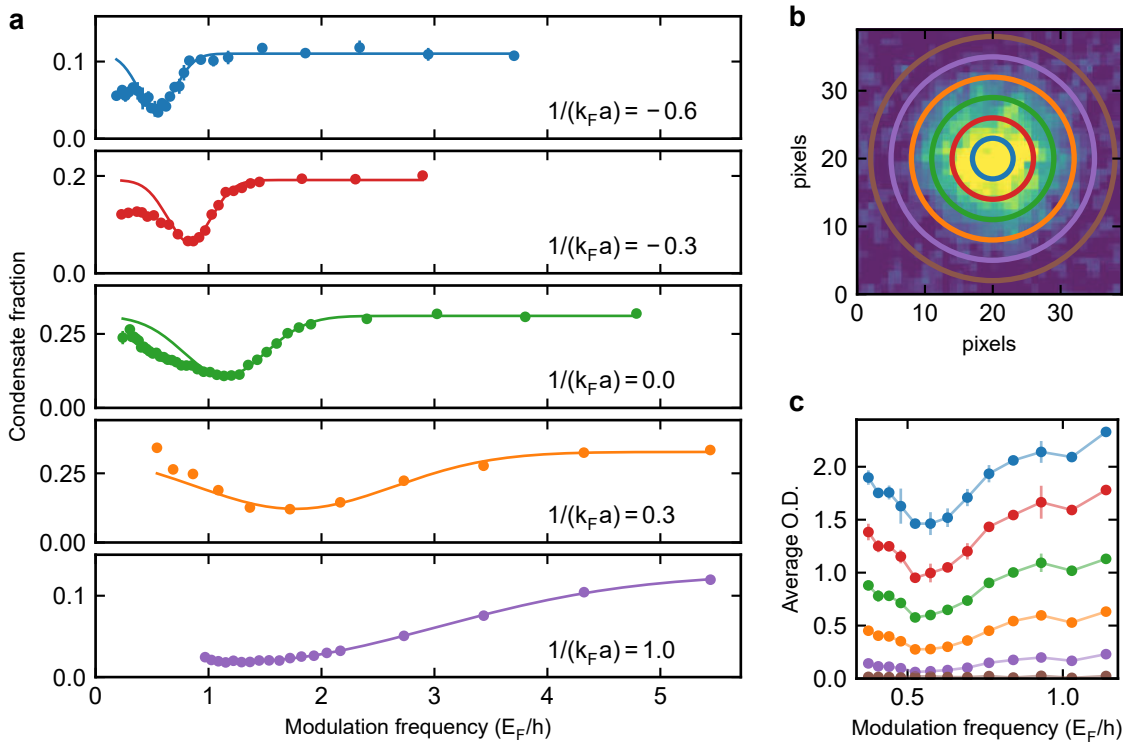

Figure 11.3: Excitation spectra of the Higgs mode. (a) Excitation spectra of the Higgs mode for different interaction strengths, $1/(k_F a)$, as labeled in the figure. The different levels of background condensate fraction are due to the different $1/(k_F a)$. The solid lines shows the Gaussian fit to the high frequency side of the spectra. The error bars show the standard deviation of approximately four measurements. (b) Time-of-flight image of the condensate with the thermal background subtracted at $1/(k_F a) \approx -0.43$. Rings indicate momentum intervals of $0.02\,k_F$. (c) Momentum-resolved analysis of the Higgs excitation inside the condensate by averaging the optical density in the color-coded rings in (b) for different modulation frequency. The resonance occurs at the same modulation frequency for all momenta.

the excitation of modes in the quantum gas. In Figure 3a we plot the measured spectra as a function of the modulation frequency for different values of $1/(k_F a)$. On the BCS-side of the Feshbach resonance up to unitarity, $1/(k_F a) < 0$, we observe clear resonances for which the condensate fraction reduces, signaling the excitation of a well defined mode. For $1/(k_F a) > 0$, the energy absorption peak is gradually washed out and broadens significantly. Far on the BEC side, for $1/(k_F a) \simeq 1$, we cannot observe a resonance and conclude that the Higgs mode is absent. The resonances generally exhibit an asymmetric line shape, which we fit with a Gaussian to the high-frequency side in order to extract the peak position and width. A contribution to the asymmetric peak shape stems from the momentum-dependence of the effective Rabi frequencies $\Omega'_{R,k}$. As indicated in Figures 2a and b, the effective detuning (and hence the modulation frequency) varies with increasing momentum k. Therefore, a resonant excitation at the Higgs mode frequency can be achieved for high momenta k even though for low momenta the modulation frequency is below the resonant excitation.

In order to demonstrate the collective mode nature of our resonance, we perform a number of checks. Firstly, we verify that the excitation resonance frequency (to within 4%) and shape is independent of the modulation strength in the range of $0.001 < \alpha < 0.2$ and modulation duration between $\tau = 0.5\,\mathrm{ms}$ and $\tau = 30\,\mathrm{ms}$ (for the definition of α, see Methods and Supplementary Figure). Secondly, we have confirmed that the observed resonance peak is not caused by single-particle excitations by measuring the excitation probability to the $|3\rangle$ state vs. modulation frequency Ω_{mod} and finding a featureless broad spectrum. This and the following checks have been performed with a modulation amplitude of $\alpha = 0.2$ and a modulation time of 0.5 ms, which is much shorter than the trap period of $\sim 5\,\mathrm{ms}$. Hence the measurement is insensitive to thermalization effects and/or density redistribution within the cloud. Thirdly, we check the momentum-dependence of the resonance. After the modulation, we perform a time-of-flight expansion for a period of 15 ms, which is approximately a quarter period of the residual harmonic potential during ballistic expansion. This procedure maps the initial momentum states to positions in the absorption image [30]. We analyse the detected condensate density in momentum intervals of $0.02\,k_F$ and find that the excitation resonance is at the same frequency for all momentum intervals, see Figure 3b and 3c. Finally, we have searched for possible quasiparticle excitations resulting from our interaction modulation by employing standard rf spectroscopy [24, 25, 31] after the interaction modulation. The spectra only show a very weak and broad background independent of the modulation frequency. This behaviour is not unexpected since the contribution of quasi-particle excitations is smeared out in the presence of a trap as we confirmed numerically using the local-density approximation.

In Figure 4a, we plot the position of the fitted peak of the energy absorption spectra vs. the interaction parameter $1/(k_F a)$ evaluated at the center of the sample. It has been suggested[8] that the Higgs mode frequency is close to twice the superconducting gap in the BCS/BEC crossover and can therefore be used as an approximative measure of the gap. In the crossover regime, the exact value of $|\Delta|$ is yet unknown and both experiments and numerical calculations are challenging. We compare our data to gap measurement using different methods[31, 32] and several numerical calculations[33, 34, 35, 36, 37, 38]. As compared to the previous experimental results, our extracted value is somewhat larger. We note that previous gap measurements rely on fitting the onset of a spectral feature whereas our method is based on fitting a Gaussian to a slightly skewed spectral feature and both methodologies could be susceptible to small systematic uncertainties. An upper bound is provided by the theoretical result of mean-field theory (dashed line), which is known to overestimate the superconducting gap.

In Figure 4b, we plot the full-width-at-half-maximum of the Gaussian fits to the energy absorption peaks. Utilizing the BCS model for the momentum-dependent excitation discussed above, we estimate the width of our excitation resonance to be of order Δ, see Supplementary Figure. Hence, we cannot directly interpret the linewidth of our spectra as the decay rate of the

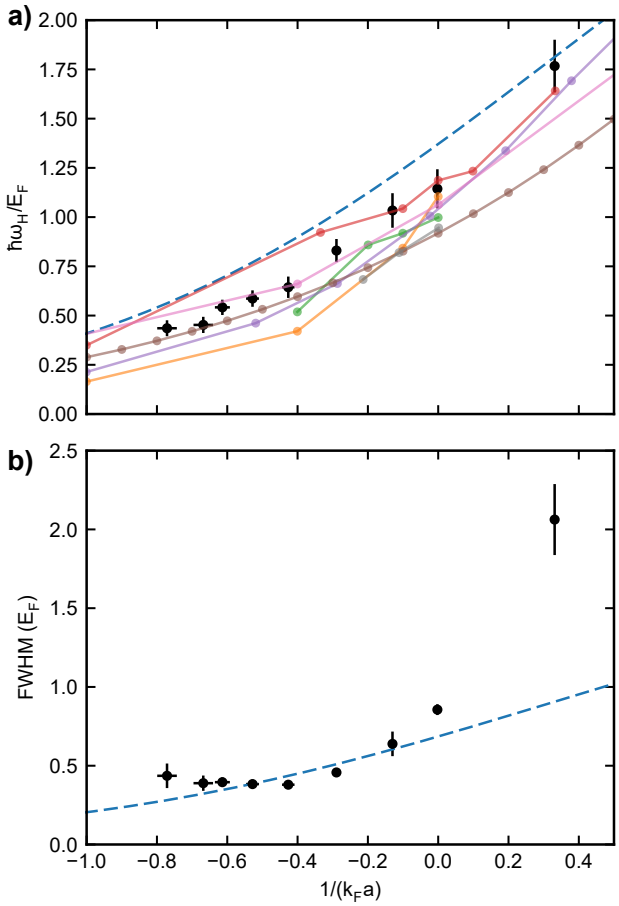

Figure 11.4: Observation of the Higgs mode. (a) Measured peak positions of the energy absorption spectra (black circles). For comparison we show numerical simulations of the gap parameter multiplied by 2: BCS mean field theory (blue dashed line), ref. [33] (red), ref. [34] (green), ref. [35] (orange), ref. [36] (purple), ref. [37] (brown), ref. [38] (pink). The grey symbols show the experimental data of ref. [32]. (b) Measured fullwidth at half maximum (FWHM) of the absorption peaks (black circles). For comparison, the BCS mean field theory gap is also shown (blue dashed line). The error bars in a and b represent the standard errors.

Higgs mode but only as lower limit of the lifetime. On the BCS side of the resonance we find good agreement with our model and towards the BEC side the measured width far exceeds the prediction, indicating that the Higgs mode becomes strongly broadened, for example, due to the violation of particle-hole symmetry resulting in a decay into Goldstone modes[39, 6, 10, 11]. Extending, in the future, our novel experimental scheme with a better momentum resolution will provide a route to finally explore the decay mechanisms of the Higgs mode, the understanding of which is a cornerstone in both high-energy particle physics and condensed-matter physics.

11.0.2 Methods

Preparation

Using standard techniques of laser cooling and sympathetic cooling in a mixture with Sodium atoms in a magnetic trap, we prepare $\sim 5 \times 10^7$ cold fermionic Lithium atoms in a crossed-beam optical dipole trap of wavelength 1070 nm in an equal mixture of the two lowest hyperfine states $|1\rangle$ and $|2\rangle$. Using subsequent evaporative cooling in a homogeneous magnetic field of 795 G, in immediate vicinity of the Feshbach resonance at 834 G, we produce a condensate in the BCS/BEC crossover regime with a temperature of $T/T_F = 0.07 \pm 0.02$. After preparation of the fermionic superfluid, the magnetic offset field is adiabatically adjusted in the range between 740 G and 1000 G in order to control the interaction parameter $1/(k_F a)$ in the range of $-0.8 < 1/(k_F a) < 1$, i.e. across the whole BCS/BEC crossover region.

Calibration of spectroscopy and analysis

We experimentally calibrate the modulation frequency and amplitude to take into account energy shifts owing to interaction effects of the initial and final states and the efficiency of the rf antenna setup. To this end, we drive Rabi oscillations with set values of detuning δ and power and measure the population $p_{|3\rangle}$ as a function of time during the rf drive $p_{|3\rangle} = \alpha \sin^2(\Omega_{\mathrm{mod}} t/2)$. This provides us with a direct measurement of the modulation frequency and amplitude. In order to model the data, we assume a Lorentzian line shape $\alpha = \frac{\Omega_R^2}{\Omega_R^2 + (\delta - \delta_0)^2}$, however, we allow for a frequency shift $\delta_0(k_F a)$ by which the detuning δ is corrected as compared to the Zeeman-energy resonance of the free atom. The fit parameter δ_0 absorbs the effects of interactions in the final state of the spectroscopy, the condensation energy of the initial state, and the averaging of different momentum states and densities in the trap. Experimentally, the calibration is performed at a value of $\alpha \simeq 4\%$ for which we obtain agreement with the Lorentzian model to a few percent.

We check for unpaired atoms in the $|2\rangle$ state for red and blue detuned radio-frequency with respect to δ_0 as a result of the modulation. This has been achieved by rapidly ramping the field to 450 G with approximately 4 G/μs, which allows for the detection of free atoms rather than paired atoms. In the case of a red-detuned radio-frequency modulation no enhancement of the signal of unpaired atoms could be observed over the whole range of modulation frequencies. However, blue detuned radio-frequency modulation increases significantly the number of unpaired atoms due to single particle excitations to the continuum, see Supplementary Figure 1.

Additionally, we vary the driving strength α and observe that the resonance position of the peak with respect to the modulation frequency does not vary, see Supplementary Figure 2.

Theoretical modelling

The experimental system can be described taking three different fermionic levels into account. Initially the system is prepared in a balanced mixture of states $|1\rangle$ and $|2\rangle$. Since we are

mainly interested in the excitation mechanism and for this mainly the presence of a difference in the interaction strength between states ($|1\rangle$ and $|2\rangle$) and ($|1\rangle$ and $|3\rangle$) is needed, we take here only the interaction between these two states into account and decouple this term within the s-wave BCS channel. Using the rotating wave approximation for the coupling between the states $|2\rangle$ and $|3\rangle$, we obtain the Hamiltonian

$$H = H_{BCS} + \sum_{\boldsymbol{k}} (\varepsilon_{\boldsymbol{k}} - \hbar\delta) n_{\boldsymbol{k},3} + \frac{\hbar\Omega_R}{2} \sum_{\boldsymbol{k}} \left(c^\dagger_{\boldsymbol{k},3} c_{\boldsymbol{k},2} + c^\dagger_{\boldsymbol{k},2} c_{\boldsymbol{k},3} \right)$$

with

$$H_{BCS} = \sum_{\boldsymbol{k}} \varepsilon_{\boldsymbol{k}} (n_{\boldsymbol{k},1} + n_{\boldsymbol{k},2}) + \sum_{\boldsymbol{k}} \left\{ \Delta^* c_{-\boldsymbol{k},2} c_{\boldsymbol{k},1} + \Delta c^\dagger_{\boldsymbol{k},1} c^\dagger_{-\boldsymbol{k},2} \right\}. \tag{11.1}$$

Here $\Delta = \frac{g}{V} \sum_{\boldsymbol{k}} \langle c_{-\boldsymbol{k},2} c_{\boldsymbol{k},1} \rangle$, Ω_R is the Rabi-frequency, g the interaction strength, V the volume, and the momentum independent detuning is $\hbar\delta = \hbar\omega_{rf} - (\varepsilon^0_3 - \varepsilon^0_2)$, where ε^0_n is the bare energy for the state $n = 2, 3$ and $\varepsilon_k = \hbar^2 k^2/(2m)$ is the single-particle dispersion. We determine g from the scattering length using the expression provided in Ref. [23].

In order to determine the time evolution of the order parameter, we derive a closed set of equations for the expectation values

$$\begin{aligned}
\hbar\frac{\partial}{\partial t}\langle c_{-\boldsymbol{k},2} c_{\boldsymbol{k},1}\rangle &= i\{-2\epsilon_{\boldsymbol{k}}\langle c_{-\boldsymbol{k},2} c_{\boldsymbol{k},1}\rangle - \frac{\hbar\Omega_R}{2}\langle c_{-\boldsymbol{k},3} c_{\boldsymbol{k},1}\rangle + \Delta(n_{\boldsymbol{k},1} + n_{-\boldsymbol{k},2} - 1)\} \\
\hbar\frac{\partial}{\partial t}\langle c_{-\boldsymbol{k},3} c_{\boldsymbol{k},1}\rangle &= i\{-\frac{\hbar\Omega_R}{2}\langle c_{-\boldsymbol{k},2} c_{\boldsymbol{k},1}\rangle - (2\epsilon_{\boldsymbol{k}} - \hbar\delta)\langle c_{-\boldsymbol{k},3} c_{\boldsymbol{k},1}\rangle + \Delta\langle c^\dagger_{-\boldsymbol{k},2} c_{-\boldsymbol{k},3}\rangle\} \\
\hbar\frac{\partial}{\partial t}\langle c^\dagger_{-\boldsymbol{k},2} c_{-\boldsymbol{k},3}\rangle &= i\{\Delta^*\langle c_{-\boldsymbol{k},3} c_{\boldsymbol{k},1}\rangle + \hbar\delta\langle c^\dagger_{-\boldsymbol{k},2} c_{-\boldsymbol{k},3}\rangle - \frac{\hbar\Omega_R}{2}(n_{-\boldsymbol{k},2} - n_{-\boldsymbol{k},3})\} \\
\hbar\frac{\partial}{\partial t} n_{\boldsymbol{k},1} &= -2\ \mathrm{Im}(\Delta^*\ \langle c_{-\boldsymbol{k},2} c_{\boldsymbol{k},1}\rangle) \\
\hbar\frac{\partial}{\partial t} n_{-\boldsymbol{k},2} &= -2\ \mathrm{Im}(\Delta^*\ \langle c_{-\boldsymbol{k},2} c_{\boldsymbol{k},1}\rangle) + \hbar\ \Omega_R\ \mathrm{Im}(\langle c^\dagger_{-\boldsymbol{k},2} c_{-\boldsymbol{k},3}\rangle) \\
\hbar\frac{\partial}{\partial t} n_{-\boldsymbol{k},3} &= -\hbar\ \Omega_R\ \mathrm{Im}(\langle c^\dagger_{-\boldsymbol{k},2} c_{-\boldsymbol{k},3}\rangle),
\end{aligned}$$

where the number densities are defined as $n_{\boldsymbol{k},m} = \langle c^\dagger_{\boldsymbol{k},m} c_{\boldsymbol{k},m}\rangle$ with $m = 1, 2, 3$. We solve these equations numerically discretizing both time t and momentum k and using the self-consistency condition $\Delta = \frac{g}{V}\sum_{\boldsymbol{k}}\langle c_{-\boldsymbol{k},2} c_{\boldsymbol{k},1}\rangle$ at each time step ensuring both the convergence for the time-step dt and the momentum spacing. Typical values taken are $dk/k_F = 5 \times 10^{-4}$, $dt = 5 \times 10^{-4}\hbar/E_F$ and the cutoff for the momentum sum is $E_c = 100\, E_F$.

The momentum resolved spectral weight of the gap shown in Figure 2c is computed as

$$A_{\boldsymbol{k}}(\omega) = V/g \left| \mathscr{F}\left\{ \left|\Delta_{\boldsymbol{k}}(t)\right| - \frac{1}{T}\int_0^T dt \left|\Delta_{\boldsymbol{k}}(t)\right| \right\} \right| \tag{11.2}$$

with the momentum-dependent order parameter $\Delta_{\boldsymbol{k}} = g/V\langle c_{-\boldsymbol{k},2} c_{\boldsymbol{k},1}\rangle$. We use $T = 400\hbar/E_F$ for the calculation.

Time evolution of the population of state $|3\rangle$

We compare the theoretical evolution of the population of atoms in state $|3\rangle$ (see Figure 1c) during the application of the rf dressing to the experimental results. Supplementary Figure 3 shows the population of the atoms in state $|3\rangle$ normalized to the initial atom number in state $|1\rangle$. The simulation and experiment were performed with the same effective modulation frequency, Ω_{mod}, and maximum atom transfer. Both curves show damped oscillations of the population of

state $|3\rangle$ with time. The initial time behaviour up to approximately three oscillations agrees well between theory and experiment which means that the dominant damping mechanism is due to a dephasing of the different momentum components. Afterwards the experimental results show a stronger damping which we attribute to other damping mechanisms such as for example the presence of collisions in the experiment which are not considered in the theoretical description.

Time evolution of the condensate fraction

We show the evolution of the condensate fraction during the application of the rf dressing in Extended Data Fig. 4. After different durations of the application, the drive time, the rapid mapping to the condensate fraction has been performed and the condensate fraction has been taken. The drive amplitude was chosen to be 0.05%. As a response, an oscillation of the condensate fraction close to the expected Rabi frequency can be observered over several oscillation periods with an amplitude of the order of 0.05 %.

Comparison of the experimental and theoretical spectra

In Supplementary Figure 5, we show a comparison of the experimentally measured spectra with the theoretical simulation. In order to gain insight into the structure expected from the excitation scheme, we theoretically extract the weight of the Higgs excitation for different effective modulation frequencies and plot these in the lower panel of Supplementary Figure 5 for $1/(k_{\mathrm{F}}a) = -0.63$. To evaluate the area under the Higgs, for each momentum, we integrate around the Higgs excitation peak (shown in Figure 2c) and then sum over all momenta along the Higgs excitation line. Let us note that this procedure leads to the artefact that at high modulation frequencies still a non-vanishing contribution to the weight is found, which, however, can be attributed to the excitation of quasi-particles in a homogeneous system and would vanish in a trapped system as considered experimentally. More importantly, we see that even though the Higgs mode has a very sharp frequency (as shown in Fig. 2c) and therefore a long life-time, the resulting spectra show a much broader peak. The width of the peak is due to the excitation procedure. In particular, a resonant excitation of the Higgs mode is already possible if the effective modulation frequency lies below the sharp frequency of the Higgs mode, since then already some of the Rabi frequencies of the higher momentum components (compare stars in Fig. 2c) can resonantly excite the Higgs mode. Thus, the broadening of the spectral feature is mainly due to the particular excitation scheme and not a measurement of the life-time of the Higgs mode. Let us conclude by pointing out that the full width at half maximum in both the theoretical and the experimental spectra is approximately $|\Delta|$.

Local density approximation for the quasi-particle excitations

To study the effect of the harmonic trapping on the quasi-particle excitations we performed a calculation of the system's dynamics within the local-density approximation (LDA). Within LDA we treat points of different density as effectively homogeneous systems with rescaled interaction $1/[k_F(\mathbf{r})a]$, Fermi energy $E_F(\mathbf{r})$ and chemical potential consistent with the system's density profile. We assume the latter to be the profile for non-interacting fermions as typically the density profiles only changes slightly for the considered interactions. The time evolution of the superconducting order parameter of the homogeneous system is performed locally for each point in the trap and rescaled to give $\frac{\Delta(\mathbf{r},t)}{E_F(\mathbf{r}=0)}$. We then take the density-weighted average of its Fourier transform. It is important to note that the Higgs - due to its collective nature - cannot be treated in this formalism, so that we remove the Higgs peak in each Fourier transform by hand before we take the trap average. Integrating the resulting spectrum gives the "background excitation weight" (cf. Supplementary Figure 6). In contrast to the peaked quasi-particle

structure of a homogeneous system, we find the trap averaged “background excitation weight” to be significantly broadened resulting in a featureless, broad background.

Part X
Other Experiments

Part XI

Another Explanations of a Typical Theories

Part XII
Appendix

.1 Appendix

.1.1 Literature

Bibliography

References

.2 Bibliography from Old, Fundamental Artiles

Bibliography from Experiments on charge imbalance in superconductors by John Clarke

Abrahams, E., P.W. Anderson, P.A. Lee and T.V. Ramakrishnan, 1981, Phys. Rev. B24, 6783.
Abrikosov, A.A., and L.P. Gor'kov, 1960, Zh. Eksp. Teor. Fiz. 39, 1781 [Sov. Phys. JETP 12, 1243]
Anderson, P.W., 1959, J. Phys. Chem. Solids 11, 26.
Andreev, A.F., 1964, Zh. Eksp. Teor. Fiz. 46, 182 [Sov. Phys. JETP 19, 1228].
Aponte, J.M., and M. Tinkham, 1983, J. Low Temp. Phys. 51, 189.
Aronov, A.G., 1974, Zh. Eksp. Teor. Fiz. 67, 178 [Sov. Phys. JETP 40, 90].
Artemenko, N., and A.F. Volkov, 1976, Zh. Eksp. Teor. Fiz. 70, 1051 [Sov. Phys. JETP 43, 548].
Artemenko, N., and A.F. Volkov, 1977, Zh. Eksp. Teor. Fiz. 72, 1018 [Sov. Phys. JETP 45, 533].
Artemenko, N., A.F. Volkov and A.V. Zaitsev, 1978, J. Low Temp. Phys. 30, 487.
Bardeen, J., L.N. Cooper and J.R. Schrieffer, 1957, Phys. Rev. 108, 1175.
Battersby, S.J., and J.R. Waldram, 1984, Phys. F14, 109.
Beyer Nielsen, J., Y.A. Ono, C.J. Pethick and H. Smith, 1980, Solid State Commun. 33, 925.
Beyer Nielsen, J., C.J. Pethick, J. Rammer and H. Smith, 1982, J. Low Temp. Phys. 46, 565.
Blonder, G.E., and M. Tinkham, 1983, Phys. Rev. B27, 112.
Blonder, G.E., M. Tinkham and T.M. Klapwijk, 1982, Phys. Rev. B25, 4515.
Chambers, R.G., 1952, Proc. Roy. Soc. (London) 215, 481.
Chang, J.-J., 1977, Phys. Rev. Lett. 39, 1352.
Chang, J.-J., 1979, Phys. Rev. B19, 1420.
Chang, J.-J., and D.J. Scalapino, 1977, Phys. Rev. B15, 2651.
Chi, C.C., and J. Clarke, 1979, Phys. Rev. B19, 4495.
Chi, C.C., and J. Clarke, 1980, Phys. Rev. B21, 333.
Christian, J.W., J.P. Jan, W.P. Pearson and I.M. Templeton, 1958, Proc. Roy. Soc. (London) A245, 213.
Clarke, J., 1972, Phys. Rev. Lett. 28, 1363.
Clarke, J., 1976, in: Superconductor Applications: SQUIDs and Machines, eds. B.B. Schwartz and S. Foner (Plenum, New York) p. 67.
Clarke, J., 1981, in: Nonequilibrium Superconductivity, Phonons, and Kapitza Boundaries (Proc. NATO ASI), ed. K.E. Gray (Plenum, New York) ch. 5.
Clarke, J., and J.L. Paterson, 1974, J. Low Temp. Phys. 15, 491.
Clarke, J. and M. Tinkham, 1980, Phys. Rev. Lett. 44, 106.
Clarke, J., U. Eckern, A. Schmid, G. Schön and M. Tinkham, 1979a, Phys. Rev. B20, 3933.
Clarke, J., B.R. Fjordbge and P.E. Lindelof, 1979b, Phys. Rev. Lett. 43, 642.
Craven, R.A., G.A. Thomas and R.D. Parks, 1971, Phys. Rev. B4, 2185.
De Gennes, P.G., 1966, Superconductivity of Metals and Alloys (Benjamin, New York).
Dolan, G.J., and L.D. Jackel, 1977, Phys. Rev. Lett. 39, 1628.
Entin-Wohlman, O., and R. Orbach, 1979, Phys. Rev. B19, 4510.
Entin-Wohlman, O., and R. Orbach, 1981, Phys. Rev. B24, 1177.

Fickett, F.R., 1971, Cryogenics 11, 349.
Fjordbge, B.R., P.E. Lindelof and J. Clarke, 1981, J. Low Temp. Phys. 44, 535.
Gal'perin, Yu. M., V.L. Gurevich and V.I. Kozub, 19'74, Zh. Eksp. Teor. Fiz. 66, 1387 [Sov. Phys. JETP 39, 680].
Ginzburg, V.L., and L.D. Landau, 1950, Zh. Eksp. Teor. Fiz. 20, 1064.
Gordon, J.M., C.J. Lobb and M. Tinkham, 1983, Phys. Rev. B28, 4046.
Gray, K.E., 1981, in: Nonequilibrium Superconductivity, Phonons, and Kapitza Boundaries (Proc. NATO ASI) ed. K.E. Gray (Plenum, New York) ch. 5.
Gschneidner, K.A., 1964, Solid State Phys. 16, 275.
Harding, G.L., A.B. Pippard and J.R. Tomlinson, 1974, Proc. Roy. Soc. (London) A340, 1.
Heidel, D.F., and J.C. Garland, 1981, J. Low Temp. Phys. 44, 295.
Hsiang, T.Y., 1980, Phys. Rev. B21, 956.
Hsiang, T.Y., and J. Clarke, 1980, Phys. Rev. B21, 945.
Jillie, D.W., J.E. Lukens and Y.H. Kao, 1977, Phys. Rev. Lett. 38, 915.
Jillie, D.W., M.A.H. Nerenberg and J.A. Blackburn, 1980, Phys. Rev. 21B, 125.
Kadin, A.M., W.J. Skocpol and M. Tinkham, 1978, J. Low Temp. Phys. 33, 481.
Kadin, A.M., L.N. Smith and W.J. Skocpol, 1980, J. Low Temp. Phys. 33, 497.
Kaplan, S.B., 1979, J. Low Temp. Phys. 37, 343.
Kaplan, S.B., C.C. Chi, D.N. Langenberg, J.-J. Chang, S. Jafarey and D.J. Scalapino, 1976, Phys. Rev. B14, 4854.
Kaplan, S.B., J.R. Kirtley and D.N. Langenberg, 1977, Phys. Rev. Lett. 39, 291.
Kirtley, J.R., D.S. Kent, S.B. Kaplan and D.N. Langenberg, 1978, J. Physique Suppl. 39, C6-511.
Kittel, C., 1976, Introduction to Solid State Physics, 5th Ed. (Wiley, New York).
Klapwijk, T.M., and J.E. Mooij, 1976, Phys. Lett. 57A, 97.
Klapwijk, T.M., G.E. Blonder and M. Tinkham, 1982, Physica 109B, 1657.
Krhenbhl, Y., and R.J. Watts-Tobin, 1978, J. Physique 39, C6-677.
Krhenbhl, Y., and R.J. Watts-Tobin, 1979, J. Low Temp. Phys. 35, 569.
Lawrence, W.E., and A.B. Meador, 1978, Phys. Rev. B18, 1154.
Lemberger, T.R., 1981, Phys. Rev. B24, 4105.
Lemberger, T.R., and J. Clarke, 1981a, Phys. Rev. B23, 1088.
Lemberger, T.R., and J. Clarke, 1981b, Phys. Rev. B23, 1100.
Lindelof, P.E., and J. Bindslev Hansen, 1977, J. Low Temp. Phys. 29, 369.
Lindelof, P.E., and J. Bindslev Hansen, 1981, in: Nonequilibrium Superconductivity, Phonons, and Kapitza Boundaries (Proc. NATO ASI), ed. K.E. Gray (Plenum, New York) ch. 19.
Maki, K., 1969, in: Superconductivity, ed. R.D. Parks (Marcel Dekker, New York).
Mamin, H.J., J. Clarke and D.J. Van Harlingen, 1983, Phys. Rev. Lett. 51, 1480.
Mamin, H.J., J. Clarke and D.J. Van Harlingen, 1984, Phys. Rev. B29, 3881.
Markowitz, D., and L.P. Kadanoff, 1963, Phys. Rev. 131, 563.
Meservey, R., and B.B. Schwartz, 1969, in: Superconductivity, ed. R.D. Parks (Marcel Dekker, New York).
Meyer, J.D., 1973, Appl. Phys. 2, 303.
Meyer, J., and G. von Minnigerode, 1972, Phys. Lett. 38A, 529.
Moody, M.V., and J.L. Paterson, 1979, J. Low Temp. Phys. 34, 83.
Nyquist, H., 1928, Phys. Rev. 32, 110.
Octavio, M., M. Tinkham, G.E. Blonder and T.M. Klapwijk, 1983, Phys. Rev. B27, 6739.
Ovchinnikov, Yu.N., 1977, J. Low Temp. Phys. 28, 43.
Ovchinnikov, Yu.N., 1978, J. Low Temp. Phys. 31, 785.
Palmer, D.W., and J.E. Mercereau, 1977, Phys. Lett. 61A, 135.
Pethick, C.J., and H. Smith, 1979a, Ann. Phys. 119, 133.

Pethick, C.J., and H. Smith, 1979b, Phys. Rev. Lett. 43. 640.
Pethick, C.J., and H. Smith, 1981a, in: Nonequilibrium Superconductivity, Phonons, and Kapitza Boundaries (Proc. NATO ASI), ed. K.E. Gray (Plenum, New York) ch. 15.
Pethick, C.J., and H. Smith, 1981b, J. Phys. C13, 6313.
Pippard, A.B., 1965, The Dynamics of Conduction Electrons (Gordon and Breach, New York).
Pippard, A.B., 1981, in: Nonequilibrium Superconductivity, Phonons, and Kapitza Boundaries (Proc. NATO ASI), ed. K.E. Gray (Plenum, New York) ch. 12.
Pippard, A.B., J.G. Shepherd and D.A. Tindall, 1971, Proc. Roy. Soc. (London) A324, 17.
Rieger, T.J., D.J. Scalapino and J.E. Mercereau, 1971, Phys. Rev. Lett. 27, 1787.
Santhanam, P., and D.E. Prober, 1984, Phys. Rev. B29, 3733.
Schmid, A., and G. Schön, 1975, J. Low Temp. Phys. 20, 207.
Schmid, A., and G. Schön, 1979, Phys. Rev. Lett. 43, 793.
Schön, G., 1981a, in: Festkörperprobleme (Advances in Solid State Physics), Vol. 21, ed. J. Treusch (Vieweg, Braunschweig) p. 341.
Schön, G., 1981b, Physica 107B, 171.
Skocpol, W.J., 1981, in: Nonequilibrium Superconductivity, Phonons, and Kapitza Boundaries (Proc. NATO ASI), ed. K.E. Gray (Plenum, New York) ch. 18.
Skocpol, W.J., and L.D. Jackel, 1981, Physica 108B, 1021.
Skocpol, W.J., M.R. Beasley and M. Tinkham, 1974, J. Low Temp. Phys. 16, 145.
Stuivinga, M., J.E. Mooij and T.M. Klapwijk, 1981, Physica 108B, 1023.
Stuivinga, M., J.E. Mooij and T.M. Klapwijk, 1982, J. Low Temp. Phys. 46, 555.
Stuivinga, M., C.L.G. Ham, T.M. Klapwijk and J.E. Mooij, 1983a, J. Low Temp. Phys. 53, 633.
Stuivinga, M., T.M. Klapwijk, J.E. Mooij and A. Bezuijen, 1983b, J. Low Temp. Phys. 53, 673.
Tinkham, M., 1972, Phys. Rev. B6, 1747.
Tinkham, M., 1975, Introduction to Superconductivity (McGraw-Hill, New York).
Tinkham, M., 1979, Festkörperprobleme (Advances in Solid State Physics), Vol. 19, ed. J. Treusch (Vieweg, Braunschweig) p. 363.
Tinkham, M., and J. Clarke, 1972, Phys. Rev. Lett. 28, 1366.
Van Harlingen, D.J., 1981, J. Low Temp. Phys. 44, 163.
Van Harlingen, D.J., 1982, Physica 109&110B + C, 1710.
Waldram, J.R., 1975, Proc. Roy. Soc. (London) A345, 231.
Webb, W.W., and R.J. Warburton, 1968, Phys. Rev. Lett. 20, 461.
Yu, M.L., and J.E. Mercereau, 1972, Phys. Rev. Lett. 28, 1117.

Bibliography from Nonequilibrium phenomena in superconducting weak links by L.G. Aslamazov and A.F. Volkov

Ambegarkar, V., and A. Baratoff, 1963, Phys, Rev. Lett. 10, 486.
Andreev, A.F., 1964, Zh. Eksp. Teor. Fiz, 46, 1823.
Artemenko, S.N., and A.F. Volkov, 1979, Usp. Fiz. Nauk 128, 4.
Artemenko, S.N., A.F. Volkov and A.V. Zaitsev, 1979a, Zh. Eksp. Teor. Fiz. 76, 1816.
Artemenko, S.N., A.F. Volkov and A.V. Zaitsev, 1979b, Solid State Commun. 30, 771.
Artemenko, S.N., A.F. Volkov and A.V. Sergeev, 1981, J. Low Temp. Phys. 44. 405.
Astamazov, L.G., and A.I. Larkin, 1969, Zh. Eksp. Teor. Fiz, Pis'ma 2, 150.
Aslamazor, L.G., and A.I. Larkin, 1976, Zh. Eksp. Teor. Fiz. 70. 1341).
Aslamazov, L.G., and A.r. Larkin, 1978, Zh. Eksp. Teor. Fiz. 74, 2184.
Barone, A., and G. Paterno, 1981, Physics and Applications of the Josephson Effect (Wile), New York).
De Gennes, P.G., 1966. Superconductivity of Metals and Alloys (Benjamin, New York).

Divin, Yu.Ya., and F.Ya.N"ad", 1978, Fiz. Nizk. Temp. 4, 1115.
Dorozhkin, S.I., 198(). Zh. Eksp. Teor. Fiz. 79, 1025.
Ellenherger, G., 1968. Z. Phys. 214, 195.
Eliashberg, G.M., 1970, Zh. Eksp. Teor. Fiz. Pis'ma 11, 186.
Eliashberg, G.M. 1971, Zh. Eksp. Teor, Fiz, 61, 1254.
Goluh. A.A., 1976, Zh. Eksp. Teor. Fiz. 71, 341.
Gorkov, L.P., and G.M. Eliashberg, 1968, Zh. Eksp. Teor. Fiz. 54. 612: 55. 2431).
Gubankov, V.N., V.P. Koshelets and G.A. Ovsyannikov. 1977. Zh. Eksp. Teor. Fiz. 73. 1435.
Ivlev, B.I., and G.M. Eliashberg. 1971. Zh. Eksp. Teor. Fiz. Pis m 13. 464.
Josephson, B.D., 1962, Phys. Lett. 1, 251; Rev. Mod. Phys. 36. 216.
Jensen. H.H.. and P.E. Lindelof. 1976. J. Low Temp. Phys. 23. 469.
Klapwijk, T.M. J.N. Van den Bergh and J.E. Mooij. 1977. J. Low Temp. Phys. 26. 385.
Klapwijk. T.M.. G.E. Blonder and M. Tinkham. 1982. Physica 109-110B. 1657.
Kulik. I.O., and A.N. Omelyanchuk. 1975, Zh. Eksp. Teor. Fiz. Pisma 21. 216.
Kulik, I.O., and A.N. Omelyanchuk, 1977, Fiz. Nizk. Temp. 3. 945.
Kulik, I.O., A.N. Omelyanchuk and R.I. Shekhter, 1977, Zh. Eksp. Teor. Fiz. Pis ma 25. 465.
Likharev, K.K., 1979, Lisp. Fiz. Nauk 127, 185.
Likharev, K.K.. and L.A. Yakobson. 1975, Zh. Eksp. Teor. Fiz. 68. 1150.
Larkin. A.I., and Yu.N. Ovchinnikov. 1966. Zh. Eksp. Teor. Fiz. 51. 1535.
Larkin, A.I., and Yu.N. Ovchinnikov. 1977. Zh. Eksp. Teor. Fiz. 73. 299.
Larkin, A.I., and Yu.N. Ovchinnikov, 1975, Zh. Eksp. Teor. Fiz. 68, 1915.
Latyshev, Yu.I., and F.Ya.Nad', 1979, Zh. Eksp. Teor. Fiz. Pis'ma 29, 54.
Mitsay, Yu.N., 1976, Fiz. Nizk. Temp. 2, 189.
Octavio, M., W.J. Skocpol and M. Tinkham, 1978, Phys. Rev. B17, 159.
Pethik, C.I., and H. Smith, 1979, Ann. Phys. 119, 133.
Schmid, A., 1981, in: Nonequilibrium Superconductivity, Phonons and Kapitza Boundaries (Proc. NATO ASI), ed. K.E. Gray (Plenum, New York) p. 423.
Schmid, A., 1981, Kinetic Equations for Dirty Superconductors, preprint.
Schmid, A., and G. Schön, 1975, J. Low Temp. Phys. 20, 207.
Schmid, A., G. Schön and M. Tinkham, 1980, Phys. Rev. B21, 5076.
Tinkham, M., 1979, in: Festkörperprobleme, Advances in Solid State Physics XIX, ed. I. Treusch (Vieweg, Braunschweig) p. 363.
Werthammer, W.R., 1966, Phys. Rev. 147, 255.
Zaitsev, A.V., 1980, Zh. Eksp. Teor. Fiz., 78, 221; 79, 2015.

Bibliography from Time-dependent superconductivity in SNS bridges: an example of TDGL theory by A.L. De Lozanne and M.R. Beasley

Alfeev, V.N., A.V. Verbilo, D.P. Kolesnikov and V.A. Ryzhkov, 1979, Fiz. Tekh. Poluprovodn. 13, 164 [Sov. Phys. Semicond. 13, 93].
Aslamazov, L.G., and A.I. Larkin, 1968, Zh. Eksp. Teor. Fiz. Pis'ma 9, 150 [1969, JETP Lett, 9, 87].
de Lozanne, A.L., 1982, Ph.D. Thesis (Stanford Univ.).
de Lozanne, A.L., M.S. DiIorio and M.R. Beasley, 1983, Appl. Phys. Lett. 42, 541; see also Proc. XVI Low Temp. Conf., 1981, Physica 108B, 1027.
Dilorio, M.S., A.L. de Lozanne and M.R. Beasley, 1983, IEEE Trans. Magn. Mag-19, 308.
Fjordbge, B.R., and P.E. Lindelof, 1978, J. Low Temp. Phys. 31, 83.
Golub, A.A., 1980, Fiz. Nizk. Temp. 6, 979 [Sov. J. Low Temp. Phys. 6, 475].
Gor'kov, L.P., and G.M. Eliashberg, 1968, Zh. Eksp. Teor. Fiz. 54, 612 [Sov. Phys. JETP 27, 328]
Gudkov, A.L., K.K. Likharev, O.V. Snigirev, E.S. Soldatov, S.S. Tinchev and V.V. Khanin,

1979, Zh. Tekh. Fiz. Pis'ma 5, 1206 [Sov. Tech. Phys. Lett. 5, 506]
Hu, C.-R., and R.S. Thompson, 1972, Phys. Rev. B6, 110; see also Tinkham (1980) p. 273.
Ivanov, Z.G., O.V. Snigirev, E.S. Soldatov, Yu.V. Maslennikov, A.V. Chervyakov and V.L. Golubev, 1981, Fiz. Nizk. Temp. 7, 1245 [Sov. J. Low Temp. Phys. 7, 603].
Kadin, A.M., and A.M. Goldman, ch. 7, this volume.
Komarovskikh, N.I., G.M. Lapir, A.N. Samus', and V.K. Semenov, 1975, Zh. Tekh. Fiz. Pis'ma 1, 1002 [Sov. Tech. Phys. Lett. 1, 432].
Kramer, L., and A. Baratoff, 1977, Phys. Rev. Lett. 38, 518; Proc. Int. Conf. on Superconductors and Quantum Devices, Berlin, 1976, eds. H.-D. Hahlbohm and H. Lbbig (W. de Gruyter, Berlin).
Kramer, L., and R.J. Watts-Tobin, 1978, Phys. Rev. Lett. 40, 1041.
Kulik, I.O., and I.K. Yanson, 1972, The Josephson Effect in Superconducting Tunneling Structures (Keter, Jerusalem).
Liengme, O., P. Lerch, W. Liu and P. Martinoli, 1983, IEEE Trans. Magn. Mag-19, 995.
Likharev, K.K., 1979, Rev. Mod. Phys. 51, 101.
Likharev, K.K., and L.A. Yakobson, 1975, Zh. Eksp. Teor. Fiz. 68, 1150 [1976 Sov. Phys. JETP 41, 570].
Ruby, R.C., and T. van Duzer, 1981, IEEE Trans. Electron. Dev. ED-28, 1394.
Russer, P., 1972, J. Appl. Phys. 43, 2008.
Schön, G., and V. Ambegaokar, 1979, Phys. Rev. B19, 3515.
Tinkham, M., 1980, Introduction to Superconductivity (Krieger, New York) pp. 250-254.
van Dover, R.B., A.L. de Lozanne, R.E. Howard, W.L. McLean and M.R. Beasley, 1980, Appl. Phys. Lett. 37, 838.
van Dover, R.B., A.L. de Lozanne and M.R. Beasley, 1981, J. Appl. Phys. 52, 7327.
Warlaumont, J., J.C. Brown and R.A. Buhrman, 1979, Appl. Phys. Lett. 34, 415.

Bibliography from Pair breaking in nonequilibrium superconductors by J. Beyer, C.J. Pethick, J. Rammer and H. Smith

Eilenberger, G., 1968, Z. Phys. 214, 195.
Eliashberg, G.M., 1971, Zh. Eksp. Teor. Fiz. 61, 1254 [1972, Sov. Phys. JETP 34, 668].
Fjordbge, B.R., P.E. Lindelof and J. Clarke, 1981, J. Low Temp. Phys. 44, 535.
Gunault, A.M., 1961, Proc. Roy. Soc. (London) A204, 420.
Keldysh, L.V., 1964, Zh. Eksp. Teor. Fiz. 47, 1515 (1965, Sov. Phys. JETP 20, 1018].
Larkin, A.I., and Yu.N. Ovchinnikov, 1968, Zh. Eksp. Teor. Fiz. 55, 2262 [1969, Sov. Phys. JETP 28, 1200].
Larkin, A.I., and Yu.N. Ovchinnikov, 1977, Zh. Eksp. Teor. Fiz. 73, 299 [Sov. Phys. JETP

[13]Ambegaokar, V., and L. Tewordt, 1964, Phys. Rev. 134A, 805.
Ambegaokar, V., and J. Woo, 1965, Phys. Rev. 139A, 1818.
Aronov, A.G., 1974, Zh. Eksp. Teor. Fiz. 67, 178 [Sov. Phys. JETP 40, 90].
Aronov, A.G., and V.L. Gurevich, 1974, Fiz. Tverd. Tela 16, 2656 [Sov. Phys. Solid State 16, 1722].
Aronov, A.G., Yu.N. Gal'perin, V.L. Gurevich and V.J. Kozub, 1981, Adv. Phys. 30, 539.
Bardeen, J., G. Rickayzen and L. Tewordt, 1959, Phys. Rev. 113, 982.
Betbeder-Matibet, O., and P. Nozires, 1969, Ann. Phys. 51, 392.
Beyer Nielsen, J., and H. Smith, 1982, Phys. Rev. Lett. 49, 689.
Beyer Nielsen, J., and H. Smith, 1985, Phys. Rev. B31, 2831.
Beyer Nielsen, J., Y.A. Ono, C.J. Pethick and H. Smith, 1980, Solid State Commun. 33, 925.
Beyer Nielsen, J., C.J. Pethick, J. Rammer and H. Smith, 1981, Physica 107B+C, 161.
Beyer Nielsen, J., C.J. Pethick, J. Rammer and H. Smith, 1982, J. Low Temp. Phys. 46, 565.
Beyer Nielsen, J., H. Smith and S.R. Yang, 1985, J. Low Temp. Phys. 55, 33.
Clarke, J., 1972, Phys. Rev. Lett. 28, 1363.
Clarke, J., and M. Tinkham, 1980, Phys. Rev. Lett. 44, 106.
Clarke, J., B.R. Fjordbge and P.E. Lindelof, 1979, Phys. Rev. Lett. 43, 642.

46, 155].
Lemberger, T.R., and J. Clarke, 1981, Phys. Rev. B23, 1088, 1100.
Mezahov-Deglin, L.P., 1979, Zh. Eksp. Teor. Fiz. 77, 733 [Sov. Phys. JETP 50, 369].
Ovchinnikov, Yu.N., A. Schmid and G. Schön, 1981, Phys. Rev. Lett. 46, 1013.
Peters, R., and H. Meissner, 1973, Phys. Rev. Lett. 30, 965.
Pethick, C.J., and H. Smith, 1978, Physica 90B, 107.
Pethick, C.J., and H. Smith, 1979a, Ann. Phys. 119, 133.
Pethick, C.J., and H. Smith, 1979b, Phys. Rev. Lett. 43, 640.
Ritger, A.J., and H. Meissner, 1980, J. Low Temp. Phys. 40, 495.
Scalapino, D.J., 1969, in: Superconductivity, Vol. I, ed. R.D. Parks (Marcel Dekker, New York) p. 445.
Schmid, A., 1968, Phys. Kondens. Mater. 8, 129.
Schmid, A., 1969, Phys. Rev. 186, 420.
Schmid, A., 1981, in: Non-equilibrium Superconductivity, Phonons and Kapitza Boundaries (Proc. NATO ASI) ed. K.E. Gray (Plenum, New York) p. 423.
Schmid, A., and G. Schön, 1975, J. Low Temp. Phys. 20, 207.
Schmid, A., and G. Schön, 1979, Phys. Rev. Lett. 43, 793.
Shelankov, A.L., 1980, Zh. Eksp. Teor. Fiz. 78, 2359 [Sov. Phys. JETP 51, 1186].
Schön, G., 1981a, Physica 107B + C, 171.
Schön, G., 1981b, in: Festkörperprobleme (Advances in Solid State Physics), vol. XXI, ed. J. Treusch (Vieweg, Braunschweig) p. 341.
Tinkham, M., 1972, Phys. Rev. B6, 1747.
Tinkham, M., and J. Clarke, 1972, Phys. Rev. Lett. 28, 1366.
Vashishta, P., and J.P. Carbotte, 1972, Phys. Rev. B5, 1859.
Watson, J.H.P., and G.M. Graham, 1963, Can. J. Phys. 41, 1738.

Bibliography from Experimental study of enhanced superconductivity by V.M. Dmitriev, V.N. Gubankov and F.Ya. Nad'

Artemenko, S.N., A.F. Volkov and A.V. Zaitsev, 1979a, Zh. Eksp. Teor. Fiz. 76, 1816.
Artemenko, S.N., A.F. Volkov and A.V. Zaitsev, 1979b, Solid State Commun. 30, 771.
Aslamazov, L.G., 1978, Zh. Eksp. Teor. Fiz. 75, 1778.
Aslamazov, L.G., and V.I. Gavrilov, 1980, Fiz. Nizk. Temp. 6, 877.
Aslamazov, L.G., and A.I. Larkin, 1969, Zh. Eksp. Teor. Fiz. Pis'ma 9, 150.
Aslamazov, L.G., and A.I. Larkin, 1976, Zh. Eksp. Teor. Fiz. 70, 1340.
Aslamazov, L.G., and A.I. Larkin, 1978, Zh. Eksp. Teor. Fiz. 74, 2184.
Aslamazov, L.G., and A.F. Volkov, 1985, ch. 2, this volume.
Aslamazov, L.G., A.I. Larkin and Yu.N. Ovchinnikov, 1968, Zh. Eksp. Teor. Fiz. 55, 323.
Bar'yakhtar, V.G., and V.P. Seminozhenko, 1976, Fiz. Nizk. Temp. 2, 1516.
Bar'yakhtar, V.P., and V.P. Seminozhenko, 1977, Fiz. Nizk. Temp. 3, 272.
Bevza, Yu.G., G.G. Zah, V.M. Karamushko and I.M. Dmitrenko, 1976, Zh. Tekhn. Fiz. Pis'ma 2, 367.
Bevza, Yu.G., V.M. Karamushko and I.M. Dmitrenko, 1977, Zh. Tekhn. Fiz. 47, 646.
Bulyzhenkov, I.E., and B.I. Ivlev, 1976, Zh. Eksp. Teor. Fiz. 70, 1405; 71, 1172.
Chang, J.J., and D.J. Scalapino, 1977, J. Low Temp. Phys. 29, 477.

[13]Anderson, P.W., 1967, in: Progress in Low Temperature Physics V, ed. C.J. Gorter (NorthHolland, Amsterdam) p. 1.

Anderson, P.W., and A.H. Dayem, 1964, Phys. Rev. Lett. 13, 195.
Andratskii, V.P., L.M. Grundel, V.N. Gubankov and N.B. Pavlov, 1973, Zh. Eksp. Teor. Fiz. 65, 1591.
Andreev, A.F., 1964, Zh. Eksp. Teor. Fiz. 46, 1823.
Artemenko, S.N., A.F. Volkov and A.V. Zaitsev, 1978, Zh. Eksp. Teor. Fiz. Pis'ma 28, 637.

Chang, J.J., and D.J. Scalapino, 1978, J. Low Temp. Phys. 31, 2.
Chi, C.C., and J. Clarke, 1979, Phys. Rev. B19, 4465.
Chien, M.K., and D.E. Farrell, 1975, J. Low-Temp. Phys. 19, 75.
Christiansen, P.V., E.B. Hansen and C.J. Sjöström, 1971, J. Low-Temp. Phys. 4, 349.
Clarke, J., and J.L. Paterson, 1974, J. Low-Temp. Phys. 15, 491.
Dayem, A.H., and C.C. Grimes, 1966, Appl. Phys. Lett. 9, 47.
Dayem, A.H., and R.J. Martin, 1962, Phys. Rev. Lett. 8, 246.
Dayem, A.H., and J.J. Wiegand, 1967, Phys. Rev. 155, 418.
Deaver, B.S., and J.M. Pierce, 1972, Phys. Lett. 38 A, 81.
Divin, Yu.Ya., and F.Ya. Nad', 1978, Fiz. Nizk. Temp. 4, 1105.
Divin, Yu.Ya., and F.Ya. Nad', 1979, Zh. Eksp. Teor. Fiz., Pis'ma, 29, 567.
Dmitriev, V.M., and E.V. Khristenko, 1978, Fiz. Nizk. Temp. 4, 821.
Dmitriev, V.M., and E.V. Khristenko, 1979, J. Physique 40, L-85.
Dmitriev, V.M., E.V. Khristenko, A.V. Trubitsyn and F.F. Mende, 1970, Ukr. Fiz. Zh. 15, 1611.
Dmitriev et al. 73 from p. 55.
Dmitriev, V.M., E.V., Khristenko and L.V. Esichko, 1976, Microwave Enhanced Superconductivity in Thin Film Bridges, in: Proc. LT-19 Conference, Minsk, 1976, p. 393.
Dmitriev, V.M., N.I. Glushchuk and E.V. Khristenko, 1978, Nonequilibrium critical current of the superconducting channels in the microwave field, in: Proc. LT-20 Conference, Moscow, 1979, v. 3, p. 194.
Dmitriev, V.M.. E.V. Khristenko and S. Shapiro, 1973, Fiz. Kond. Sost., 28, 3.
Dorozhkin, S.I., 1980, Temperature Dependence of the S-N Point Contacts Conductivity, in: Proc. LT-21 Conference, Kharkov, 1980, v. 1, p. 221.
Eckern, U., A. Schmid, M. Schmutz and G. Schön, 1979, J. Low Temp. Phys. 36, 643.
Eliashberg, G.M., 1970, Zh. Eksp. Teor. Fiz. Pis'ma 11, 186.
Eliashberg, G.M., 1971, Zh. Eksp. Teor. Fiz. 61, 1254.
Eliashberg, G.M., and B.I. Ivlev, 1985, ch. 6, this volume.
Fil', V.D., V.I. Denisenko and P.A. Bezuglyi, 1975, Zh. Eksp. Teor. Fiz. Pis'ma 21, 693.
Fil', V.D., V.I. Denisenko, P.A. Bezuglyi and A.S. Pirogov, 1976, Fiz. Nizk. Temp. 2, 1506.
Fil', V.D., A.L. Gaiduk and V.I. Denisenko, 1980, Zh. Eksp. Teor. Fiz. 78, 1464.
Galaiko, V.P., V.S. Shumeiko and T. Kshishton', 1981, Zh. Eksp. Teor. Fiz., 80, 2078.
Gor'kov, L.P., 1959, Zh. Eksp. Teor. Fiz. 37, 1407.
Gor'kov, L.P., and G.M. Eliashberg, 1969, Zh. Eksp. Teor. Fiz. Pis'ma 8, 329; Zh. Eksp. Teor. Fiz. 56, 1297.
Gray, K.E., 1978, Solid State Commun. 26, 633.
Gregers-Hansen, P.E., and M.T. Levinsen, 1971, Phys. Rev. Lett. 27, 847.
Gubankov, V.N., and N.M. Margolin, 1979, Zh. Eksp. Teor. Fiz. Pis'ma 29, 733.
Gubankov, V.N., and N.M. Margolin, 1981, Zh. Eksp. Teor. Fiz. 79, 1419.
Gubankov, V.N., V.P. Koshelets, K.K. Likharev and G.A. Ovsyannikov, 1973, Zh. Eksp. Teor. Fiz. Pis'ma 18, 292.
Gubankov, V.N., V.P. Koshelets and G.A. Ovsyannikov, 1975, Zh. Eksp. Teor. Fiz. Pis'ma 21, 489.
Gubankov, V.N., V.P. Koshelets and G.A. Ovsyannikov, 1976, Zh. Eksp. Teor. Fiz. 71, 348.
Gubankov, V.N., V.P. Koshelets and G.A. Ovsyannikov, 1977, Zh. Eksp. Teor. Fiz. 73, 1435.
Gubankov, V.N., V.P. Koshelets and G.A. Ovsyannikov, 1978, J. Physique 39 (suppl. No 8) c. 6-535.
Gubankov, V.N., V.P. Koshelets and G.A. Ovsyannikov, 1979, Zh. Tekhn. Fiz. 49, 832.
Gubankov, V.N., V.P. Koshelets and G.A. Ovsyannikov, 1980, Fiz. Nizk. Temp. 6, 50.

Hall, J.T., L.B. Holdeman and R.J. Sonlen, 1980, Phys. Rev. Lett. 45, 1011.
Hansen, J.B., P. Jespersen and P.E. Lindelof, 1978, J. Physique 39 (suppl. No 8) c. 6-500.
Hunt, T.K., 1969, Phys. Rev. 177, 749.
Hunt, T.K., and J.E. Mercereau, 1967, Phys. Rev. Lett. 18, 551.
Ivlev, B.I., 1972, Zh. Eksp. Teor. Fiz. 72, 1197.
Ivlev, B.I., and G.M. Eliashberg, 1971, Zh. Eksp. Teor. Fiz. Pis'ma 13, 464.
Ivlev, B.I., S.G. Lisitsyn and G.M. Eliashberg, 1973, J. Low-Temp. Phys. 10, 449.
Jillie, D.W., J. Lukens and Y.H. Kao, 1975, IEEE Trans. Magn. MAG-11, 671.
Kirichenko, I.K., S.A. Peskovatskii and V.P. Seminozhenko, 1979, Solid State Commun. 26, 633.
Klapwijk, T.M., and J.E. Mooij, 1976, Physica 81B, 132.
Klapwijk, T.M., J.N. Van den Bergh and J.E. Mooij, 1977, J. Low-Temp. Phys. 26, 385.
Klapwijk, T.M., H.B. van Linden van den Heuvell and J.E. Mooij, 1978, J. Physique 39 (suppl. No 8) c. 6-525.
Kommers, T.M., and J. Clarke, 1977, Phys. Rev. Lett. 38, 1091.
Kulik, I.O., and A.N. Omelyanchuk, 1978, Fiz. Nizk. Temp. 4, 296.
Latyshev, Yu.I., and F.Ya. Nad', 1974, Zh. Eksp. Teor. Fiz. Pis'ma 19, 737.
Latyshev, Yu.I., and F.Ya. Nad', 1975, IEEE Trans. Magn. MAG-11, 877.
Latyshev, Yu.I., and F.Ya. Nad', 1976, Zh. Eksp. Teor. Fiz. 71, 2158.
Latyshev, Yu.I., and F.Ya Nad', 1977, Zh. Eksp. Teor. Fiz. Pis'ma 26, 488.
Latyshev, Yu.I., and F.Ya. Nad', 1978, J. Physique 39 (suppl. No. 8) c. 6-531.
Latyshev, Yu.I., and F.Ya. Nad', 1979, Zh. Eksp. Teor. Fiz. Pis'ma 29, 58.
Levinsen, M.T., 1974, Phys. Rev. Appl. 9, 135.
Likharev, K.K., and L.A. Yakobson, 1975, Zh. Eksp. Teor. Fiz. 68, 1150.
Likharev, K.K., and B.T. Ulrich, 1978, Systems with Josephson contacts (Moscow University, Moscow).
Lindelof, P.E., 1976, Solid State Commun. 18, 283.
McCumber, D.E., 1968, J. Appl. Phys. 39, 3113.
Mitsen, K.V., G.P. Motulevich, A.I. Golovashkin, O.M. Ivanchenko and M.V. Tihansky, 1980, Superconductivity Enhancement in Tin by Quasiparticle Tunneling, in: Proc. LT-21 Conference, Kharkov, USSR, 1980, (FTINT, Kharkov) v. 1, p. 173.
Mooij, J.E., N. Lambert and T.M. Klapwijk, 1980, Solid State Commun. 36, 585.
Nad', F.Ya., and O.Yu. Polanskii, 1973, Radiotekhn. Elektron. 18, 2448.
Octavio, M., 1978, Thesis (Harvard Univ.).
Octavio, M., M.J. Skocpol and M. Tinkham, 1977, IEEE Trans. Magn. MAG-13, 739.
Octavio, M., M.J. Skocpol and M. Tinkham, 1978, Phys. Rev. 17B, 159.
Ovchinnikov, Yu.A., 1973, Zh. Eksp. Teor. Fiz. 64, 719.
Pals, J.A., and J. Dobben, 1978, J. Physique 40, L-85.
Pals, J.A., and J. Dobben, 1979, Phys. Rev. 20B. 935.
Pankove, J.J., 1966, Phys. Lett. 21, 406.
Parmenter, R.H., 1961, Phys. Rev. Lett. 7, 274.
Peskovatskii, S.A., and V.P. Seminozhenko, 1976, Fiz. Nizk. Temp. 2, 943.
Peskovatskii, S.A., and L.P. Strizhko, 1979, Zh. Eksp. Teor. Fiz. Pis'ma 29, 68.
Rieger, T.J., D.J. Scalapino and J.E. Mercereau, 1972, Phys. Rev. B6, 1734.
Schmid, A., 1977, Phys. Rev. Lett. 38, 922.
Seminozhenko, V.P., and A.A. Yatsenko, 1980, Solid State Commun. 33, 753.
Shepard, K.W., 1971, Physica 55, 786.
Skocpol, W.J., M.R. Beasley and M. Tinkham, 1974, J. Low-Temp. Phys. 16, 145.
Stewart, W.S., 1968, Appl. Phys. Lett. 12, 277.
Tredwell, T.J., and E.H. Jakobson, 1975, Phys. Rev. Lett. 35, 244.

Volkov, A.F., N.V. Zavaritskii, and F.Ya Nad', 1978, Electronic Devices on the Base of the Weakly Coupled Superconductors, ed. N.V. Zavaritskii (Sov. Radio, Moscow).
Weitz, D.A., W.J. Skocpol and M. Tinkham, 1978, Phys. Rev. Lett. 40, 253.
Wyatt, A.F.G., V.M. Dmitriev, and W.S. Moore, 1966a, The Effect of Microwaves on Constricted Tin Films, in: Proc. LT-10 Int. Conference Moscow, v. 2-A, p. 242.
Wyatt, A.F.G., V.M. Dmitriev, W.S. Moore and F.W. Sheard, 1966b, Phys. Rev. Lett. 16, 1166.
Zaitsev, A.V., 1980a, To the Theory of the Variable Thickness Bridges, in: Proc LT-21 Conference, Kharkov, ed. N.V. Zavaritskii (FTINT, Kharkov) v. 1, p. 132.
Zaitsev, A.V., 1980b, Zh. Eksp. Teor. Fiz. 79, 1025.
Zhilinskii, S.K., Yu.I. Latyshev and F.Ya. Nad', 1980, Temperature Dependence of Excess Current in Short Superconducting Bridges, in: Proc. LT-21 Conference, Kharkov, ed. (FTINT, Kharkov) v. 1, p. 223.

Bibliography from Theory of superconductivity stimulation by G.M.Eliashberg and B. I. Ivlev

Aronov, A.G., and V. L. Gurevich, 1972, Zh. Eksp. Teor. Fiz. 63, 1809.
Artemenko, S.N., and A.F. Volkov, 1975, Zh. Eksp. Teor. Fiz. Pis'ma 21, 662.
Artemenko, S.N., A.F. Volkov and A.V. Zaitsev, 1978, J. Low Temp. Phys. 30, 487.
Aslamazov, L.G., and V.I. Gavrilov, 1980, Fiz. Nizk. Temp. 6, 877.
Aslamazov, L.G., and A.I. Larkin, 1978, Zh. Eksp. Teor. Fiz. 74, 2184.
Bulyzhenkov, I.E., and B.I. Ivlev, 1976a, Zh. Eksp. Teor. Fiz. 70, 1405.
Bulyzhenkov, I.E., and B.I. Ivlev, 1976b, Zh. Eksp. Teor. Fiz. 71, 1112.
Bulyzhenkov, I.E., and B.I. Ivlev, 1978, Zh. Eksp. Teor. Fiz. 74, 224.
Bulyzhenkov, I.E., and B.I. Ivlev, 1979, Fiz. Tverd. Tela 21, 2325.
Chang, J.J., 1978, Phys. Rev. B11, 20.
Chang, J.J., and D.J. Scalapino, 1977, J. Low Temp. Phys. 29, 477.
Chi, C.C., and J. Clarke, 1979, Phys. Rev. B11, 20.
Dayem, A.H., and J.J. Wiegand, 1967, Phys. Rev. 155, 419.
Dmitriev, V.M., and E.V. Khristenko, 1978, Fiz. Nizk. Temp. 4, 821.
Dmitriev, V.M., V.N. Gubankov and F. Nad', 1985, ch. 5, this volume.
Douglass, D., and L. Falicov, 1964, Energy gap in superconductors, in: Progress in Low Temperature Physics IV, ed. C. Gorter (North-Holland, Amsterdam) p. 97.
Eckern, U., A. Schmid, M. Schmutz and G. Schön, 1979, J. Low Temp. Phys. 36, 643.
Eliashberg, G.M., 1970, Zh. Eksp. Teor. Fiz. Pis'ma 11, 186.
Eliashberg, G.M., 1971, Zh. Eksp. Teor. Fiz. 61, 1254.
Galaiko, V.P., 1974, Zh. Eksp. Teor. Fiz. 66, 379.
Ginzburg, E.V., and B.Z. Spivak, 1981, Zh. Eksp. Teor. Fiz. 80, 2013.
Gor'kov, L.P., and G.M. Eliashberg, 1968, Zh. Eksp. Teor. Fiz. 56, 612.
Gor'kov, L.P., and N.B. Kopnin, 1973, Zh. Eksp. Teor. Fiz. 65, 396.
Gray, K.E., 1978, Solid State Commun. 26, 633.
Ivlev, B.I., and G.M. Eliashberg, 1971, Zh. Eksp. Teor. Fiz. Pis'ma 13, 464.
Ivlev, B.I., S.G. Lisitsyn and G.M. Eliashberg, 1973, J. Low Temp. Phys. 10, 449.
Ivlev, B.I.. 1978, Zh. Eksp. Teor. Fiz. 75, 1771.
Kaplan, S.B., J.R. Kirtley and D.N. Langenberg, 1977, Phys. Rev. Lett. 39, 291.
Keldysh, L.V., 1964, Zh. Eksp. Teor. Fiz. 47, 1515.
Kittel, G., 1963, Quantum theory of solids (Wiley, New York).
Klapwijk, T.M., and J.E. Mooij, 1976, Physica 81B + C, 132.
Kommers, T., and J. Clarke, 1977, Phys. Rev. Lett. 38, 1091.
Kozub, V.I., and B.Z. Spivak, 1981. J. Low Temp. Phys. 42, N5/6.

Larkin, A.I., and Yu.N. Ovchinnikov, 1977, Zh. Eksp. Teor. Fiz. 73, 299.
Latyshev, Yu.I., and F.Ya. Nad', 1974, Zh. Eksp. Teor. Fiz. Pis'ma 19, 737.
Latyshev, Yu.I., and F.Ya. Nad', 1976, Zh. Eksp. Teor. Fiz. 71, 2158.
Parmenter, R.H., 1961, Phys. Rev. Lett. 11, 274.
Peskovatski, S.A., and V.P. Seminozhenko, 1976, Fiz. Nizk. Temp. 2, 943.
Schmid, A., and G. Schön, 1975, J. Low Temp. Phys. 20, 207.
Tinkham, M., and J. Clarke, 1972, Phys. Rev. Lett. 28, 1366.
Tredwell, T.J., and E.H. Jacobsen, 1975, Phys. Rev. Lett. 35, 244.
Vardanyan, R.A., and B.1. Ivlev, 1973, Zh. Eksp. Teor. Fiz. 65, 2315.
Volkov, A.F., and A.V. Zaitsev, 1975, Zh. Eksp. Teor. Fiz. 69, 2222.
Wyatt, A.F., V.M. Dmitriev, W.S. Moore and F.W. Sheard, 1966, Phys. Rev. Lett. 16, 1166.

Bibliography from Dynamical effects in nonequilibrium superconductors: some experimental perspectives by A.M. Kadin and A.M. Goldman

Abraham, D.W., C.J. Lobb, M. Tinkham and T.M. Klapwijk, 1982, Phys. Rev. B26, 5268.
Anderson, J.T., and A.M. Goldman, 1970, Phys. Rev. Lett. 25, 743.
Anderson, J.T., R.V. Carlson and A.M. Goldman, 1972, J. Low Temp. Phys. 8, 29.
Anderson, P.W., 1958, Phys. Rev. 110, 827.
Andreev, A.F., 1964, Zh. Eksp. Teor. Fiz. 19, 1228 [Sov. Phys. JETP 19, 1228].
Aponte, J., and M. Tinkham, 1983, J. Low Temp. Phys. 51, 189.
Aronov, A.G., and B.Z. Spivak, 1978, Fiz. Nizk. Temp. 4, 1365 [Sov. J. Low Temp. Phys. 4, 641].
Artemenko, S.N., and A.F. Volkov, 1975, Zh. Eksp. Teor. Fiz. 69, 1764 [1976, Sov. Phys. JETP 42, 896].
Artemenko, S.N., and A.F. Volkov, 1979, Usp. Fiz. Nauk 128, 3 [1980, Sov. Phys. Usp. 22, 295].
Artemenko, S.N., A.F. Volkov and A.V. Zaitsev, 1978a, J. Physique 39, C6-588.
Artemenko, S.N., A.F. Volkov and A.V. Zaitsev, 1978b, Zh. Eksp. Teor. Fiz. Pis'ma 27, 122 [JETP Lett. 27, [13].
Artemenko, S.N., A.F. Volkov and A.V. Zaitsev, 1979, Zh. Eksp. Teor. Fiz. 76, 1816 [Sov. Phys. JETP 49, 924].
Aslamazov, L.G., and A.I. Larkin, 1976, Zh. Eksp. Teor. Fiz. 70, 1340 [Sov. Phys. JETP 43, 698].
Aslamazov, L.G., and A.F. Volkov, 1985, ch. 2, this volume.
Aspen, F.E., and A.M. Goldman, 1979, Phys. Rev. Lett. 43, 307.
Aspen, F.E., and A.M. Goldman, 1981a, J. Low Temp. Phys. 43, 559.
Aspen, F.E., and A.M. Goldman, 1981b, Phys. Rev. B22, 3508.
Baratoff, A., 1982a, Phys. Rev. Lett. 48, 434.
Baratoff, A., 1982b, Physica 109+110B, 2058.
Baru, V.G., and A.A. Sukhanov, 1975, Zh. Eksp. Teor. Fiz. Pis'ma 21, 209 [JETP Lett. 21, 93].
Bindslev Hansen, J., 1982, Phys. Scripta 25, 844.
Bindslev Hansen, J., and P.E. Lindelof, 1981, Nonequilibrium Phenomena in Josephson Junctions, in: Proc. 2nd IC-SQUID Conf., Berlin 1980, eds. H.-D. Hahlbohm and H. Lubbig (W. de Gruyter, Berlin), p. 29.
Bindslev Hansen, J., P.E. Lindelof and T.F. Finnegan, 1981, IEEE Trans. Magn. MAG-17, 95.
Blackburn, J.A., 1983, J. Low Temp. Phys. 50, 475.
Blonder, G.E., and M. Tinkham, 1983, Phys. Rev. B27, 6747.
Blonder, G.E., M. Tinkham and T.M. Klapwijk, 1982, Phys. Rev. B25, 4515.
Boone, B.G., C.A. Arrington, L.K. Wang and B.S. Deaver, 1977, IEEE Trans. Magn. MAG-13,

735.

Carlson, R.V., and A.M. Goldman, 1973, Phys. Rev. Lett. 31, 880.

Carlson, R.V., and A.M. Goldman, 1975, Phys. Rev. Lett. 34, 11.

Carlson, R.V., and A.M. Goldman, 1976, J. Low Temp. Phys. 27, 67.

Chang, J.-J., and D.J. Scalapino, 1974, Phys. Rev, B10, 4047.

Chang, J.-J., and D.J. Scalapino, 1978, J. Low Temp. Phys. 31, 1.

Chaudhari, P., A.N. Broers, C.C. Chi, R. Laibowitz, E. Spiller and J. Viggiano, 1980, Phys. Rev. Lett. 45, 930.

Chi, C.C., and J. Clarke, 1979, Phys. Rev. B20, 4465.

Chi, C.C., M.M.T. Loy and D.C. Cronemeyer, 1981, Phys. Rev. B23, 124.

Clarke, J., 1972, Phys. Rev. Lett. 28, 1363.

Clarke, J., 1985, ch. 1, this volume.

Clarke, J., and J.L. Paterson, 1974, J. Low Temp. Phys. 15, 491.

Cyrot, M., 1973, Rep. Prog. Phys. 36, 103.

Dahlberg, E.D., R.L. Orbach and I.K. Schuller, 1979, J. Low Temp. Phys. 36, 367.

Davidson A., 1981, IEEE Trans. Magn. MAG-17, 108.

de Lozanne, A., and M.R. Beasley, 1985, ch. 3, this volume.

Dinter, M., 1977, J. Low Temp. Phys. 26, 39.

Dinter, M., 1978, J. Low Temp. Phys. 32, 529.

Divin, Yu.Ya., and F.Ya. Nad', 1979, Zh. Eksp. Teor. Fiz. Pis'ma 29 [JETP Lett. 29, 516].

Dmitriev, V.M., and E.V. Khristenko, 1978, Fiz. Nizk. Temp. 4, 821 [Sov. J. Low Temp. Phys. 4, 387].

Dmitriev, V.M., V.N. Gubankov and F.Ya. Nad', 1985, ch. 5, this volume.

Dolan, G.J., and L.D. Jackel, 1977, Phys. Rev. Lett. 39, 1628.

Dynes, R.C., V. Narayanamurti and J.P. Garno, 1977, Phys. Rev. Lett. 39, 229.

Eckern, U., A. Schmid, M. Schmutz and G. Schön, 1979, J. Low Temp. Phys. 36, 643.

Elesin, V.F., 1974, Zh. Eksp. Teor. Fiz. 66, 1755 [Sov. Phys. JETP. 39, 862].

Elesin, V.F., 1976, Zh. Eksp. Teor. Fiz. 71, 1490 [Sov. Phys. JETP 44, 780].

Elesin, V.F., 1977a, Zh. Eksp. Teor. Fiz. 73, 355 [Sov. Phys. JETP 46, 185].

Elesin, V.F., 1977b, Fiz. Tverd. Tela 19, 2977 [Sov. Phys. Solid State 19, 1744].

Eliashberg, G.M., 1970, Zh. Eksp. Teor. Fiz. Pis'ma 11, 186 [JETP Lett. 11, 114].

Eliashberg, G.M., and B.I. Ivlev, 1985, ch. 6, this volume.

Entin-Wohlman, O., and R. Orbach, 1978, Ann. Phys. 116, 35.

Entin-Wohlman, O., and R. Orbach, 1979, Ann. Phys. 122, 64.

Faris, S.M., 1980, Appl. Phys. Lett. 36, 1005.

Faris, S.M., S.I. Raider, W.J. Gallagher and R.E. Drake, 1983, IEEE Trans. Magn. MAG-19, 1293.

Ferrell, R.A., 1969, J. Low Temp. Phys. 1, 423.

Frank, D.J., and M. Tinkham, 1983, Phys. Rev. B28, 5345.

Frank, D.J., M. Tinkham, A. Davidson and S.M. Faris, 1983, Phys. Rev. Lett. 50, 1611.

Galako, V.P., and N.B. Kopnin, 1985, ch. 12, this volume.

Geier, A., and G. Schön, 1982, J. Low Temp. Phys, 46, 151.

Goldman, A.M., 1981, Collective Modes of the Superconducting Order Parameter, in: Nonequilibrium Superconductivity, Phonons, and Kapitza Boundaries (Proc. NATO ASI), ed. K.E. Gray (Plenum, New York) ch. 17.

Golub, A.A., 1976, Zh. Eksp. Teor. Fiz. 71, 341 [Sov. Phys. JETP 44, 178].

Gordon, J.M., C.J. Lobb and M. Tinkham, 1983, Phys. Rev. B28, 4046.

Gor'kov, L.P., and G.M. Eliashberg, 1968, Zh. Eksp. Teor. Fiz. 54, 612 [Sov. Phys. JETP 27, 328].

Gorlach, A.F., and R.P. Huebner, 1983, J. Low Temp. Phys. 53, 619.

Gorter, C.J., and H.B.J. Casimir, 1934, Phys. Z. 35, 963.
Gray, K.E., 1978a, Solid State Commun. 26, 633.
Gray, K.E., 1978b, Appl. Phys. Lett. 32, 392.
Gray, K.E., ed., 1981a, Nonequilibrium Superconductivity, Phonons, and Kapitza Boundaries (Proc. NATO ASI) (Plenum, New York).
Gray, K.E., 1981b, Tunneling: A Probe of Nonequilibrium Superconductivity, in: Nonequilibrium Superconductivity, Phonons and Kapitza Boundaries (Proc. NATO ASI), ed. K.E. Gray (Plenum, New York) ch. 5.
Gray, K.E., and H.W. Willemsen, 1978, J. Low Temp. Phys. 31, 911.
Gubankov, V.N., V.P. Koshelets and G.A. Ovsyannikov, 1977, Zh. Eksp. Teor. Fiz. 73, 1435 [Sov. Phys. JETP 46, 755].
Gubankov, V.N., V.P. Koshelets and G.A. Ovsyannikov, 1980, Fiz. Nizk. Temp. 6, 50 [Sov. J. Low Temp. Phys. 6].
Hall, J.T., L.B. Holdeman and R.J. Soulen Jr, 1980, Phys. Rev. Lett. 45, 1011.
Hsiang, T.Y., and J. Clarke, 1980, Phys. Rev. B21, 945.
Hunt, B.D., and R.A. Buhrman, 1983, IEEE Trans. Magn. MAG-19, 1155.
Iguchi, I., 1978a, J. Low Temp. Phys. 31, 605.
Iguchi, I., 1978b, J. Low Temp. Phys. 33, 439.
Iguchi, I., and D.N. Langenberg, 1980, Phys. Rev. Lett. 44, 486.
Ivlev, B.I., and N.B. Kopnin, 1980, J. Low Temp. Phys. 39, 137.
Ivlev, B.I., and N.B. Kopnin, 1981, J. Low Temp. Phys. 44, 453.
Ivlev, B.I., and N.B. Kopnin, 1982, Solid State Commun. 41, 107.
Jain, A.K., P. Mankiewich, A.M. Kadin, R.H. Ono and J.E. Lukens, 1981, IEEE Trans. Magn. MAG-17, 99.
Jillie, D.W., 1976, Doctoral dissertation (State University of New York) unpublished.
Jillie, D.W., J. Lukens and Y.H. Kao, 1977, Phys. Rev. Lett. 38, 915.
Jillie, D.W., M.A.H. Nerenberg and J.A. Blackburn, 1980, Phys. Rev. B21, 125.
Kadin, A.M., and A.M. Goldman, 1982, Phys. Rev. B25, 6701.
Kadin, A.M., W.J. Skocpol and M. Tinkham, 1978, J. Low Temp. Phys. 33, 481.
Kadin, A.M., L.N. Smith and W.J. Skocpol, 1980, J. Low Temp. Phys. 38, 497.
Kadin, A.M., C. Varmazis and J.E. Lukens, 1981, Physica 107B + C, 159.
Kaplan, S.B., 1979, J. Low Temp. Phys. 37, 343.
Kaplan, S.B., C.C. Chi, D.N. Langenberg, J.-J. Chang, S. Jafarey and D.J. Scalapino, 1976, Phys. Rev. B14, 4854.
Klapwijk, T.M., and J.E. Mooij, 1975, IEEE Trans. Magn. MAG-11, 858.
Klapwijk, T.M., and J.E. Mooij, 1976a, Physica 81B, 132.
Klapwijk, T.M., and J.E. Mooij, 1976b, Phys. Lett. 57A, 97.
Klapwijk, T.M., J.N. van den Bergh and J.E. Mooij, 1977, J. Low Temp. Phys. 26, 385.
Klapwijk, T.M., G.E. Blonder and M. Tinkham, 1982, Physica 109+110B, 1657.
Kommers, T., and J. Clarke, 1977, Phys. Rev. Lett. 38, 1091.
Kramer, L., and R.J. Watts-Tobin, 1978, Phys. Rev. Lett. 40, 1041.
Kulik, I.O., 1980, Solid State Commun. 35. 383.
Langenberg, D.N., 1974, in: Festkörperprobleme XIV (Advances in Solid State Physics) ed. H.J. Queisser (Pergamon, Oxford) pp. 67-86.
Latyshev, Yu.I., and F.Ya. Nad', 1976, Zh. Eksp. Teor. Fiz. 71, 2158 [Sov. Phys. JETP 44, 1136].
Lemberger, T.R., 1981a, Phys. Rev. B24, 4105.
Lemberger, T.R., 1981b, Physica 107B + C, 163.
Lemberger, T.R., and J. Clarke, 1981a, Phys. Rev. B23, 1088.
Lemberger, T.R., and J. Clarke, 1981b, Phys. Rev. B23, 1100.

Likharev, K.K., 1979, Rev. Mod. Phys. 51, 101.
Likharev, K.K., and L.A. Yacobson, 1975, Zh. Tekh. Fiz. 20, 1950 [Sov. Phys. Tech. Phys. 20, 950].
Likharev, K.K., L.S. Kuzmin and G.A. Ovsyannikov, 1981, IEEE Trans. Magn. MAG-17, 111.
Lindelof, P.E., 1981, Rep. Prog. Phys. 44, 949.
Lindelof, P.E., and J. Bindslev Hansen, 1977, J. Low Temp. Phys. 29, 369.
Lindelof, P.E., and J. Bindslev Hansen, 1981, Short-range interaction between two superconduct-
ing weak links, in: Nonequilibrium Superconductivity, Phonons and Kapitza Boundaries (Proc. NATO ASI), ed. K.E. Gray (Plenum, New York) ch. 19.
Meyer, J., and G. von Minnigerode, 1972, Phys. Lett. 38A, 529.
Meyer, J.D., and R. Tidecks, 1976, Solid State Commun. 18, 305.
Mooij, J.E., N. Lambert and T.M. Klapwijk, 1980, Solid State Commun. 36, 585.
Mller, W.H.G., and F. Baumann, 1978, Thin Solid Films 48, 193.
Octavio, M., and W.J. Skocpol, 1981, Physica 107B + C, 173.
Octavio, M., W.J. Skocpol and M. Tinkham, 1977, IEEE Trans. Magn. MAG-13, 739.
Octavio, M., W.J. Skocpol and M. Tinkham, 1978, Phys. Rev. B17, 159.
Octavio, M., M. Tinkham, G.E. Blonder and T.M. Klapwijk, 1983, Phys. Rev. B27, 6739.
Owen, C.S., and D.J. Scalapino, 1972, Phys. Rev. Lett. 28, 1559.
Palmer, D.W., and J.E. Mercereau, 1974, Appl. Phys. Lett. 25, 467.
Palmer, D.W., and J.E. Mercereau, 1977, Phys. Lett. 61A, 135.
Pals, J.A., and J. Dobben, 1979, Phys. Rev. B20, 935.
Pals, J.A., and J. Dobben, 1980, Phys. Rev. Lett. 44, 1143.
Pals, J.A., and J. Wolter, 1979, Phys. Lett. 70A, 150.
Pals, J.A., K. Weiss, P.M. Van Attekum, R.E. Horstman and J. Wolter, 1982, Phys. Rep. 89, 323.
Parker, W.H., 1975, Phys. Rev. B12, 3667.
Paterson, J.L., 1978, J. Low Temp. Phys. 33, 285.
Pethick, C.J., and H. Smith, 1979, Ann. Phys. 119, 133.
Pethick, C.J., and H. Smith, 1980, J. Phys. C13, 6313.
Pippard, A.B., J.G. Shephard and D.A. Tindall, 1971, Proc. Roy. Soc. (London) A324, 17.
Resnick, D.J., T.C. Garland, J.T. Boyd, S. Shoemaker and R.S. Newrock, 1981, Phys. Rev. Lett. 47, 1542.
Riedel, E., 1964, Z. Naturforsch. 19, 1634.
Rieger, T.J., D.J. Scalapino and J.E. Mercereau, 1972, Phys. Rev. B6, 1734.
Sandell, R.D., C. Varmazis, A.K. Jain and J.E. Lukens, 1979, IEEE Trans. Magn. MAG-15, 462.
Santhanam, P., and D.E. Prober, 1984, Phys. Rev. B29, 3733.
Scalapino, D.J., 1970, Phys. Rev. Lett. 24, 1052.
Schmid, A., 1978, J. Physique 39, C6-1360.
Schmid, A., 1981, in:Nonequilibrium Superconductivity, Phonons, and Kapitza Boundaries (Proc. NATO ASI), ed. K.E. Gray (Plenum, New York) ch. 14.
Schmid, A., and G. Schön, 1975a, J. Low Temp. Phys. 20, 207.
Schmid, A., and G. Schön, 1975b, Phys. Rev. Lett. 34, 941.
Schmid, A., G. Schön and M. Tinkham, 1980, Phys. Rev. B11, 5076.
Schön, G., 1985, ch., this volume.
Schön, G., and V. Ambegaokar, 1979, Phys. Rev. B19, 3515.
Schrieffer, J.R., and J.W. Wilkins, 1963, Phys. Rev. Lett. 10, 17.
Schuller, I., and K.E. Gray, 1976, Phys. Rev. Lett. 36, 429.
Schuller, I., and K.E. Gray, 1977, Solid State Commun. 23, 337.

Seligson, D., and J. Clarke, 1983, Phys. Rev. B28, 6297.
Simanek, E., and J.C. Hayward, 1974, Physica 78, 199.
Skocpol, W.J., 1981, Nonequilibrium effects in 1-D superconductors, in: Nonequilibrium Superconductivity, Phonons, and Kapitza Boundaries (Proc. NATO ASI), ed. K.E. Gray (Plenum, New York) ch. 18.
Skocpol, W.J. and L.D. Jackel, 1981, Physica 108B + C, 1021.
Skocpol, W.J., and M. Tinkham, 1975, Rep. Prog. Phys. 38, 1049.
Skocpol, W.J., M.R. Beasley and M. Tinkham, 1974a, J. Low Temp. Phys. 16, 145.
Skocpol, W.J., M.R. Beasley and M. Tinkham, 1974b, J. Appl. Phys. 45, 4054.
Smith, A.D., W.J. Skocpol and M. Tinkham, 1980, Phys. Rev. B22, 4346.
Smith, L.N., 1977, J. Low Temp. Phys. 28, 519.
Smith, L.N., 1980, J. Low Temp. Phys. 38, 553.
Solymar, L., 1972, Superconductive Tunneling and Applications (Wiley, New York).
Stuivinga, M., J.E. Mooij and T.M. Klapwijk, 1982, J. Low Temp. Phys. 46, 555.
Stuivinga, M., C.L.G. Ham, T.M. Klapwijk and J.E. Mooij, 1983, J. Low Temp. Phys. 53, 633.
Thouless, D.J., and D.R. Tilley, 1961, Proc. Phys. Soc. (London) 77, 1175.
Tidecks, R., and J.D. Meyer, 1979, Z. Phys. B32, 363.
Tinkham, M., 1972, Phys. Rev. B6, 1747.
Tinkham, M., 1979, Nonequilibrium superconductivity, in: Advances in Solid State Physics XIX, ed. J. Treusch (Pergamon, Oxford) pp. 363-385.
Tinkham, M., 1981, Heating and dynamic enhancement in metallic weak links, in: Nonequilibrium Superconductivity, Phonons, and Kapitza Boundaries (Proc. NATO ASI), ed. K.E. Gray (Plenum, New York) ch. 8.
Tinkham, M., and J. Clarke, 1972, Phys. Rev. Lett. 28, 1366.
Tinkham, M., M. Octavio and W.J. Skocpol, 1977, J. Appl. Phys. 48, 1311.
Tredwell, T.J., and E.H. Jacobsen, 1975, Phys Rev. Lett. 35, 244.
Tredwell, T.J., and E.H. Jacobsen, 1976, Phys. Rev. B13, 293.
Van Attekum, P.M., and J.J. Ramekers, 1982, Solid State Commun. 43, 735.
Van Attekum, P.M., J.J. Ramekers, J.A. Pals and A.M. Hoeben, 1983, Phys. Rev. B27, 1623.
Volkov, A.F., and A.V. Zaitsev, 1975, Zh. Eksp. Teor. Fiz. 69, 222 [Sov. Phys. JETP 42, 1130].
Voss, R.F., and R.A. Webb, 1982, Phys. Rev. B25, 3446.
Waldram, J.R., 1975, Proc. Roy. Soc. (London) A345, 231.
Watts-Tobin, R.J., Y. Krhenbhl and L. Kramer, 1981, J. Low Temp. Phys. 42, 459.
Werthamer, N.R., 1966, Phys. Rev. 147, 255.
Wolter, J., P.M. Van Attekum, R.E. Horstman and M.C.H.M. Wouters, 1981a, Solid State Commun. 40, 433.
Wolter, J., P.M. Van Attekum, R.E. Horstman and M.C.H.M. Wouters, 1981b, Physica 108B, 781. Yoshihiro, K., and K. Kajimura, 1970, Phys. Lett. 32A, 269.
Yu, M.L., and J.E. Mercereau, 1972, Phys. Rev. Lett. 28, 1117.
Yu, M.L., and J.E. Mercereau, 1975, Phys Rev. B12, 4909.

Bibliography from Nonequilibrium properties of superconductors (transport equation approach) by A.G. Aronov, Yu.M. Gal'perin, V.L. Gurevich and V.I. Kozub

Akhieser, A.I., 1938, Zh. Eksp. Teor. Fiz. 8, 1900.
Akhieser, A.I., M.I. Kaganov and G.Ya. Ljubarskii, 1957, Zh. Eksp. Teor. Fiz. 32, 837.
Aronov, A.G., 1974, Zh. Eksp. Teor. Fiz. 67, 178 [1975, Sov. Phys. JETP 40, 908].
Aronov, A.G., 1976, Zh. Eksp. Teor. Fiz. 70, 1477 [Sov. Phys. JETP 43, 770].
Aronov, A.G., and V.L. Gurevich, 1974, Fiz. Tverd. Tela 16, 2656 [1975, Sov. Phys. Solid.

State 16. 1722].
Aronov, A.G., and V.L. Gurevich, 1976, Zh. Eksp. Teor. Fiz. 70, 955 [Sov. Phys. JETP 43, 498].
Aronov, A.G., and B.Z. Spivak, 1977, J. Low Temp. Phys. 29, 149.
Aronov, A.G., and B.Z. Spivak, 1978, Fiz. Nizk. Temp. 4, 1305.
Aronov, A.G., M.A. Zelikman and B.Z. Spivak, 1976, Fiz. Tverd. Tela 18, 2209.
Artemenko, S.N., and A.F. Volkov, 1975a, Zh. Eksp. Teor. Fiz. Pis'ma 21, 662.
Artemenko, S.N., and A.F. Volkov, 1975b, Zh. Eksp. Teor. Fiz. 69, 1764 [Sov. Phys. JETP 42, 896].
Artemenko, S.N., and A.F. Volkov, 1976, Zh. Eksp. Teor. Fiz. 70, 1061 [Sov. Phys. JETP 43, 548]. Artemenko, S.N., and A.F. Volkov, 1979, Usp. Fiz. Nauk 128, 3.
Azbel', M.Ya., 1970, Zh. Eksp. Teor. Fiz. 59, 295 [1971, Sov. Phys. JETP 32, 159].
Betbeder-Matibet, O., and P. Nozires, 1969, Ann. Phys. 51, 392.
Bulyzhenkov, I.E., and B.I. Ivlev, 1976a, Zh. Eksp. Teor. Fiz. 70, 1405.
Bulyzhenkov, I.E., and B.I. Ivlev, 1976b, Zh. Eksp. Teor. Fiz. 71, 1172.
Carlson, P.L., and A.M. Goldman, 1975, Phys. Rev. Lett. 34, 11.
Clarke, J., and M. Tinkham, 1972, Phys. Rev. Lett. 28, 1366.
Clarke, J., B.R. Fjordbge and P. E. Lindelof, 1979, Phys. Rev. Lett. 43, 642.
De Gennes, P., 1968, Superconductivity of Metals and Alloys (Benjamin, New York).
Eliashberg, G.M., 1970, Zh. Eksp. Teor. Fiz. Pis'ma 11, 186 [Sov. Phys. JETP. Lett. 11, 114].
Eliashberg, G.M., 1971, Zh. Eksp. Teor. Fiz. 61, 1254 [Sov. Phys. JETP 34, 668].
Eliashberg, G.M., and B.I. Ivlev, 1985, ch. 6, this volume.
Eilenberger, G., 1968, Z. Phys. 214, 195.
Galaiko, V.P., 1973, Zh. Eksp. Teor. Fiz. 64, 1824 [Sov. Phys. JETP 37, 922].
Galaiko, V.P., 1974, Zh. Eksp. Teor. Fiz. 66, 379 [Sov. Phys. JETP 39, 181].
Galaiko, V.P., 1975, Zh. Eksp. Teor. Fiz. 68, 223 [Sov. Phys. JETP 41, 108].
Galaiko, V.P., and N.B. Kopnin, 1985, ch. 12, this volume.
Galako, V.P., and V.S. Shumeiko, 1976, Zh. Eksp. Teor. Fiz. 71, 671 [Sov. Phys. JETP 44, 353].
Galako, V.P., V.S. Shumeko and T. Kshishton', 1981, Zh. Eksp. Teor. Fiz. 80. 2078.
Galitskii, V.M., V.F. Elesin and Yu.V. Kopaev, 1985, ch. 9, this volume.
Gal'perin, Yu.M., 1974, Zh.Eksp.Teor.Fiz. 67, 2195 [Sov. Phys. JETP 40, 1088].
Gal'perin, Yu.M., 1978, Zh. Eksp. Teor. Fiz. 74, 1126.
Gal'perin, Yu.M., and V.I. Kozub, 1977, Fiz. Nizk. Temp. 3, 1512.
Gal'perin, Yu.M., V.D. Kagan and V.I. Kozub, 1972, Zh. Eksp. Teor. Fiz. 62, 1521 [Sov. Phys. JETP. 35, 798].
Gal'perin, Yu.M., V.L. Gurevich and V.I. Kozub, 1973a, Zh. Eksp. Teor. Fiz. 65, 1045 [1974, Sov. Phys. JETP 38, 517].
Gal'perin, Yu.M., V.L. Gurevich and V.I. Kozub, 1973b, Zh. Eksp. Teor. Fiz. Pis'ma 17, 687.
Gal'perin, Yu.M., V.L. Gurevich and V.I. Kozub, 1974a, Zh. Eksp. Teor. Fiz. 66, 1387 [Sov. Phys. JETP, 39, 680].
Gal'perin, Yu.M., V.L. Gurevich and V.I. Kozub, 1974b, Fiz. Tverd. Tela 16, 1151.
Gal'perin, Yu.M., V.L. Gurevich and V.I. Kozub, 1978, Phys. Rev. B18, 5116.
Gantsevich, S.V., V.L. Gurevich and R. Katilius, 1974, Phys. Kond. Mater. 18, 165.
Garland, J.C., and D.J. Van Harlingen, 1974, Phys. Lett. A47, 423.
Gelikman, B.T., 1958, Zh. Eksp. Teor. Fiz. 34, 1042 [Sov. Phys. JETP 34, 721].
Geilikman, B.T., and M.Yu. Reizer, 1975, Fiz. Tverd. Tela 17, 2002 [Sov. Phys. Solid State 17, 1309].
Ginzburg, V.L., 1944, Zh. Eksp. Teor. Fiz. 14, 177.

Gor'kov, L.P., and G.M. Eliashberg, 1968, Zh. Eksp. Teor. Fiz. 54, 612 [Sov. Phys. JETP 27, 328].
Gor'kov, L.P., and G.M. Eliashberg, 1969, Zh. Eksp. Teor. Fiz. 56, 1297 [Sov. Phys. JETP 29, 698].
Gurevich, L.E., and E.T. Krylov, 1975, Zh. Eksp. Teor. Fiz. Pis'ma 22, 467 [Sov. Phys. JETP Lett. 22, 226].
Kagan, V.D., 1967, Fiz. Tverd. Tela 9, 3293.
Keldysh, L.V., 1964, Zh. Eksp. Teor. Fiz. 47, 1515 [1965, Sov. Phys. JETP 20, 1018].
Kemoklidze, M.P., and L.P. Pitaevskii, 1967, Zh. Eksp. Teor. Fiz. 52, 1556 [Sov. Phys. JETP 25, 1036].
Kon, L.Z., 1975, Fiz. Tverd. Tela 17, 1711 [Sov. Phys. Solid State 17, 1113].
Kon, L.Z., and Yu.N. Nika, 1976, Fiz. Tverd. Tela 18, 3474.
Kozub, V.I., 1978, Zh. Eksp. Teor. Fiz. 74, 344 [Sov. Phys. JETP 47, 178].
Kresin, V.Z., 1959, Zh. Eksp. Teor. Fiz. 36, 1947 [Sov. Phys. JETP 36, 1385].
Landau, L.D., 1946, Zh. Eksp. Teor. Fiz. 16, 574.
Larkin, A.I., and Yu.N. Ovchinnikov, 1973, J. Low Temp. Phys. 10, 407.
Larkin, A.I., and Yu.N. Ovchinnikov, 1977, Zh. Eksp. Teor. Fiz. 73, 299 [Sov. Phys. JETP 46. 155].
Larkin, A.I., and Yu.N. Ovchinnikov, 1985, ch. 11, this volume.
Luttinger, J.M., 1964, Phys. Rev. 136A. 1481.
Ovchinnikov, Yu.N., 1977, Zh. Eksp. Teor. Fiz. 72, 773 [Sov. Phys. JETP 45, 404].
Owen, T.S., and D.J. Scalapino, 1972, Phys. Rev. Lett. 28, 1559.
Pegrum, C.M., and A.M. Gunault, 1976, Solid State Commun. 25, 419.
Pegrum, C.M., A.M. Gunault and C.R. Picket, 1975, Proc. 14th Int. Conf. on Low Temperature Physics (Otaniemi, Finland) vol. 2, 513.
Prange, R.E., and L.P. Kadanoff, 1964, Phys. Rev. 134A, 566.
Privorotskii, I.A., 1962, Zh. Eksp. Teor. Fiz. 42, 450 [Sov. Phys. JETP 42, 315].
Rieger, T.J., D.J. Scalapino and J.E. Mercereau, 1971, Phys. Rev, Lett. 27, 1787.
Rothwarf, A., and B.M. Taylor, 1967, Phys. Rev. Lett. 19, 27.
Schmid, A., 1968, Phys. Kond. Mater. 8, 129.
Schmid, A., 1969, Phys. Rev. 186, 480.
Schmid, A., and G. Schön, 1975a, J. Low Temp. Phys. 20, 207.
Schmid, A., and G. Schön, 1975b, Phys. Rev. Lett. 34, 941.
Schmid, A., and G. Schön, 1979, Phys. Rev. Lett. 43, 793.
Schrieffer, J.R., and D.M. Ginsberg, 1962, Phys. Rev. Lett. 8, 207.
Selzer, P.M., and W.W. Fairbank, 1974, Phys. Lett. 48A, 279.
Shelankov, A.L., 1977, Fiz. Tverd. Tela 19, 3256.
Shelankov, A.L., 1980, Zh. Eksp. Teor. Fiz. 78, 2359.
Stephen, M.J., 1965, Phys. Rev. 139A, 197.
Tinkham, M., 1972, Phys. Rev. B6, 1747.
Van Harlingen, D.J., and J.C. Garland, 1978, Solid State Commun. 25, 419.
Vardanyan, R.A., and B.I. Ivlev, 1973, Zh. Eksp. Teor. Fiz. 65, 2315.
Volkov, A.F., 1974, Zh. Eksp. Teor. Fiz. 66, 758.
Weinreich, G., 1957, Phys. Rev. 107, 317.
Zavaritskii, N.V., 1974, Zh. Eksp. Teor. Fiz. Pis'ma 19, 205.

Bibliography from The kinetic theory of superconductors with excess quasiparticles by V.M. Galitskii, V.F. Elesin and Yu.V. Kopaev

Abrikosov, A.A., and L.P. Gor'kov, 1960, Zh. Eksp. Teor. Fiz. 39, 1781.
Abrikosov, A.A., and I.M. Khalatnikov, 1958, Usp. Fiz. Nauk 65, 551.

Abrikosov, A.A., L.P. Gor'kov and I.E. Dzyaloshinskii, 1962, Metody kvantovoi teorii polya v statisticheskoi fizike (Quantum Field Theoretical Methods in Statistical Physics), Fizmatgiz, Moscow (Engl. trans.: Pergamon Press, Oxford, 1965).
Aronov, A.G., and V.L. Gurevich, 1972, Zh. Eksp. Teor. Fiz. Pis'ma 13, 564.
Aronov, A.G., and V.L. Gurevich, 1973, Zh. Eksp. Teor. Fiz. 65, 1111.
Aronov, A.G., and B.Z. Spivak, 1976, Fiz. Tverd. Tela 18, 541.
Aronov, A.G., and B.Z. Spivak, 1978, Fiz. Nizk. Temp. 4, 1365.
Aronov, A.G., and B.Z. Spivak, 1979, Zh. Eksp. Teor. Fiz, 21, 2868.
Artemenko, S.N., and A.F. Volkov, 1979, Usp. Fiz. Nauk 128, 3.
Balkashin, O.P., I.K. Yanson and A.V. Khotkevich, 1977, Zh. Eksp. Teor. Fiz. 72, 1182.
Baru, V.G., and A.A. Sukhanov, 1975, Zh. Eksp. Teor. Fiz. Pis'ma 21, 209.
Blazhin, A.G., and A.S. Selivanenko, 1970, Fiz. Tekhn. Poluprovodn. 4, 239.
Buimistrov, V.M., 1968, Zh. Eksp. Teor. Fiz. Pis'ma 8, 274.
Buisson, R., R. Chicauft, F. Madeore and R. Romestain, 1978, Phys. Lett. 39, 130.
Chang, J.J., and D.J. Scalapino, 1974, Phys. Rev. B10, 4047.
Chang, J.J., and D.J. Scalapino, 1977, Phys. Rev. B15, 2651.
Chang, J.J., Y.L. Warren and D.J. Scalapino, 1979, Phys. Rev. B20, 2739.
Dmitriev, V.M., and E.V. Khristenko, 1978, Fiz. Nizk Temp. 4, 821.
Dynes, R.C., and V. Narayanamurti, 1972, Phys. Rev. B6, 143.
Dynes, R.C., V. Narayanamurti and J.P. Garno, 1977, Phys. Rev. Lett. 39, 229.
Eckern, V., A. Schmid, M. Schmutz and G. Schön, 1979, J. Low Temp. Phys. 36, 643.
Elesin, V.F., 1969, Fiz. Tverd. Tela 11, 1820.
Elesin, V.F., 1970a, Zh. Eksp. Teor. Fiz. 59, 602.
Elesin, V.F., 1970b, Fiz. Tekhn. Poluprovodn. 4, 1520.
Elesin, V.F., 1974, Zh. Eksp. Teor. Fiz. 66, 1755.
Elesin, V.F., 1975, Zh. Eksp. Teor. Fiz. 69, 572.
Elesin, V.F., 1976, Zh. Eksp. Teor. Fiz. 71, 1490.
Elesin, V.F., 1977a, Zh. Eksp. Teor. Fiz. 72, 365.
Elesin, V.F., 1977b, Fiz. Tverd. Tela 19, 2977.
Elesin, V.F., 1979a, Fiz. Tverd. Tela 21, 2868.
Elesin, V.F., 1979b, Zh. Eksp. Teor. Fiz. 76, 2218.
Elesin, V.F., 1980, Fiz. Tverd. Tela 22, 3097.
Elesin, V.F., 1981, Zh. Eksp. Teor. Fiz. 80, 293.
Elesin, V.F., and Yu.V. Kopaev, 1972, Fiz. Tverd. Tela 14, 669.
Elesin, V.F., and Yu.V. Kopaev, 1974, Fiz. Tverd. Tela 16, 840.
Elesin, V.F., and Yu.V. Kopaev, 1981, Usp. Fiz. Nauk 133, 259.
Elesin, V.F., and E.B. Levchenko, 1978, Fiz. Tverd. Tela 20, 2454.
Elesin, V.F., Yu.V. Kopaev and R.Kh. Timerov, 1973, Zh. Eksp. Teor. Fiz. 65, 2343.
Elesin, V.F., V.V. Kapaev and Yu.V. Kopaev, 1976a, Zh. Eksp. Teor. Fiz. 71, 714.
Elesin, V.F., V.E. Kondrashov and Yu.M. Sklyarov, 1976b, Fiz. Tverd. Tela 18, 3393.
Elesin, V.F., V.E. Kondrashov and B.N. Shamraev, 1977a, Fiz. Tverd. Tela 19, 1525.
Elesin, V.F., V.E. Kondrashov, B.N. Shamraev and A.S. Sukhikh, 1977b, Fiz. Tverd. Tela 19, 3702.
Elesin, V.F., V.E. Kondrashov and A.S. Sukhikh, 1979, Fiz. Tverd. Tela 21, 3225.
Elesin, V.F., V.E. Kondrashov, E.B. Levchenko and A.S. Sukhikh, 1980a, Fiz. Tverd. Tela 22, 1571.
Elesin, V.F., V.E. Kondrashov, E.B. Levchenko and A.S. Sukhikh, 1980b, VINITI, No 1862-80, UDK 537.312.62.
Eliashberg, G.M., 1970, Zh. Eksp. Teor. Fiz. Pis'ma 11, 186.
Eliashberg, G.M., 1971a, Zh. Eksp. Teor. Fiz. 61, 1274.

Eliashberg, G.M., 1971b, Thesis (Landau Inst. Teor. Fiz., Moskva-Chernogolovka).
Fush, J., P.W. Eppelrein, M. Welte and W. Eisenmenger, 1977, Phys. Rev. Lett. 38, 919.
Galitskii, V.M., and V.F. Elesin, 1973, Zh. Eksp. Teor. Fiz. 64, 691.
Galitskii, V.M., S.P. Goreslavskii and V.F. Elesin, 1969, Zh. Eksp. Teor. Fiz. 57, 207.
Galitskii, V.M., V.F. Elesin and Yu.V. Kopaev, 1973, Zh. Eksp. Teor. Fiz. Pis'ma 18, 50.
Galitskii, V.M., V.F. Elesin and V.E. Kondrashov, 1978, Preprint IAE, 3055.
Geilikman, B.T., and V.Z. Kresin, 1969, Usp. Fiz. Nauk 99, 51.
Golovashkin, A.I., K.V. Mitsen and G.P. Motulevich, 1975, Zh. Eksp. Teor. Fiz. 68, 1408.
Golovashkin, A.I., O.M. Ivanenko, K.V. Mitsen, G.P. Motulevich and A.L. Shubin, 1978, Zh. Eksp. Teor. Fiz. 75, 1515.
Golovashkin, A.I., O.M. Ivanenko, K.V. Mitsen, G.P. Motulevich and V.F. Elesin, 1979a, Proc. XX Conf. Fiz. Nizk Temp. (Moskva) ed. W.F. Gantmaher (Institute of Chemical Physics, Academy of Science, USSR) v.3, p. 210.
Golovashkin, A.I., O.M. Ivanenko, K.V. Mitsen and G.P. Motulevich, 1979b, Proc. XVIII Conf. Fiz. Nizk. Temp. (Dresden) p. 24.
Golovashkin, A.I., V.F. Elesin, O.M. Ivanenko, K.V. Mitsen and G.P. Motulevich, 1980, Fiz. Tverd. Tela 21, 105.
Gor'kov, L.P., and L.M. Eliashberg, 1968, Zh. Eksp. Teor. Fiz. 54, 612.
Gor'kov, L.P. and L.M. Eliashberg, 1969. Zh. Eksp. Teor. Fiz. 56, 1297.
Gray, K.E., and H.W. Willemsen, 1978, J. Low Temp. Phys. 31, 911.
Hida, K., 1978a, J. Low Temp. Phys. 32. 881.
Hida, K., 1978b, Phys. Lett. 68 A, 71.
Hu, P., R.C. Dynes and V. Narayanamurti, 1974, Phys. Rev. B10, 2786.
Iguchi, I., 1977. Phys. Rev. B16, 1954.
Iguchi, I., D. Kent, H. Gilmartin and D.N. Langenberg, 1981, Phys. Rev. 23, 3240.
Imai, S., 1980, J. Low Temp. Phys. 40, 595.
Janik, R., L. Morli, N.C. Cirillo, T.N. Lechevet, W.D. Gregory and W.L. Goodman, 1975, IEEE Trans. Magn. Mag-11, 687.
Jaworsky, F., and W.H. Parker, 1979, Phys. Rev. B20, 945.
Kaplan, S.B., J.R. Kirtley and D.N. Langenberg, 1977, Phys. Rev. Lett. 39, 291.
Keldysh, L.V., 1964, Zh. Eksp. Teor. Fiz. 47, 1515.
Keldysh, L.V., and Yu.V. Kopaev, 1964, Fiz. Tverd. Tela 6, 2791.
Kemoklidze, M.L., and L.P. Pitaevskii, 1967, Zh. Eksp. Teor. Fiz. 52, 1556.
Kirichenko, I.K., and V.P. Seminozhenko, 1977, Fiz. Nizk. Temp. 3, 987.
Kirichenko, I.K., S.A. Peskovatskii and V.P. Seminozhenko, 1976, Preprint, IAE Akad. Nauk, No 74. Kiev.
Kirzhnits, D.A., and Yu.V. Kopaev, 1973, Zh. Eksp. Teor. Fiz. Pis'ma 17, 379.
Kumar, N., and K.P. Sinha, 1968, Phys. Rev. 174, 482.
Lambert, D., D. Salin, and T. Joffin, 1977, J. Phys. Lett. 38, 368.
Langenberg, D.N., 1975, Proc. LT-14, 14th Int. Conf. on Low Temperature Physics (Otaniemi, Finland) eds. M. Krusius and M. Vuorio vol. 5, p. 223.
Mitsen, K.V., 1979, Fiz. Tverd. Tela 21, 3475.
Mitsen, K.V., 1981, Thesis (FIAN, Moskva).
Mitsen, K.V., G.P. Motulevich, A.I. Golovashkin and O.M. Ivanenko, 1981, Solid State Commun. 38. 6366.
Owen, C.S., and D.J. Scalapino, 1972, Phys. Rev. Lett. 28, 1559.
Pan, V.M., and E.M. Rudenko, 1981, Zh. Eksp. Teor. Fiz. Pis'ma 34, 57.
Parker, W.H., 1975, Phys. Rev. B12, 3667.
Ryvkin, S.M., 1963, Fotoelectricheskie Yavleniya v Poluprovodnikakh (Fizmatgiz, Moskva).
Sai-Halasz, C.A., C.C. Chi, A. Denstein and D.N. Langenberg, 1974, Phys. Rev. Lett. 33, 215.

Scalapino, D.N., and B.A. Huberman, 1977, Phys. Rev. Lett. 39, 1365.
Schön, A., and M. Tremblay, 1979, Phys. Rev. Lett. 42, 1086.
Smith, L.N., 1977, J. Low Temp. Phys. 28, 519.
Smith, L.N., 1980, J. Low Temp. Phys. 38, 553.
Testardi, L.R., 1971, Phys. Rev. B4, 2189.
Tremblay, A.-M.S., 1981, Stability of nonequilibrium superconductivity states, in: Nonequilibrium Superconductivity, Phonons, and Kapitza Boundaries (Proc. NATO ASI), ed. K.E. Gray (Plenum, New York) chs. 10 and 11.
Vardanyan, R.A., and B.I. Ivlev, 1973, Zh. Eksp. Teor. Fiz. 52, 1556.
Volkov, A.F., and Sh.M. Kogan, 1968, Usp. Fiz. Nauk 96, 633.
Willemsen, H.W. and K.E. Gray, 1978, Phys. Rev. Lett. 41, 812.

Bibliography from Kinetic equations in superconducting thin films by Jhy-Jiun Chang

Chang, Jhy-Jiun, and D.J. Scalapino, 1977c, Phys. Rev. B15, 2651.
Chang, Jhy-Jiun, and D.J. Scalapino, 1978, J. Low Temp. Phys. 31, 1.
Chang, Jhy-Jiun, W.Y. Lai and D.J. Scalapino, 1979, Phys. Rev. B20, 2739.
Chi, C.C., and J. Clarke, 1979a, Phys. Rev. B19, 4495.
Chi, C.C., and J. Clarke, 1979b, Phys. Rev. B20, 4465.
Clarke, J., 1972, Phys. Rev. Lett. 28, 1363.
Clarke, J., 1981, Charge imbalance, in: Nonequilibrium Superconductivity, Phonons and Kapitza Boundaries (Proc. NATO ASI), ed. K.E. Gray (Plenum, New York) ch. 13.
Cohen, M.G., L.N. Falicov and J.C. Phillips, 1962, Phys. Rev. Lett. 8, 316.
Dayem, A.H., and J.J. Wiegand, 1967, Phys. Rev. 155, 419.
Dayem, A.H., and J.J. Wiegand, 1972, Phys. Rev. B5, 4390.
Dynes, R.C., and V. Narayanamurti, 1972, Phys. Rev. B6, 143.
Dynes, R.C., V. Narayanamurti and M. Chin, 1971, Phys. Rev. Lett. 26, 181.
Eisenmenger, W., 1981, Nonequilibrium phonons, in: Nonequilibrium Superconductivity, Phonons, and Kapitza Boundaries (Proc. NATO ASI), ed. K.E. Gray (Plenum, New York) ch. 3.
Eisenmenger, W., and A.H. Dayem, 1967, Phys. Rev. Lett. 18, 125.
Elesin, V.F., 1979, Sov. Phys. JETP 49, 1121.
Eliashberg, G.M., 1970a, JETP Lett. 11, 696.
Eliashberg, G.M.. 1970b, JETP Lett. 11, 114.
Eliashberg, G.M., 1972, Sov. Phys. JETP 34, 668.

[13]Ambegaokar, V., and L. Tewordt 1964, Phys. Rev. A134, 805.
Bardeen, J., 1961, Phys. Rev. Lett. 6, 57.
Bardeen, J., 1962, Phys. Rev. Lett. 9, 147.
Bardeen, J., L.N. Cooper and J.R. Schrieffer, 1957, Phys. Rev. 108, 1175.
Bardeen, J., G. Rickayzen and L. Tewordt, 1959, Phys. Rev. 113, 982.
Chang, Jhy-Jiun, 1977, Phys. Rev. Lett. 39, 1352.
Chang, Jhy-Jiun, 1978, Phys. Rev. B17, 2137.
Chang, Jhy-Jiun, 1979, Phys. Rev. B19, 1420.
Chang, Jhy-Jiun, 1981, Properties of nonequilibrium superconductors: A kinctic equation approach, in: Nonequilibrium Superconductivity, Phonons, and Kapitza Boundaries (Proc. NATO ASI), ed. K.E. Gray (Plenum, New York) ch. 9.
Chang, Jhy-Jiun, and D.J. Scalapino, 1974, Phys. Rev. B10, 4047.
Chang, Jhy-Jiun, and D.J. Scalapino, 1976, Phys. Rev. Lett. 37, 522.
Chang, Jhy-Jiun, and D.J. Scalapino, 1977a, IEEE Trans. Magn. MAG-13, 747.
Chang, Jhy-Jiun, and D.J. Scalapino, 1977b, Hot superconductors- The physics and application of nonequilibrium superconductivity, in: Superconductor Applications: SQUIDS and Machines, eds. B.B. Schwartz and S. Foner (Plenum, New York).

Entin-Wohlman, O., and R. Orbach, 1979a, Ann. Phys. 122, 64.
Entin-Wohlman, O., and R. Orbach, 1979b, Phys. Rev. B19, 4510.
Gray, K.E., 1969, Quasiparticle lifetime in superconducting aluminium, Ph.D. Thesis (Cambridge Univ.).
Gray, K.E., 1978, Solid State Commun. 26, 633.
Hall, J.T., L.B. Holdeman and R.J. Soulen, 1980, Phys. Rev. Lett. 45, 1011.
Hall, J.T., L.B. Holdeman and R.J. Soulen, 1981, Physica 108 B + C, 827.
Hida, K., 1978, J. Low Temp. Phys. 32, 881.
Horstman, R.E., J. Wolter and E.J. Bartels, 1981, Physica B + C, 833.
Ivlev, B.I., and G.M. Eliashberg, 1971, JETP Lett. 13, 333.
Ivlev, B.I., S.G. Lisitsyn and G.M. Eliashberg, 1973, J. Low Temp. Phys. 10, 449.
Jaworski, F., and W.H. Parker, 1979, Phys. Rev. B20, 945.
Kaplan, S.B., C.C. Chi, D.N. Langenberg, Jhy-Jiun Chang, S. Jafarey and D.J. Scalapino, 1976, Phys. Rev. B14, 4854.
Kaplan, S.B., J.R., Kirtley and D.N. Langenberg, 1977, Phys. Rev. Lett. 39, 291.
Kirtley, J.R., D.S. Kent, D.N. Langenberg, S.B. Kaplan, Jhy-Jiun Chang and Chi-Chung Yang, 1980, Phys. Rev. B22, 1218.
Kommer, T., and J. Clarke, 1977, Phys. Rev. Lett. 38, 1091.
Lemberger, T.R., and J. Clarke. 1981, Phys. Rev. B23, 1088, 1100.
Little, W.A., 1959, Can. J. Phys. 37, 334.
Mattis, D.C., and J. Bardeen, 1958, Phys. Rev. 111, 412.
Moody, M.V., and J.L. Paterson, 1978 J. Low Temp. Phys. 34, 83.
Moody, M.V., and J.L. Paterson, 1981, Phys. Rev. B23, 133.
Mooij, J.E., 1981, Enhancement of superconductivity, in: Nonequilibrium Superconductivity, Phonons, and Kapitza Boundaries (Proc. NATO ASI), ed. K.E. Gray (Plenum, New York) ch. 7.
Narayanamurti, V., and R.C. Dynes, 1971, Phys. Rev. Lett. 27, 410.
Owen, C.S., and D.J. Scalapino, 1972, Phys. Rev. Lett. 28, 1559.
Parker, W.H., 1975, Phys. Rev. B12, 3667.
Parmenter, R.H., 1961, Phys. Rev. Lett. 7, 274.
Paterson, J.L., 1978, J. Low Temp. Phys. 33, 285.
Peskovatskii, S.A., and V.P. Seminozenko, 1976, Sov. J. Low Temp. Phys. 2, 464.
Pethick, C.J., and H. Smith, 1980, J. Phys. C13, 6313.
Prange, R.E., and L.P. Kadanoff, 1964, Phys. Rev. A134, 566.
Rothwarf, A., and B.N. Taylor, 1967, Phys. Rev. Lett. 19, 27.
Rutledge, J.R., R.C. Dynes and V. Narayanamurti, 1979, Bull. Am. Phys. Soc. 24, 330.
Scalapino, D.J., 1969, The electron-phonon coupling and strong superconductors, in: Superconductivity, ed. R.D. Parks (Marcel Dekker, New York) ch. 10.
Scalapino, D.J., and B.A. Huberman, 1977, Phys. Rev. Lett. 39, 1365.
Schmid, A., 1977, Phys. Rev. Lett. 38, 922.
Schmid, A., and G. Schön, 1975, J. Low Temp. Phys. 20, 207.
Schrieffer, J.R., 1964, Theory of superconductivity (Benjamin, New York) chs. 2 and 3.
Seligson, D., and J. Clarke, 1982, Bull. Am. Phys. Soc. 27, 252.
Smith, A.D., W.J. Skocpol, and M. Tinkham, 1980, Phys. Rev. B21, 3879.
Tinkham, M., 1972, Phys. Rev. B6, 1747.
Tinkham, M., and J. Clarke, 1972, Phys. Rev. Lett. 28, 1366.
Tremblay, A.-M.S., 1981, Stability of nonequilibrium superconducting states, in: Nonequilibrium Superconductivity, Phonons, and Kapitza Boundaries (Proc. NATO ASI), ed. K.E. Gray (Plenum, New York) chs. 10 and 11.
Willemsen, H.W., and K.E. Gray, 1978. Phys. Rev. Lett. 41, 812.

Wyatt, A.F.G., V.M. Dmitriev, W.S. Moore and R.W. Sheard, 1966, Phys. Rev. Lett. 16, 1166.

Bibliography from Vortex motion in superconductors by A.J. Larkin and Yu.N. Ovchinnikov

Abrikosov, A.A., 1957, On magnetic properties of type II superconductors, Zh. Eksp. Teor. Fiz. 32, 1442 [Sov. Phys. JETP 5, 1174].
Bardeen, J., and R.D. Sherman, 1975, Flux flow in nearly pure low- κ superconductors, Phys. Rev. B12, 2634.
Bardeen, J., and M.J. Stephen, 1965, Theory of the motion in superconductors, Phys. Rev. 140, A1197.
Brandt, E.H., 1976, On the shear modulus of the flux line lattice, Phys. Stat. Sol. (b) 77, 551.
Brandt, E.H., 1977, Elastic energy of the vortex state in type II superconductors. I. High Inductions, J. Low Temp. Phys. 26, 709; II. Low Induction, 735.
Borka, S., I.N. Goncharov, D. Frichevski and I.S. Khukhareva, 1977, Investigation of vortex pinning forces in superconducting $Nb - Zr$ alloys with low j_c, Fiz. Nizk. Temp. 3, 716.
Caroli, C., M. Cyrot and P.G. De Gennes, 1966, The magnetic behaviour of dirty superconductors, Solid State Commun. 4, 17.
Chang, C.C., and J.B. McKinnon, 1968, On the occurrence of the peak effect in type-II superconductors, Phys. Lett. 27 A, 414.
Chang, C.C., J.B. McKinnon and A.C. Rose-Innes, 1969, Peak effect in Type-II Superconductors: Yield point of the Fluxon lattice, Phys. Stat. Sol. 36, 205.
Danilov, V.V., M.Yu. Kupriyanov and K.K. Likharev, 1974, On resistance of superconductors in a dynamic mixed state, Fiz. Tverd. Tela 16, 935.
Eilenberger, G., 1968, Transformation of Gor'kov's equation for type II superconductors into transport-like equations, Z. Phys. 214, 195.
Eliashberg, G.M., 1971, Electron inelastic collisions and nonequilibrium stationary states in superconductors, Zh. Eksp. Teor. Fiz. 61, 1254.
Fiory, A.T., 1971, Quantum interference effects of a moving vortex lattice in Al films, Phys. Rev. Lett. 27, 501.
Gor'kov, L.P., 1958, On the energy spectrum of superconductors, Zh. Eksp. Teor. Fiz. 34, 735.
Gorkov, L.P., 1959, Theory of superconducting alloys in a strong magnetic field near the critical temperature, Zh. Eksp. Teor. Fiz. 37, 1407 [1960, Sov. Phys. JETP 10, 998].
Gor'kov, L.P., and N.B. Kopnin, 1973a, Some features of viscous flow of vortexes in superconducting alloys near the critical temperature, Zh. Eksp. Teor. Fiz. 64, 356 [Sov. Phys. JETP 37, 183].
Gor'kov, L.P., and N.B. Kopnin, 1973b, Viscous flow of vortexes in type II superconducting alloys, Zh. Eksp. Teor. Fiz. 65, 396 [1974, Sov. Phys. JETP 38, 195].
Ioffe, L., and A.I. Larkin, 1981, Properties of Superconductors with Smearing-out Transition Temperature, Zh. Eksp. Teor. Fiz. 81, 707 [Sov. Phys. JETP 54, 378].
Keldysh, L.V., 1964, Diagram technique for nonequilibrium processes, Zh. Eksp. Theor. Fiz. 47, 1515 [1965, Sov. Phys. JETP 20, 1018].
Kramer, E.J., 1978, Summation curves for flux pinning in superconductors, J. Appl. Phys. 49, 742.
Kramer, L., and W. Pesch, 1974, Core structure and low-energy spectrum of isolated vortex lines in clean superconductors as $T \ll T_c$, Z. Phys. 269, 59.
Kpfer, H., and A.A. Manuel, 1979, Summation and Saturation Behaviour of the Volume Pinning Force in Neutron Irradiated V_3Si, Phys. Stat. Sol. (a) 54, 153.
Labusch, R., 1967, Elastische Konstanten des Flussfadengitters in Supraleitern zweiter Art,

Phys. Stat. Sol. 19, 715.
Labusch, R., 1969a, Elastic constants of the fluxoid lattice near the upper critical field, Phys. Stat. Sol. 32, 493.
Labusch, R., 1969b, Calculation of the critical field gradient in type II superconductors, Cryst. Lattice Defects 1, 1.
Larkin, A.I., 1970, Effect of inhomogeneities on the structure of the mixed state of superconductors, Zh. Eksp. Teor. Fiz. 58, 1466 [Sov. Phys. JETP 31, 784].
Larkin, A.L., and Yu.N. Ovchinnikov, 1968, On the quasiclassical method in superconductivity theory, Zh. Eksp. Teor. Fiz. 55, 2262 [1969, Sov. Phys. JETP 28, 1200].
Larkin, A.L., and Yu.N. Ovchinnikov, 1973a, Fluctuation conductivity in the vicinity of the superconducting transition, J. Low Temp. Phys. 10, 407.
Larkin, A.I., and Yu.N. Ovchinnikov, 1973b, Resistance of superconductors near the critical field H_{C2}, Zh. Eksp. Teor. Fiz. 64, 1096 [Sov. Phys. JETP 37, 557].
Larkin, A.I., and Yu.N. Ovchinnikov, 1973c, Electrodynamics of inhomogeneous type II superconductors, Zh. Eksp. Teor. Fiz. 65, 1704 [1974, Sov. Phys. JETP 38, 854].
Larkin, A.I., and Yu.N. Ovchinnikov, 1975, Nonlinear conductivity of superconductors in the mixed state, Zh. Eksp. Teor. Fiz. 68, 1915 [1976, Sov. Phys. JETP 41, 960].
Larkin, A.I., and Yu.N. Ovchinnikov, 1976, Vortex viscosity in clean superconductors, Zh. Eksp. Teor. Fiz. Pis'ma 23, 210.
Larkin, A.I., and Yu.N. Ovchinnikov, 1977, Nonlinear effects during the motion of vortexes in superconductors, Zh. Eksp. Teor. Fiz. 73, 299 [Sov. Phys. JETP 46, 155].
Larkin, A.I., and Yu.N. Ovchinnikov, 1978, Peak-effect in the dependence of the superconductor critical current on the magnetic field, Zh. Eksp. Teor. Fiz. Pis'ma 27, 301.
Larkin, A.I., and Yu.N. Ovchinnikov, 1979, Pinning in type II superconductors, J. Low Temp. Phys. 34, 409.
Larkin, A.I., and Yu.N. Ovchinnikov, 1981, Volt-ampere characteristic of superconductors with large-size defects, Zh. Eksp. Teor. Fiz. 80, 2334 [Sov. Phys. JETP 53, 1221].
Maki, K., 1966, Electrodynamics of superconducting alloys in high magnetic fields, Phys. Rev. 141, 331.
Meier-Hirmer, R., M. David Maloney and M. Gey, 1976, Temperature dependence of the flux flow resistance near H_{C2} in $Pb-In$ alloys, Z . Phys. B23, 139.
Musienko, L.E., I.M. Dmitrenko and V.G. Volotskaya, 1980, On nonlinear conductivity of thin films in a mixed state, Zh. Eksp. Teor. Fiz. Pis'ma 31, 603.
Osborne, K.E., and E.J. Kramer, 1974, The influence of plastic deformation on the peak effect in a type II superconductor, Phil. Mag. 29, 685.
Ovchinnikov, Yu.N., 1974, Conductivity of type II superconductors near the critical field H_{C2} for arbitrary free paths, Zh. Eksp. Teor. Fiz. 66, 1100 [Sov. Phys. JETP 39, 538].
Ovchinnikov, Yu.N., 1980, Metastable states and one-particle pinning in type II superconductors near the critical field- H_{C2}, Zh. Eksp. Teor. Fiz. 79, 1825 [Sov. Phys. JETP 52, 923].
Ovchinnikov, Yu.N., and E.H. Brandt, 1975, Properties of type-II superconductors with arbitrary impurity concentration near H_{C2}, Phys. Stat. Sol. (b) 67, 301.
Reichert, T., R. Meier-Hirmer and H. Kpfer, 1981, Annealing behavior of the critical current density and the superconducting parameters T_c, κ, and H_{C2} in a neutron-irradiated V_3 Si single crystal, Phys. Stat. Sol. (a) 64, 585.
Schmid, A., 1981, Kinetic equations for dirty superconductors, in: Nonequilibrium Superconductivity, Phonons, and Kapitza Boundaries (Proc. NATO ASI), ed. K.E. Gray (Plenum, New York).
Schmid, A., and W. Hauger, 1973, On the theory of vortex motion in an inhomogeneous superconducting film, J. Low Temp. Phys. 11, 667.
Schmid, A., and G. Schön, 1975, Linearized kinetic equations and relaxation processes of a

superconductor near T_c, J. Low Temp. Phys. 20, 207.
Shelankov, A.L., 1980, Normal component drag by the condensate in nonequilibrium superconductors, Zh. Eksp. Teor. Fiz. 78, 2359 [Sov. Phys. JETP 51, 1186].
Shubnikov, L.V., V.I. Khotkevich, Yu.D. Shepelev and Yu.N. Ryabinin, 1937, Magnetic properties of superconducting metals and alloys, Zh. Eksp. Teor. Fiz. 7, 221.
Strnad, A.R., C.F. Hempstead and Y.B. Kim, 1964, Dissipative mechanism in type-II superconductors, Phys. Rev. Lett. 13, 794.
Thompson, R.S., 1970, Microwave, flux flow and fluctuation resistance of dirty type-II superconductors, Phys. Rev. B1, 327.
Tinkham, M., 1964, Viscous flow of flux in type-II superconductors, Phys. Rev. Lett. 13, 804.
Truble, H., and U. Essmann, 1968, Flux-line arrangement in superconductors as revealed by direct observation, J. Appl. Phys. 39, 4052.
Vinnikov, L.Ya., V.I. Grigoriev and O.V. Zharikov, 1976, The resistive state and pinning in deformed niobium single crystals, Zh. Eksp. Teor. Fiz. 71, 252 [Sov. Phys. JETP 44, 1976].
Watts-Tobin, R.J., Y. Krhenbhl and L. Kramer, 1981, Nonequilibrium theory of dirty current carrying superconductors: phase-slip oscillators in narrow filaments near T_c, J. Low Temp. Phys. 42, 459.

Bibliography from Theory of the resistive state in narrow superconducting channels by V.P. Galaiko and N.B. Kopnin

Galako, V.P., 1976a, Zh. Eksp. Teor. Fiz. 71, 273.
Galako, V.P., 1976b, Fiz. Nizk. Temp. 2, 807.
Galaiko, V.P., 1977, J. Low Temp. Phys. 26, 483.
Galaiko, V.P., and V.S. Shumeko, 1976, Zh. Eksp. Teor. Fiz. 71, 761.
Galako, V.P., V.M. Dmitriev and G. E. Churilov, 1973, Zh. Eksp. Teor. Fiz. Pis'ma 18, 362.
Galako, V.P., V.M. Dmitriev and G.E. Churilov, 1976, Fiz. Nizk. Temp. 2, 299.
De Gennes, P.G., 1966, Superconductivity of Metals and Alloys (Benjamin, New York).
Golub, A.A., 1976, Zh. Eksp. Teor. Fiz. 71, 341.
Gor'kov, L.P., 1970, Zh. Eksp. Teor. Fiz. Pis'ma 11, 52.
Gor'kov, L.P., and G.M. Eliashberg, 1968, Zh. Eksp. Teor. Fiz. 54, 612.
Gor'kov, L.P., and G.M. Eliashberg, 1969, Zh. Eksp. Teor. Fiz. 56, 1297.
Gor'kov, L.P., and N.B. Kopnin, 1975, Usp. Fiz. Nauk 116, 413.
Huebner, R.P., and D.E. Gallus, 1973, Phys. Rev. B7, 4089.
Ivlev, B.I., and N.B. Kopnin, 1978, Zh. Eksp. Teor. Fiz. Pis'ma 28, 640.
Ivlev, B.I., and N.B. Kopnin, 1980, Zh. Eksp. Teor. Fiz. 79, 672.
Ivlev, B.I., and N.B. Kopnin, 1981, J. Low Temp. Phys. 44, 453.
Ivlev, B.I., and N.B. Kopnin, 1982, Solid State Commun. 41, 107.
Ivlev, B.I., N.B. Kopnin and L.A. Maslova, 1980a, Fiz. Tverd. Tela 22, 252.
Ivlev, B.I., N.B. Kopnin and L.A. Maslova, 1980b, Zh. Eksp. Teor. Fiz. 78, 1963.
Ivlev, B.I., N.B. Kopnin and V.I. Mel'nikov, 1980c, Fiz. Tverd. Tela 22, 3386.
Ivlev, B.I., N.B. Kopnin and C.J. Pethick, 1980d, Zh. Eksp. Teor. Fiz. 79, 1017.
Ivlev, B.I., N.B. Kopnin and C.J. Pethick, 1980e, J. Low Temp. Phys. 41, 297.
Kadin, A.M., W.J. Skocpol and M. Tinkham, 1978, J. Low Temp. Phys. 33, 481.
Kramer, L., and A. Baratoff, 1977, Phys. Rev. Lett. 38, 518.
Kramer, L., and R.J. Watts-Tobin, 1978a, Phys. Rev. Lett. 40, 1041.
Kramer, L., and R.J. Watts-Tobin, 1978b, in: Proc. 15th Int. Conf. on Low Temperature Physics, J. Physique, Suppl. no. 8, tome 39, C6-554.
Kulik, I.O., 1970, Zh. Eksp. Teor. Fiz. 59, 584.
Landau, I.L., and Yu.V. Sharvin, 1969, Zh. Eksp. Teor. Fiz. Pis'ma 10, 192.
Landau, I.L., and Yu.V. Sharvin, 1972, Zh. Eksp. Teor. Fiz. Pis'ma 15, 88.

Langer, J.S., and V. Ambegaokar, 1967, Phys. Rev. 164, 498.
Larkin, A.I., and Yu.N. Ovchinnikov, 1985, ch. this volume.
Likharev, K.K., 1974, Zh. Eksp. Teor. Fiz. Pis'ma 20, 730.
Little, W.A., 1967, Phys. Rev. 156, 396.
Lukens J.E., R.J. Warburton and W.W. Webb, 1970, Phys. Rev. Lett. 25, 1180.
McCumber, D.E., and B.I. Halperin, 1970, Phys. Rev. B1, 1054.
Meyer, J., and G. von Minnigerode, 1972, Phys. Lett. 38 A, 529.
Newbower, R.S., M.R. Beasley and M. Tinkham, 1972, Phys. Rev. B6, 864.
Rieger, T.J., D.J. Scalapino and J.E. Mercereau, 1972, Phys. Rev. B6, 1734.
Schmid, A., 1966, Phys. Kondens. Mater. 5, 302.
Schmid, A., and G. Schön, 1975, J. Low Temp. Phys, 20, 207.
Schön, G., and V. Ambegaokar, 1979, Phys. Rev. B19, 3515.
Skocpol, W.J., M.R. Beasley and M. Tinkham, 1974, J. Low Temp. Phys. 16, 145.
Smith, L.N., 1980, J. Low Temp. Phys. 38, 553.
Tinkham, M., 1972, Phys. Rev. B6, 1747.
Tinkham, M., 1979, J. Low Temp. Phys. 35, 147.
Tinkham, M., and J. Clarke, 1972, Phys. Rev. Lett. 28, 1366.
Tucker, J.R., and B.I. Halperin, 1971, Phys. Rev. B3, 3768.
Volkov, A.F., and Sh. M. Kogan, 1974, JETP Lett. 19, 4.
Watts-Tobin, R.J., Y. Krhenbhl and L. Kramer, 1981, J. Low Temp. Phys. 42, 459.
Webb, W.W., and R.J. Warburton, 1968, Phys. Rev. Lett. 20, 461.

Bibliography from Collective modes in superconductors by G. Schon

Abrahams, E., and T. Tsuneto, 1966, Phys. Rev. 152, 416.
Ambegaokar, V., and L.P. Kadanoff, 1961, Nuovo Cimento 22, 914.
Anderson, J.T., R.V. Carlson and A.M. Goldman, 1972, J. Low Temp. Phys. 8, 29.
Anderson, P.W., 1958, Phys. Rev. 110, 827; 112, 1900.
Aronov, A.G., and V.L. Gurevich, 1974, Fiz. Tverd. Tela 16, 2656 [1975, Sov. Phys. Solid State 16, 1722].
Artemenko, S.A., and A.F. Volkov, 1975, Zh. Eksp. Teor. Fiz. 69, 1764 [Sov. Phys. JETP 42, 896].
Artemenko, S.A., and A.F. Volkov, 1979, Usp. Fiz. Nauk 128, 3 [1980, Sov. Phys. Usp. 22, 295].
Aspen, F.E., and A.M. Goldman, 1979, Phys. Rev. Lett. 43, 307.
Aspen, F.E., and A.M. Goldman, 1981, J. Low Temp. Phys. 43, 559.
Balseiro, C.A., and L.M. Falicov, 1980, Phys. Rev. Lett. 45, 662.
Baratoff, A., 1982, in: Proc. 16th Int. Conf. on Low Temperature Physics, Part III, Physica 109 & **110B** + **C**, 2058.
Bardeen, J., 1957, Nuovo Cimento 5, 1766.
Bardeen, J., 1958, Phys. Rev. Lett. 1, 399.
Bardeen, J., L.N. Cooper and J.R. Schrieffer, 1957, Phys. Rev. 108, 1175.
Bardeen, J., G. Rickayzen and L. Tewordt, 1959, Phys. Rev. 113, 982.
Baym, G., 1962, Phys. Rev. 127, 1391.
Baym, G., and L.P. Kadanoff, 1961, Phys. Rev. 124, 287.
Bezuglyi, E.V., and E.N. Bratus', 1981, Physica 107B, 167.
Bezuglyi, E.V., E.N. Bratus' and V.P. Galaiko, 1982, J. Low Temp. Phys. 47, 511.
Bogoliubov, N.N., V.V. Tolmachev and D.N. Shirkov, 1959, New Method in the Theory of Superconductivity (Consultants Bureau, New York).
Bray, A.J., and H. Schmidt, 1975a, J. Low Temp. Phys. 21, 669.
Bray, A.J., and H. Schmidt, 1975b, Solid State Commun. 17, 1175.

Brieskorn, G., M. Dinter and H. Schmidt, 1974, Solid State Commun. 15, 757.
Byrd, P.F., and M.D. Friedman, 1971, Handbook of Elliptic Integrals for Engineers and Scientists (Springer, Berlin).
Carlson, R.V., 1975, Thesis (Univ. of Minnesota).
Carlson, R.V., and A.M. Goldman, 1973, Phys. Rev. Lett. 31, 880.
Carlson, R.V., and A.M. Goldman, 1975, Phys. Rev. Lett. 34, 11.
Carlson, R.V., and A.M. Goldman, 1976, J. Low Temp. Phys. 27, 67.
Cheishvili, O.D., 1977, Fiz. Nizk. Temp. 3, 736 [Sov. J. Low Temp. Phys. 3, 357].
Cheishvili, O.D., 1982, J. Low Temp. Phys. 48, 445.
Chi, C.C., and J. Clarke, 1979, Phys. Rev. B19, 4495.
Clarke, J., 1972, Phys. Rev. Lett. 28, 1363.
Dinter, M., 1978a, Phys. Rev. B18, 3163.
Dinter, M., 1978b, J. Low Temp. Phys. 32, 529.
Eckern, U., and A. Schmid, 1981, J. Low Temp. Phys. 45, 137.
Eckern, U., and G. Schön, 1978, J. Low Temp. Phys. 32, 821.
Eilenberger, G., 1968, Z. Phys. 214, 195.
Eliashberg, G.M., 1971, Zh. Eksp. Teor. Fiz. 61, 1254 [1972, Sov. Phys. JETP 34, 668].
Entin-Wohlman, O., and R. Orbach, 1978, Ann. Phys. 116, 35.
Enz, C.P., 1974, Rev. Mod. Phys. 46, 705.
Ferrell, R.A., 1969, J. Low Temp. Phys. 1, 423.
Galako, V.P., N.I. Glushchik and V.S. Shumeko, 1978, Fiz. Nizk. Temp. 4, 289 [Sov. J. Low Temp. Phys. 4, 139].
Ginzburg, V.L., 1961, Zh. Eksp. Teor. Fiz. 41, 828 [1962, Sov. Phys. JETP 14, 594].
Goldman, A.M., 1981, in: Nonequilibrium Superconductivity, Phonons and Kapitza Boundaries (Proc. NATO ASI), ed. K.E. Gray, (Plenum, New York).
Gor'kov, L.P., and G.M. Eliashberg, 1970, J. Low Temp. Phys. 2, 161.
Hu, C.R., 1980, Phys. Rev. B21, 2775.
Jillie, D.W., J.E. Lukens and Y.H. Kao, 1977, IEEE Trans. Magn. Mag 13, 578.
Kadanoff, L.P.. and P.C. Martin, 1961, Phys. Rev: 124, 670.
Kadin, A.M., and A.M. Goldman, 1982, Phys. Rev. B25, 6701.
Kadin, A.M., L.N. Smith and W.J. Skocpol, 1980, J. Low Temp. Phys. 38, 497.
Kadin, A.M., C. Varmazis and J.E. Lukens, 1981, Physica 107B, 159.
Kaplan, S.B., C.C. Chi, D.N. Langenberg, J.-J. Chang, S. Jafarey and D.J. Scalapino, 1976, Phys. Rev. B14, 4854.
Keldysh, L.V., 1964, Zh. Eksp. Teor. Fiz. 47, 1515 [1965 Sov. Phys. JETP 20, 1018].
Khalatnikov, I.M., 1965, An Introduction to the Theory of Superfluidity (Benjamin, New York).
Khalatnikov, I.M., 1969, Zh. Eksp. Teor. Fiz. 57, 489 [Sov. Phys. JETP 30, 268].
Kulik, I.O., 1979, Fiz. Nizk. Temp. 5, 1391 [Sov. J. Low Temp. Phys. 5, 656].
Kulik, I.O., O. Entin-Wohlman and R. Orbach, 1981, J. Low Temp. Phys. 43, 591.
Landau, L.D., 1956, Zh. Eksp. Teor. Fiz. 30, 1058 [1957, Sov. Phys. JETP 3, 920].
Landau, L.D., 1957, Zh. Eksp. Teor. Fiz. 32, 59 [Sov. Phys. JETP 5, 101].
Landau, L.D., 1958, Zh. Eksp. Teor. Fiz. 35, 95 [1959, Sov. Phys. JETP 8, 70].
Landau, L.D., and E.M. Lifshitz, 1959, Fluid Mechanics (Addison-Wesley, Reading, MA), $78.
Larkin, A.I., and A.B. Migdal, 1963, Zh. Eksp. Teor. Fiz. 44, 1703 [Sov. Phys. JETP 17, 1146].
Larkin, A.I., and Yu.N. Ovchinnikov, 1968, Zh. Eksp. Teor. Fiz. 55, 2262 [1969, Sov. Phys. JETP 28, 1200].
Larkin, A.I., and Yu.N. Ovchinnikov, 1977, Zh. Eksp. Teor. Fiz. 73, 295 [Sov. Phys. JETP 46, 155].
Larkin, A.I., and Yu.N. Ovchinnikov, 1981, preprint; see their chapter in the present volume.

Leggett, A.J., 1965, Phys. Rev. A140, 1869.
Leggett, A.J., 1966, Phys. Rev. 147, 119.
Leggett, A.J., 1975, Rev. Mod. Phys. 47, 331.
Lemberger, T.R., and J. Clarke, 1981, Phys. Rev. B23, 1100.
Lindelof, P.E., and J. Bindslev Hansen, 1977, J. Low Temp. Phys. 29, 369.
Littlewood, P.B., and C.M. Varma, 1981, Phys. Rev. Lett. 47, 811.
Maki, K., and H. Sato, 1974, J. Low Temp. Phys. 16, 557.
Martin, P.C., 1969, in: Superconductivity, vol. 1, ed. R.D. Parks (Marcel Dekker, New York), ch. 7.
Mattis, D.C., and J. Bardeen, 1958, Phys. Rev. 111, 412.
Nambu, Y., 1960, Phys. Rev. 117, 648.
Ovchinnikov, Yu.N., 1970, Zh. Eksp. Teor. Fiz. 59, 128 [1971, Sov. Phys. JETP 32, 72].
Ovchinnikov, Yu.N., 1977, Zh. Eksp. Teor. Fiz. 72, 773 [Sov. Phys. JETP 45, 404].
Ovchinnikov, Yu.N., and G. Schön, 1981, preprint.
Ovchinnikov, Yu. N., A. Schmid and G. Schön, 1981, Phys. Rev. Lett. 46, 1013.
Palmer, D. W., and J.E. Mercereau, 1977, Phys. Lett. 61 A, 135.
Paulson, D.N., R.T. Johnson and J.C. Wheatley, 1973, Phys. Rev. Lett. 30, 829.
Pethick, C.J., and H. Smith, 1979, Ann. Phys. 119, 133.
Putterman, S.J., 1974, Superfluid Hydrodynamics (North-Holland, Amsterdam).
Putterman, S.J., 1977, J. Low Temp. Phys. 28, 339.
Scalapino, D.J., 1970, Phys. Rev. Lett. 24, 1052.
Schmid, A., 1966, Phys. Kondens. Mater. 5, 302.
Schmid, A., 1968, Phys. Kondens. Mater. 8, 129.
Schmid, A., 1980, J. Low Temp. Phys. 41, 37.
Schmid, A., 1981, in: Nonequilibrium Superconductivity, Phonons, and Kapitza Boundaries (Proc. NATO ASI), ed. K.E. Gray, (Plenum, New York).
Schmid, A., and G. Schön, 1975a, J. Low Temp. Phys. 20, 207.
Schmid, A., and G. Schön, 1975b, Phys. Rev. Lett. 34, 941.
Schmid, A., and G. Schön, 1975c, in: Proc. 14th Int. Conf. on Low Temperature Physics (Otaniemi, Finland), eds. M. Krusius and M. Vuorio (North-Holland, Amsterdam) vol. 5.
Schön, G., 1976, Thesis (Univ. of Dortmund).
Schön, G., and V. Ambegaokar, 1979, Phys. Rev. B19, 3515.
Shenoy, S.R., and P.A. Lee, 1974, Phys. Rev. B10, 2744.
Skocpol, W.J., M.R. Beasley and M. Tinkham, 1974, J. Low Temp. Phys. 16, 145.
Sooryakumar, R., and M.V. Klein, 1980, Phys. Rev. Lett. 45, 660.
Takayama, H., 1971, Prog. Teor. Phys. 46, 71.
Tinkham, M., 1972, Phys. Rev. B6, 1747.
Tinkham, M., and J. Clarke, 1972, Phys. Rev. Lett. 28, 1366.
Usadel, K.S., 1970, Phys. Rev. Lett. 25, 507.
Wölfle, P., 1973, Phys. Rev. Lett. 31, 1437.
Wölfle, P., 1977, Physica 90B, 96.
Wölfle, P., 1978, in: Progress in Low Temperature Physics VIII, ed. D.F. Brewer (North-Holland, Amsterdam).

Bibliography from resistive states of type-I superconductors by V.T. Dolgopolov and I.L. Landau

Alekseevskii, N.E., 1938, Zh. Eksp. Teor. Fiz. 8, 342.
Andreev, A.F., 1966, Zh. Eksp. Teor. Fiz. 51, 1510 [1967, Sov. Phys. JETP 24, 1019].
Andreev, A.F., 1967, Zh. Eksp. Teor. Fiz. 52, 1106 [Sov. Phys. JETP 25, 735].
Andreev, A.F., 1968, Zh. Eksp. Teor. Fiz. 54, 1510 [Sov. Phys. JETP 27, 809].

Andreev, A.F., 1972, private communication.
Andreev, A.F., and W. Bestgen, 1973, Zh. Eksp. Teor. Fiz. 64, 1865 [Sov. Phys. JETP 37, 942].
Andreev, A.F., and Yu.K. Dzhikaev, 1977, Zh. Eksp. Teor. Fiz. Pis'ma 26, 756, [JETP Lett. 26, 590].
Andreev, A.F., and Yu.V. Sharvin, 1967, Zh. Eksp. Teor. Fiz. 53, 1499 [1968, Sov. Phys. JETP 26, 865].
Andreev, A.F., and P. Tekel, 1972, Zh. Eksp. Teor. Fiz. 76, 1740 [Sov. Phys. JETP 35, 807].
Baird, D.C., and B.C. Mukherjee, 1968, Phys. Rev. Lett. 21, 996.
Balashova, V.M., and Yu.V. Sharvin, 1956, Zh. Eksp. Teor. Fiz. 31, 40 [1957, Sov. Phys. JETP 4, 54].
Bestgen, W., 1973, Zh. Eksp. Teor. Fiz. 65, 2097 [1974, Sov. Phys. JETP 38, 1048].
Bestgen, W., 1979, Zh. Eksp. Teor. Fiz. 76, 556 [Sov. Phys. JETP 49, 285].
Chandrasekhar, B.S., D.E. Farrel and S. Huang, 1967, Phys. Rev. Lett. 18, 43.
Chien, M.K., and D.E. Farrel, 1974, Phys. Rev. B9, 2092.
Dolgopolov, V.T., and S.I. Dorozhkin, 1978, Zh. Eksp. Teor. Fiz. Pis'ma 27, 459 [JETP Lett. 27. 430].
Dolgopolov, V.T., and S.S. Murzin, 1976, Zh. Eksp. Teor. Fiz. Pis'ma 24, 434 [1977, Sov. Phys. JETP Lett. 24, 397].
Dolgopolov, V.T., and S.S. Murzin, 1977, Zh. Eksp. Teor. Fiz. 73, 2281 [Sov. Phys. JETP 46, 1195].
Dolgopolov, V.T., and S.S. Murzin, 1979, Zh. Eksp. Teor. Fiz. 76, 1740 [Sov. Phys. JETP 49, 885].
Dorozhkin, S.I., and V.T. Dolgopolov, 1979a, Solid State Commun. 30, 205.

From The Behavior of a Superconductor in a Variable Field by Gor'kov, Eliashberg

[1] L. P. Gor'kov and G. M. Éliashberg, Zh. Eksp. Teor. Fiz. 54, 612 (1968) [Soviet Phys.-JETP 27, 328 (1968)].

[2] V. L. Ginzburg and L. D. Landau, Zh. Eksp. Teor. Fiz. 20, 1064 (1950).

[3] I. M. Lifshitz, Zh. Eksp. Teor. Fiz. 20, 834 (1950); Dokl. Akad. Nauk SSSR 90, 363 (1953).

[4] V. L. Ginzburg, Zh. Eksp. Teor. Fiz. 34, 113 (1958) [Soviet Phys.-JETP 7, 78 (1958)].

[5] G. E. Churilov, V. M. Dmitriev, F. F. Mende, E. V.

[6] Khristenko and I. M. Dmitrenko, ZhETF Pis. Red. 6, 752 (1967) [JETP Lett. 7, 222 (1967)].

[7] V. V. Golubev, Lektsii po analiticheskoĭ teorii differentsial'nykh uravnenii (Lectures on the Analytic Theory of Differential Equations), Gostekhizdat, 1950.

[8] D. Saint-James and P. G. de Gennes, Phys. Lett. 7, 306 (1963).

[9] P. G. de Gennes, Superconductivity of Metals and Alloys, Pt. 6, Benjamin, 1966.

From Inelastic Electron Collisions and Nonequilibrium Stationary States in Superconductors G. M. Eliashberg

[1] J. Bardeen, L. Cooper, and J. Schrieffer, Phys. Rev., 108, 1175 (1957).

[2] M. P. Kemoklidze and L. P. Pitaevskiĭ, Zh. Eksp. Teor. Fiz. 52, 1556 (1967) [Sov. Phys.-

JETP 25, 1036 (1967)].
[3] L. P. Gor 'kov and G. M. Éliashberg, ibid. 54, 612 (1968) [27, 328 (1968)].
[4] G. M. Eliashberg, ibid. 55, 2443 (1968) [28, 1298 (1969)].
[5] L. D. Landau and E. M. Lifshitz, Mekhanika sploshnykh sred (Fluid Mechanics), Gostekhizdat, 1953, Sec. 65.
[6] A. B. Migdal, Zh. Eksp. Teor. Fiz. 34, 1438 (1958) [Sov. Phys.-JETP 7, 996 (1958)].
[7] G. M. Éliashberg, ZhETF Pis. Red. 11, 186 (1970) [JETP Lett. 11, 114 (1970)].
[8] G. M. Éliashberg, Zh. Eksp. Teor. Fiz. 39, 1437 (1960) [Sov. Phys.-JETP 12, 1000 (1961)].
[9] L. V. Keldysh, ibid. 47, 1515 (1964) [20, 1018 (1965)].
[10] V. L. Pokrovskiĭ and S. K. Savvinykh, ibid. 43, 564 (1962) [16, 404 (1963)].
[11] G. Eilenberger, Zs. Phys., 214, 195 (1968).
[12] A. A. Abrikosov and L. P. Gor'kov, Zh. Eksp. Teor. Fiz. 39, 1781 (1960) [Sov. Phys.-JETP 12, 1243 (1961)].
[13] G. M. Éliashberg, ibid. 42, 1658 (1962) [15, 1151 (1962)].
[14] I. O. Kulik, ibid. 57, 600 (1969) [30, 329 (1970)].
[15] L. P. Gor'kov and G. M. Éliashberg, ibid. 56, 1297 (1969) [29, 698 (1969)].
Translated by J. G. Adashko 129

From A Time Dependent Ginzburg-Landau Equation and its Application to the Problem of Resistivity in the Mixed State by A. Schmid, 1966

[1] Ginzburg, V. L., and L. D. Landau: J. Exptl. Theoret. Phys. (U.S.S.R) 20, 1064 (1950).
[2] Abrikosov, A. A.: J. Exptl. Theoret. Phys. (U.S.S.R.) 32, 1442 (1957) [translation: Soviet Phys. - JETP 5, 1174 (1957)].
[3a] Gorkov, L. P.: J. Exptl. Theoret. Phys. (U.S.S.R.) 36, 1918 (1959) [translation: Soviet Phys. - JETP 9, 1364 (1959)].
[3b] - J. Exptl. Theoret. Phys. (U.S.S.R.) 37, 1407 (1959) [translation: Soviet Phys. JETP 10, 998 (1960)].
[4] Bardeen, J., L. N. Cooper, and J. R. Sohrieffer: Phys. Rev. 108, 1175 (1957).
[5a] Kim, Y. B., C. F. Hempstead, and A. R. Strnad: Phys. Rev. 139 A, 1163 (1965).
[5b] Strnad, A. R., C. F. Hempstead, and Y. B. Kim: Phys. Rev. Letters 13, 794 (1964).
[5c] Hempstead, C. F., and Y. B. Kım: Phys. Rev. Letters 12, 145 (1964). See for similar observations:
Druyvesteyn, W. F., and J. Volger: Philips Res. Repts 19, 359 (1964);
Farrell, D. E., I. Dinewitz, and B. S. Chandrasekhar: Phys. Rev. Letters 16, 91 (1966).
[6] Stephen, M. J., and J. Bardeen: Phys. Rev. Letters 14, 112 (1965). Bardeen, J., and M. J. Stephen: Phys. Rev. 140 A, 1197 (1965). A model with some similar features has been considered by van Vijfeijken, A. G. and A. K. Niessen: Philips Res. Repts 20, 505 (1965).
[7] Tinkham, M.: Phys. Rev. Letters 13, 804 (1964).
[8] Stefhen, M. J., and H. Suhl: Phys. Rev. Letters 13, 797 (1964).
[9] Anderson, P. W., N. R. Werthamer, and J. M. Luttinger: Phys. Rev. 138 A, 1157 (1965).
[10] Jakeman, E., and E. R. Pike: Phys. Letters 20, 593 (1966).
[11] Gorkov, L. P.: J. Exptl. Theoret. Phys. (U.S.S.R.) 34, 735 (1958) [translation: Soviet Phys. - JETP 8, 505 (1958)].
[12] Landau, L. D., and I. M. Khalatnikov: Dokl. Akad. Nauk SSSR, 96, 469 (1954) [translation: Collected Papers of L. D. Landau, edited by D. ter Haar. Oxford: Pergamon Press, pag. 626].
[13] Kadanoff, L. P., and G. Baym: Quantum Statistical Mechanics. New York: W. A. Benjamin, Inc. 1962, chap. 8-2.
[14] Maki, K.: Physics 1, 21 (1964).
[15] Bateman manuscript project. New York-Toronto-London: McGraw-Hill Book Company,

Inc. 1953; Higher transcendental functions II, chap. VIII.
[16] Jones, R. G., E. H. Rhoderick, and A. C. Rose-Innes: Phys. Letters 15, 214 (1965); Josephson, B. D.: Phys. Letters 16, 242 (1965).
[17] Kleiner, W. H., L. M. Roth, and S. H. Autler: Phys. Rev. 138 A, 1226 (1964).

From Stability of nonequilibrium Fermi distributions with respect to Cooper pairing by Aronov, Gurevich

Comments:

[2)] We have learned that D. A. Kirzhnits and Yu. V. Kopaev are also studying a similar problem.

[3)] A similar formalism has also been used by Elesin [[16]] in order to solve the problem of a semiconductor in the field of a strong electromagnetic wave.

[4)] In this representation the factors $\mathbf{u_p}$ and $\mathbf{v_p}$ are determined by other expressions (see [[11]]). We take this opportunity to mention that in [[11]] in expression (2.18) for the collision operator the last two terms were erroneously omitted. Taking these terms into account leads to a change of the numerical coefficients in the final formulas, namely, it leads to the replacement in formula (43) of the coefficient associated with Δ/kT by $1/2 + \pi/4$ and it also leads to the addition of the term $(\,1 - \ln 2)/2$ in the expression for $\ln C$.

[5)] This implies, as one can easily see, a "negative temperature" of the superconducting excitations.

[6)] This state has subsequently been studied in detail experimentally. [[20]]

[7)] Equation (4.3), which we have derived, differs slightly from the corresponding equation in [[12]].

Refs:

[1] V. M. Dmitriev, E. V. Khristenko, A. V. Trubitsyn, and F. F. Mende, UFZh 15, 1611 (1970).
[2] L. R. Testardi, Phys. Rev. B4, 2189 (1971).
[3] R. H. Parmenter, Phys. Rev. Letters 7, 274 (1961).
[4] É. G. Batyev, ZhETF Pis. Red. 5, 45 (1967) [JETP Lett. 5, 35 (1967)].
[5] G. M. Éliashberg, ZhETF Pis. Red. 11, 186 (1970) [JETP Lett. 11, 114 (1970)].
[6] G. M. Éliashberg, Zh. Eksp. Teor. Fiz. 61, 1254 (1971) [Sov. Phys.-JETP 34, 668 (1972)].
[7] B. I. Ivlev and G. M. Éliashberg, ZhETF Pis. Red. 13, 464 (1971) [JETP Lett. 13, 333 (1971)].
[8] A. G. Aronov and V. L. Gurevich, Fiz. Tverd. Tela 14, 1129 (1972) [Sov. Phys.-Solid State 14, 966 (1972)].
[9] A. G. Aronov and V. L. Gurevich, ZhETF Pis. Red. 15, 564 (1972) [JETP Lett. 15, 400 (1972)].
[10] A. G. Aronov and V. L. Gurevich, Fiz. Tverd. Tela 14, 2675 (1972) [Sov. Phys.-Solid State 14, 2309 (1973)].
[11] A. G. Aronov and V. L. Gurevich, Zh. Eksp. Teor. Fiz. 63, 1809 (1972) [Sov. Phys.-JETP 36, 957 (1973)].
[12] C. S. Owen and D. J. Scalapino, Phys. Rev. Lett. 28, 1559 (1972).
[13] a) A. A. Abrikosov, L. P. Gor'kov, and I. E. Dzyaloshinskiĭ, Metody kvantovoĭ teorii polya v statisticheskoĭ fizike (Quantum Field Theoretical Methods in Statistical Physics), Fizmatgiz, 1962, p. 367 (English Transl., Pergamon Press, 1965); b) V. L. Ginzburg, Usp. Fiz. Nauk 69, 537 (1959) [Sov. Phys.-Uspekhi 2, 874 (1960)].
[14] L. V. Keldysh, Zh. Eksp. Teor. Fiz. 47, 1515 (1964) [Sov. Phys.-JETP 20, 1018 (1965)].
[15] E. F. Gross, V. I. Perel', and R. I. Shekhmamet'ev, ZhETF Pis. Red. 13, 320 (1971) [JETP Lett. 13, 229 (1971)].
[16] V. F. Elesin, Zh. Eksp. Teor. Fiz. 59, 602 (1970) [Sov. Phys.-JETP 32, 328 (1971)].

[17] A. B. Migdal, Zh. Eksp. Teor. Fiz. 40, 684 (1961) [Sov. Phys.-JETP 13, 478 (1961)].
[18] N. N. Bogolyubov, V. V. Tolmachev, and D. V. Shirokov, Novyĭ metod v teorii sverkhprovodimosti (A New Method in the Theory of Superconductivity), 1958, p. 38 (English Transl., Consultants Bureau, 1959).
[19] P. W. Anderson, Phys. Rev. 112, 1900 (1958).
[20] W. H. Parker and W. D. Williams, Phys. Rev. Lett. 29, 924 (1972).

.3 Bibliography from Well-known, Important Artiles

From Quantum quench phase diagrams of an s-wave BCS-BEC condensate by Yuzbashyan, Dzero, Gurarie, Foster

References

[Anderson(1958)] P. W. Anderson, Phys. Rev. **112**, 1900 (1958).

[Galaiko(1972)] V. P. Galaiko, Sov. Phys. JETP **34**, 203 (1972).

[Volkov and Kogan(1974)] A. F. Volkov and S. M. Kogan, Zh. Eksp. Teor. Fiz **65**, 2038 (1974), English translation: Sov. Phys. JETP, **38**, 1018 (1974).

[Galperin et al.(1981)] Y. M. Galperin, V. I. Kozub, and B. Z. Spivak, Sov. Phys. JETP **54**, 1126 (1981).

[Littlewood and Varma(1982)] P. B. Littlewood and C. M. Varma, Phys. Rev. B (1982).

[Shumeiko(1990)] V. S. Shumeiko, *Dynamics of electronic system with off-diagonal order parameter and non-linear resonant phenomena in superconductors* (Doctoral Thesis, Institute for Low Temperature Physics and Engineering, Kharkov, Ukraine, 1990).

[Barankov et al.(2004)] R. A. Barankov, L. S. Levitov, and B. Z. Spivak, Phys. Rev. Lett. **93**, 160401 (2004).

[Amin et al.(2004)] M. Amin, E. Bezuglyi, A. Kijko, and A. Omelyanchouk, Low Temp. Phys. **30**, 661 (2004).

[Andreev et al.(2004)] A. V. Andreev, V. Gurarie, and L. Radzihovsky, Phys. Rev. Lett. **93**, 130402 (2004).

[Barankov and Levitov(2004)] R. A. Barankov and L. S. Levitov, Phys. Rev. Lett. **93**, 130403 (2004).

[Szymanska et al.(2005)] M. H. Szymanska, B. D. Simons, and K. Burnett, Phys. Rev. Lett. **94**, 170402 (2005).

[Warner and Leggett(2005)] G. L. Warner and A. J. Leggett, Phys. Rev. B **71**, 034514 (2005).

[Yuzbashyan et al.(2005a)] E. A. Yuzbashyan, B. L. Altshuler, V. B. Kuznetsov, and V. Z. Enolskii, J. Phys. A **38**, 7831 (2005a).

[Yuzbashyan et al.(2005b)] E. A. Yuzbashyan, B. L. Altshuler, V. B. Kuznetsov, and V. Z. Enolskii, Phys. Rev. B **72**, 220503(R) (2005b).

[Yuzbashyan et al.(2005c)] E. A. Yuzbashyan, V. B. Kuznetsov, and B. L. Altshuler, Phys. Rev. B **72**, 144524 (2005c).

[Yuzbashyan et al.(2006)] E. A. Yuzbashyan, O. Tsyplyatyev, and B. L. Altshuler, Phys. Rev. Lett. **96**, 097005 (2006), erratum: Phys. Rev. Lett. **96**, 179905 (2006).

[Barankov and Levitov(2006)] R. A. Barankov and L. S. Levitov, Phys. Rev. Lett. **96**, 230403 (2006).

[Yuzbashyan and Dzero(2006)] E. A. Yuzbashyan and M. Dzero, Phys. Rev. Lett. **96**, 230404 (2006).

[Dzero et al.(2007)] M. Dzero, E. A. Yuzbashyan, B. L. Altshuler, and P. Coleman, Phys. Rev. Lett. **99**, 160402 (2007).

[Barankov and Levitov(2007)] R. A. Barankov and L. S. Levitov, arXiv:0704.1292 (2007).

[Tomadin et al.(2008)] A. Tomadin, M. Polini, M. P. Tosi, and R. Fazio, Phys. Rev. A **77**, 033605 (2008).

[Nahum and Bettelheim(2008)] A. Nahum and E. Bettelheim, Phys. Rev. B **78**, 184510 (2008).

[Gurarie(2009)] V. Gurarie, Phys. Rev. Lett. **103**, 075301 (2009).

[Faribault et al.(2009)] A. Faribault, P. Calabrese, and J.-S. Caux, J. Math. Phys. **50**, 095212 (2009).

[Matsunaga et al.(2013)] R. Matsunaga, Y. I. Hamada, K. Makise, Y. Uzawa, H. Terai, Z. Wang, and R. Shimano, Phys. Rev. Lett. **111**, 057002 (2013).

[Matsunaga et al.(2014)] R. Matsunaga, N. Tsuji, H. Fujita, A. Sugioka, K. Makise, Y. Uzawa, H. Terai, Z. Wang, H. Aoki, and R. Shimano, Science **345**, 1145 (2014).

[Papenkort et al.(2007)] T. Papenkort, V. M. Axt, and T. Kuhn, Physical Review B **76** (2007).

[Papenkort et al.(2009)] T. Papenkort, T. Kuhn, and V. M. Axt, Journal of Physics **193**, 012050 (2009).

[Krull et al.(2013)] H. Krull, D. Manske, G. S. Uhrig, and A. P. Schnyder, arXiv:1309.7318 (2013).

[Tsuji(2014)] H. Tsuji, Naoto; Aoki, arXiv:1404.2711 (2014).

[Matsunaga and Shimano(2012)] R. Matsunaga and R. Shimano, Phys. Rev. Lett. **109**, 187002 (2012).

[Beck et al.(2013)] M. Beck, I. Rousseau, M. Klammer, P. Leiderer, M. Mittendorff, S. Winnerl, M. Helm, G. N. Gol'tsman, and J. Demsar, Phys. Rev. Lett. **110**, 267003 (2013).

[Brierley et al.(2011)] R. T. Brierley, P. B. Littlewood, and P. R. Eastham, Phys. Rev. Lett. **107**, 040401 (2011).

[Pehlivan et al.(2011)] Y. Pehlivan, T. Balantekin, A. B.; Kajino, and T. Yoshida, Phys. Rev. D **84**, 065008 (2011).

[Raffelt et al.(2013)] G. Raffelt, S. Sarikas, and D. d. S. Seixas, Phys. Rev. Lett. **111** (2013).

[Foster et al.(2013)] M. S. Foster, M. Dzero, V. Gurarie, and E. A. Yuzbashyan, Phys. Rev. B **88**, 104511 (2013).

[Foster et al.(2014)] M. S. Foster, V. Gurarie, M. Dzero, and E. A. Yuzbashyan, Phys. Rev. Lett. **113**, 076403 (2014).

[Gaudin(1983)] M. Gaudin, *La fonction d'onde de Bethe* (Masson, Paris, 1983).

[Richardson(2002)] R. W. Richardson, arXiv:cond-mat/0203512 (unpublished) (2002).

[Ibanez et al.(2009)] M. Ibanez, J. Links, G. Sierra, and S.-Y. Zhao, Phys. Rev. B **79**, 180501(R) (2009).

[Dunning et al.(2010)] C. Dunning, M. Ibanez, J. Links, G. Sierra, and S.-Y. Zhao, J. Stat. Mech. p. P08025 (2010).

[Rombouts et al.(2010)] S. M. A. Rombouts, J. Dukelsky, and G. Ortiz, Phys. Rev. B **82**, 224510 (2010).

[Dukelsky et al.(2004)] J. Dukelsky, S. Pittel, and G. Sierra, Rev. Mod. Phys. **76**, 643 (2004).

[Ortiz et al.(2005)] G. Ortiz, R. Somma, J. Dukelsky, and S. Rombouts, Nucl.Phys. B **707**, 421 (2005).

[J. Dukelsky(2001)] P. S. J. Dukelsky, C. Esebbag, Phys. Rev. Lett. **87**, 066403 (2001).

[L. Amico(2001)] A. O. L. Amico, A. di Lorenzo, Phys. Rev. Lett. **86**, 5759 (2001).

[Regal et al.(2004)] A. Regal, M. Greiner, and D. S. Jin, Phys. Rev. Lett. **92**, 040403 (2004).

[Zwierlein et al.(2004)] M. W. Zwierlein, C. A. Stan, C. H. Schunck, S. M. F. Raupach, A. J. Kerman, and W. Ketterle, Phys. Rev. Lett. **92**, 120403 (2004).

[Calabrese and Cardy(2006)] P. Calabrese and J. Cardy, Phys. Rev. Lett. **96**, 136801 (2006).

[Kollath et al.(2007)] C. Kollath, A. M. Läuchli, and E. Altman, Phys. Rev. Lett. **98**, 180601 (2007).

[Leggett(1980)] A. Leggett, in *Modern Trends in the Theory of Condensed Matter* (Springer-Verlag, Berlin, 1980), pp. 13–27.

[Nozières and Schmitt-Rink(1985)] P. Nozières and S. Schmitt-Rink, J. Low Temp. Phys. **59**, 195 (1985).

[Gurarie and Radzihovsky(2007)] V. Gurarie and L. Radzihovsky, Ann. Phys. **322**, 2 (2007).

[Burovski et al.(2006)] E. Burovski, N. Prokof'ev, B. Svistunov, and M. Troyer, New J. Phys. **8**, 153 (2006).

[Bulgac and Yoon(2009)] A. Bulgac and S. Yoon, Phys. Rev. Lett. **102**, 085302 (2009).

[Levinsen and Gurarie(2006)] J. Levinsen and V. Gurarie, Phys. Rev. A **73**, 053607 (2006).

[Richardson(1977)] R. Richardson, J. Math. Phys. **18**, 1802 (1977).

[Sträter et al.(2012)] C. Sträter, O. Tsyplyatyev, and A. Faribault, Phys. Rev. B **86**, 195101 (2012).

[Pekker and Varma(2014)] D. Pekker and C. M. Varma, arXiv:1406.2968 (2014).

[Anderson(1959)] P. W. Anderson, J. Phys. Chem. Solids **11**, 26 (1959).

[Kurland et al.(2000)] I. L. Kurland, I. L. Aleiner, and B. L. Altshuler, Phys. Rev. B **62**, 14886 (2000).

[not(a)] The integrand in Eq. (**??**) generally has a nonvanishing zeroth Fourier mode, i.e. it contributes to both linear and periodic parts.

[Arnold(1978)] V. I. Arnold, *Mathematical Methods of Classical Mechanics* (Springer-Verlag, New York, 1978).

[Tabor(1989)] M. Tabor, *Chaos and Integrability in Nonlinear Dynamics* (Wiley, New York, 1989).

[H. Goldstein(2002)] J. S. H. Goldstein, C. Poole, *Classical Mechanics*, Ch. 10 (Addison Wesley, 2002), 3rd ed.

[Carlson and Gustafson(1994)] B. C. Carlson and J. L. Gustafson, SIAM J. Math. Anal., 25(2) p. 288 (1994).

[DLMF()] DLMF, *NIST Digital Library of Mathematical Functions*, Ch. 19, Release date 2014-04-25, URL `http://dlmf.nist.gov/`.

[Chin et al.(2004)] C. Chin, M. Bartenstein, A. Altmeyer, S. Riedl, S. Jochim, J. H. Denschlag, and R. Grimm, Science **305**, 1128 (2004).

[Zwierlein et al.(2005)] M. W. Zwierlein, A. S. J. R. Abo-Shaeer, C. H. Schunck, and W. Ketterle, Nature **435**, 1047 (2005).

[Schrieffer(1989)] R. Schrieffer, *Theory of Superconductivity* (Perseus Books Group, N.Y., 1989).

[Bardeen et al.(1957)] J. Bardeen, L. N. Cooper, and J. R. Schrieffer, Phys. Rev. **108**, 1175 (1957).

[not(b)] See Ref. [Foster et al.(2013)] for a detailed calculation of analogous Green's functions and expectation values.

[Törmä and Zoller(2000)] P. Törmä and P. Zoller, Phys. Rev. Lett. **85**, 487 (2000).

[Regal and Jin(2003)] C. A. Regal and D. S. Jin, Phys. Rev. Lett. **90**, 230404 (2003).

[et al.(2003)] S. G. et al., Science **300**, 1723 (2003).

[Kinnunen et al.(2004)] J. Kinnunen, M. Rodriguez, and P. Törmä, Science **305**, 1131 (2004).

[Schunk et al.(2008)] C. H. Schunk, Y. Shin, A. Schirotzek, and W. Ketterle, Nature **454**, 739 (2008).

[Basu and Mueller(2008)] S. Basu and E. J. Mueller, Phys. Rev. Lett. **101**, 060405 (2008).

[Schirotzek et al.(2008)] A. Schirotzek, Y. Shin, C. H. Schunck, and W. Ketterle, Phys. Rev. Lett. **101**, 140403 (2008).

[not(c)] We note that the contribution of stimulated emission processes is missing in Ref. [Dzero et al.(2007)]. This mistake is fixed in Ref. [Foster et al.(2013)]. Moreover, we computed the RF response for the two-channel model taking this term into account and we find that the absorbed intensity is not significantly affected by this term for quenches to both BCS and BEC final detunings at least for the values of the relevant parameters considered.

[Dong et al.(2014)] Y. Dong, L. Dong, M. Gong, and H. Pu, arXiv:1406.3821 (2014).

[Duyckaerts et al.(2013)] T. Duyckaerts, C. Keni, and F. Merle, Cambridge Journal of Mathematics **1**, 75 (2013).

[Phillips(2003)] P. Phillips, *Advanced Solid State Physics* (Westview Press, Boulder, CO, 2003).

From relaxation and persistent oscillations of the order parameter in the non-stationary BCS theory by A. Yuzbashyan, Tsyplyatyev, Altshuler

References

[1] P. W. Anderson: Phys. Rev. 112, 1900 (1958).

[2] V. P. Galaiko: Sov. Phys. JETP 34, 203 (1972).

[3] A. F. Volkov and Sh. M. Kogan: Sov. Phys. JETP 38, 1018 (1974).

[4] Yu. M. Gal'perin, V. I. Kozub, and B. Z. Spivak: Sov. Phys. JETP 54, 1126 (1981).

[5] R. A. Barankov, L. S. Levitov, and B. Z. Spivak: PRL 93, 160401 (2004); A. V. Andreev, V. Gurarie, and L. Radzihovsky: PRL 93, 130402 (2004); R. A. Barankov and L. S. Levitov: PRL 93, 130403 (2004).

[6] R. A. Barankov and L. S. Levitov: cond-mat/0508215 (2005).

[7] M.H.S. Amin, E.V. Bezuglyi, A.S. Kijko, A.N. Omelyanchouk: Low Temp. Phys. 30, 661 (2004).

[8] E. A. Yuzbashyan, B. L. Altshuler, V. B. Kuznetsov, V. Z. Enolskii: J. Phys. A 38, 7831, (2005); cond-mat/0505493 (2005).

[9] E. A. Yuzbashyan, V. B. Kuznetsov, B. L. Altshuler: Phys. Rev. B 72, 144524 (2005).

[10] M. H. Szymanska, B. D. Simons, and K. Burnett: PRL 94 , 170402 (2005).

[11] G.L. Warner and A. J. Leggett: Phys. Rev. B 71, 134514 (2005).

[12] N. B. Kopnin: Theory of Nonequilibrium Superconductivity, Clarendon Press, Oxford (2001).

[13] T. Loftus et. al.: PRL 88, 173201 (2002); J. L. Bohn: Phys. Rev. A 61, 053409 (2000); M. W. Zwierlein et. al.: PRL 92, 120403 (2004); C. Chin et. al.: Science 305, 1128 (2004).

[14] Y. Nakamura, Yu. A. Pashkin and J. S. Tsai: Nature 398, 786, (1999); O. Astafiev et. al.: PRL 93, 267007 (2004); D. Vion et. al.: Science, 296, 886 (2002).

[15] E. A. Yuzbashyan and M. Dzero, unpublished.

[16] An m-spin solution can be expressed in terms of a Riemann theta function of genus $m-1$[8]. In particular, 2-spin solutions are genus one – ordinary elliptic functions.

[17] If the initial state is particle-hole symmetric k is equal to the integer part of $m/2$. In this case the effective m-spin problem is also particle-hole symmetric, which reduces the number of independent degrees of freedom and therefore the number of incommensurate frequencies.

[18] Far from the Fermi level $s_z(\epsilon) = -\text{sgn}\epsilon$. Therefore, the total number of jumps in $s_z(\epsilon)$ for normal states is always odd. For anomalous stationary states the number of discontinuities in the spin distribution is even by the same argument.

[19] E. Abrahams and T. Tsuneto: Phys. Rev. 152, 416 (1966).

[20] A. Schmid: Phys. Kond. Mat. 5, 302 (1966).

[21] The two solutions merge for Δ_{in} comparable to the mean level spacing d. Here we consider the thermodynamic limit $d/\Delta_{in} \to 0$.

From Onset of superconductivity in a voltage-biased NSN microbridge by Serbyn, Skvortsov

References

[Kopnin(2001)] N. B. Kopnin, *Theory of Nonequilibrium Superconductivity* (Oxford University Press, New York, 2001).

[Gray(1981)] K. Gray, ed., *Nonequilibrium superconductivity, phonons, and Kapitza boundaries* (Plenum Press, New York, 1981).

[Gulian and Zharkov(1999)] A. Gulian and G. Zharkov, *Nonequilibrium Electrons and Phonons in Superconductors*, Selected Topics in Superconductivity (Springer, 1999).

[Langenberg and Larkin(1986)] D. Langenberg and A. Larkin, *Nonequilibrium superconductivity*, Modern problems in condensed matter sciences (North-Holland, 1986).

[Vodolazov *et al.*(2003)] D. Y. Vodolazov, F. M. Peeters, L. Piraux, S. Mátéfi-Tempfli, and S. Michotte, Phys. Rev. Lett. **91**, 157001 (2003).

[Xiong *et al.*(1997)] P. Xiong, A. V. Herzog, and R. C. Dynes, Phys. Rev. Lett. **78**, 927 (1997).

[Rogachev *et al.*(2006)] A. Rogachev, T.-C. Wei, D. Pekker, A. T. Bollinger, P. M. Goldbart, and A. Bezryadin, Phys. Rev. Lett. **97**, 137001 (2006).

[Li *et al.*(2011)] P. Li, P. M. Wu, Y. Bomze, I. V. Borzenets, G. Finkelstein, and A. M. Chang, Phys. Rev. B **84**, 184508 (2011).

[Astafiev *et al.*(2012)] O. V. Astafiev, L. B. Ioffe, S. Kafanov, Y. A. Pashkin, K. Y. Arutyunov, D. Shahar, O. Cohen, and J. S. Tsai, Nature **484**, 355 (2012).

[Ivlev and Kopnin(1984)] B. I. Ivlev and N. B. Kopnin, Adv. Phys. **33**, 47 (1984).

[Meyer and Minnigerode(1972)] J. Meyer and G. Minnigerode, Physics Letters A **38**, 529 (1972).

[Langer and Ambegaokar(1967)] J. S. Langer and V. Ambegaokar, Phys. Rev. **164**, 498 (1967).

[McCumber and Halperin(1970)] D. E. McCumber and B. I. Halperin, Phys. Rev. B **1**, 1054 (1970).

[Keizer *et al.*(2006)] R. S. Keizer, M. G. Flokstra, J. Aarts, and T. M. Klapwijk, Phys. Rev. Lett. **96**, 147002 (2006).

[Vercruyssen *et al.*(2012)] N. Vercruyssen, T. G. A. Verhagen, M. G. Flokstra, J. P. Pekola, and T. M. Klapwijk, Phys. Rev. B **85**, 224503 (2012).

[Snyman and Nazarov(2009)] I. Snyman and Y. V. Nazarov, Phys. Rev. B **79**, 014510 (2009).

[Gorkov and Eliashberg(1968)] L. P. Gorkov and G. M. Eliashberg, Sov. Phys. JETP **27**, 328 (1968).

[Kramer and Watts-Tobin(1978)] L. Kramer and R. J. Watts-Tobin, Phys. Rev. Lett. **40**, 1041 (1978).

[Michotte *et al.*(2004)] S. Michotte, S. Mátéfi-Tempfli, L. Piraux, D. Y. Vodolazov, and F. M. Peeters, Phys. Rev. B **69**, 094512 (2004).

[Vodolazov(2007)] D. Y. Vodolazov, Phys. Rev. B **75**, 184517 (2007).

[Elmurodov *et al.*(2008)] A. K. Elmurodov, F. M. Peeters, D. Y. Vodolazov, S. Michotte, S. Adam, F. d. M. de Horne, L. Piraux, D. Lucot, and D. Mailly, Phys. Rev. B **78**, 214519 (2008).

[Rubinstein *et al.*(2007)] J. Rubinstein, P. Sternberg, and Q. Ma, Phys. Rev. Lett. **99**, 167003 (2007).

[Chtchelkatchev and Vinokur(2009)] N. Chtchelkatchev and V. Vinokur, Europhys. Lett. **88**, 47001 (2009).

[Giazotto *et al.*(2006)] F. Giazotto, T. T. Heikkilä, A. Luukanen, A. M. Savin, and J. P. Pekola, Rev. Mod. Phys. **78**, 217 (2006).

[Chen *et al.*(2009)] Y. Chen, S. D. Snyder, and A. M. Goldman, Phys. Rev. Lett. **103**, 127002 (2009).

[Tian *et al.*(2005)] M. Tian, N. Kumar, S. Xu, J. Wang, J. S. Kurtz, and M. H. W. Chan, Phys. Rev. Lett. **95**, 076802 (2005).

[Boogaard *et al.*(2004)] G. R. Boogaard, A. H. Verbruggen, W. Belzig, and T. M. Klapwijk, Phys. Rev. B **69**, 220503 (2004).

[Larkin and Varlamov(2002)] A. I. Larkin and A. A. Varlamov, *Theory of Fluctuations in Superconductors* (Oxford University Press, New York, 2002).

[Levchenko and Kamenev(2007)] A. Levchenko and A. Kamenev, Phys. Rev. B **76**, 094518 (2007).

[Feigel'man *et al.*(2000)] M. V. Feigel'man, A. I. Larkin, and M. A. Skvortsov, Phys. Rev. B **61**, 12361 (2000).

[Kamenev(2011)] A. Kamenev, *Field Theory of Non-Equilibrium Systems* (Cambridge University Press, 2011).

[Nagaev(1995)] K. E. Nagaev, Phys. Rev. B **52**, 4740 (1995).

[Pothier *et al.*(1997)] H. Pothier, S. Guéron, N. O. Birge, D. Esteve, and M. H. Devoret, Phys. Rev. Lett. **79**, 3490 (1997).

[Bender and Boettcher(1998)] C. M. Bender and S. Boettcher, Phys. Rev. Lett. **80**, 5243 (1998).

[Bender(2007)] C. M. Bender, Rep. Prog. Phys. **70**, 947 (2007).

[Vodolazov and Peeters(2007)] D. Y. Vodolazov and F. M. Peeters, Phys. Rev. B **75**, 104515 (2007).

[Serbyn and Skvortsov()] M. Serbyn and M. A. Skvortsov, in preparation.

From Observing Dynamical Phases of BCS Superconductors in a Cavity QED Simulator by Young et al.

References

[Bardeen *et al.*(1957)] J. Bardeen, L. N. Cooper, and J. R. Schrieffer, Phys. Rev. **108**, 1175 (1957).

[Yuzbashyan *et al.*(2006)] E. A. Yuzbashyan, O. Tsyplyatyev, and B. L. Altshuler, Phys. Rev. Lett. **96**, 097005 (2006).

[Barankov and Levitov(2006)] R. A. Barankov and L. S. Levitov, Phys. Rev. Lett. **96**, 230403 (2006).

[Yuzbashyan and Dzero(2006)] E. A. Yuzbashyan and M. Dzero, Phys. Rev. Lett. **96**, 230404 (2006).

[Gurarie and Radzihovsky(2007)] V. Gurarie and L. Radzihovsky, Ann. Phys. **322**, 2 (2007), January Special Issue 2007.

[Gurarie(2009)] V. Gurarie, Phys. Rev. Lett. **103**, 075301 (2009).

[Foster *et al.*(2013)] M. S. Foster, M. Dzero, V. Gurarie, and E. A. Yuzbashyan, Phys. Rev. B **88**, 104511 (2013).

[Yuzbashyan *et al.*(2015)] E. A. Yuzbashyan, M. Dzero, V. Gurarie, and M. S. Foster, Phys. Rev. A **91**, 033628 (2015).

[Lewis-Swan *et al.*(2021)] R. J. Lewis-Swan, D. Barberena, J. R. Cline, D. J. Young, J. K. Thompson, and A. M. Rey, Phys. Rev. Lett. **126**, 173601 (2021).

[Kelly *et al.*(2022)] S. P. Kelly, J. K. Thompson, A. M. Rey, and J. Marino, Phys. Rev. Res. **4**, L042032 (2022).

[Stewart(2017)] G. R. Stewart, Adv. Phys. **66**, 75 (2017).

[Sato and Ando(2017)] M. Sato and Y. Ando, Rep. Prog. Phys. **80**, 076501 (2017).

[Zhou *et al.*(2021)] X. Zhou, W.-S. Lee, M. Imada, N. Trivedi, P. Phillips, H.-Y. Kee, P. Törmä, and M. Eremets, Nat. Rev. Phys. **3**, 462 (2021).

[Shuryak(2017)] E. Shuryak, Rev. Mod. Phys. **89**, 035001 (2017).

[Harlow(2016)] D. Harlow, Rev. Mod. Phys. **88**, 015002 (2016).

[Marino *et al.*(2022)] J. Marino, M. Eckstein, M. Foster, and A.-M. Rey, Rep. Prog. Phys. **85**, 116001 (2022).

[Volkov and Kogan(1974)] A. F. Volkov and S. M. Kogan, JETP **38**, 1018 (1974), [Russian original - Zh. Eksp. Teor. Fiz. **65**, 2038 (1973)].

[Yuzbashyan *et al.*(2005)] E. A. Yuzbashyan, B. L. Altshuler, V. B. Kuznetsov, and V. Z. Enolskii, J. Phys. A: Math. Gen. **38**, 7831 (2005).

[Barankov *et al.*(2004)] R. A. Barankov, L. S. Levitov, and B. Z. Spivak, Phys. Rev. Lett. **93**, 160401 (2004).

[Yuzbashyan(2008)] E. A. Yuzbashyan, Phys. Rev. B **78**, 184507 (2008).

[Foster *et al.*(2014)] M. S. Foster, V. Gurarie, M. Dzero, and E. A. Yuzbashyan, Phys. Rev. Lett. **113**, 076403 (2014).

[Collado *et al.*(2023)] H. P. O. Collado, N. Defenu, and J. Lorenzana, Phys. Rev. Res. **5**, 023011 (2023).

[Mansart *et al.*(2013)] B. Mansart, J. Lorenzana, A. Mann, A. Odeh, M. Scarongella, M. Chergui, and F. Carbone, Proc. Natl. Acad. Sci. U.S.A. **110**, 4539 (2013).

[Matsunaga *et al.*(2013)] R. Matsunaga, Y. I. Hamada, K. Makise, Y. Uzawa, H. Terai, Z. Wang, and R. Shimano, Phys. Rev. Lett. **111**, 057002 (2013).

[Matsunaga *et al.*(2014)] R. Matsunaga, N. Tsuji, H. Fujita, A. Sugioka, K. Makise, Y. Uzawa, H. Terai, Z. Wang, H. Aoki, and R. Shimano, Science **345**, 1145 (2014).

[Randeria and Taylor(2014)] M. Randeria and E. Taylor, Annu. Rev. Condens. Matter Phys. **5**, 209 (2014).

[Behrle *et al.*(2018)] A. Behrle, T. Harrison, J. Kombe, K. Gao, M. Link, J.-S. Bernier, C. Kollath, and M. Köhl, Nature Physics **14**, 781 (2018).

[Anderson(1958)] P. W. Anderson, Phys. Rev. **112**, 1900 (1958).

[Davis *et al.*(2020)] E. J. Davis, A. Periwal, E. S. Cooper, G. Bentsen, S. J. Evered, K. Van Kirk, and M. H. Schleier-Smith, Phys. Rev. Lett. **125**, 060402 (2020).

[Norcia *et al.*(2018a)] M. A. Norcia, R. J. Lewis-Swan, J. R. Cline, B. Zhu, A. M. Rey, and J. K. Thompson, Science **361**, 259 (2018a).

[Allred *et al.*(2002)] J. C. Allred, R. N. Lyman, T. W. Kornack, and M. V. Romalis, Phys. Rev. Lett. **89**, 130801 (2002).

[Kleine *et al.*(2008)] A. Kleine, C. Kollath, I. P. McCulloch, T. Giamarchi, and U. Schollwoeck, New J. Phys. **10**, 045025 (2008).

[Deutsch *et al.*(2010)] C. Deutsch, F. Ramirez-Martinez, C. Lacroûte, F. Reinhard, T. Schneider, J. N. Fuchs, F. Piéchon, F. Laloë, J. Reichel, and P. Rosenbusch, Phys. Rev. Lett. **105**, 020401 (2010).

[Smale *et al.*(2019)] S. Smale, P. He, B. A. Olsen, K. G. Jackson, H. Sharum, S. Trotzky, J. Marino, A. M. Rey, and J. H. Thywissen, Sci. Adv. **5**, eaax1568 (2019).

[Muniz *et al.*(2020)] J. A. Muniz, D. Barberena, R. J. Lewis-Swan, D. J. Young, J. R. Cline, A. M. Rey, and J. K. Thompson, Nature **580**, 602 (2020).

[Baghdad *et al.*(2023)] M. Baghdad, P.-A. Bourdel, S. Schwartz, F. Ferri, J. Reichel, and R. Long, Nat. Phys. **19**, 1104 (2023).

[Sauerwein *et al.*(2023)] N. Sauerwein, F. Orsi, P. Uhrich, S. Bandyopadhyay, F. Mattiotti, T. Cantat-Moltrecht, G. Pupillo, P. Hauke, and J.-P. Brantut, Nat. Phys. **19**, 1128 (2023).

[Richardson and Sherman(1964)] R. Richardson and N. Sherman, Nuclear Physics **52**, 221 (1964).

[Gaudin(1976)] M. Gaudin, J. Phys. (Paris) **37**, 1087 (1976).

[Weiner *et al.*(2012)] J. M. Weiner, K. C. Cox, J. G. Bohnet, Z. Chen, and J. K. Thompson, Appl. Phys. Lett. **101**, 261107 (2012).

[Bohnet *et al.*(2013)] J. G. Bohnet, Z. Chen, J. M. Weiner, K. C. Cox, and J. K. Thompson, Phys. Rev. A **88**, 013826 (2013).

[Norcia *et al.*(2016)] M. A. Norcia, M. N. Winchester, J. R. Cline, and J. K. Thompson, Sci. Adv. **2**, e1601231 (2016).

[Rey *et al.*(2008)] A. M. Rey, L. Jiang, M. Fleischhauer, E. Demler, and M. D. Lukin, Phys. Rev. A **77**, 052305 (2008).

[Black-Schaffer(2012)] A. M. Black-Schaffer, Phys. Rev. Lett. **109**, 197001 (2012).

[Nandkishore *et al.*(2012)] R. Nandkishore, L. S. Levitov, and A. V. Chubukov, Nat. Phys. **8**, 158 (2012).

[Kiesel *et al.*(2012)] M. L. Kiesel, C. Platt, W. Hanke, D. A. Abanin, and R. Thomale, Phys. Rev. B **86**, 020507 (2012).

[Kiesel *et al.*(2013)] M. L. Kiesel, C. Platt, W. Hanke, and R. Thomale, Phys. Rev. Lett. **111**, 097001 (2013).

[Fischer *et al.*(2014)] M. H. Fischer, T. Neupert, C. Platt, A. P. Schnyder, W. Hanke, J. Goryo, R. Thomale, and M. Sigrist, Phys. Rev. B **89**, 020509 (2014).

[Shankar *et al.*(2022)] A. Shankar, E. A. Yuzbashyan, V. Gurarie, P. Zoller, J. J. Bollinger, and A. M. Rey, PRX Quantum **3**, 040324 (2022).

[Laughlin(1998)] R. Laughlin, Phys. Rev. Lett. **80**, 5188 (1998).

[Balatsky *et al.*(2006)] A. V. Balatsky, I. Vekhter, and J.-X. Zhu, Rev. Mod. Phys. **78**, 373 (2006).

[Schäfer and Teaney(2009)] T. Schäfer and D. Teaney, Rep. Prog. Phys. **72**, 126001 (2009).

[Pehlivan *et al.*(2011)] Y. Pehlivan, A. Balantekin, T. Kajino, and T. Yoshida, Phys. Rev. D **84**, 065008 (2011).

[Norcia *et al.*(2018b)] M. A. Norcia, J. R. Cline, J. A. Muniz, J. M. Robinson, R. B. Hutson, A. Goban, G. E. Marti, J. Ye, and J. K. Thompson, Phys. Rev. X **8**, 021036 (2018b).

[Young *et al.*(2023)] D. J. Young, A. Chu, E. Y. Song, D. Barberena, D. Wellnitz, Z. Niu, V. Schäfer, R. J. Lewis-Swan, A. M. Rey, and J. K. Thompson, Data for: Observing dynamical phases of BCS superconductors in a cavity QED simulator (2023), dryad dataset.

[Reiter and Sørensen(2012)] F. Reiter and A. S. Sørensen, Phys. Rev. A **85**, 032111 (2012).

From Theory of Anderson pseudospin resonance with Higgs mode in SC

References

[Anderson(1958)] P. W. Anderson, Phys. Rev. **112**, 1900 (1958).

[Volkov,Kogan (1973)] A. F. Volkov and S. M. Kogan, Sov. Phys. JETP **38**, 1018 (1974).

[Littlewood (1981)] P. B. Littlewood and C. M. Varma, Phys. Rev. Lett. **47**, 811 (1981); Phys. Rev. B **26**, 4883 (1982).

[Varma(2002)] C. Varma, J. Low Temp. Phys. **126**, 901 (2002).

[Pekker and Varma(2015)] D. Pekker and C. Varma, Annual Review of Condensed Matter Physics **6**, 269 (2015).

[Eng()] F. Englert and R. Brout, Phys. Rev. Lett. **13** 321, (1964).

[Hig()] P. W. Higgs, Phys. Lett. **12**, 132 (1964); Phys. Rev. Lett. **13**, 508 (1964).

[Gur()] G. S. Guralnik, C. R. Hagen, and T. W. B. Kibble, Phys. Rev. Lett. **13**, 585 (1964).

[Nam(a)] Y. Nambu and G. Jona-Lasinio, Phys. Rev. **122**, 345 (1961).

[Anderson(1963)] P. W. Anderson, Phys. Rev. **130**, 439 (1963).

[Sooryakumar and Klein(1980)] R. Sooryakumar and M. V. Klein, Phys. Rev. Lett. **45**, 660 (1980).

[Méasson et al.(2014)] M.-A. Méasson, Y. Gallais, M. Cazayous, B. Clair, P. Rodière, L. Cario, and A. Sacuto, Phys. Rev. B **89**, 060503 (2014).

[Matsunaga et al.(2013)] R. Matsunaga, Y. I. Hamada, K. Makise, Y. Uzawa, H. Terai, Z. Wang, and R. Shimano, Phys. Rev. Lett. **111**, 057002 (2013).

[Mat()] R. Matsunaga, N. Tsuji, H. Fujita, A. Sugioka, K. Makise, Y. Uzawa, H. Terai, Z. Wang, H. Aoki, and R. Shimano, Science **345**, 1145 (2014).

[ATL()] ATLAS Collaboration, Phys. Lett. B **716**, 1 (2012).

[CMS()] CMS Collaboration, Phys. Lett. B **716**, 30 (2012).

[Gor()] L. P. Gor'kov, Sov. Phys. JETP **9**, 1364 (1959).

[Bogoliubov et al.(1958)] N. N. Bogoliubov, V. V. Tolmachev, and D. V. Shirkov, *A New Method in the Theory of Superconductivity* (Achademy of Sciences of USSR, Moscow, 1958).

[Nam(b)] Y. Nambu, Physica **15D**, 147 (1985).

[Vol(b)] G. E. Volovik and M. A. Zubkov, Phys. Rev. D **87**, 075016 (2013); J. Low Temp. Phys. **175**, 486 (2014).

[Barankov et al.(2004)] R. A. Barankov, L. S. Levitov, and B. Z. Spivak, Phys. Rev. Lett. **93**, 160401 (2004).

[Yuzbashyan et al.(2005)] E. A. Yuzbashyan, B. L. Altshuler, V. B. Kuznetsov, and V. Z. Enolskii, Phys. Rev. B **72**, 220503 (2005).

[Man()] B. Mansart, J. Lorenzana, A. Mann, A. Odeh, M. Scarongella, M. Chergui, and F. Carbone, Proc. Natl. Acad. Sci. **110**, 4539 (2013).

[Lor()] J. Lorenzana, B. Mansart, A. Mann, A. Odeh, M. Chergui, and F. Carbone, Eur. Phys. J. Special Topics **222**, 1223 (2013).

[Tsuji et al.(2009)] N. Tsuji, T. Oka, and H. Aoki, Phys. Rev. Lett. **103**, 047403 (2009).

[Barankov and Levitov(2006)] R. A. Barankov and L. S. Levitov, Phys. Rev. Lett. **96**, 230403 (2006).

[Yuzbashyan and Dzero(2006)] E. A. Yuzbashyan and M. Dzero, Phys. Rev. Lett. **96**, 230404 (2006).

[Zimmermann et al.(1991)] W. Zimmermann, E. Brandt, M. Bauer, E. Seider, and L. Genzel, Physica C: Supercond. **183**, 99 (1991).

[Freericks et al.(2006)] J. K. Freericks, V. M. Turkowski, and V. Zlatić, Phys. Rev. Lett. **97**, 266408 (2006).

[Aoki et al.(2014)] H. Aoki, N. Tsuji, M. Eckstein, M. Kollar, T. Oka, and P. Werner, Rev. Mod. Phys. **86**, 779 (2014).

[not()] Note that what essentially matters in the DMFT calculation here is the density of states near the Fermi energy and the α_1 parameter. Thus, one may take our model adopted here as a certain infinite-dimensional lattice model that has the corresponding density of states and α_1, to which DMFT can be applied.

[Tsuji and Werner(2013)] N. Tsuji and P. Werner, Phys. Rev. B **88**, 165115 (2013).

[Tsuji et al.(2013)] N. Tsuji, M. Eckstein, and P. Werner, Phys. Rev. Lett. **110**, 136404 (2013).

[Turkowski and Freericks(2005)] V. Turkowski and J. K. Freericks, Phys. Rev. B **71**, 085104 (2005).

From Dynamical vanishing of the order parameter in a fermionic condensate by Yuzbashyan, Dzero

References

[1] C. A. Regal, M. Greiner and D. S. Jin, Phys. Rev. Lett. **92**, 040403 (2004).

[2] M. W. Zwierlein *et.al.*, Phys. Rev. Lett. **92**, 120403 (2004).

[3] J. Kinast *et. al.* Phys. Rev. Lett. **92**, 150402 (2004).

[4] C. Chin *et.al.*, Science **305**, 1128 (2004).

[5] R. A. Barankov, L. S. Levitov, and B. Z. Spivak, Phys. Rev. Lett. **93**, 160401 (2004).

[6] E. A. Yuzbashyan, B. L. Altshuler, V. B. Kuznetsov, V. Z. Enolskii, J. Phys. A **38**, 7831,(2005); Phys. Rev. B **72**, 220503(R) (2005).

[7] M. H. Szymanska, B. D. Simons, and K. Burnett: Phys. Rev. Lett. **94**, 170402 (2005).

[8] G.L. Warner and A. J. Leggett, Phys. Rev. B **71**, 134514 (2005).

[9] E. A. Yuzbashyan, O. Tsyplyatyev, B. L. Altshuler, Phys. Rev. Lett. **96**, 097005 (2006).

[10] K. M. O'Hara *et. al.*, Science **298**, 2179 (2002).

[11] T. Loftus, C. A. Regal, C. Ticknor, J. L. Bohn, D. S. Jin, Phys. Rev. Lett. **88**, 173201 (2002).

[12] P. W. Anderson, Phys. Rev. **112**, 1900 (1958).

[13] A. F. Volkov and Sh. M. Kogan, Sov. Phys. JETP **38**, 1018 (1974).

[14] M. E. Fisher, M. N. Barber, and D. Jasnow, Phys. Rev. A **8**, 1111 (1973).

[15] J. R. Schrieffer, *Theory of superconductivity*, W. A. Benjamin, New York, 1964, Ch. 8.

[16] W. Kohn and D. Sherrington, Rev. Mod. Phys, **42**, 1 (1970).

[17] K. Maki, in *Superconductivity* (edited by R. D. Parks), Marcel Dekker, New York, 1969, v.2, p. 1035.

[18] R. B. Diener and T. L. Ho, cond-mat/0404517; E. Altman and A. Vishwanath, Phys. Rev. Lett. 95, 110404 (2005).

[19] R. A. Barankov and L. S. Levitov, cond-mat/0603317.

From Dynamical vanishing of the order parameter in a confined Bardeen-Cooper-Schrieffer Fermi gas after an interaction quench by Hannibal et al.

References

[Bloch et al.(2008)] I. Bloch, J. Dalibard, and W. Zwerger, Rev. Mod. Phys. **80**, 885 (2008).

[Goldman et al.(2016)] N. Goldman, J. Budich, and P. Zoller, Nature Physics **12**, 639 (2016).

[Galitski and Spielman(2013)] V. Galitski and I. B. Spielman, Nature **494**, 49 (2013).

[Wu et al.(2016)] Z. Wu, L. Zhang, W. Sun, X.-T. Xu, B.-Z. Wang, S.-C. Ji, Y. Deng, S. Chen, X.-J. Liu, and J.-W. Pan, Science **354**, 83 (2016).

[Liao et al.(2010)] Y.-a. Liao, A. S. C. Rittner, T. Paprotta, W. Li, G. B. Partridge, R. G. Hulet, S. K. Baur, and E. J. Mueller, Nature **467**, 567 (2010).

[Giorgini et al.(2008)] S. Giorgini, L. Pitaevskii, and S. Stringari, Rev. Mod. Phys. **80**, 1215 (2008).

[Chin et al.(2010)] C. Chin, R. Grimm, P. Julienne, and E. Tiesinga, Rev. Mod. Phys. **82**, 1225 (2010).

[Regal et al.(2004)] C. A. Regal, M. Greiner, and D. S. Jin, Phys. Rev. Lett. **92**, 040403 (2004).

[Zwerger(2011)] W. Zwerger, *The BCS-BEC crossover and the unitary Fermi gas*, vol. 836 (Springer, 2011).

[Grimm et al.(2000)] R. Grimm, M. Weidemüller, and Y. B. Ovchinnikov, Adv. At., Mol., Opt. Phys. **42**, 95 (2000).

[Shanenko et al.(2012)] A. A. Shanenko, M. D. Croitoru, A. V. Vagov, V. M. Axt, A. Perali, and F. M. Peeters, Phys. Rev. A **86**, 033612 (2012).

[Polkovnikov et al.(2011)] A. Polkovnikov, K. Sengupta, A. Silva, and M. Vengalattore, Rev. Mod. Phys. **83**, 863 (2011).

[Yin and Radzihovsky(2013)] X. Yin and L. Radzihovsky, Phys. Rev. A **88**, 063611 (2013).

[Yin and Radzihovsky(2016)] X. Yin and L. Radzihovsky, Phys. Rev. A **94**, 063637 (2016).

[Collaboration(2012)] C. Collaboration, Physics Letters B **716**, 30 (2012), ISSN 0370-2693.

[Sooryakumar and Klein(1980)] R. Sooryakumar and M. V. Klein, Phys. Rev. Lett. **45**, 660 (1980).

[Littlewood and Varma(1981)] P. B. Littlewood and C. M. Varma, Phys. Rev. Lett. **47**, 811 (1981).

[Endres et al.(2012)] M. Endres, T. Fukuhara, D. Pekker, M. Cheneau, P. Schauß, C. Gross, E. Demler, S. Kuhr, and I. Bloch, Nature **487**, 454 (2012).

[Papenkort et al.(2007)] T. Papenkort, V. M. Axt, and T. Kuhn, Phys. Rev. B **76**, 224522 (2007).

[Papenkort et al.(2008)] T. Papenkort, T. Kuhn, and V. M. Axt, Phys. Rev. B **78**, 132505 (2008).

[Matsunaga et al.(2014)] R. Matsunaga, N. Tsuji, H. Fujita, A. Sugioka, K. Makise, Y. Uzawa, H. Terai, Z. Wang, H. Aoki, and R. Shimano, Science **345**, 1145 (2014).

[Matsunaga et al.(2013)] R. Matsunaga, Y. I. Hamada, K. Makise, Y. Uzawa, H. Terai, Z. Wang, and R. Shimano, Phys. Rev. Lett. **111**, 057002 (2013).

[Matsunaga and Shimano(2012)] R. Matsunaga and R. Shimano, Phys. Rev. Lett. **109**, 187002 (2012).

[Fröhlich et al.(2011)] B. Fröhlich, M. Feld, E. Vogt, M. Koschorreck, W. Zwerger, and M. Köhl, Phys. Rev. Lett. **106**, 105301 (2011).

[Clark et al.(2015)] L. W. Clark, L.-C. Ha, C.-Y. Xu, and C. Chin, Phys. Rev. Lett. **115**, 155301 (2015).

[Yuzbashyan et al.(2015)] E. A. Yuzbashyan, M. Dzero, V. Gurarie, and M. S. Foster, Phys. Rev. A **91**, 033628 (2015).

[Yuzbashyan et al.(2006)] E. A. Yuzbashyan, O. Tsyplyatyev, and B. L. Altshuler, Phys. Rev. Lett. **96**, 097005 (2006).

[Yuzbashyan and Dzero(2006)] E. A. Yuzbashyan and M. Dzero, Phys. Rev. Lett. **96**, 230404 (2006).

[Yuzbashyan et al.(2005)] E. A. Yuzbashyan, B. L. Altshuler, V. B. Kuznetsov, and V. Z. Enolskii, Phys. Rev. B **72**, 220503 (2005).

[Barankov and Levitov(2006)] R. A. Barankov and L. S. Levitov, Phys. Rev. Lett. **96**, 230403 (2006).

[Bruun et al.(1999)] G. Bruun, Y. Castin, R. Dum, and K. Burnett, Eur. Phys. J. D **7** 433 (1999).

[Bruun(2014)] G. Bruun, Phys. Rev. A **90**, 023621 (2014).

[Scott et al.(2012)] R. G. Scott, F. Dalfovo, L. P. Pitaevskii, and S. Stringari, Phys. Rev. A **86**, 053604 (2012).

[Hannibal et al.(2015)] S. Hannibal, P. Kettmann, M. D. Croitoru, A. Vagov, V. M. Axt, and T. Kuhn, Phys. Rev. A **91**, 043630 (2015).

[Zachmann et al.(2013)] M. Zachmann, M. D. Croitoru, A. Vagov, V. M. Axt, T. Papenkort, and T. Kuhn, New J. Phys. **15**, 055016 (2013).

[Kettmann et al.(2017)] P. Kettmann, S. Hannibal, M. Croitoru, A. Vagov, V. Axt, and T. Kuhn, Physica C **533**, 133 (2017).

[Papenkort et al.(2009)] T. Papenkort, T. Kuhn, and V. M. Axt, Journal of Physics: Conference Series **193**, 012050 (2009).

[Chou et al.(2017)] Y.-Z. Chou, Y. Liao, and M. S. Foster, Phys. Rev. B **95**, 104507 (2017).

[Datta and Bagwell(1999)] S. Datta and P. F. Bagwell, Superlattices and Microstructures **25**, 1233 (1999).

[De Gennes(1989)] P. De Gennes, *Superconductivity of metals and alloys* (Addison-Wesley New York, 1989).

[Anderson(1959)] P. W. Anderson, J. Phys. Chem. Solids **11**, 26 (1959).

[Bruun and Heiselberg(2002)] G. M. Bruun and H. Heiselberg, Phys. Rev. A **65**, 053407 (2002).

[Leggett(2006)] A. J. Leggett, *Quantum liquids: Bose condensation and Cooper pairing in condensed-matter systems* (Oxford University Press, 2006).

From Pure Goldstone mode in the quench dynamics of a confined ultracold Fermi gas in the BCS-BEC crossover regime by Kettmann et al.

References

[Giorgini *et al.*(2008)] S. Giorgini, L. Pitaevskii, and S. Stringari, "Theory of ultracold atomic Fermi gases," Rev. Mod. Phys. **80**, 1215–1274 (2008).

[Bloch *et al.*(2008)] I. Bloch, J. Dalibard, and W. Zwerger, "Many-body physics with ultracold gases," Rev. Mod. Phys. **80**, 885 (2008).

[Weinberg(1996)] Steven Weinberg, *The quantum theory of fields*, Vol. 2 (Cambridge university press, 1996) pp. 332–352.

[Higgs(1964)] P. W. Higgs, "Broken symmetries and the masses of gauge bosons," Phys. Rev. Lett. **13**, 508–509 (1964).

[Burgess(2000)] C. P. Burgess, "Goldstone and pseudo-Goldstone bosons in nuclear, particle and condensed-matter physics," Phys. Reports **330**, 193–261 (2000).

[Paulson *et al.*(1973)] D. Paulson, R. Johnson, and J. Wheatley, "Propagation of collisionless sound in normal and extraordinary phases of liquid ^{3}He below 3 mK," Phys. Rev. Lett. **30**, 829 (1973).

[Lawson *et al.*(1973)] D. Lawson, W. Gully, S. Goldstein, R. Richardson, and D. Lee, "Attenuation of zero sound and the low-temperature transitions in liquid ^{3}He," Phys. Rev. Lett. **30**, 541 (1973).

[Anderson(1958)] P. W. Anderson, "Random-phase approximation in the theory of superconductivity," Phys. Rev. **112**, 1900 (1958).

[Pekker and Varma(2015)] David Pekker and CM Varma, "Amplitude/higgs modes in condensed matter physics," Annu. Rev. Condens. Matter Phys. **6**, 269–297 (2015).

[Bissbort *et al.*(2011)] U. Bissbort, S. Götze, Y. Li, J. Heinze, J. S Krauser, M. Weinberg, C. Becker, K. Sengstock, and W. Hofstetter, "Detecting the amplitude mode of strongly interacting lattice bosons by Bragg scattering," Phys. Rev. Lett. **106**, 205303 (2011).

[Endres *et al.*(2012)] M. Endres, T. Fukuhara, D. Pekker, M. Cheneau, P. Schauß, C. Gross, E. Demler, S. Kuhr, and I. Bloch, "The 'Higgs' amplitude mode at the two-dimensional superfluid/Mott insulator transition," Nature **487**, 454–458 (2012).

[Matsunaga *et al.*(2013)] R. Matsunaga, Y. I. Hamada, K. Makise, Y. Uzawa, H. Terai, Z. Wang, and R. Shimano, "Higgs amplitude mode in the BCS superconductors Nb 1-x Ti x n induced by terahertz pulse excitation," Phys. Rev. Lett. **111**, 057002 (2013).

[Matsunaga *et al.*(2014)] R. Matsunaga, N. Tsuji, H. Fujita, A. Sugioka, K. Makise, Y. Uzawa, H. Terai, Z. Wang, H. Aoki, and R. Shimano, "Light-induced collective pseudospin precession resonating with Higgs mode in a superconductor," Science **345**, 1145–1149 (2014).

[Barankov *et al.*(2004)] R.A. Barankov, L.S. Levitov, and B.Z. Spivak, "Collective Rabi oscillations and solitons in a time-dependent BCS pairing problem," Phys. Rev. Lett. **93**, 160401 (2004).

[Barankov and Levitov(2006)] R. A. Barankov and L. S. Levitov, "Synchronization in the BCS pairing dynamics as a critical phenomenon," Phys. Rev. Lett. **96**, 230403 (2006).

[Yuzbashyan *et al.*(2006)] E. A. Yuzbashyan, O. Tsyplyatyev, and B. L. Altshuler, "Relaxation and persistent oscillations of the order parameter in fermionic condensates," Phys. Rev. Lett. **96**, 097005 (2006).

[Dzero *et al.*(2007)] M. Dzero, E.A. Yuzbashyan, B.L. Altshuler, and P. Coleman, "Spectroscopic signatures of nonequilibrium pairing in atomic Fermi gases," Phys. Rev. Lett. **99**, 160402 (2007).

[Scott *et al.*(2012)] R.G. Scott, F. Dalfovo, L.P. Pitaevskii, and S. Stringari, "Rapid ramps across the BEC-BCS crossover: A route to measuring the superfluid gap," Phys. Rev. A **86**, 053604 (2012).

[Bruun(2014)] G. Bruun, "Long-lived Higgs mode in a two-dimensional confined Fermi system," Phys. Rev. A **90**, 023621 (2014).

[Hannibal *et al.*(2015)] S. Hannibal, P. Kettmann, M. D. Croitoru, A. Vagov, V. M. Axt, and T. Kuhn, "Quench dynamics of an ultracold Fermi gas in the BCS regime: Spectral properties and confinement-induced breakdown of the Higgs mode," Phys. Rev. A **91**, 043630 (2015).

[Kinast *et al.*(2004a)] J. Kinast, S.L. Hemmer, M.E. Gehm, A. Turlapov, and J.E. Thomas, "Evidence for superfluidity in a resonantly interacting Fermi gas," Phys. Rev. Lett. **92**, 150402 (2004a).

[Kinast *et al.*(2004b)] J. Kinast, A. Turlapov, and J.E. Thomas, "Breakdown of hydrodynamics in the radial breathing mode of a strongly interacting Fermi gas," Phys. Rev. A **70**, 051401 (2004b).

[Bartenstein *et al.*(2004)] M. Bartenstein, A. Altmeyer, S. Riedl, S. Jochim, C. Chin, J. H. Denschlag, and R. Grimm, "Collective excitations of a degenerate gas at the BEC-BCS crossover," Phys. Rev. Lett. **92**, 203201 (2004).

[Altmeyer *et al.*(2007a)] A. Altmeyer, S. Riedl, M. J. Wright, C. Kohstall, J. H. Denschlag, and R. Grimm, "Dynamics of a strongly interacting Fermi gas: The radial quadrupole mode," Phys. Rev. A **76**, 033610 (2007a).

[Altmeyer *et al.*(2007b)] A. Altmeyer, S. Riedl, C. Kohstall, M. J. Wright, R. Geursen, M. Bartenstein, C. Chin, J. H. Denschlag, and R. Grimm, "Precision measurements of collective oscillations in the BEC-BCS crossover," Phys. Rev. Lett. **98**, 040401 (2007b).

[Riedl *et al.*(2008)] S. Riedl, E. R. Sánchez Guajardo, C. Kohstall, A. Altmeyer, M. J. Wright, J. H. Denschlag, R. Grimm, G. M. Bruun, and H. Smith, "Collective oscillations of a Fermi gas in the unitarity limit: Temperature effects and the role of pair correlations," Phys. Rev. A **78**, 053609 (2008).

[Baranov and Petrov(2000)] M. A. Baranov and D. S. Petrov, "Low-energy collective excitations in a superfluid trapped Fermi gas," Phys. Rev. A **62**, 041601 (2000).

[Bruun and Mottelson(2001)] G. M. Bruun and B. R. Mottelson, "Low energy collective modes of a superfluid trapped atomic Fermi gas," Phys. Rev. Lett. **87**, 270403 (2001).

[Bruun(2002)] G. M. Bruun, "Low-energy monopole modes of a trapped atomic Fermi gas," Phys. Rev. Lett. **89**, 263002 (2002).

[Hu *et al.*(2004)] H. Hu, A. Minguzzi, X. J. Liu, and M. P. Tosi, "Collective modes and ballistic expansion of a Fermi gas in the BCS-BEC crossover," Phys. Rev. Lett. **93**, 190403 (2004).

[Heiselberg(2004)] H. Heiselberg, "Collective modes of trapped gases at the BEC-BCS crossover," Phys. Rev. Lett. **93**, 040402 (2004).

[Stringari(2004)] S. Stringari, "Collective oscillations of a trapped superfluid Fermi gas near a Feshbach resonance," Europhys. Lett. **65**, 749–752 (2004).

[Grasso *et al.*(2005)] M. Grasso, E. Khan, and M. Urban, "Temperature dependence and finite-size effects in collective modes of superfluid-trapped Fermi gases," Phys. Rev. A **72**, 043617 (2005).

[Korolyuk *et al.*(2011)] A. Korolyuk, J. J. Kinnunen, and P. Törmä, "Density response of a trapped Fermi gas: A crossover from the pair vibration mode to the Goldstone mode," Phys. Rev. A **84**, 033623 (2011).

[Clark *et al.*(2015)] L. W. Clark, L. C. Ha, C. Y. Xu, and C. Chin, "Quantum dynamics with spatiotemporal control of interactions in a stable Bose-Einstein condensate," Phys. Rev. Lett. **115**, 155301 (2015).

[De Gennes(1989)] P. De Gennes, *Superconductivity of metals and alloys* (Addison-Wesley New York, 1989).

[Datta and Bagwell(1999)] S. Datta and P. F. Bagwell, "Can the Bogoliubov-de Gennes equation be interpreted as a one-particle wave equation?" Superlattices and Microstruct. **25**, 1233–1250 (1999).

[Lord(1949)] R. D. Lord, "Some integrals involving Hermite polynomials," Journal of the London Mathematical Society **1**, 101–112 (1949).

[Shanenko *et al.*(2012)] A.A. Shanenko, M. D. Croitoru, A.V. Vagov, V.M. Axt, A. Perali, and F.M. Peeters, "Atypical BCS-BEC crossover induced by quantum-size effects," Phys. Rev. A **86**, 033612 (2012).

[Jain(2017)] Akash Jain, "Theory of non-abelian superfluid dynamics," Phys. Rev. D **95**, 121701 (2017).

[Yuzbashyan *et al.*(2015)] Emil A. Yuzbashyan, Maxim Dzero, Victor Gurarie, and Matthew S. Foster, "Quantum quench phase diagrams of an s-wave BCS-BEC condensate," Physical Review A **91**, 033628 (2015).

[Stewart *et al.*(2008)] J. Stewart, J. Gaebler, and D. Jin, "Using photoemission spectroscopy to probe a strongly interacting Fermi gas," Nature **454**, 744–747 (2008).

[Stewart *et al.*(2010)] J.T. Stewart, J.P. Gaebler, T.E. Drake, and D.S. Jin, "Verification of universal relations in a strongly interacting Fermi gas," Phys. Rev. Lett. **104**, 235301 (2010).

[Ketterle and Zwierlein(2008)] W. Ketterle and M. Zwierlein, "Making, probing and understanding ultracold Fermi gases," ArXiv (2008).

From Synchronization in the BCS Pairing Dynamics as a Critical Phenomenon by Barankov, Levitov

References

[1] C. A. Regal, M. Greiner, and D. S. Jin, Phys. Rev. Lett. **92**, 040403 (2004).

[2] M. W. Zwierlein, C. A. Stan, C. H. Schunck, S. M. F. Raupach, A. J. Kerman, and W. Ketterle, Phys. Rev. Lett. **92**, 120403 (2004).

[3] E. Timmermans, P. Tommasini, M. Hussein, and A. Kerman, Physics Reports **315**, 199 (1999).

[4] F. Dalfovo, S. Giorgini, L. P. Pitaesvkii, and S. Stringari, Rev. Mod. Phys. **71**, 463 (1999).

[5] H. J. Lewandowski, D. M. Harber, D. L. Whitaker, and E. A. Cornell, Phys. Rev. Lett. **88**, 070403 (2002); J. M. McGuirk, H. J. Lewandowski, D. M. Harber, T. Nikuni, J. E. Williams, and E. A. Cornell, Phys. Rev. Lett. **89**, 090402 (2002).

[6] C. Chin, M. Bartenstein, A. Altmeyer, S. Riedl, S. Jochim, J. H. Denschlag, and R. Grimm, Science, **305**, 1128 (2004).

[7] T. M. O'Neil, Phys. Fluids **8**, 2255 (1965).

[8] I. B. Bernstein, J. M. Green, and M. D. Kruskal, Phys. Rev. **108**, 546 (1957)

[9] J. R. Danielson, F. Anderegg, and C. F. Driscoll, Phys. Rev. Lett. **92**, 245003 (2004).

[10] M.Ö. Oktel and L. S. Levitov, Phys. Rev. Lett. **83**, 6 (1999).

[11] T. Nikuni and J. E. Williams, J. Low Temp. Phys. **133**, 323 (2003).

[12] R. J. Ragan, W. J. Mullin, and E. B. Wiita, cond-mat/0502189

[13] S. Tsuchiya and A. Griffin, Phys. Rev. A **72**, 053621 (2005).

[14] R. A. Barankov, L. S. Levitov, and B. Z. Spivak, Phys. Rev. Lett. **93**, 160401 (2004).

[15] A. V. Andreev, V. Gurarie, and L. Radzihovsky, Phys. Rev. Lett. **93**, 130402 (2004); R. A. Barankov and L. S. Levitov, Phys. Rev. Lett. **93**, 130403 (2004).

[16] M. H. Szymańska, B. D. Simons, and K. Burnett, Phys. Rev. Lett. **94**, 170402 (2005).

[17] G. L. Warner and A. J. Leggett, Phys. Rev. B **71**, 134514 (2005).

[18] A. F. Volkov and Sh. M. Kogan, Zh. Eksp. Teor. Fiz. **65**, 2038, (1973) [Sov. Phys. JETP **38**, 1018 (1974)].

[19] E. A. Yuzbashyan, O. Tsyplyatyev, and B. L. Altshuler, Phys. Rev. Lett. **96**, 097005 (2006).

[20] E. A. Yuzbashyan, B. L. Altshuler, V. B. Kuznetsov, and V. Z. Enolskii, Phys. Rev. B **72**, 220503 (2005).

[21] P. W. Anderson, Phys. Rev. **112**, 1900 (1958)

[22] M. H. S. Amin, E. V. Bezuglyi, A. S. Kijko, and A. N. Omelyanchouk, Low Temp. Phys. **30**, 661 (2004), cond-mat/0404401

[23] R. W. Richardson and N. Sherman, Nucl. Phys. **52**, 221 (1964).

[24] M. C. Cambiaggio, A. M. F. Rivas, and M. Saraceno, Nucl. Phys. A **424**, 157 (1997).

[25] L. P. Gor'kov and T. K. Melik-Barkhudarov, Zh. Eksp. Teor. Fiz. **40**, 1452, (1961) [Sov. Phys. JETP, **13**, 1018 (1961)].

From Higgs Mode in Superconductors by Shimano, Tsuji

References

[1] Nambu Y. 2011. *BCS: 50 Years*, edited by L. N. Cooper and D. Feldman (World Scientific, Singapore)

[2] Ginzburg VL, Landau LD. 1950. *Zh. Eksp. Teor. Fiz.* 20:1064

[3] Bogoliubov NN. 1958. *J. Exptl. Theoret. Phys.* 34:58 [1958. *Sov. Phys.* 34:41]

[4] Anderson PW. 1958. *Phys. Rev.* 110:827

[5] Anderson PW. 1958. *Phys. Rev.* 112:1900

[6] Nambu Y. 1960. *Phys. Rev.* 117:648

[7] Goldstone J. 1961. *Nuovo Cim.* 19:154

[8] Goldstone J, Salam A, Weinberg S. 1962. *Phys. Rev.* 127:965

[9] Anderson PW. 1963. *Phys. Rev.* 130:439

[10] Englert F, Brout R. 1964. *Phys. Rev. Lett.* 13:321.

[11] Higgs PW. 1964. *Phys. Lett.* 12:132

[12] Higgs PW. 1964. *Phys. Rev. Lett.* 13:508

[13] Guralnik GS, Hagen CR, Kibble TWB. 1964. *Phys. Rev. Lett.* 13:585

[14] Anderson PW. 2015. *Nat. Phys.* 11:93

[15] Bardeen J, Cooper LN, Schrieffer JR. 1957. *Phys. Rev.* 108:1175

[16] Volkov AF, Kogan SM. 1974. *Sov. Phys. JETP* 38:1018

[17] Kulik IO, Entin-Wohlman O, Orbach R. 1981. *J. Low Temp. Phys.* 43:591

[18] Littlewood PB, Varma CM. 1981. *Phys. Rev. Lett.* 47:811

[19] Littlewood PB, Varma CM. 1982. *Phys. Rev. B* 26:4883

[20] Nambu Y, Jona-Lasinio G. 1961. *Phys. Rev.* 122:345

[21] Nambu Y. 1985. *Physica* 15D:147

[22] Volovik GE, Zubkov MA. 2014. *J. Low Temp. Phys.* 175:486

[23] ATLAS Collaboration. 2012. *Phys. Lett. B* 716:1

[24] CMS Collaboration. 2012. *Phys. Lett. B* 716:30

[25] Sooryakumar R, Klein MV. 1980. *Phys. Rev. Lett.* 45:660

[26] Sooryakumar R, Klein MV. 1981. *Phys. Rev. B* 23:3213

[27] Varma C. 2002. *J. Low Temp. Phys.* 126:901

[28] Méasson MA, Gallais Y, Cazayous M, Clair B, Rodière P, Cario L, Sacuto A. 2014. *Phys. Rev. B* 89:060503(R)

[29] Cea T, Benfatto L. 2014. *Phys. Rev. B* 90:224515

[30] Grasset R, Cea T, Gallais Y, Cazayous M, Sacuto A, Cario L, Benfatto L, Méasson MA. 2018. *Phys. Rev. B* 97:094502

[31] Barankov RA, Levitov LS, Spivak BZ. 2004. *Phys. Rev. Lett.* 93:160401

[32] Yuzbashyan EA, Altshuler BL, Kuznetsov VB, Enolskii VZ. 2005. *Phys. Rev. B* 72:220503

[33] Barankov RA, Levitov LS. 2006. *Phys. Rev. Lett.* 96:230403

[34] Yuzbashyan EA, Tsyplyatyev O, Altshuler BL. 2006. *Phys. Rev. Lett.* 96:097005

[35] Yuzbashyan EA, Dzero M. 2006. *Phys. Rev. Lett.* 96:230404

[36] Gurarie V. 2009. *Phys. Rev. Lett.* 103:075301

[37] Tsuji N, Eckstein M, Werner P. 2013. *Phys. Rev. Lett.* 110:136404

[38] Papenkort T, Axt VM, Kuhn T. 2007. *Phys. Rev. B* 76:224522

[39] Papenkort T, Kuhn T, Axt VM. 2008. *Phys. Rev. B* 78:132505

[40] Schnyder AP, Manske D, Avella A. 2011. *Phys. Rev. B* 84:214513

[41] Krull H, Manske D, Uhrig GS, Schnyder AP. 2014. *Phys. Rev. B* 90:014515

[42] Tsuji N, Aoki H. 2015. *Phys. Rev. B* 92:064508

[43] Kemper AF, Sentef MA, Moritz B, Freericks JK, Devereaux TP. 2015. *Phys. Rev. B* 92:224517

[44] Chou Y-Z, Liao Y, Foster M. S. 2017. *Phys. Rev. B*95:104507

[45] Matsunaga R, Hamada YI, Makise K, Uzawa Y, Terai H, Wang Z, Shimano R. 2013. *Phys. Rev. Lett.* 111:057002

[46] Matsunaga R, Tsuji N, Fujita H, Sugioka A, Makise K, Uzawa Y, Terai H, Wang Z, Aoki H, Shimano R. 2014. *Science* 345:1145

[47] Cea T, Castellani C, Benfatto L. 2016. *Phys. Rev. B* 93:180507(R)

[48] Tsuji N, Murakami Y, Aoki H. 2016. *Phys. Rev. B* 94:224519

[49] Matsunaga R, Tsuji N, Makise K, Terai H, Aoki H, Shimano R. 2017 *Phys. Rev. B* 96:020505(R)

[50] Cea T, Barone P, Castellani C, Benfatto L. 2018. *Phys. Rev. B* 97:094516

[51] Jujo T. 2015. *J. Phys. Soc. Jpn.* 84:114711

[52] Jujo T. 2018. *J. Phys. Soc. Jpn.* 87:024704

[53] Murotani Y, Shimano R. 2019. arXiv:1902.01104

[54] Silaev M. 2019. arXiv:1902.01666

[55] Katsumi K, Tsuji N, Hamada YI, Matsunaga R, Schneeloch J, Zhong RD, Gu GD, Aoki H, Gallais Y, Shimano R. 2018. *Phys. Rev. Lett.* 120:117001

[56] Chu H, Kim M-J, Katsumi K, Kovalev S, Dawson RD, Schwarz L, Yoshikawa N, Kim G, Putzky D, Li ZZ, Raffy H, Germanskiy S, Deinert J-C, Awari N, Ilyakov I, Green B, Chen M, Bawatna M, Christiani G, Logvenov G, Gallais Y, Boris AV, Keimer B, Schnyder A, Manske D, Gensch M, Wang Z, Shimano R, Kaiser S. 2019. arXiv:1901.06675

[57] Moor A, Volkov AF, Efetov KB. 2017. *Phys. Rev. Lett.* 118:047001

[58] Nakamura S, Iida Y, Murotani Y, Matsunaga R, Terai H, Shimano R. 2018. arXiv:1809.10335

[59] Vollhardt D, Wölfle P. 1990. *The Superfluid Phases of Helium 3* (Taylor & Francis)

[60] Endres M, Fukuhara T, Pekker D, Cheneau M, Schauβ P, Gross C, Demler E, Kuhr S, Bloch I. 2012. *Nature* 487:454

[61] Behrle A, Harrison T, Kombe J, Gao K, Link M, Bernier J-S, Kollath C, Köhl M. 2018. *Nat. Phys.* 14:781

[62] Rüegg C, Normand B, Matsumoto M, Furrer A, McMorrow DF, et al. 2008. *Phys. Rev. Lett.* 100:205701

[63] Pekker D, Varma CM. 2015. *Annu. Rev. Condens. Matter Phys.* 6:269

[64] Abraham E, Tsuneto T. 1966. *Phys. Rev.* 152:416

[65] Schmid A. 1966. *Phys. Kond. Mater.* 5:302

[66] Caroli C, Maki K. 1967. *Phys. Rev.* 159:306

[67] Ebisawa H, Fukuyama H. 1971. *Prog. Theor. Phys.* 46:1042

[68] Sá de Melo CAR, Randeria M, Engelbrecht JR. 1993. *Phys. Rev. Lett.* 71:3202

[69] Tsuchiya S, Yamamoto D, Yoshii R, Nitta M. 2018. *Phys. Rev. B* 98:094503

[70] Gor'kov LP, Eliashberg GM. 1968. *Sov. Phys. JETP* 27:328

[71] Gulian AM, Zharkov GF. 1999. *Nonequilibrium electrons and phonons in superconductors* (Kluwer Academic/Plenum Publishers)

[72] Kopnin N. 2001. *Theory of Nonequilibrium Superconductivity* (Oxford University Press)

[73] Schrieffer JR. 1999. *Theory of Superconductivity* (Westview Press)

[74] Kihlstrom KE, Simon RW, Wolf SA. 1985. *Phys. Rev. B* 32:1843

[75] Brorson SD, Kazeroonian A, Moodera JS, Face DW, Cheng TK, Ippen EP, Dresselhaus MS, Dresselhaus G. 1990. *Phys. Rev. Lett.* 64:2172

[76] Chockalingam SP, Chand M, Jesudasan J, Tripathi V, Raychaudhuri P. 2008. *Phys. Rev. B* 77:214503

[77] Aoki H, Tsuji N, Eckstein M, Kollar M, Oka T, Werner P. 2014. *Rev. Mod. Phys.* 86:779

[78] Murakami Y, Werner P, Tsuji N, Aoki H. 2016. *Phys. Rev. B* 93:094509

[79] Murakami Y, Werner P, Tsuji N, Aoki H. 2016. *Phys. Rev. B* 94:115126

[80] Nosarzewski B, Moritz B, Freericks JK, Kemper AF, Devereaux TP. 2017. *Phys. Rev. B* 96:184518

[81] Kumar A, Kemper AF. 2019. arXiv:1902.09549

[82] Yu T, Wu MW. 2017. *Phys. Rev. B* 96:155311

[83] Yu T, Wu MW. 2017. *Phys. Rev. B* 96:155312

[84] Yang F, Wu MW. 2018. *Phys. Rev. B* 98:094507

[85] Yang F, Wu MW. 2018. arXiv:1812.06622

[86] Leggett AJ. 1966. *Prog. Theor. Phys.* 36:901

[87] Akbari A, Schnyder AP, Manske D, Eremin I. 2013. *Europhys. Lett.* 101:17002

[88] Krull H, Bittner N, Uhrig GS, Manske D, Schnyder AP. 2016. *Nat. Commun.* 7:11921

[89] Cea T, Benfatto L. 2016. *Phys. Rev. B* 94:064512

[90] Murotani Y, Tsuji N, Aoki H. 2017. *Phys. Rev. B* 95:104503

[91] Barlas Y, Varma CM. 2013. *Phys. Rev. B* 87:054503

[92] Peronaci F, Schiró M, Capone M. 2015. *Phys. Rev. Lett.* 115:257001

[93] Foster MS, Dzero M, Gurarie V, Yuzbashyan EA. 2013. *Phys. Rev. B* 88:104511

[94] Fauseweh B, Schwarz L, Tsuji N, Cheng N, Bittner N, Krull H, Berciu M, Uhrig GS, Schnyder AP, Kaiser S, Manske D. 2017. arXiv:1712.07989

[95] Grasset R, Gallais Y, Sacuto A, Cazayous M, Mañas-Valero S, Coronado E, Méasson MA. 2019. Phys. Rev. Lett. 122:127001

[96] Hebling J, Yeh KL, Hoffmann MC, Bartal B, Nelson KA. 2008. *J. Opt. Soc. Am. B* 25:B6

[97] Watanabe S, Minami N, Shimano R. 2011. *Optics Express* 19:1528

[98] Shimano R, Watanabe S, Matsunaga R. 2012. *J. Infrared Millim. Terahz Waves* 33:861

[99] Matsunaga R, Shimano R. 2012. *Phys. Rev. Lett.* 109:187002

[100] Matsunaga R, Shimano R. 2017. *Phys. Scr.* 92:024003

[101] Beck M, Klammer M, Lang S, Leiderer P, Kabanov VV, Gol'tsman GN, Demsar J. 2011. *Phys. Rev. Lett.* 107:177007

[102] Mansart B, Lorenzana J, Mann A, Odeh A, Scarongella M, Chergui M, Carbone F. 2013. *Proc. Natl. Acad. Sci. USA* 110:4539

[103] Gor'kov LP, Eliashberg GM. 1969. *Sov. Phys. JETP* 29:698

[104] Amato JC, McLean WL. 1976. *Phys. Rev. Lett.* 37:930

[105] Entin-Wohlman O. 1978. *Phys. Rev. B* 18:4762

[106] Bardasis A, Schrieffer JR. 1961. *Phys. Rev.* 121:1050

[107] Mattis DC, Bardeen J. 1958. *Phys. Rev.* 111:412

[108] Zimmermann W, Brandt EH, Bauer M, Seider E, Genzel L. 1991. *Physica C: Supercond.* 183:99

[109] Podolsky D, Auerbach A, Arovas DP. 2011. *Phys. Rev. B* 84:174522

[110] Gazit S, Podolsky D, Auerbach A. 2013. *Phys. Rev. Lett.* 110:140401

[111] Sachdev S. 1999. *Phys. Rev. B* 59:14054

[112] Zwerger W. 2004. *Phys. Rev. Lett.* 92:027203

[113] Sherman D, Pracht US, Gorshunov B, Poran S, Jesudasan J, Chand M, Raychaudhuri P, Swanson M, Trivedi N, Auerbach A, Scheffler M, Frydman A, Dressel M. 2015. *Nat. Phys.* 11:188

[114] Cea T, Bucheli D, Seibold G, Benfatto L, Lorenzana J, Castellani C. 2014. *Phys. Rev. B* 89:174506

[115] Cea T, Castellani C, Seibold G, Benfatto L. 2015. *Phys. Rev. Lett.* 115:157002

[116] Pracht US, Cea T, Bachar N, Deutscher G, Farber E, Dressel M, Scheffler M, Castellani C, García-García AM, Benfatto L. 2017. *Phys. Rev. B* 96:094514

[117] Seibold G, Benfatto L, Castellani C. 2017. *Phys. Rev. B* 96:144507

[118] Cheng B, Wu L, Laurita NJ, Singh H, Chand M, Raychaudhuri P, Armitage NP. 2016. *Phys. Rev. B* 93:180511

[119] Maiti S, Hirschfeld PJ. 2015. *Phys. Rev. B* 92:094506

[120] Müller MA, Shen P, Dzero M, Eremin I. 2018. *Phys. Rev. B* 98:024522

[121] Blumberg G, Mialitsin A, Dennis BS, Klein MV, Zhigadlo ND, Karpinski J. 2007. *Phys. Rev. Lett.* 99:227002

[122] Giorgianni F, Cea T, Vicario C, Hauri CP, Withanage WK, Xi X, Benfatto L. 2019. *Nat. Phys.* online publication

[123] Scott RG, Dalfovo F, Pitaevskii LP, Stringari S. 2012. *Phys. Rev. A* 86:053604

[124] Yuzbashyan EA, Dzero M, Gurarie V, Foster MS. 2015. *Phys. Rev. A* 91:033628

[125] Tokimoto J, Tsuchiya S, Nikuni T. 2019. *J. Phys. Soc. Jpn.* 88:023601

[126] Wölfle P. 1977. *Physica B* 90:96

[127] Fausti D, Tobey RI, Dean N, Kaiser S, Dienst A, Hoffmann MC, Pyon S, Takayama T, Takagi H, Cavalleri A. 2011. *Science* 331:189

[128] Kaiser S, Hunt CR, Nicoletti D, Hu W, Gierz I, Liu HY, Le Tacon M, Loew T, Haug D, Keimer B, Cavalleri A. 2014. *Phys. Rev. B* 89:184516

[129] Hu W, Kaiser S, Nicoletti D, Hunt CR, Gierz I, Hoffmann MC, Le Tacon M, Loew T, Keimer B, Cavalleri A. 2014. *Nat. Mater.* 13:705

[130] Mitrano M, Cantaluppi A, Nicoletti D, Kaiser S, Perucchi A, Lupi S, Di Pietro P, Pontiroli D, Riccò M, Clark SR, Jaksch D, Cavalleri A. 2016. *Nature* 530:461

.4 Bibliography from Other Artiles

From Nonequilibrium Cooper pairing in the nonadiabatic Regime by Yuzbashyan et al.

References

[1] N. B. Kopnin: Theory of Nonequilibrium Superconductivity, Clarendon Press, Oxford (2001).

[2] E. Abrahams and T. Tsuneto: Phys. Rev. **152**, 416 (1966).

[3] A. Schmid: Phys. Kond. Mat. **5**, 302 (1966).

[4] L. P. Gor'kov and G. M. Eliashberg: Sov. Phys. JETP **27**, 328 (1968).

[5] O. Betbeder-Matibet and P. Nozieres: Ann. Phys. **51**, 392 (1969).

[6] A. G. Aronov et. al.: Adv. Phys. **30**, 539 (1981); In: Nonequilibrium Superconductivity (ed. D. N. Landenberg and A. I. Larkin), Elsevier (1986).

[7] M. W. Zwierlein et. al.: Phys. Rev. Lett. **92**, 120403 (2004). C. A. Regal, M. Greiner, and D. S. Jin: Phys. Rev. Lett. **92**, 040403 (2004).

[8] C. A. Regal, M. Greiner, and D. S. Jin: Phys. Rev. Lett. 92, 040403 (2004); M. W. Zwierlein et. al.: Phys. Rev. Lett. 92, 120403 (2004); J. Kinast et. al.: Phys. Rev. Lett. 92, 150402 (2004); M. W. Zwierlein et. al.: cond-mat/0412675.

[9] E. A. Yuzbashyan, V. B. Kuznetsov, B. L. Altshuler: unpublished.

[10] R. W. Richardson: J. Math. Phys. **18**, 1802 (1977).

[11] P. W. Anderson: Phys. Rev. **112**, 1900 (1958).

[12] A. F. Volkov and Sh. M. Kogan: Sov. Phys. JETP **38**, 1018 (1974).

[13] Yu. M. Gal'perin, V. I. Kozub, and B. Z. Spivak: Sov. Phys. JETP **54**, 1126 (1981).

[14] V. S. Shumeiko: Doctoral Thesis, Institute for Low Temperature Physics and Engineering, Kharkov, 1990.

[15] R. A. Barankov, L. S. Levitov, and B. Z. Spivak: Phys. Rev. Lett. 93, 160401 (2004).

[16] A. V. Andreev, V. Gurarie, and L. Radzihovsky: Phys. Rev. Lett. 93, 130402 (2004).

[17] R. A. Barankov and L. S. Levitov: Phys. Rev. Lett. 93, 130403 (2004).

[18] M. H. Szymanska, B. D. Simons, and K. Burnett: Phys. Rev. Lett. 94 , 170402 (2005).

[19] M.H.S. Amin, E.V. Bezuglyi, A.S. Kijko, A.N. Omelyanchouk: Low Temp. Phys. 30, 661 (2004).

[20] J. Bardeen, L.N. Cooper, and J.R. Schriefer: Phys. Rev. **108** 1175 (1957).

[21] P. W. Anderson: J. Phys. Chem. Solids **11**, 26 (1959).

[22] I. L. Kurland, I. L. Aleiner, and B. L. Altshuler: Phys. Rev. B **62**, 14886 (2000).

[23] In the presence of spatial symmetries additional quantum numbers are needed to distinguish states. For example, if there is translational invariance, time-reversed pairs of states are $|j\uparrow\rangle = |\mathbf{p}\uparrow\rangle$ and $|j\downarrow\rangle = |-\mathbf{p}\downarrow\rangle$.

[24] R. W. Richardson and N. Sherman: Nucl. Phys. **52**, 221 (1964); **52**, 253 (1964).

[25] M. Gaudin: La fonction d'onde de Bethe, Masson, Paris (1983).

[26] M. C. Cambiaggio, A. M. F. Rivas, and M. Saraceno: Nucl. Phys. A **424**, 157 (1997).

[27] Each of H_j can be viewed as a Hamiltonian of a system of classical spins, these Hamiltonians are known as classical Gaudin magnets[25].

[28] V. I. Arnold: Mathematical Methods of Classical Mechanics, Springer-Verlag, New York, (1978); M. Tabor, Chaos and Integrability in Nonlinear Dynamics, Wiley, New York, (1989).

[29] E. K. Sklyanin: J. Sov. Math. **47**, 2473 (1989); Progr. Theoret. Phys. Suppl. **118**, 35 (1995); V. B. Kuznetsov: J. Math. Phys. **33**, 3240, (1992).

[30] E. A. Yuzbashyan, B. L. Altshuler, V. B. Kuznetsov, V. Z. Enolskii: J. Phys. A **38**, 7831, (2005); cond-mat/0407501.

[31] E.D. Belokolos, A.I. Bobenko, V.Z. Enolskii, A.R. Its: *Algebro-geometric approach to nonlinear-integrable equations*, (Springer-Verlag, Berlin, 1994); D. Mumford: *Tata Lectures on Theta*, (Birkhauser, Boston, 1983, 1984) Vols. 1-2.

[32] J. C. Eilbeck, V. Z. Enolskii, and H. Holden: Proc. R. Soc. Lond. A **459**, 1581, (2003).

[33] R. Bonifacio and G. Preparata: Phys. Rev. A **2**, 336 (1970).

[34] A. Vardi, V. A. Yurovsky and J. R. Anglin: Phys. Rev. A **64**, 063611 (2001).

[35] For certain initial conditions the dynamics in the thermodynamic limit can reduce to that of a few spin solution *asymptotically* at long times. For example, we expect $m = 3, 5, \ldots$ spin solutions at long times if the coupling is changed abruptly while the condensate is in an excited state.

[36] G.L. Warner and A. J. Leggett: Phys. Rev. B **71**, 134514 (2005).

From Nonequilibrium dynamics of weakly and strongly paired superconductors by Gurarie

References

[Calabrese and Cardy(2006)] P. Calabrese and J. Cardy, Phys. Rev. Lett. **96**, 136801 (2006).

[Kollath et al.(2007)] C. Kollath, A. M. Läuchli, and E. Altman, Phys. Rev. Lett. **98**, 180601 (2007).

[Volkov and Kogan(1973)] A. F. Volkov and S. M. Kogan, Zh. Eksp. Teor. Fiz **65**, 2038 (1973), English translation: Sov. Phys. JETP, **38**, 1018 (1974).

[Barankov et al.(2004)] R. A. Barankov, L. S. Levitov, and B. Z. Spivak, Phys. Rev. Lett. **93**, 160401 (2004).

[Dukelsky et al.(2004)] J. Dukelsky, S. Pittel, and G. Sierra, Rev. Mod. Phys. **76**, 643 (2004).

[Barankov and Levitov(2006)] R. A. Barankov and L. S. Levitov, Phys. Rev. Lett. **96**, 230403 (2006).

[Yuzbashyan and Dzero(2006)] E. A. Yuzbashyan and M. Dzero, Phys. Rev. Lett. **96**, 230404 (2006).

[Eagles(1969)] D. M. Eagles, Phys. Rev. **186**, 456 (1969).

[Leggett(1980)] A. Leggett, in *Modern Trends in the Theory of Condensed Matter* (Springer-Verlag, Berlin, 1980), pp. 13–27.

[Nozières and Schmitt-Rink(1985)] P. Nozières and S. Schmitt-Rink, J. Low Temp. Phys. **59**, 195 (1985).

[Regal et al.(2004)] A. Regal, M. Greiner, and D. S. Jin, Phys. Rev. Lett. **92**, 040403 (2004).

[Zwierlein et al.(2004)] M. W. Zwierlein, C. A. Stan, C. H. Schunck, S. M. F. Raupach, A. J. Kerman, and W. Ketterle, Phys. Rev. Lett. **92**, 120403 (2004).

[Andreev et al.(2004)] A. V. Andreev, V. Gurarie, and L. Radzihovsky, Phys. Rev. Lett. **93**, 130402 (2004).

[Barankov and Levitov(2004)] R. A. Barankov and L. S. Levitov, Phys. Rev. Lett. **93**, 130403 (2004).

[Holland et al.(2001)] M. Holland, J. Park, and R. Walser, Phys. Rev. Lett. **86**, 1915 (2001).

[Giorgini et al.(2008)] S. Giorgini, L. P. Pitaevskii, and S. Stringari, Rev. Mod. Phys. **80**, 1215 (2008).

[Levinsen and Gurarie(2006)] J. Levinsen and V. Gurarie, Phys. Rev. A **73**, 053607 (2006).

[Bulgac and Yoon(2009)] A. Bulgac and S. Yoon, Phys. Rev. Lett. **102**, 085302 (2009).

[Timmermans et al.(1999)] E. Timmermans, P. Tommasini, M. Hussein, and A. Kerman, Physics Reports **315**, 199 (1999).

[Gurarie and Radzihovsky(2007)] V. Gurarie and L. Radzihovsky, Ann. Phys. **322**, 2 (2007).

From Solitons and Rabi Oscillations in a Time-Dependent BCS Pairing Problem by Barankov, Levitov, Spivak

References

[1] B. DeMarco, *et al.*, Phys. Rev. Lett. **82**, 4208 (1999); Science **285**, 1703 (1999); Phys. Rev. Lett. **86**, 5409 (2001); Phys. Rev. Lett. **88**, 040405 (2002); A. G. Truscott *et al.*, Science **291**, 2570 (2001); T. Loftus *et al.*, Phys. Rev. Lett. **88**, 173201 (2002); K. M. O'Hara, *et al.*, Science **298**, 2179 (2002); Phys. Rev. A **66**, 041401 (2002)

[2] H. T. C. Stoof, M. Houbiers, C. A. Sackett, and R. G. Hulet, Phys. Rev. Lett. **76**, 10 (1996)

[3] Tin-Lun Ho and S. Yip, Phys. Rev. Lett. **82**, 247 (1999)

[4] J. L. Bohn, Phys. Rev. A**61**, 053409 (2000)

[5] M. Holland, S. J. J. M. F. Kokkelmans, M. L. Chiofalo, and R. Walser, Phys. Rev. Lett. **87**, 120406 (2001)

[6] S. J. J. M. F. Kokkelmans, J. N. Milstein, M. L. Chiofalo, R. Walser, and M. J. Holland, Phys. Rev. A**65**, 053617 (2002)

[7] J. N. Milstein, S. J. J. M. F. Kokkelmans, and M. J. Holland, Phys. Rev. A**66**, 043604 (2002)

[8] Y. Ohashi, and A. Griffin, Phys. Rev. Lett. **89**, 130402 (2002); Phys. Rev. A**67**, 033603 (2003); Phys. Rev. A**67**, 063612 (2003)

[9] J. Stajic, J. N. Milstein, Q. Chen, M. L. Chiofalo, M. J. Holland, and K. Levin, cond-mat/0309329

[10] H. Heiselberg, C. J. Pethick, H. Smith, and L. Viverit, Phys. Rev. Lett. **85**, 2418 (2000)

[11] M. A. Baranov, M. S. Marenko, V. S. Rychkov, and G. V. Shlyapnikov, Phys. Rev. A **66**, 013606 (2002)

[12] H. Heiselberg and B. Mottelson, Phys. Rev. Lett. **88**, 190401 (2002)

[13] C. P. Search, H. Pu, W. Zhang, B. P. Anderson, and P. Meystre, Phys. Rev. A **65**, 063616 (2002)

[14] J. Carlson, S.-Y. Chang, V. R. Pandharipande, and K. E. Schmidt, Phys. Rev. Lett. **91**, 050401 (2003)

[15] H. Heiselberg, Phys. Rev. A **68**, 053616 (2003)

[16] M. Houbiers and H. T. C. Stoof, Phys. Rev. A**59**, 1556 (1999)

[17] M. Tinkham, *Introduction to Superconductivity*, (McGraw-Hill, 1996)

[18] A. Schmid, Phys. Kond. Mat. **5**, 302 (1966)

[19] E. Abrahams and T. Tsuneto, Phys. Rev. **152**, 416 (1966)

[20] L. P. Gor'kov, G. M. Eliashberg, Zh. Eksp. Teor. Fiz. **54**, 612 (1968) [Sov. Phys. JETP **27**, 328 (1968)]

[21] A. G. Aronov and V. L. Gurevich, Sov. Phys. Solid State, **16**, 1722, (1974); Sov. Phys. JETP, **38**, 550, (1974);

[22] A. I. Larkin, Yu. N. Ovchinnikov, Sov. Phys. JETP, **46**, 155, (1977)

[23] P. W. Anderson, Phys. Rev. **112**, 1900 (1958)

[24] A. F. Volkov and Sh. M. Kogan, Sov. Phys. JETP, **38**, 1018 (1974);

[25] Yu. M. Gal'perin, V. I. Kozub, and B. Z. Spivak, Sov. Phys. JETP, **54**, 1126 (1981)

[26] S. L. McCall and E. L. Hahn, Phys. Rev. Lett. **18**, 908 (1967); Phys. Rev. **183**, 457 (1968)

From Collisionless relaxation of the energy gap in superconductors by Volkov, Kogan, 1973

[1)] We note that the term $(2\pi)^4(\omega)\delta(\mathbf{k})$ in Eq. (13) of Éliashberg's paper [[5]] should be discarded.

[T] E. Abrahams and T. Tsuneto, Phys. Rev., 152, 416 (1966).

[2] L. P. Gor'kov and G. M. Éliashberg, Zh. Eksp. Teor. Fiz. 54, 612 (1968) [Sov. Phys.-JETP 27, 328 (1968)].

[3] G. M. Éliashberg, ibid. 55, 2443 (1968) [28, 1298 (1969)].

[4] B. I. Ivlev, ZhETF Pis. Red. 15, 441 (1972) [JETP Lett. 15, 313 (1972)].

[5] G. M. Eliashberg, Zh. Eksp. Teor. Fiz. 61, 1254 (1971) [Sov. Phys.-JETP 34, 668 (1972)]. .

[6] L. V. Keldysh, Zh. Eksp. Teor. Fiz. 47, 1515 (1964) [Sov. Phys.-JETP 20, 1018 (1965)].
[7] J. R. Schrieffer, Theory of Superconductivity, Benjamin, 1964.
[8] A. A. Abrikosov, L. P. Gor'kov, and I. E. Dzyaloshinskiĭ, Metody kvantovoĭ teorii polya v statisticheskoĭ fizike (Quantum Field-Theoretical Methods in Statistical Physics), Fizmatgiz, 1962 [Pergamon, 1965)]. [9] L. D. Landau, Zh. Eksp. Teor. Fiz. 16, 574 (1946).

From Higgs mode in a strongly interacting fermionic superfluid by Behrle, Harrison et al.

References

[1] Higgs, P. W. Broken symmetries and the masses of gauge bosons. *Phys. Rev. Lett.* **13**, 508–509 (1964). URL https://link.aps.org/doi/10.1103/PhysRevLett.13.508.

[2] Littlewood, P. B. & Varma, C. M. Gauge-invariant theory of the dynamical interaction of charge density waves and superconductivity. *Phys. Rev. Lett.* **47**, 811–814 (1981). URL http://link.aps.org/doi/10.1103/PhysRevLett.47.811.

[3] Sooryakumar, R. & Klein, M. V. Raman scattering by superconducting-gap excitations and their coupling to charge-density waves. *Phys. Rev. Lett.* **45**, 660–662 (1980). URL http://link.aps.org/doi/10.1103/PhysRevLett.45.660.

[4] Matsunaga, R. *et al.* Higgs amplitude mode in the BCS superconductors $Nb_{1-x}Ti_xN$ induced by terahertz pulse excitation. *Phys. Rev. Lett.* **111**, 057002 (2013). URL http://link.aps.org/doi/10.1103/PhysRevLett.111.057002.

[5] Sherman, D. *et al.* The Higgs mode in disordered superconductors close to a quantum phase transition. *Nature Physics* **11**, 188–192 (2015).

[6] Pekker, D. & Varma, C. Amplitude/Higgs modes in condensed matter physics. *Annual Review of Condensed Matter Physics* **6**, 269–297 (2015).

[7] Podolsky, D., Auerbach, A. & Arovas, D. P. Visibility of the amplitude (Higgs) mode in condensed matter. *Phys. Rev. B* **84**, 174522 (2011). URL http://link.aps.org/doi/10.1103/PhysRevB.84.174522.

[8] Scott, R. G., Dalfovo, F., Pitaevskii, L. P. & Stringari, S. Rapid ramps across the BEC-BCS crossover: A route to measuring the superfluid gap. *Phys. Rev. A* **86**, 053604 (2012). URL http://link.aps.org/doi/10.1103/PhysRevA.86.053604.

[9] Barlas, Y. & Varma, C. M. Amplitude or Higgs modes in *d*-wave superconductors. *Phys. Rev. B* **87**, 054503 (2013). URL https://link.aps.org/doi/10.1103/PhysRevB.87.054503.

[10] Liu, B., Zhai, H. & Zhang, S. Evolution of the Higgs mode in a fermion superfluid with tunable interactions. *Phys. Rev. A* **93**, 033641 (2016). URL http://link.aps.org/doi/10.1103/PhysRevA.93.033641.

[11] Han, X., Liu, B. & Hu, J. Observability of Higgs mode in a system without Lorentz invariance. *Phys. Rev. A* **94**, 033608 (2016). URL http://link.aps.org/doi/10.1103/PhysRevA.94.033608.

[12] Littlewood, P. B. & Varma, C. M. Amplitude collective modes in superconductors and their coupling to charge-density waves. *Phys. Rev. B* **26**, 4883–4893 (1982). URL http://link.aps.org/doi/10.1103/PhysRevB.26.4883.

[13] Rüegg, C. *et al.* Quantum magnets under pressure: Controlling elementary excitations in $TlCuCl_3$. *Phys. Rev. Lett.* **100**, 205701 (2008). URL https://link.aps.org/doi/10.1103/PhysRevLett.100.205701.

[14] Halperin, W. & Varoquax, E. Order-parameter collective modes in superfluid 3He. In Halperin, W. & Pitaevskii, L. (eds.) *Helium Three*, 353–522 (Elsevier Science Publishers, 1990).

[15] Bissbort, U. *et al.* Detecting the amplitude mode of strongly interacting lattice bosons by Bragg scattering. *Phys. Rev. Lett.* **106**, 205303 (2011). URL http://link.aps.org/doi/10.1103/PhysRevLett.106.205303.

[16] Endres, M. *et al.* The 'Higgs' amplitude mode at the two-dimensional superfluid/Mott insulator transition. *Nature* **487**, 454–458 (2012).

[17] Hoang, T. M. *et al.* Adiabatic quenches and characterization of amplitude excitations in a continuous quantum phase transition. *Proceedings of the National Academy of Sciences* **113**, 9475–9479 (2016). URL http://www.pnas.org/content/113/34/9475.abstract. http://www.pnas.org/content/113/34/9475.full.pdf.

[18] Leonard, J., Morales, A., Zupancic, P., Donner, T. & Esslinger, T. Monitoring and manipulating Higgs and Goldstone modes in a supersolid quantum gas. *Science* **358**, 1415–1418 (2017).

[19] Yuzbashyan, E. A. & Dzero, M. Dynamical vanishing of the order parameter in a fermionic condensate. *Phys. Rev. Lett.* **96**, 230404 (2006). URL http://link.aps.org/doi/10.1103/PhysRevLett.96.230404.

[20] Hannibal, S. *et al.* Quench dynamics of an ultracold Fermi gas in the BCS regime: Spectral properties and confinement-induced breakdown of the Higgs mode. *Phys. Rev. A* **91**, 043630 (2015). URL http://link.aps.org/doi/10.1103/PhysRevA.91.043630.

[21] Greiner, M., Regal, C. A. & Jin, D. S. Probing the excitation spectrum of a Fermi gas in the BCS-BEC crossover regime. *Phys. Rev. Lett.* **94**, 070403 (2005). URL https://link.aps.org/doi/10.1103/PhysRevLett.94.070403.

[22] Chin, C. *et al.* Observation of the pairing gap in a strongly interacting Fermi gas. *Science* **305**, 1128–1130 (2004).

[23] Ketterle, W. & Zwierlein, M. W. Making, probing and understanding ultracold Fermi gases. *Proceedings of the International School of Physics "Enrico Fermi"* **164**, 95–287 (2007).

[24] Stewart, J. T., Gaebler, J. P. & Jin, D. S. Using photoemission spectroscopy to probe a strongly interacting Fermi gas. *Nature* **454**, 744–747 (2008).

[25] Feld, M., Fröhlich, B., Vogt, E., Koschorreck, M. & Köhl, M. Observation of a pairing pseudogap in a two-dimensional Fermi gas. *Nature* **480**, 75–78 (2011).

[26] Bruun, G. M. Low-energy monopole modes of a trapped atomic Fermi gas. *Phys. Rev. Lett.* **89**, 263002 (2002). URL https://link.aps.org/doi/10.1103/PhysRevLett.89.263002.

[27] Korolyuk, A., Kinnunen, J. J. & Törmä, P. Density response of a trapped fermi gas: A crossover from the pair vibration mode to the goldstone mode. *Phys. Rev. A* **84**, 033623 (2011). URL https://link.aps.org/doi/10.1103/PhysRevA.84.033623.

[28] Korolyuk, A., Kinnunen, J. J. & Törmä, P. Collective excitations of a trapped fermi gas at finite temperature. *Phys. Rev. A* **89**, 013602 (2014). URL https://link.aps.org/doi/10.1103/PhysRevA.89.013602.

[29] Tokimoto, J., Tsuchiya, S. & Nikuni, T. Higgs mode in a trapped superfluid Fermi gas. *Journal of Low Temperature Physics* 1–6 (2017). URL http://dx.doi.org/10.1007/s10909-017-1766-2.

[30] Ries, M. G. *et al.* Observation of pair condensation in the quasi-2D BEC-BCS crossover. *Phys. Rev. Lett.* **114**, 230401 (2015). URL https://link.aps.org/doi/10.1103/PhysRevLett.114.230401.

[31] Schirotzek, A., Shin, Y.-i., Schunck, C. H. & Ketterle, W. Determination of the superfluid gap in atomic Fermi gases by quasiparticle spectroscopy. *Phys. Rev. Lett.* **101**, 140403 (2008). URL https://link.aps.org/doi/10.1103/PhysRevLett.101.140403.

[32] Hoinka, S. *et al.* Goldstone mode and pair-breaking excitations in atomic Fermi superfluids. *Nature Physics* **13**, 943—-946 (2017).

[33] Chang, S. Y., Pandharipande, V. R., Carlson, J. & Schmidt, K. E. Quantum Monte Carlo studies of superfluid Fermi gases. *Phys. Rev. A* **70**, 043602 (2004). URL https://link.aps.org/doi/10.1103/PhysRevA.70.043602.

[34] Gezerlis, A. & Carlson, J. Strongly paired fermions: Cold atoms and neutron matter. *Phys. Rev. C* **77**, 032801 (2008). URL https://link.aps.org/doi/10.1103/PhysRevC.77.032801.

[35] Bulgac, A., Drut, J. E. & Magierski, P. Quantum Monte Carlo simulations of the BCS-BEC crossover at finite temperature. *Phys. Rev. A* **78**, 023625 (2008). URL https://link.aps.org/doi/10.1103/PhysRevA.78.023625.

[36] Chen, Q. Effect of the particle-hole channel on BCS-–Bose–Einstein condensation crossover in atomic Fermi gases. *Scientific Reports* **6**, 25772 (2016).

[37] Haussmann, R., Rantner, W., Cerrito, S. & Zwerger, W. Thermodynamics of the BCS-BEC crossover. *Phys. Rev. A* **75**, 023610 (2007). URL https://link.aps.org/doi/10.1103/PhysRevA.75.023610.

[38] Pieri, P., Pisani, L. & Strinati, G. C. BCS-BEC crossover at finite temperature in the broken-symmetry phase. *Phys. Rev. B* **70**, 094508 (2004). URL https://link.aps.org/doi/10.1103/PhysRevB.70.094508.

[39] Ohashi, Y. & Griffin, A. Superfluidity and collective modes in a uniform gas of Fermi atoms with a Feshbach resonance. *Phys. Rev. A* **67**, 063612 (2003). URL https://link.aps.org/doi/10.1103/PhysRevA.67.063612.